ELECTRON BEAM CHEMICAL VAPOR DEPOSITION OF PLATINUM AND CARBON

A Thesis

Presented to

The Academic Faculty

By

David Cartier Beaulieu

In Partial Fulfillment

Of the Requirements for the Degree

Master of Science in Mechanical Engineering

Georgia Institute of Technology

April 2005

ELECTRON BEAM CHEMICAL VAPOR DEPOSITION OF PLATINUM AND CARBON

Approved by:

Dr. W. Jack Lackey, Chair
School of Mechanical Engineering
Georgia Institute of Technology

Dr. Thomas Orlando
School of Chemistry
Georgia Institute of Technology

Dr. Suresh K. Sitaraman
School of Mechanical Engineering
Georgia Institute of Technology

Date Approved: April 11, 2005

ACKNOWLEDGEMENT

I would like to thank Dr. Lackey for the guidance he has given me for this research and throughout graduate school. He has provided me with help and support whenever I have needed it, and it has been a pleasure to work under him. I would also like to thank my fellow graduate students who have worked under Dr. Lackey. Ryan Johnson, Scott Bondi, Jian Mi, and Josh Gillespie have all helped me along the way. Lastly, I would like to give thanks to Dr. S. K. Sitaraman and Dr. T. Orlando for being on my reading committee.

TABLE OF CONTENTS

LIST OF TABLES

LIST OF FIGURES

SUMMARY

Electron Beam Chemical Vapor Deposition (EBCVD) is a process by which an electron beam is used to decompose adsorbed reagent molecules to produce a deposit. Typically, this process occurs in a modified Scanning Electron Microscope (SEM) or Transmission Electron Microscope (TEM), and the reagent gas molecules are an organometallic compound or a hydrocarbon. The primary electrons from the beam, and especially the secondary electrons emitted from the substrate as a result of the beam, dissociate the adsorbed molecules. Important factors for the deposition process include beam current, accelerating voltage, deposition time, and reagent gas composition. Simple structures can be fabricated through utilization of the various scanning modes of an SEM. Fibers (pillar-like structures) can be deposited using the spot scan mode, in which the electron beam remains in a fixed location. Lines (wall-like structures) can be deposited using the line scan mode, in which the beam moves back and forth over a fixed number of pixels.

This investigation focuses on the process parameters controlling deposition rate and geometry for platinum and carbon fibers and lines. Platinum deposition was performed using a gas injection system that featured a small diameter needle for supplying a localized flow of gas from an organometallic compound, $(CH_3)_3Pt((C_5H_5)CH_3)$. Carbon deposition was performed in the Environmental mode of the microscope, in which the chamber is filled with a specified pressure of the reagent gas.

Statistically designed experiments were performed for platinum fiber and line deposition. Analysis indicated that the beam current and deposition time were dominant factors in determining the deposition rate. The voltage also had a significant effect on fiber deposition. For platinum line deposition, the effects of varying the dwell time and line time were also studied. The dwell time refers to the time that the beam spends on a single pixel, and the line time refers to the amount of time required for the beam to return to a specific pixel. Thus the line time is an exact measure of time available for reagent molecules to re-adsorb on the surface. This factor also had a significant effect on the line height deposited per scan. The dwell time was not found to have any statistically significant effects. Optimization analysis was performed to maximize growth rate and aspect ratio and to minimize deposit size for platinum. Depositions were made at the specified parameters, and results indicated that high voltage (30 kV) and high beam current (5,400 pA) led to higher aspect ratios for both platinum lines and fibers. Medium voltage (15.8 kV), low beam current (60 pA or less), and longer dwell times (420 μs) were found to be preferable for depositing minimal width lines, which were under 200 nm. Low voltage (5 kV) and high beam current (20,000 pA) were preferable for maximum deposition rates. Optimal settings for a specific application would be determined by the sizes required for that application. If size is a critical parameter, then lower beam currents would be necessary, but this would slow down the process. If speed is the most critical parameter, then higher beam currents would be used, but this would lead to less control over deposit size and geometry. If size and speed are equally important, the optimal beam settings may be somewhere in the middle (i.e., 15-20 kV, 1,500 pA), depending on the specific requirements. EDS performed for platinum fibers

in a TEM indicated that the fibers were amorphous with no carbon content detected. This differs significantly from previously reported results which utilized a similar precursor and found platinum crystals and upwards of 70% carbon content.

Statistically designed experiments were also performed for carbon line deposition. The voltage, beam current, and dwell/line time were the factors that were studied for carbon lines. An increase in the line time led to a significant increase in the line height/scan and appeared to be the dominant factor. There was no statistically significant correlation between the line time and the line width. An increase in voltage led to a non-statistically significant increase in the height/scan, but a larger effect on the line width. Increasing voltage led to a statistically significant decrease in the line width for one experiment, and was just outside of the 95% confidence level for another. The beam current had a statistically significant effect on the line width for one study (and was just below the 95% confidence level for another), with increasing beam current corresponding to increasing line width. This effect is likely attributable to the wider beam diameter associated with larger beam currents. TEM analysis indicated that carbon fiber deposits were mostly amorphous, which agrees with previously reported results.

CHAPTER I

INTRODUCTION AND BACKGROUND

1.1. Electron Beam Chemical Vapor Deposition

Electron Beam Chemical Vapor Deposition (EBCVD) is a technology that uses an electron beam to provide localized deposition for fabrication of nanoscale structures or devices. In EBCVD, impinging electrons dissociate adsorbed precursor molecules, forming a deposit on the substrate and volatiles that are evacuated from the chamber. Alternative names for the process are Electron Beam Induced Deposition (EBID) and Focused Electron Beam Induced Deposition (FEBID). Often a scanning electron microscope (SEM) or a transmission electron microscope (TEM), modified to permit operation with chemical reagents present, are used for EBCVD.

Standard IC manufacturing methods such as photolithography and chemical etching generally have resolution limits on the order of 1 μm. Electron beam lithography can achieve resolutions on the order of 50 nm. These methods are, however, indirect in that they require several intermediate steps to produce the final desired structure. Direct fabrication technologies such as Laser CVD[1] (LCVD) have resolutions on the order of 10-100 μm, which is approximately ten times the wavelength of the laser. While LCVD is a thermally driven process, EBCVD is driven by electron-induced dissociation of adsorbed molecules, meaning it can occur at low temperatures. A Focused Ion Beam (FIB)[2,3] can also be used as a direct fabrication technology, with deposition occurring via ion beam decomposition of adsorbed precursor molecules. The ion beam typically

consists of Ga^+ ions from a liquid source, but other materials have been used. Typical resolutions for FIB are on the order of 100 nm. FIB technology has been used for device modification and mask repair. Inherent problems associated with FIB technology include damage to the sample in the form of milling and ion implantation. EBCVD is capable of resolution as small as 20 nm for a 30 kV beam and 7 nm for a 200 kV beam along with deposition rates as large as 150 nm/s, allowing fabrication of nanometer scale devices. High aspect ratio and three-dimensional deposits are also possible. EBCVD thus features superior resolution and does not have inherent deposit impurities in comparison with FIB. EBCVD can be thought of as a localized CVD process since growth rate can be limited by mass transport or reaction rate. An example of device fabrication possible with EBCVD is a nanometer scale probe for an AFM[4]. Currently, EBCVD has limited industrial use, but there is potential for applications that require high precision processing and flexible manufacturing such as rapid prototyping, prototype microelectronic circuit repair, or direct fabrication of nanoscale devices.

1.2. Research Scope

The scope of this investigation is to use a modified SEM to fabricate platinum and carbon structures and analyze them with respect to growth rates, geometry, and microstructure. Emphasis will be placed on maximizing the deposition rates for both line and fiber deposits. The process variables of voltage, beam current, and deposition time were controlled and manipulated in statistically designed experiments in order to study the effects on fiber deposition. Voltage, beam current, dwell time, and line time were varied to study the effects on line deposition. Specimen geometry was observed via scanning

electron microscopy, and deposit composition was determined by EDS and EELS. Transmission electron microscopy was used to observe the microstructure of the deposits. Optimization analysis and experimentation was performed for deposition rates and deposit aspect ratio.

CHAPTER II

LITERATURE REVIEW AND PREVIOUS WORK

2.1. EBCVD Overview

Electron Beam Chemical Vapor Deposition (EBCVD) is a process by which an electron beam is used to provide localized deposition for fabrication of nanoscale structures or devices. A focused electron beam, such as in an SEM or TEM, can be used to from structures with high aspect ratios. In EBCVD, primary electrons from the beam impact a substrate, causing secondary electrons to be emitted. These secondary electrons play a prominent role in dissociating adsorbed reagent molecules to form a deposit on the substrate and volatiles that are evacuated from the chamber. The deposition process depends on many factors including the precursor properties and the electron beam properties. If the electron beam is not moved relative to the substrate, a dot is grown. A fiber is grown if the growth time is increased. If the beam is moved, lines or other structures can be deposited as in rapid prototyping. If a gas such as Cl or HCl is present, etching is possible. Alternative names for the process are Electron Beam Induced Deposition (EBID) and Focused Electron Beam Induced Deposition (FEBID). The progress that has been made in this emerging technology in terms of capabilities, modeling, and control is reviewed here.

2.2. Materials

The EBCVD process was inadvertently discovered when carbon was deposited in an electron microscope because of the presence of hydrocarbons which were emitted from the vacuum pump oil.[5-7] Starting in the mid 1980's, more extensive work was done in this area by pioneers such as Koops and colleagues[8,9] and Matsui and Mori.[10] Since this discovery, a variety of materials have been deposited through the EBCVD process.[7-34] Many gases that have been used for traditional CVD reactions have been used for analogous deposition of metals and ceramics by EBCVD. Table 2-1 summarizes some of the different materials that have been deposited thus far.

Table 2-1. Various Materials Deposited by EBCVD

Material Depsosited	Precursor	Substrate	Apparatus	Substrate Temperature (°C)	Voltage (kV)	Current/Current Density	Growth Rate (nm/min)	Ref.
Al	$(CH_3)_3Al$	GaAs	SEM	18-80	6	10pA	20	11
	$AlH_3{\cdot}N(CH_3)_3$	SiO_2	TEM	120-170	120	NR*	1.2-2.4	12
Au	$CH_3CH_2AuP(CH_3)_3$	Si	TEM	125-200	120	NR	NR	13
	$Au(CH_3)_2(C_5H_7O_2)$	TEM grid	SEM	NR	10	0.2 nA	1500	14
	PF_3AuCl	Si (w/ SiO_2 layer)	SEM	NR	3-25	400-500 pA	NR	15
	$Me_2Au(tfac)$*	Si (w/ SiO_2 layer)	SEM	20-100	20-30	20-2000 pA	NR	16
C	Hydrocarbon contamination	Au-Pd	SEM	NR	45	10-50 pA	NR	7
	Hydrocarbon contamination	Si	SEM	NR	30	15-100 pA	NR	17
Co	$Co_2(CO)_8$	Carbon TEM grid	SEM	NR	25	84-100 pA	120-2700	18
Cr	$Cr(C_6H_6)_2$	Si	SEM	NR	15	40 pA	NR	10
	$Cr(CO)_6$	Si	SEM	280-330	0.25	20 $\mu A/cm^2$	25-100	19
Cu	(hfac)CuVTMS*	Si	SEM	NR	25	20 pA-1nA	960	20
Diamond	CH_4-H_2	Si	SEM	NR	10	30 nA	1.7	21
Fe	$Fe(CO)_5$	Si	Kaufman source	125	1 kV	70 pA	30-50	19
	$Fe(CO)_5$	Carbon film	SEM	NR	30	800 pA	NR	22
GaAs	$Ga(CH_3)_3/AsH_3$	Si	SEM	NR	NR	1-100 A/cm^2	1.7-33.3	23
Mo	$Mo(CO)_6$	Cu TEM grid	SEM	NR	20	500 pA	NR	24
Os	$Os_3(CO)_{12}$	Si, Carbon foil	Electron Gun	90-120	40	0.8-15 mA/cm^2	0.19	8
Pt	$C_5H_5Pt(CH_3)_3$	Si (w/ SiO_2 layer)	SEM	NR	20	200 pA	200	25
	$C_5H_5Pt(CH_3)_3$	Si (w/ Si_3N_4 layer)	SEM	NR	NR	NR	NR	26
	$C_5H_5Pt(CH_3)_3$	Cu	SEM	NR	20	75-1100 pA	9000	27
	$C_5H_5Pt(CH_3)_4$	Si (w/ SiO_2 layer)	SEM	NR	30	70-100 pA	NR	28
Rh	$RhCl(PF_3)_2$	Si (w/ SiO_2 layer)	SEM	NR	25	90 pA	1200	20
Ru	$Ru_3(CO)_{12}$	Si, Carbon foil		90-120	40	0.8-15 mA/cm^2	0.23	8
Si	SiH_4	Alumina	TEM	900-1000	100	1 mA/cm^2	1-3	29
SiO_2	TEOS ($SiO_4C_8H_{20}$)	Quartz (w/ SnO_2 layer)	SEM	NR	2-25	10 pA-1nA	120-480	30
	N_2O/SiH_4	Si	Electron Gun	150-400	1-5	40-400 mA/cm^2	5-25	31
	TEOS ($SiO_4C_8H_{20}$)	Si	SEM	NR	25	90 pA	360	20
Si_3N_4	Nitrogen on surface of Si	Si	LEED	-220	0.4-0.9	5 μA	NR	32
W	WCl_6	Si	SEM	NR	15	40 pA	NR	10
	WF_6	Si on TEM grid	TEM	NR	120	100 A/cm^2	NR	33
WC	$W(CO)_6$	Si	SEM	NR	1.5-30	115-482 pA	1550nm/(nC)*	34

Note*: NR=Not Reported; tfac=trifluoroacetylacetonate; hfac=hexafluoroacetylacetonate; VTMS=vinyltrimethoxysilane; nC= nanoCoulomb

2.2.1. Properties of Deposited Materials

There has been limited analysis thus far of the material properties of EBCVD materials. The primary focus has been on deposit composition and electrical resistivity, as these characteristics are important for micro- or nanoscale electronics. There has been very limited analysis of mechanical properties and deposit adherence.

2.2.2. Composition/Structure

The composition of EBCVD deposits is an important characteristic, and has probably been the most studied feature of this process aside from deposit shape. The ability to deposit high purity materials is critical if specific properties, such as high conductivity or strength, are desired. The dissociation mechanisms of the process have led to difficulty in obtaining high purity deposits. Deposits from precursor gases containing C and O typically contain significant levels of contamination of these two elements, especially C. Some of the relevant investigations into composition for various materials are detailed here.

Kunz and Mayer[37] characterized the morphology and chemical purity for Fe and Cr films. Auger electron spectroscopy indicated low carbon contamination, with no detectable carbon in the Fe film. Shimojo et al.[22] deposited Fe using $Fe(CO)_5$ and reported amorphous deposits containing Fe and C. After annealing at 600^{o}C for 1 hour, the deposits were crystalline, with α-Fe, Fe_5C_2, Fe_7C_3, and Fe_2C being formed. Ishibashi et al.[11] characterized Al line deposits from trimethyl aluminum as consisting of aluminum mixed with carbon, and concluded that higher purity could be achieved at higher

deposition temperature or with longer growth time and lower source gas pressure. Rotkina et al.[26] deposited Pt lines using $C_5H_5Pt(CH_3)_3$ and reported a structure consisting of clustered Pt crystals in an amorphous C matrix. Koops et al.[16] deposited Pt fibers using $C_5H_5Pt(CH_3)_3$ and reported Pt contents ranging from 4 to 14%. Platinum crystals of 1.8 to 2.1 nm were observed in the body of the fiber, and surface crystals up to 8 nm were also observed. The matrix surrounding the crystals was not visible due to projection in the TEM image. Koops et al.[27] also reported Pt nanocrystalline material deposition as shown in Figure 2-1. Takai et al.[28] also deposited Pt using $C_5H_5Pt(CH_3)_3$ and measured the composition to be 21.5% Pt, 73% C, and 5.5% O using Auger electron spectroscopy.

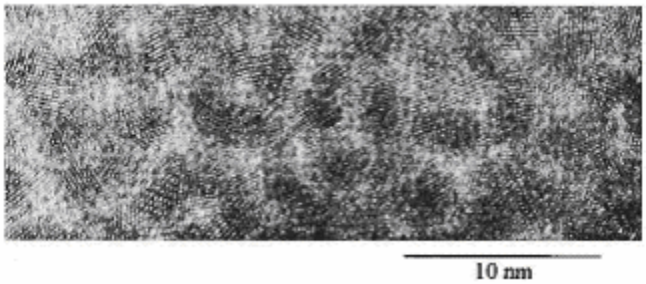

Figure 2-1. 400 kV TEM Image of 2 nm Pt Single Crystals in a Carbon Matrix[27]

Koops et al.[9] determined the composition of W and Au deposited from $W(CO)_6$ and $Me_2Au(tfac)$. For the former, the deposits consisted of up to 75 at.% W. Typical composition values were 55% W, 30% C, and 15% O. For the Au films, typical compositions were 40% Au, 55% C, and 1.5% O. Bauerdick et al.[34] performed energy dispersive x-ray analysis (EDX) on deposits from $W(CO)_6$ and found a W content of about 4%. Hoffmann et al.[15] found that Au depositions from PF_3AuCl resulted in high metal content. Au deposits from Me_2Au-(tfac) were only able to achieve a maximum of 50% Au content. Figure 2-2 shows percolating gold crystals from PF_3AuCl. Matsui and Mori[10] analyzed W (from WCl_6) and Cr (from $Cr(C_6H_6)_2$) with Auger spectroscopy and

found that W deposits were 58% W, 16% Cl, 8%C, and 18%O. Cr deposits were 16% Cr, 62% C, and 22% O.

Folch et al.[35,36] deposited Au from $Au(CH_3)_2$(hexafluoroacetylacetonate) using an ESEM and found that the presence of water vapor or an Ar/O_2 mixture could increase the Au content in the deposit from less than 5% to over 50%. This effect was attributed to the C in the deposits being desorbed in the form of CO or CO_2 molecules as the deposition occurred. Molhave et al.[14] deposited Au fibers from dimethylaceytlacetonate gold(III) and characterized the deposits as having three distinct concentric layers. A core layer consisted of dense gold surrounded by a crust layer consisting of gold nanocrystals embedded in an amorphous carbon matrix. A contamination layer consisting of amorphous carbon and low gold content was observed to surround the crust layer. Kouvetakis et al.[13] deposited high purity gold from $CH_3CH_2AuP(CH_3)_3$ and diffraction patterns indicated polycrystalline gold. Microanalysis did not reveal any C or P impurities. Koops et al.[16] deposited Au from Me_2Au(tfac) and reported Au content varying with deposition temperature, from 40% at 20^{o}C to approximately 90% at 100^{o}C.

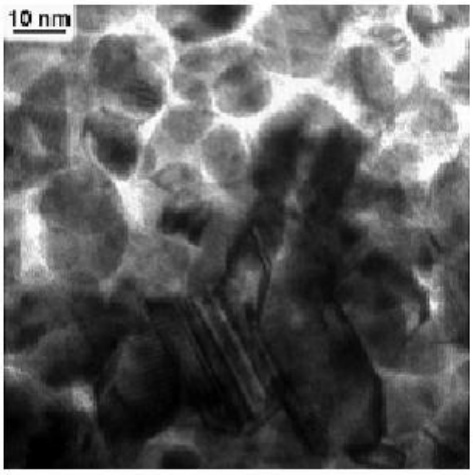

Figure 2-2. Percolating Gold Crystals[15]

Utke et al.[18] deposited Co from cobalt carbonyl and found that increasing the beam current from 20 pA to 3 μA at 25 kV led to an increase in Co content from 12 to 80 at.%. The deposits were characterized as dispersed Co nanocrystals (1-2 nm) in a carbon-rich matrix during initial stages of deposition. In later stages, corrugated and polycrystalline surfaces were observed. Fibers with a smooth surface morphology were found to consist of metal nanocrystals in a carbonaceous matrix. The average Co nanocrystal spacing was calculated to be 0.4-0.8 nm for a 30% Co composition. Cross-sections of the Co fibers were found to contain a dark contrast Co-rich core region surrounded by a lighter contrast carbon-rich material when viewed in TEM bright field. The Co-rich core corresponded roughly to the diameter of the electron beam.

Rhodium deposits from $(PF_3)_4Rh_2Cl_2$ by Hoffmann et al.[15] resulted in compositions of 60% Rh, 16% P, 9% N, 7% Cl, 7% O, and 1%F. Weber et al.[24] deposited Mo fibers from $Mo(CO)_6$, and used EDX to determine the composition of the deposits. It was determined that the Mo content increased from approximately 2% at a beam current of

450 pA to 5% at 1550 pA for a voltage of 20 kV. The maximum Mo content obtained was less than10%, as shown in Figure 2-3.

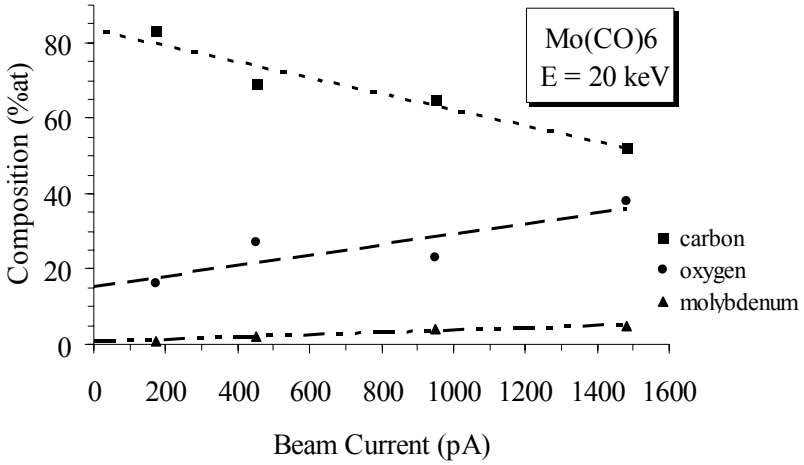

Figure 2-3. Composition of Material Deposited at 20 kV from $Mo(Co)_6$[24]

Akama et al.[38] analyzed the structure and composition of carbon fibers deposited on Si from hydrocarbon contamination. It was concluded from TEM and Auger analysis that the material was amorphous and composed of C and O. Schiffmann[39] deposited fibers from hydrocarbon contamination and performed electron probe microanalysis (EPMA) which showed almost 100% carbon content with only trace amounts of oxygen. Kiyohara et al.[21] deposited diamond film from H_2 and CH_4 and analyzed them with micro-Raman spectroscopy. The spectra indicated diamond, graphite, and amorphous material.

Thompson et al.[31] characterized SiO_2 film deposition as powdery for depositions performed at temperatures less than approximately 150^{o}C and glasslike above this temperature. Perentes et al.[30] deposited SiO_2 from TEOS and performed EDX analysis

and found a Si:C:O ratio of 1:2.88:2.45. TEM analysis showed that the deposits were amorphous. Chin and Ehrlich[32] deposited silicon nitride films and examined them with Auger analysis which indicated no impurities.

As shown from the aforementioned studies, there is a large variation in deposit composition and morphology that is dependent upon the material, the type of precursor used, and the deposition parameters. Deposition from metalorganic precursors typically led to metal nanocrystals in an amorphous carbon matrix.

2.2.3. Electrical Properties

The electrical properties of EBCVD deposits are very important if the deposits are desired for use in micro- or nanoscale electrical devices. In general, deposits have very high resistivity values due to large amounts of impurities, especially carbon. Careful selection of precursor gas and deposition parameters may be able to improve purity and hence conductivity of the deposits.

Koops et al.[9] measured the resistivity of deposited W and Au films. The W deposits had a resistivity that was four orders of magnitude greater than bulk W, and the Au films had a resistivity two orders of magnitude greater than bulk Au. These measured values were attributed to the high carbon content of the films. Komuro and Hiroshima[40] measured the electrical resistivity of W lines deposited for WF_6 and observed a rapid decrease in resistivity with increasing beam dose. They also observed lower resistivities at lower temperatures. Resistivities exhibited a wide range for differing deposition conditions,

from 100 Ωcm to $4x10^{-3}$ Ωcm. Hoffmann et al.[15] determined the resistivity of Au and Rh deposits. They found Au resistivities as low as 22 μΩcm for high purity deposits, which is 10 times the bulk resistivity for Au. Rh resistivity values of 1 Ωcm were measured, which were much larger than the bulk value of 4.5 μΩcm. Koops et al.[27] measured electrical resistivity of Pt arches and bar structures and recorded values of 1 Ωcm. They also noted a decrease in resistivity with increasing Pt content. In a separate study, Koops et al.[16] characterized the electrical properties of deposited Au and Pt resistors. I-V curves and resistance were measured from room temperature up to 180°C. Annealing at 180°C reduced the resistivity by two to three orders of magnitude and stabilized the resistors. For Au, the conductivity was better than 10^{-4} Ωcm. Poole-Frenkel plots indicated that field electron emission and hopping of electrons were the primary conduction mechanisms. Increasing Au content (corresponding to increased deposition temperature) resulted in a decrease in resistance. This was attributed to the reduced C content allowing the Au nanocrystals to be closer to each other, raising the probability for tunneling of electrons. Takai et al.[28] measured the resistivity of Pt deposited from $C_5H_5Pt(CH_3)_3$ and reported a value of 30 μΩcm, which is three times higher than the value for bulk Pt.

Kunz and Mayer[37] measured the electrical resistivity for Fe and Cr films and found that for both materials the film resistivities were 6 to 12 times higher than bulk values for the pure materials. Depositing the Cr film at higher temperatures led to a decrease in resistivity. Rangelow et al.[41] deposited Pt for a thermal nanoprobe and reported a resistivity of 900 Ωcm. This high value was attributed to carbon contamination. Utke et

al.[18] tested the electrical resistivity of Co deposits and found values that were 10^4 greater than those for pure Co.

2.2.4. Mechanical Properties

The mechanical properties of EBCVD deposits are important if complex structures are to be made. To date there have been limited studies on the mechanical properties of metal deposits. Carbon fibers deposited from hydrocarbon contamination have been studied and are summarized here.

Akama et al.[38] deposited carbon fibers on STM tips and detected no traces of vibration when using the tips for measurements, indicating sufficient mechanical stiffness of the EBCVD fiber for this process. Bøggild et al.[42] tested the mechanical properties of fibrous carbon structures by applying an increasing load until breaking of the fibers was achieved. They determined the critical load to be 10^{-5} N. The tips, which were less than 3.5 μm in length and less than 200 nm in diameter, were able to sustain deflections greater than 1 μm. It was concluded that the material composing the tips was substantially stronger than the SiO_2 that was used for the cantilevers. Hoffmann et al.[43] measured the modulus of elasticity for carbon deposited from hydrocarbon contamination and found a very high value of 0.4 TPa. While testing has been very limited thus far, it appears that carbon deposits possess good mechanical properties which could be of use for more complex nanoscale structures.

2.2.5. Adherence

Adherence to the substrate is an important property for deposits, but to date there has been little in the way of quantitative adherence studies. There have not been any reported instances of poor adherence. Thompson et al.[31] measured adherence values for deposited SiO_2 films and found values greater than 10^9 dynes/cm^2, indicating good adherence.

2.3. Deposition Mechanisms and Process Modeling

Models of the EBCVD process can facilitate understanding of the process parameters that dictate deposit growth rate, geometry, and properties. Hoffmann et al.[43] point out that the study of the deposition process is hindered by the small quantity of material involved and its complexity since surface catalyzed reactions, rearrangements, and polymerization reactions are likely involved. Early models focused primarily on basic deposition principles, while recent models have become more complex, using Monte Carlo simulations for electron scattering to attempt to correlate observed structures to a predicted model. The knowledge of molecular excitation and fragmentation resulting in deposition is in its infancy. Thermal effects have also been investigated. Process monitoring and control is in its early stages, and there have been some recent attempts to improve in this area. The process can be thought of as a localized CVD process, in that growth rate can be limited by mass transport of reagent or reaction rate. As with Laser CVD,[1] the rate limiting step may vary from the periphery to the center of the deposit. The consumption of reagent at the periphery makes it more likely that the rate limiting step at the center of the deposit is mass transport. This is further encouraged by the fact that the current density is highest at the center of the deposit.

In general, the deposition rate can be modeled by Equation 2-1,[19]

$$R(x) = \int_0^{E_0} f(x,E)\sigma_{diss}(E)N\mathrm{d}E \tag{2-1}$$

where *f(x,E)* is the flux of electrons (primary and secondary), $\sigma_{diss}(E)$ is the electron-induced dissociation cross-section, and *N* is the surface density of adsorbed molecules. This illustrates the importance of current density (electron flux) and precursor supply. The dissociation cross-section is specific to certain molecules, and is dependent upon the electron energy Cross sections typically peak at low energies (~100eV). Values are known only for a limited number of precursors and are in the range of 10^{-16} to 10^{-17} cm^2.[43] Figure 2-4 illustrates the probability of dissociative excitation p_{diss} for carbon monoxide which is obtained by multiplying the secondary electron spectrum N_{SE} with the dissociation cross section σ_{diss} of CO. As shown the dissociation cross section peaks at low energies.

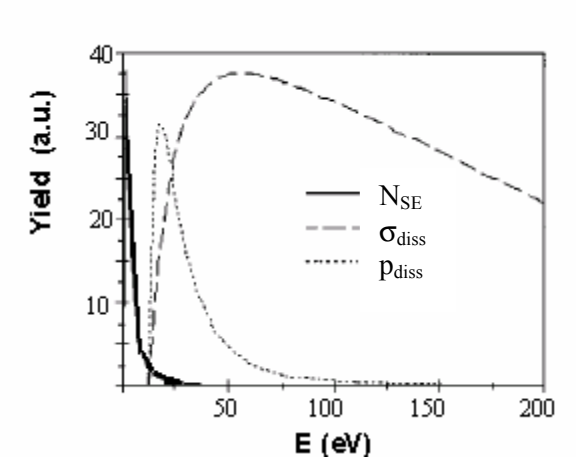

Figure 2-4. Probability of Dissociative Excitation p_{diss}, Dissociation Cross Section σ_{diss}, and Secondary Electron Spectrum N_{SE} for Carbon Monoxide[27]

2.3.1. Theoretical Deposition Models

Kunz and Mayer[19] modeled the formation of a nucleated layer occurring by electron-impact dissociation of adsorbed molecules in or near the vicinity of the surface as given in Equation 1. It was determined that since dissociation cross sections typically have maxima at less than 100 eV, impingement of a high energy electron beam in the kV range would lead to a flux contribution consisting primarily of secondary electrons. Secondary electrons are electrons of lower kinetic energy that are created in the substrate (or deposit) by the primary electrons. In other words, the secondary electrons are often responsible for the majority of the dissociation of adsorbed reagent molecules. A Monte Carlo model for scattering of low-energy primary electrons was also developed, and it indicated lateral spreading of backscattered electrons with increasing energy. This spreading, however, was relatively small (on the order of 40 nm for an increase from 250 to 2000 eV). Takai et al.[28] compared the secondary electron yield from Si with the deposition rate using $C_5H_5Pt(CH_3)_3$ as functions of the beam energy and found corresponding behaviors. As shown in Figure 2-5, as the secondary electron yield from

the Si decreases with increased beam energy, the volumetric deposition rate decreases in a similar fashion. The secondary electron yield at the surface decreases with increasing beam energy because they are created deeper within the substrate at higher voltages. This further illustrates the influence of secondary electrons on the deposition process.

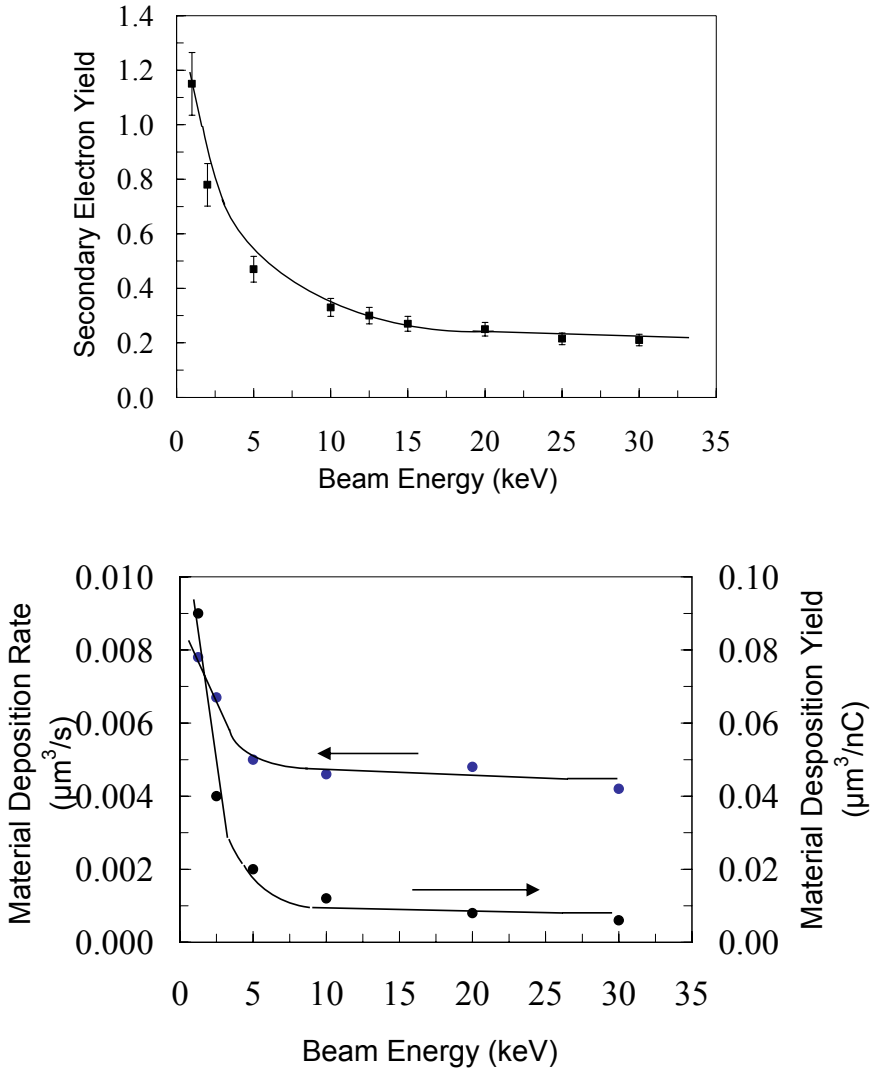

Figure 2-5. Secondary Electron Yield from (100) Si (Top) and Material Deposition Rate (Bottom) in $C_5H_5Pt(CH_3)_3$ as a Function of Electron Beam Energy[28]

Scheuer et al.[8] modeled the adsorption rate for the EBCVD process with terms to account for adsorption at the surface, reevaporation, and dissociation. The density of adsorbed

molecules on the substrate surface was assumed to vary with time by factoring in the mean lifetime of an adsorbed molecule. The growth rate for a deposited layer was modeled as a function of volume per dissociated molecule, dissociation cross-section, density of adsorbed molecules, and electron flux. The total number of electrons required to incorporate a molecule into the deposited layer was also calculated. This value was then used to determine the cross-section for layer deposition, and it was found to equal the total inelastic electron scattering cross-section. From this result it was concluded that the deposition process was not enhanced by any chemical reaction.

Koops et al.[9] modeled the physics of material supply and deposition for EBCVD in the manner originally described in Scheuer et al.[8] The authors' analysis of the model showed that increasing either the electron or the molecule flux to infinity while keeping the other constant increased the growth rate by a factor of 2. Decreasing either of these quantities by a factor of 10 led to a reduction in growth rate by a factor of 5. Hoffmann et al.[41] modeled the adsorption rate for precursor molecules as a function of the sticking coefficient, precursor flux, monolayer density, mean dwell time, dissociation cross-section, diffusion coefficient, and the electron flux. This was a modified form of the adsorption rate used by Koops et al.[9] Solving for equilibrium conditions (and neglecting diffusion) gave a constant growth rate, but it was noted that experimentally observed growth rates decrease with time. The observed results were attributed to an increasing adsorbate molecule diffusion path with time, meaning the reagent molecules diffusing from the original substrate to the top of the deposit have a longer surface diffusion path as the deposit size increases.

Ishibashi et al.[11] modeled the growth rate as a function of the number of activated gas molecules per primary electron, the effective radius of the gas molecule, and the collision rate of the gas atoms with the primary electron beam. Calculated growth rates using this model were seven orders of magnitude less than observed rates. This discrepancy was attributed to several assumptions used to generate the model, including elastic collisions at the substrate surface. Attempts to make adjustments to the model were only able to provide a precision of 2-3 orders of magnitude.

Silvis-Cividjian et al.[44] constructed a detailed model for the role of secondary electrons in EBCVD spatial resolution. The model was developed for the deposition of a fiber from a stationary electron beam. During growth, the diameter of the deposited conical fiber increases rapidly initially, eventually reaching a saturation value that exceeds the diameter of the electron beam. This behavior was modeled in several steps. The secondary electrons generated by the impinging beam form an area larger than the beam diameter, and these electrons dissociate adsorbed molecules, leading to the rapid initial growth. As the conical structure grows, secondary electron emission in the growing fiber becomes more prominent and secondary electron emission from the substrate becomes less prominent. This was modeled as the cause of lateral widening, with saturation occurring when the secondary electrons can no longer exit the side of the structure. A Monte Carlo simulation was developed which took into account secondary electrons emitted from the fiber. The growth rate for this model was a function of electron flux, electron-induced dissociation cross-section, and surface density of adsorbed precursor

molecules (similar to Eq.1). The simulation was in good agreement with experimental observations. Figure 2-6 shows fiber deposition with increasing time as generated from the Monte Carlo simulation.

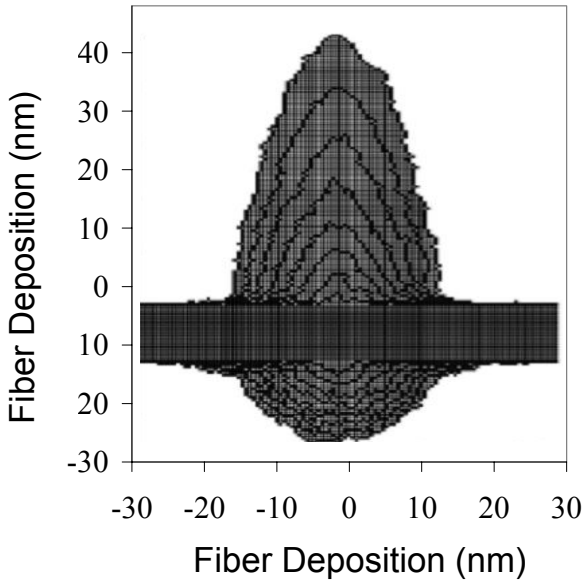

Figure 2-6. Fiber Deposition Profile with Time[44]

Kunz and Mayer[19] also made a qualitative comparison between thermally activated and electron beam stimulated nucleation. The limiting growth rate for a fully covered surface was modeled. It was found that for a specified electron flux, the limiting growth rate ensued much earlier in the presence of the electron beam than for thermally activated nucleation. It was also predicted that the initial nucleation stage for film deposition under electron beam irradiation had a time to the fourth power dependence. This agreed with experimental observations of deposited mass versus time.

2.3.2. Process Monitoring/Control

Bauerdick et al.[34] performed in situ monitoring of EBCVD using an atomic force microscope (AFM) in an SEM. A piezoresistive AFM cantilever and a micromanipulator were integrated with the SEM, and patterned tungsten lines were used to test the system. The in situ AFM allowed precise determination of topography and lateral dimensions without having to remove the sample from the SEM.

Bret et al.[20] were able to accomplish some measure of in situ control for the EBCVD process. A picoamperemeter was used to monitor the electron current flowing through the sample. At all new deposition sites, a substrate current was detected. It was observed that this current reproducibly dropped to a plateau value during deposition of a fiber structure. This drop in detected current was presumably due to electron scattering in the growing fiber. The characteristic plateau value corresponded to the completion of the formation of the conical structure of the fiber. At this point, the saturation diameter for the structure was reached and the fiber growth was cylindrical from then on. It was observed that fibers with larger diameters resulted in larger current drops. Monte Carlo simulations were performed for various stages of fiber growth. The simulated currents were modeled as a fraction of the primary electron current by factoring in backscattered and emitted secondary electrons. Simulated results for the plateau current were in very good agreement with measured values.

2.3.3. Thermal Effects

Utke et al.[18] studied the thermal effects of EBCVD for Co fibers. They calculated the local temperature rise at the apex of a cylindrical fiber tip using adjustments to the formula given originally by Reimer.[45] This rise was dependent upon the current, accelerating voltage, backscatter yield, thermal conductivity, and length and diameter of the tip. The formula was adjusted for small diameters, and it was concluded that beam power and tip length were determining factors for temperature rise in this range. Increasing current and tip length led to increasing decomposition by thermal methods, as these parameters correspond to a larger temperature rise. Higher purity deposits were also predicted for deposits on substrates with low thermal conductivity.

2.4. Shapes and Structures

The basic shapes formed through the EBCVD process are lines, fibers/dots, and films. Lines are deposited by using a line scan mode, and with today's process capabilities it is possible to produce deposits that are very linear and have excellent uniformity in width and height. Fiber/dot deposition is characterized by the initial deposition of a conical tip structure, which widens until it reaches a saturation diameter (corresponding to the range at which secondary electrons cannot exit the sidewall of the structure). At this point, the fiber grows with an essentially constant diameter as a cylindrical structure with a conical top. Film deposition can be accomplished by using the frame scan mode, during which the beam scans repeatedly over a specific area. Film deposition can also be achieved by using an unfocused electron beam, and this is typically done at low accelerating voltages (~100 eV).

2.4.1. Deposition Parameters

Important deposition parameters for the EBCVD process include the electron beam current, voltage, scan rate, and the precursor pressure. The scan rate of the beam is defined by the dwell time and loop time. The dwell time for the beam refers to the time that the beam spends on a specific pixel when in a scanning mode, and the loop time refers to the amount of time required to return to that pixel. General trends that have been observed are that increasing beam current leads to increasing growth rate (in the reaction rate limited regime), and that increasing voltage leads to an increase in deposit size. Specific observations for various materials are detailed here.

Schiffmann[39] investigated deposition parameters for carbon tips, i.e., fibers. It was observed that increasing deposition time led to an increase in fiber length and an increase in diameter to a saturation value. Increasing beam current led to a general decrease in fiber length. This was attributed to a possible temperature increase at higher current that reduced the adsorbate lifetimes on the substrate. Figure 2-7 shows plots of these characteristics. Increasing accelerating voltage led to a general increase in fiber length, while increasing working distance led to a general decrease in fiber length. Miura et al.[17] studied carbon deposition parameters and also found that increasing beam current led to decreasing deposit height. This was also attributed to increasing current leading to local heating and re-evaporation of the deposited carbon. Hoffmann et al.[43] also investigated deposition parameters for contamination deposition of carbon. They noted a decrease in growth rate with increasing time and increasing current, which was attributed

to surface diffusion limitation. The effect of increasing current was attributed to the corresponding increase in beam size, for which precursor molecules were decomposed on their way to the center of the beam. Decrease of the growth rate was attributed to lateral deposition, which reduces the amount of precursor reaching the center of the electron beam. Wendel et al.[46] also noted a higher deposition rate at lower beam currents (in the 20 pA range) for carbon fibers.

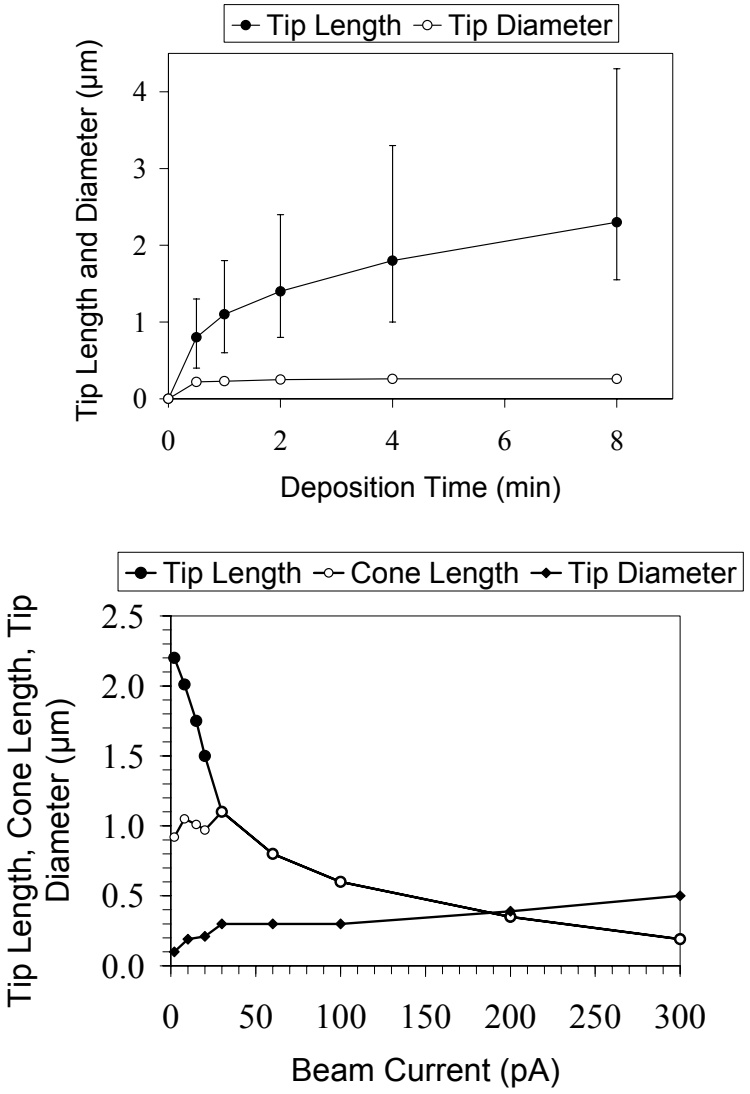

Figure 2-7. Tip Growth vs. Time (Top) and Beam Current (Bottom)[39]

Utke et al.[18] investigated deposition parameters for Co. Increasing beam current and diameter led to an increase in the diameter of the structure and an increase in the initial growth rate for various depositions. It was noted that the apex diameter of a fiber became larger than the beam diameter for currents above 10 nA, and this effect was attributed to an additional thermal decomposition mechanism due to localized heating from the electron beam. It is worth noting that an increase in beam current led to an increase in deposit purity. Perentes et al.[30] studied SiO_2 deposition parameters and found an increase in growth rate with beam current that followed a 0.25 power law relation. They also observed that the saturation diameter of a fibrous deposit increased with increasing current. In summary, it appears that increasing the beam current can either increase or decrease the growth rate depending on the current range and perhaps current flux.

Hoffmann et al.[15] studied deposition parameters for Au and Rh. Higher (25 kV) and lower (3 kV) accelerating voltages were studied for Au line deposition. It was noted that an area of sparser Au grains were deposited surrounding the line deposit up to several microns away from the incident beam. This was correlated to be roughly equivalent to the Bethe range (the average distance traveled by an electron within a specimen) for the emitted secondary electrons. A lower voltage corresponds to a smaller Bethe range, so at lower accelerating voltages, the size of the area of gold grains deposited away from the incident beam was smaller. Bauerdick et al.[34] studied deposition parameters for WC. It was noted that both dot size and deposition rate decreased strongly in a similar fashion with increasing acceleration voltage. The effect of exposure dose variation was studied by decreasing the loop time for a constant dwell time and constant voltage. The observed

trend was that feature size decreased with decreasing dose, while the deposition rate decreased slightly with increasing dose.

Kunz and Mayer[19] studied parameters for low energy deposition of Fe. They observed an increase in deposition rate when the electron beam was tilted 60^{o} to normal from the values observed for deposition with the beam normal to the substrate. This increase was attributed to an observed twofold increase in secondary electron emission for the tilted beam. The observed growth rate was found to decrease with increasing beam energy (for a range of 100 to 1500 eV). Deposition at low energy (250 eV) was studied due to the peak secondary electron emission that occurs near this value. An anomalously high deposition yield was found to occur for this value, and this was attributed to the high secondary electron yield and/or high dissociation cross sections (which peak near 100 to 150 eV) for this process.

Kohlmann-von Platen et al.[47] studied the effects of dwell and loop times on deposition yield. It was observed that holding the loop time constant and increasing the dwell time led to a trend of decreasing deposition yield due to progressing consumption of the adsorbate layer. Holding the dwell time constant and increasing the loop time led to an increase in deposition yield to a saturation level due to a longer time for replenishment of the adsorbate layer. These effects are illustrated in Figure 2-8. The saturation was attributed to the time necessary for a complete monolayer of adsorbate molecules to form. Increasing the current density of the beam was also found to lead to increasing growth rate, with higher rates being achieved for higher reagent gas flux.

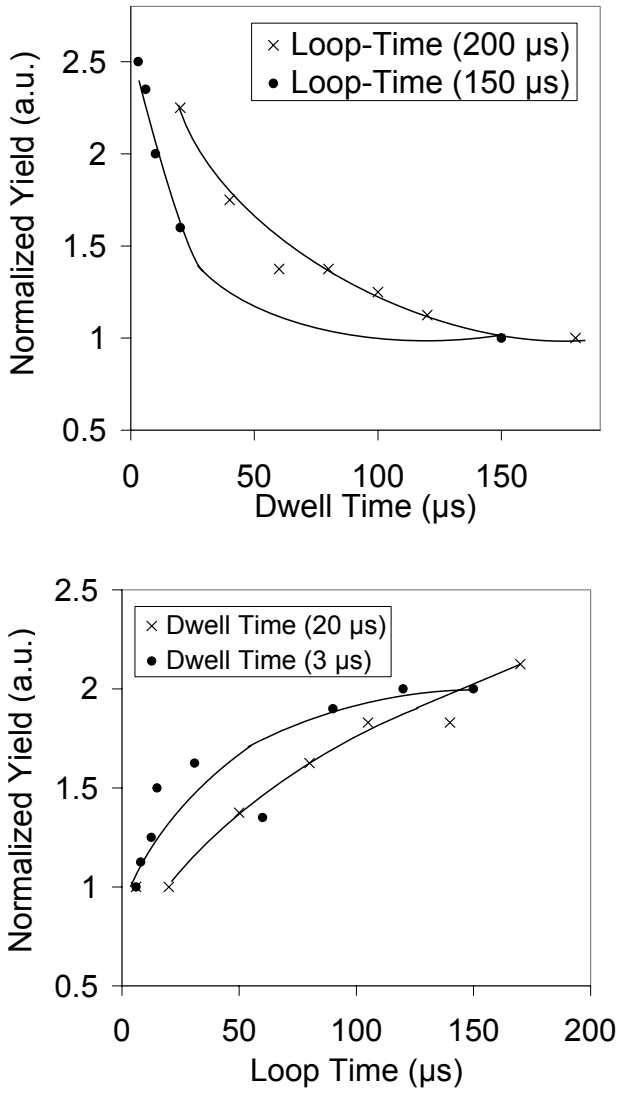

Figure 2-8. Normalized Deposition Yield vs. Variation of Dwell Time (Top) and Variation of Loop Time (Bottom)[47]

Liu et al.[48] studied the effects of focus change on W line deposition. By controlling the focus, dense and dilute line deposits were achieved. Self-supporting lines (grown out of the substrate) were also investigated. It was observed that overfocusing kept the upward features with a dense deposit, while underfocusing did the same for the downward features. Upward and downward refer to the direction with relation the surface plane of the substrate. The effects of beam scan speed were also investigated. The dark field

outlines of line deposits are shown in Figure 2-9, with scan speed ranging from 4 nm/s (top line) to 12 nm/s (bottom line). The effects of scan are further illustrated in Figure 2-10, in which line width is plotted as a function of beam scan speed for a scan speed range of 1-48 nm/s. As shown, the line width decreases sharply with increasing scan speed until it reaches a minimal saturation value of approximately 7 nm.

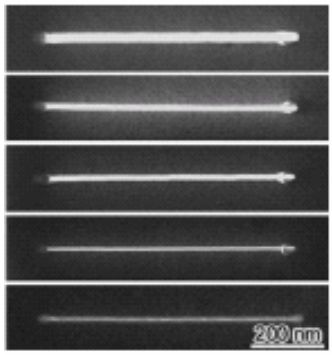

Figure 2-9. Dark Field Images of Deposited Tungsten Lines[48]

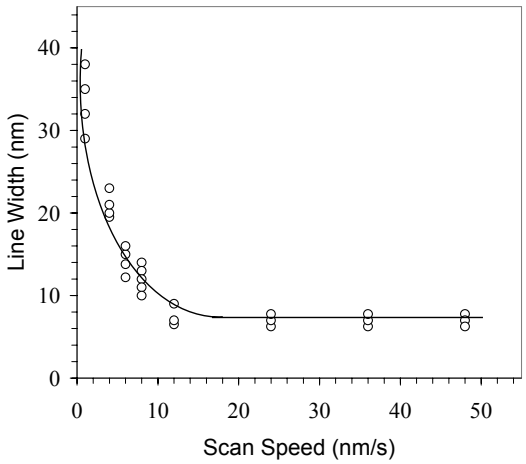

Figure 2-10. Line Width of Tungsten Line Deposits vs. Beam Scan Speed[48]

There have been limited studies of the effects of temperature on EBCVD. Ishibashi et al.[11] studied temperature dependence of the growth rate for EBCVD of Al deposits on an independently heated substrate. It was found that an increase in temperature led to a

decrease in growth rate. This was attributed to weaker adsorption of molecules to the substrate surface at higher temperatures. Koops et al.[16] also noted this behavior for Au deposits.

2.5. Applications

Several complex structures have been fabricated using the EBCVD process. These include mechanical, electrical, and optical structures, illustrating the flexibility of the process. The ability to precisely control the scanning of the electron beam allows for good uniformity in deposited structures, which is an important characteristic for reproducible feature production.

Kohlmann-von Platen et al.[47] demonstrated the ability to deposit W lines using EBCVD to produced an etch mask, but noted residue deposited in the vicinity of the electron beam pattern. W deposition was also used to successfully repair x-ray and open stencil masks with high resolution. Wendel et al.[46] demonstrated the ability to deposit arrays of carbon fibers and to use these fibers to pattern holes in photoresist through an AFM lithography technique. Hübner et al.[49] demonstrated the feasibility of incorporating a four-channel gas feeding system into a commercial electron beam lithography system and deposited Pt dots, fibers, and line structures by depositing dots in very close proximity to one another.

Perentes et al.[30] fabricated a two-dimensional photonic band gap structure through deposition using a TEOS ($SiO_4C_8H_{20}$) precursor. The structure consisted of a 2D hexagonal lattice with its central pillar missing. The goal was to create a micro-cavity on

the surface of an SiO_2 prism in order to create a focused low volume point light source when excited by total internal reflection. A micrograph of the structure is shown in Figure 2-11.

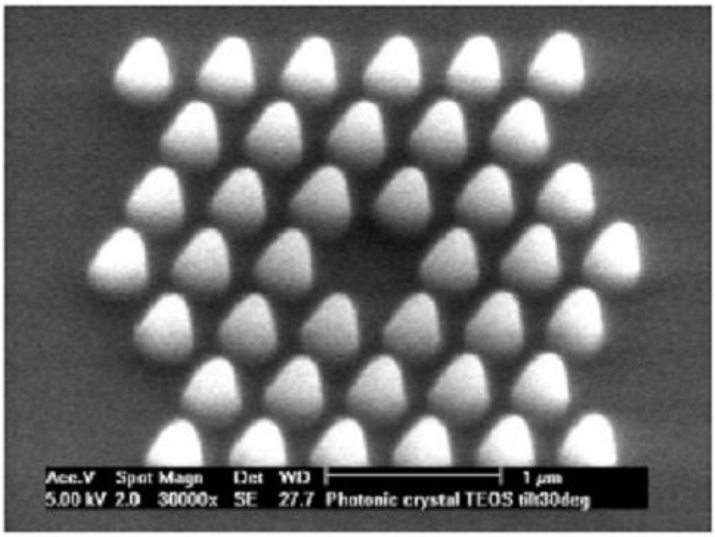

Figure 2-11. PBG Structure with Hexagonal Lattice and Microcavity[30]

Rangelow et al.[41] fabricated a thermal nanoprobe which involved the deposition of a Pt filament. The filament was integrated into a piezoresistive cantilever structure that was fabricated separately. The filament consisted of angular deposits of two platinum fibers that were grown until they were joined. After this, a shorter 70 nm diameter fiber was grown vertically from the junction of the two original fibers in order to increase sensitivity. Upon testing the probe exhibited a strong linear relationship between temperature and resistance change. A micrograph of the thermal nanoprobe is shown in Figure 2-12.

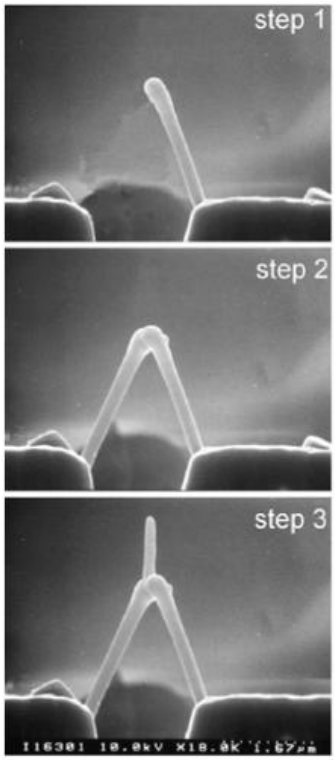

Figure 2-12. Deposition of Platinum Thermal Nanoprobe[41]

Komuro and Hiroshima[40] fabricated a single electron transistor structure by deposition of W. The structure was produced by depositing a line and connecting it to several deposited dots of various pitches, and a gate electrode was located 300 nm from the dot region. The current-voltage characteristics between the source and drain for a 7 dot structure with 10 nm pitch was measured and it was found that Couloumb block characteristics were exhibited at 12 K. It was speculated that the boundary between adjacent dots might be semi-insulating, leading to a leaky drain-source current. Miura et al.[17] fabricated a metal-insulator-metal (MIM) diode through carbon film deposition onto Au electrodes. The current-voltage characteristics of this structure were measured and the carbon film was found to function as an insulator for low biases. For higher biases, the current began to flow through the film, and this was attributed to thermionic emission and/or tunneling.

Floreani et al.[25] fabricated field electron emitters by deposition of Pt and Au. The emitters were able to reach high emission currents (~2 μA) at relatively low voltages. Koops et al.[16] examined field emission from deposited fibers and also noted high emission currents at low extraction voltages. Takai et al.[28] fabricated a field emitter array using FIB and EBCVD techniques. FIB etching was used to create a gate opening, and EBCVD was used to deposit a Pt cathode. Testing of the array indicated emission began at less than 80 V. I-V characteristics of the array showed a leakage current between the cathode tip and the gate. This was attributed to contamination of Ga atoms (from the FIB process) to the insulating sidewall.

Akama et al.[38] fabricated modified STM tips by depositing vertical fibers at the tips of existing STM tips. The deposited tips were approximately 100 nm in diameter, and they proved to be beneficial for topographical measurements of surfaces with narrow or deep grooves or holes. Schiffmann[39] deposited carbon tips for use in atomic force microscopy. AFM imaging showed that the deposited tips provided improved resolution for structures with steep topography. Utke et al.[18] deposited magnetic tips onto commercial pyramidal Si scanning microscopy tips and determined that magnetic resolution scaled linearly with tip apex diameter and allowed high resolution (~50 nm). A micrograph of the STM tip and resulting resolution enhancements are shown in Figure 2-13.

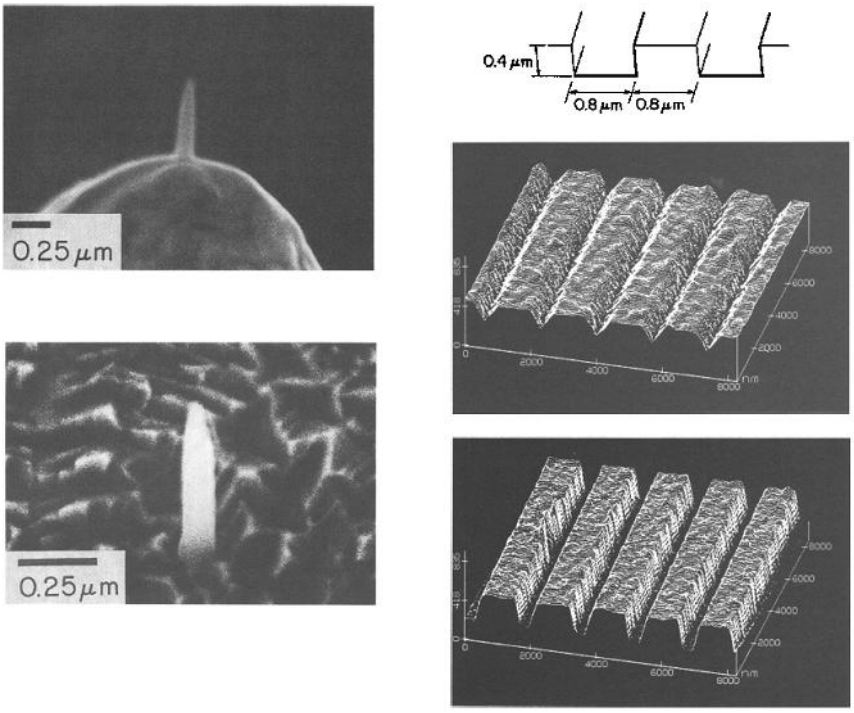

Figure 2-13. Carbon Fiber Deposited on STM Tip and Resulting Improvement in Resolution[38]

Bøggild et al.[50] fabricated nanotweezers out of hydrocarbon contamination onto silicon oxide cantilevers that were covered with a thin metal layer so that they could serve as electrodes. Four cantilevers were used, and applying a voltage to the outer electrodes with respect to the inner two electrodes allowed the gap between them to be opened and closed. The carbon deposit served as the tips structure for the tweezers, and gaps between the tweezers as small as 25 nm were achieved. A micrograph of the nanotweezer structure is shown in Figure 2-14. Ooi et al.[51] constructed hooked carbon nanoprobes for the purpose of handling DNA fibers. DNA fibers were extracted from rice nuclei and from human chromosomes using this probe.

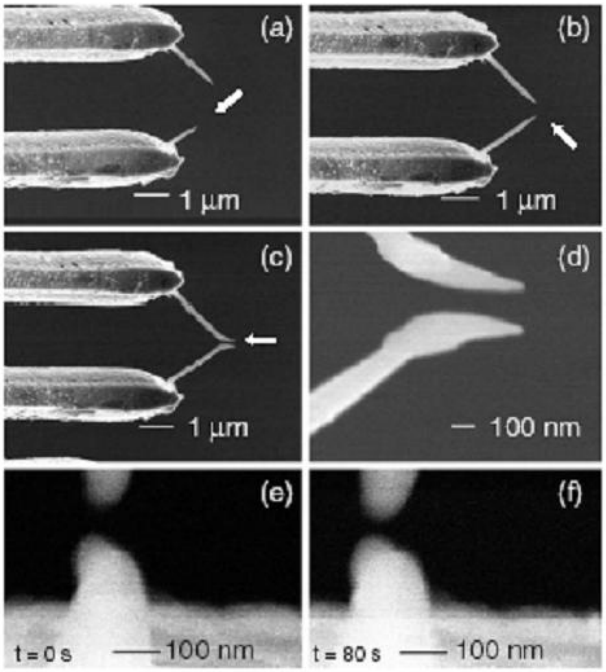

Figure 2-14. Nanotweezers Fabricated from Carbon Deposition[50]

CHAPTER III

EXPERIMENTAL APPARATUS AND PROCEDURE

3.1. EBCVD System

The EBCVD system at Georgia Tech consists of a modified FEI Quanta 200 Environmental Scanning Electron Microscope (ESEM). The system was installed in May 2004. The modifications to the system include a gas injection system for Pt and the use of the auxiliary port to fill the chamber with reagent gas when in the Environmental mode. Figure 3-1 shows a diagram of the modified SEM system found at Georgia Tech, and photographs of the microscope and gas injection needle are shown in Figure 3-2.

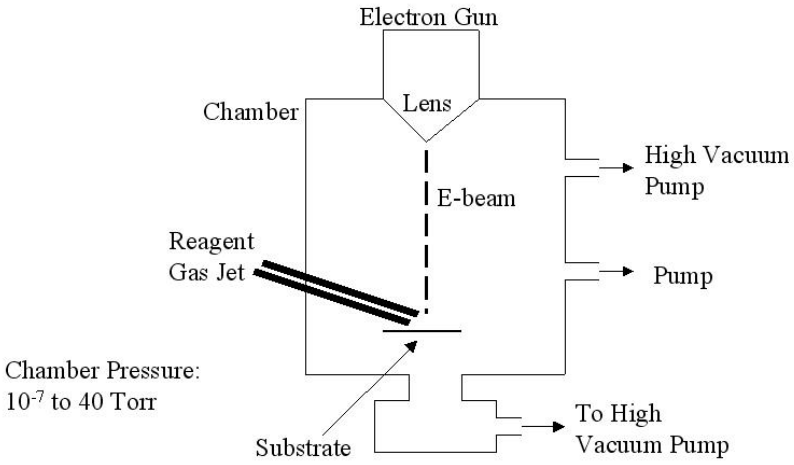

Figure 3-1. EBCVD System with Gas Jet

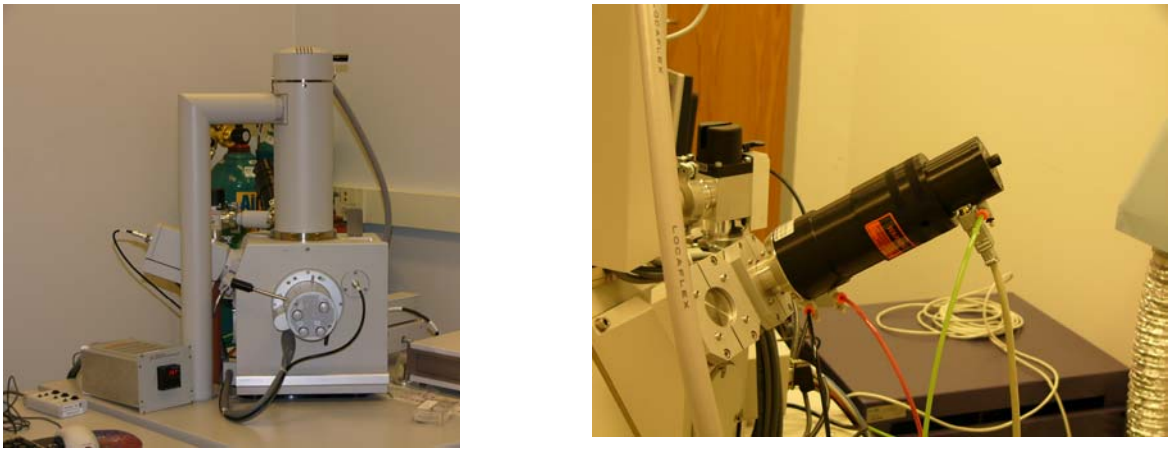

(a) (b)

Figure 3-2. (a) Modified ESEM used for EBCVD (b) Close-up View of Gas Injection System

The microscope features software control with settings pertaining to chamber pressure and various settings for the electron beam. The scan modes for the beam are spot (in which the electron beam stays in a fixed location), line (in which the beam scans back and forth continuously over the same set of pixels), and full frame (in which the beam scans a set of pixels in the x-direction and then moves in the y-direction and scans a different set of pixels). The vacuum modes for the microscope are High Vacuum, Low Vacuum, and Environmental. High Vacuum mode is used for standard imaging, and can reach pressures on the order of 10^{-7} Torr. The Low Vacuum mode is for pressures ranging from 0.1 to 1.0 Torr, and the Environmental mode features chamber pressures that can be adjusted form 0.1 to 40 Torr. When operating in the Environmental mode, the Environmental Backing Valve (EBV) must be opened. Opening the EBV opens the chamber to the rotary vacuum pump, drawing gas off before it reaches the second pressure-limiting aperture (PLA) and enters the column. The stage on which the sample sits in the microscope chamber features controls for the x, y, and z directions as well as

rotational and tilt controls. The tilt control allows the specimen stage to be tilted over a range of -15^{o} to 75^{o}.

Control of the microscope is accomplished through the used of software provided by the manufacturer. The software allows the user to select which vacuum mode to operate in and to turn the electron beam on and off. It also allows the user to select magnification, set working distance, and move the sample relative to the beam. There are currently no automated controls for controlling the electron beam or the sample. The primary electron beam parameters are the voltage (values range from 0.2 to 30 kV) and the spot size (values are on an arbitrary scale from 1.0 to 8.0). The spot size encompasses both the physical diameter of the electron beam as well as the beam current, and both of these values increase with increasing spot size. The magnification values for the microscope range from 40x up to 300,000x. Typical magnification values for deposition were 4,000x to 10,000x for fiber deposition and 15,000x to 40,000x for line deposition. The magnification is a more important factor for line deposition because it determines the length of the line to be deposited. Higher magnifications are necessary to be deposit thicker lines in a shorter amount of time since they correspond to a shorter line length.

Image analysis and measurements were performed using the XT-DOCU software program. When images are saved in the proper format (TIFF-16), the program can measure distances with resolutions as small as 2 nm, depending upon magnification. The software also features a zoom feature which allow the user to more accurately take measurements. The resolution for each measurement thus stems from the magnification

at which the image was taken. For the purposes of this research, the resolution was taken to be the distance corresponding to the distance across a single pixel.

The FEI gas injection system (GIS) consists of a 0.5 mm inner diameter needle that inserts and retracts pneumatically along with a heating system. The reagent gas is generated from a Pt containing chemical paste that is located in a crucible integrated into the base of the needle of the GIS. The heating system is a Micro-Infinity temperature controller that heats the Pt containing paste to 40^{o}C. The Pt compound is $(CH_3)_3Pt(CpCH_3)$, with a melting point of 30^{o}C. The needle insertion point is set to 9.9 mm vertically from the point where the electron beam exits the final aperture from the column. This distance was chosen so that the surface of the sample could be set to approximately 0.1 mm away from the end of the needle when operating at a working distance of 10.0 mm. Once the Pt compound is heated and the needle is inserted, a valve is manually opened to allow the flow of a localized stream of gas. When using the GIS, it is possible to stay in High Vacuum mode, meaning the pressure in the chamber is still on the order of 10^{-6} Torr. This allows for better imaging capabilities and ensures that the beam can be tightly focused.

The auxiliary gas port was used while the SEM was in the Environmental mode to flow a pre-mixed 90% Ar, 10% CH_4 gas into the chamber. A low flow pressure regulator, rated from 0.2 to 2.0 psig (10.3 to 103.4 Torr) was connected to the gas cylinder to regulate the flow to the microscope. Low flow is required by the metering valve used by the microscope to stabilize chamber pressure while in the Environmental mode.

The SEM is used in the High Vacuum mode to image the samples after they are deposited, with overhead and profile views taken for each sample. Accompanying software allows measurements to be taken from features captured in the micrographs, allowing dimensions to be determined for the deposits. The microstructure and composition of the deposits were investigated using a Transmission Electron Microscope (TEM) under the supervision of Dr. Z. L. Wang.

3.2. Design of Experiments

The design of experiments consisted of a two level three factor (2^3 factorial) design and a 2^3 central composite design with star points for both lines and fibers. The factors that were investigated for Pt fibers were voltage, beam current, and deposition time, and for C fibers the factors were voltage, beam current, and chamber pressure. The factors that were investigated for Pt and C lines were voltage, beam current, and dwell time. The response variable of primary interest was the deposition rate. The central composite designs allowed estimation of any interaction between variables.

3.3. Spot Size Equivalency

The spot size is defined in the software interface on an arbitrary scale from 1.0 to 8.0, with each value corresponding to a specific beam diameter and beam current. Data for these quantities were obtained from the manufacturer. Listed in Table 3-1 are typical beam current values at various spot sizes and voltages. As shown in the table, the beam current values increase exponentially with increasing spot size. From the given data, least squares fit lines were constructed in order to interpolate in between integer values

for spot sizes. The fit lines were exponential, with correlation coefficients exceeding 99.9%. Figure 3-3 shows the beam currents plotted on a logarithmic scale for selected voltages to illustrate this relationship. Listed in Table 3-2 are beam diameters corresponding to various spot sizes and voltages. The beam diameter values decrease in an exponential fashion with increasing voltage.

Table 3-1. Typical Beam Current Values at Various Voltages and Spot Sizes

	Beam Current (pA) for Indicated Spot Size							
High Voltage	**1**	**2**	**3**	**4**	**5**	**6**	**7**	**8**
30 kV	6.3	24	100	390	1500	5400	20000	74000
25 kV	6.1	23.4	89	339	1290	4900	18700	71000
20 kV	5.6	20.5	86	330	1200	4400	16000	65000
15 kV	5.1	19	71	270	1000	3750	14000	53000
10 kV	4.2	16.4	63	240	890	3200	11000	41000
5 kV	3.2	12.6	47	180	650	2200	7900	27000
2 kV	3.9	15	56	210	740	2500	8400	27000
1 kV	3.9	14.7	54	200	720	2400	7700	23000
0.5 kV	2.2	8.2	30	110	350	1100	3300	9600
0.2 kV		1.7	6.7	20	68	200		

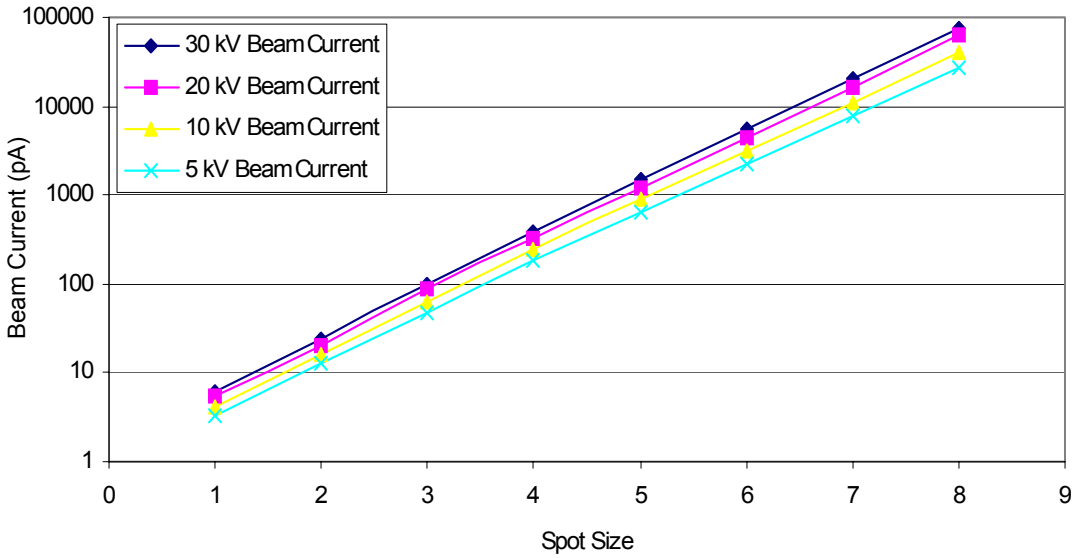

Figure 3-3. Beam Current vs. Spot Size for Selected Voltages

Table 3-2. Beam Diameter (nm) at Various Voltages at a Working Distance of 10 mm

Spot Size	30 kV	5 kV	2kV	1kV
1	10	24	40	61
2	19	48	77	110
3	40	97	160	220
4	82	200	320	450
5	170	430	670	940
6	370	900	1400	2000
7	810	2000	3100	4400
8	1900	4500	7200	10000

The current densities were calculated for various voltages to determine if comparison of this quantity was possible for a wide range of voltages. As shown in Figure 3-4, the current density increases significantly with increasing voltage. This makes it very difficult to factor in the current density as an experimental variable in a factorial design, because it greatly limits the range of voltages and spot sizes that could be used.

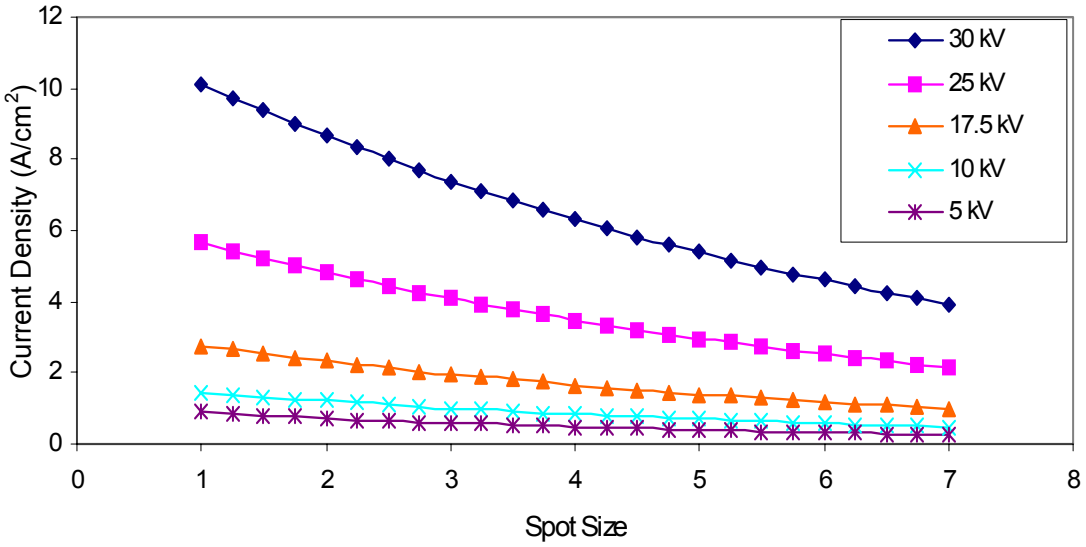

Figure 3-4. Current Density vs. Spot Size for Selected Voltages

3.4. Hypotheses on Factor Effects

3.4.1. Beam Current

The beam current should significantly influence deposition, as it indicates the number of electrons that are directed at the sample. This should affect the rate at which the adsorbed molecules are decomposed and thus the volumetric growth rate of the deposits. A larger beam current would mean that more electrons are available to initiate the dissociation of the adsorbed reagent molecules.

3.4.2. Voltage

The voltage of the beam indicates the energy with which the electrons from the beam strike the substrate surface. Higher energy primary electrons could in theory lead to a larger scattering range for the resulting secondary electrons. This could limit the minimum deposit size achievable. An increase in voltage also correlates to an increase in current density. The effects of current density are thus also indirectly indicated through the voltage. The current density increases in an exponential manner with increasing voltage.

3.4.3. Chamber Pressure

The chamber pressure in the Environmental mode could affect the supply of reagent molecules to the substrate surface. A higher chamber pressure would mean that there are potentially more molecules to adsorb on the substrate. A higher chamber pressure also makes it more difficult to properly focus the beam. The presence of gas molecules in the

chamber leads to scattering of the beam before it reaches the sample, leading to a more diffuse beam. Inability to focus at higher magnifications would therefore limit the minimum size of deposits generated when the chamber is filled with a reagent gas.

3.4.4. Dwell/Line Time

The dwell time is a measure of the length of time that the electron beam rests on a single pixel, and the line time indicates the amount of time required for the beam to return to that pixel when in line scan mode. The dwell time could affect the number of molecules decomposed per scan. The line time would affect the time for molecules to adsorb on the surface of the newly created deposits. A longer line time would be beneficial for a chemical the does not adsorb as readily as others. For a fixed dwell time, the line time can be adjusted by changing the pixel resolution. The usable resolutions available through the software are 512x442, 1024x884, 2048x1768, with the first value representing the horizontal pixels used for line scan mode. When operating in the line scan mode, the line time can be doubled by switching from 512 to 1024 pixels and quadrupled by switching from 512 to 2048 pixels. This will also double the number of scans performed if the magnification is held constant. The magnification controls the length across which the scan is performed, effectively determining the physical size of the area associated with a single pixel.

3.4.5. Deposition Time

The deposition time is an indirect indicator of the change in secondary electron yield for fiber deposition. Scattering of the electron beam occurs inside the growing deposit, leading to a lowering of the total secondary electron yield. When the electron beam rests

in a single spot, the secondary electron yield is greatest initially when the beam impacts the substrate. As the fiber grows, primary electrons from the beam scatter within the newly deposited material. This effect leads to a decrease in growth rate with increasing deposition time.

3.5. Experimental Procedure

Experiments for platinum deposition using the Gas Injection System were performed in the High Vacuum mode, while experiments for carbon deposition were performed in the Environmental mode. The experiments were performed using small pieces of a polished (100) p-type silicon wafer as substrates. Suitable deposition sites were chosen on the substrates, typically near an edge to allow for easier post-deposition imaging. The experiments were performed in a randomized fashion so as to minimize any bias.

3.5.1. Platinum Deposition Experiments

The effect of deposition time on fiber growth rate was studied by holding the voltage and spot size fixed and depositing fibers with incrementally increasing deposition times. The effect of the current density on fiber deposition was investigated by holding the voltage constant and incrementally increasing the spot size (thus decreasing the current density). This was done for two different voltages. These experiments also provided initial data regarding the general range of deposition rates, and was used to determine deposition time ranges for later experiments.

Factorial and central composite experiments were performed for platinum line and fiber deposition. For fiber deposition, the variables investigated were the deposition time, the voltage, and the beam current. The factorial fiber experiments were a two-level, three factor design, with the high and low values shown in Table 3-3.

Table 3-3. Factor Settings for Platinum Fiber Factorial Design

Trial	Voltage (kV)	Beam Current (pA)	Deposition Time (min)
T1	10	5400	5
T2	30	50	5
T3	10	5400	15
T4	10	50	5
T5	30	5400	5
T6	30	50	15
T7	30	5400	15
T8	10	50	15

A second platinum fiber factorial experiment was performed, with the same factors investigated as in the first design. The levels of the voltage and beam current factors were changed, with these values shown in Table 3-4.

Table 3-4. Factor Settings for 2nd Platinum Fiber Factorial Design

Trial	Voltage (kV)	Beam Current (pA)	Deposition Time (min)
T9	5	20000	5
T10	5	1500	5
T11	30	20000	5
T12	30	20000	15
T13	5	1500	15
T14	30	1500	5
T15	5	20000	15
T16	30	1500	15

The central composite platinum fiber experiment investigated the same variables as in the factorial design. The settings for the variables are shown in Table 3-5.

Table 3-5. Factor Settings for Platinum Fiber Central Composite Design

Trial	Voltage (kV)	Beam Current (pA)	Deposition Time (min)
1	30.1	775	9
2	25	1200	14
3	17.5	1489.8	9
4	25	350	4
5	10	1200	4
6	25	350	14
7	17.5	775	0.59
8	17.5	60.2	9
9	17.5	775	9
10	17.5	775	17.4
11	17.5	775	9
12	4.9	775	9
13	10	350	4
14	10	350	14
15	25	1200	4
16	10	1200	14

Factorial and central composite experiments were also performed to study platinum line deposition. The variables studied for these experiments were the voltage, beam current, dwell time, and line time. The first factorial experiment performed was a two level, three factor design with voltage, beam current, and dwell/line time as the variables. The dwell time and line time are proportional to each other (for the same resolution), so for this experiment it was not possible to separate out the effects of one from the other. As the dwell time was increased, the line time increased a proportional amount. The factor levels for this design are shown in Table 3-6.

Table 3-6. Factor Levels for Platinum Line Factorial Design

Trial	Voltage (kV)	Beam Current (pA)	Dwell Time (µs)	Line Time (ms)
T1	30	5400	10	10.60
T2	10	50	10	10.60
T3	30	5400	1000	1060
T4	30	50	10	10.60
T5	10	50	1000	1060
T6	30	50	1000	1060
T7	10	5400	10	10.60
T8	10	5400	1000	1060

The same variables were investigated for the platinum line central composite design, and the levels that were used for these factors are shown in Table 3-7. A smaller range of factor settings was used for the central composite design than for the factorial design, but the central composite design is more powerful for investigating interaction effects.

Table 3-7. Factor Settings for Platinum Line Central Composite Design

Trial	Voltage (kV)	Beam Current (pA)	Dwell Time (µs)	Line Time (s)
1	25	1200	100	0.11
2	10	1200	100	0.11
3	17.5	1489.8	237.5	0.25
4	25	350	100	0.11
5	17.5	775	237.5	0.25
6	10	350	100	0.11
7	17.5	775	468.75	0.5
8	30.1	775	237.5	0.25
9	25	350	375	0.4
10	17.5	775	237.5	0.25
11	10	1200	375	0.4
12	25	1200	375	0.4
13	17.5	775	6.25	0.00662
14	17.5	60.2	237.5	0.25
15	4.9	775	237.5	0.25
16	10	350	375	0.4

Factorial experiments were also performed in order to separate out the effects of the line time and the dwell time. For the line time experiment, a two-level, three factor design was used. The factor levels for this design are shown in Table 3-8. For this experiment,

the dwell time was held constant at 1 μs and the line time was varied by varying the pixel resolution. The other factors studied were the voltage and the beam current.

Table 3-8. Factor Levels for Platinum Line Time Study

Trial	Voltage (kV)	Beam Current (pA)	Line Time (ms)
1	30	5400	0.53
2	30	100	0.53
3	10	100	0.53
4	10	5400	0.53
5	30	100	2.12
6	30	5400	2.12
7	10	100	2.12
8	10	5400	2.12

Another factorial experiment of two-level, three factor design was performed to study the effects of the dwell time with the line time held constant. This was performed in a similar manner to the previously described line time investigation. The line time was held fixed at 1.06 ms and the dwell time varied by changing the pixel resolution. The other factors studied were the voltage and beam current. The factor levels for this experiment are shown in Table 3-9.

Table 3-9. Factor Levels for Platinum Line Dwell Time Study

Trial	Voltage (kV)	Beam Current (pA)	Dwell Time (ms)
1	30	5400	0.25
2	10	100	1.0
3	30	100	1.0
4	10	5400	0.25
5	10	100	0.25
6	30	5400	1.0
7	30	100	0.25
8	10	5400	1.0

Platinum fibers were deposited on a copper TEM grid for later analysis. This was performed by tilting the grid to a 40^{o} angle and focusing the beam on the inner wall of the TEM grid. The beam was then operated in the spot scan mode and angled fibers were deposited (i.e. deposits were made on the approximately 20 μm thickness dimension of the grid). The fibers were deposited in this fashion so that when the grid was mounted for analysis in the TEM, the fiber extended into open space to allow for easy examination.

3.5.2. Carbon Deposition Experiments

The effect of deposition time on carbon fiber growth rate was studied by holding the voltage and spot size constant and depositing fibers with incrementally increasing growth times. The purpose of this experiment was to obtain a general feel for the deposition rates in order to establish suitable deposition times to be used for later experiments.

Factorial experiments were performed for carbon deposition from methane. The variables studied for the first experiment were voltage, beam current, and dwell/line time. The factors and settings were the same as for the first platinum line factorial experiment. The line time varied proportionately with the dwell time, so the individual effects of each could not be separated out. Experimental settings for the carbon line deposition factorial experiment are shown in Table 3-10.

Table 3-10. Factor Levels for Carbon Line Factorial Design

Trial	Voltage (kV)	Beam Current (pA)	Dwell Time (μs)	Line Time (ms)
T1	10	5400	1000	1060
T2	10	50	10	10.60
T3	30	50	10	10.60
T4	30	5400	1000	1060
T5	30	50	1000	1060
T6	10	50	1000	1060
T7	10	5400	10	10.60
T8	30	5400	10	10.60

Another factorial study was performed to study the effects of varying the line time while holding the dwell time constant. The other factors studied were the voltage and beam current. The dwell time was fixed at 1 μs and the line time was varied by changing the pixel resolution. The factor levels for this experiment are shown in Table 3-11.

Table 3-11. Factorial Settings for Carbon Line Time Study

Trial	Voltage (kV)	Beam Current (pA)	Line Time (ms)
T1	30	5400	1.06
T2	10	100	2.12
T3	30	100	2.12
T4	10	5400	2.12
T5	30	100	1.06
T6	30	5400	2.12
T7	10	5400	1.06
T8	10	100	1.06

Carbon fibers were deposited on a copper TEM grid for analysis using the same procedure as was described previously for platinum fibers.

3.6. Post Experimental Procedure

Upon completion of the deposition experiments, the silicon substrates were mounted on a small piece of 90^{o} angle aluminum to allow imaging of the profile views of the deposits.

Once overhead and profile images were taken of the deposits, measurements were taken from these images using the XT-DOCU software program. Measurements for fiber deposits were made for the diameter at the base and the height from base to tip. Measurements for line deposits for the height and width were taken at the midpoint of the deposits. This was done to provide a characteristic value for each line deposit that did not take into account the build up that occurred at the ends of the lines on some of the deposits.

CHAPTER IV

EXPERIMENTAL RESULTS

4.1. Typical Deposit Geometry

Typical deposit geometry is illustrated in Figure 4-1 for fibers and Figure 4-2 for lines. As shown, fiber deposits are often needle-like or conical in shape, depending upon the deposition parameters. Line deposits are typically fairly uniform, although there are some cases in which build up has been observed at the ends of the lines (shown in Figure 4-3). Measurements for the line height and width were taken at the midpoint of the line, thus the end build up was not factored in for the analyses reported here.

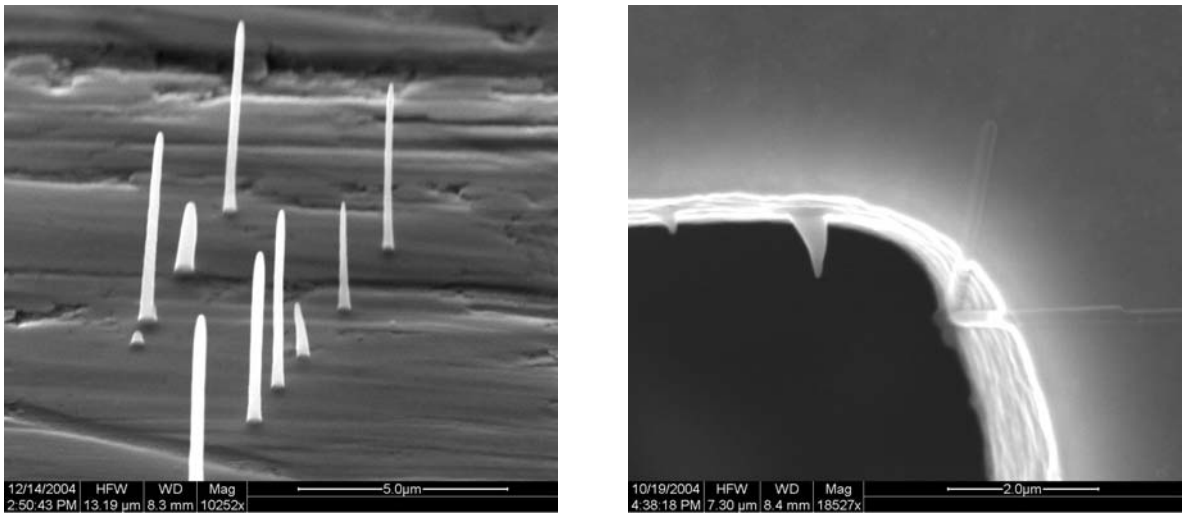

Figure 4-1. Needle- Like (Left, Pt Fibers on W Substrate) and Conical (Right, C Fibers on Cu TEM Grid) Fiber Deposits

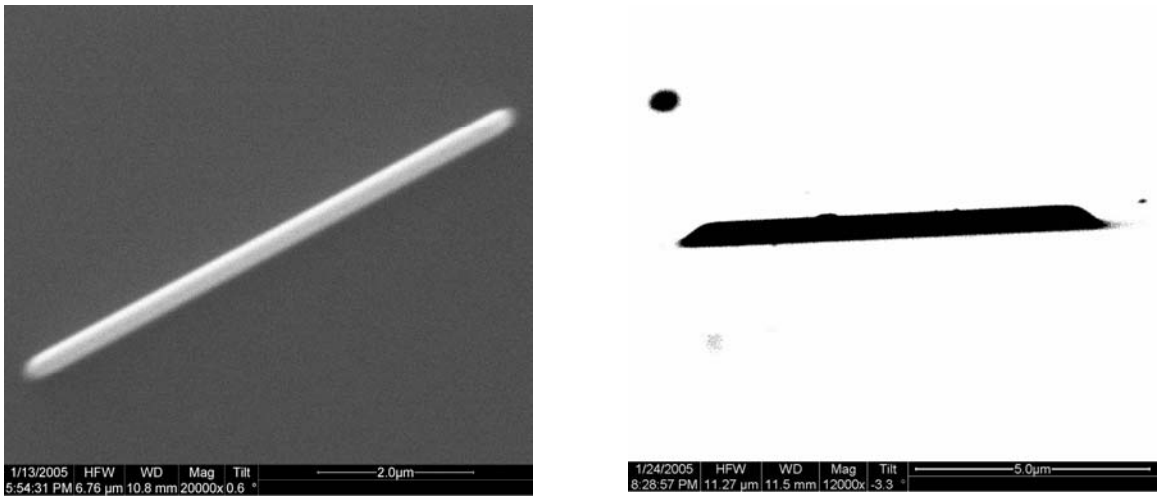

Figure 4-2. Typical Pt Line Deposits: Overhead View (Left) and Profile View (Right)

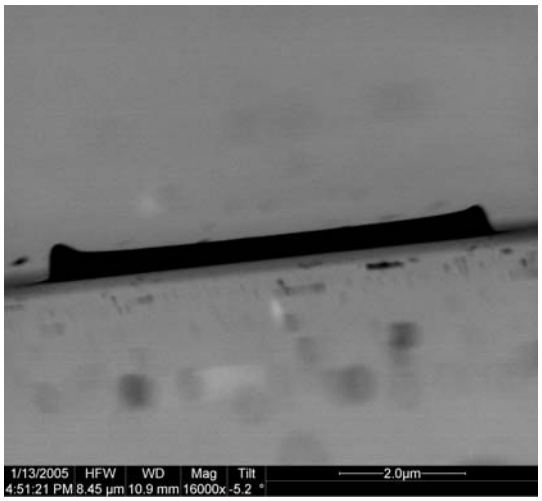

Figure 4-3. Pt Line Deposit with End Build Up

4.2. Platinum Deposition Experiments

4.2.1. Platinum Deposition Rate Study

The deposition rate as a function of time for platinum fibers was studied by holding the voltage and spot size fixed and incrementally increasing the deposition time. Fibers were chosen for the study of deposition rate due to the shorter deposition times required in comparison with line deposits. A voltage of 30 kV and a spot size of 3.0 were used,

along with deposition times of 1, 2, 3, 4, 5, 7, 10, and 15 minutes. A spot size of 3.0 at 30 kV corresponds to a beam current of 100 pA. The working distance was set to 10.1 mm. The resulting fibers were examined, and measurements were taken from images of the profiles of the fibers for the height and the base diameter. The values for vertical growth rate vs. deposition time are shown in Figure 4-4. Figure 4-5 shows the fiber bottom diameter growth rate vs. deposition time.

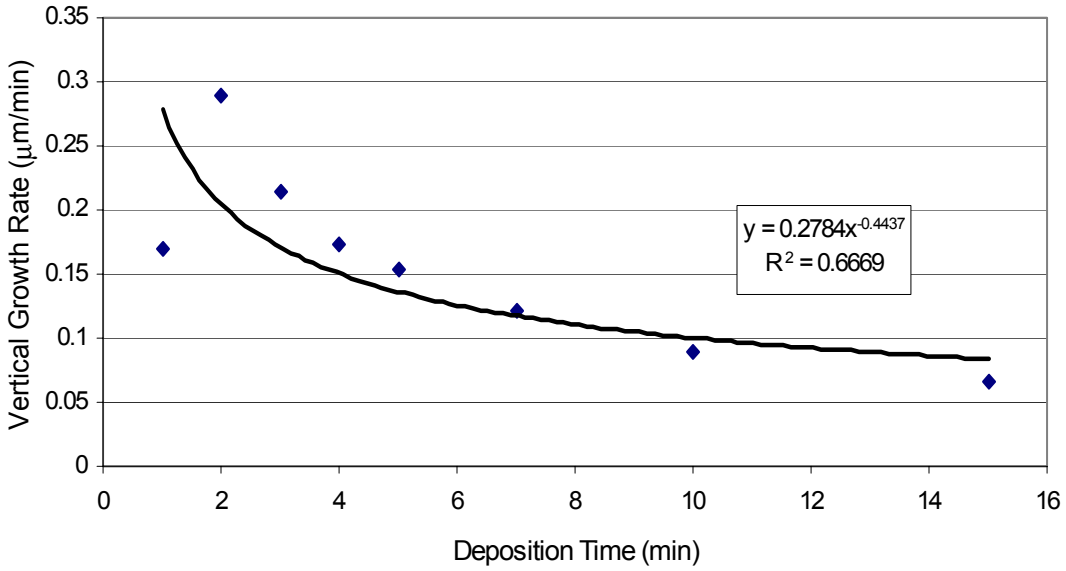

Figure 4-4. Pt Fiber Vertical Growth Rate vs. Deposition Time for 3.0 Spot Size

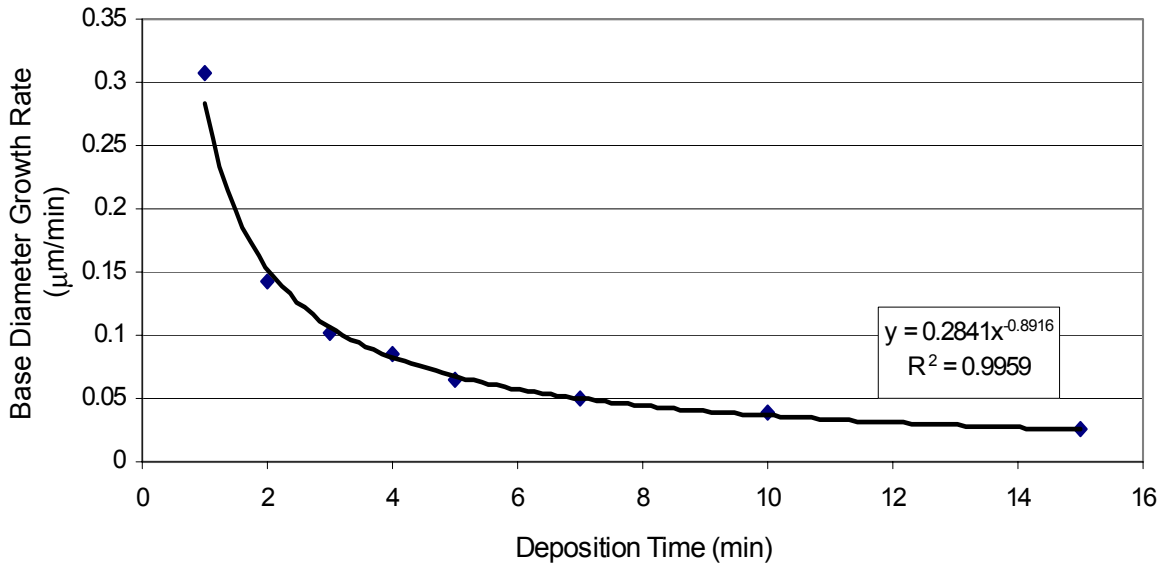

Figure 4-5. Pt Fiber Base Diameter Growth Rate vs. Deposition Time for 3.0 Spot Size

As shown in the figures, the growth rates decrease in an exponential fashion as the deposition time increases. This is to be expected, as the secondary electron yield from the substrate decreases as the fiber height increases. The primary electrons from the beam must first pass through the growing fiber for increasing deposition times, and scattering occurs within the growing fiber. This effect accounts for the decrease in secondary electron yield and corresponding decrease in growth rate. The profile views of the deposited fibers are shown in Figure 4-6. Measurements for these fibers are shown in Appendix A.1.

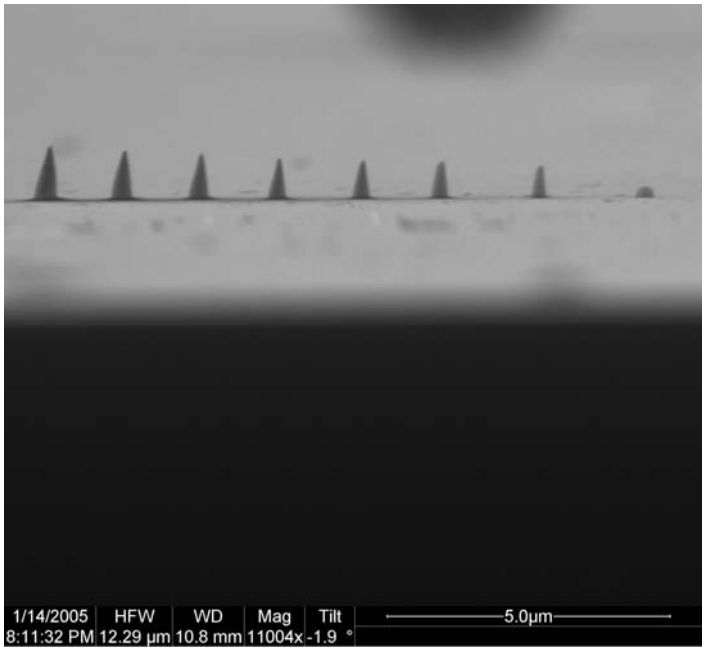

Figure 4-6. Profile View of Pt Fibers, from Longest Deposition Time to Shortest

The growth rate experiments for Pt fibers were performed again at a higher beam current setting. The fixed parameters were a voltage of 30 kV, a spot size of 6.0 (corresponding to a 5400 pA beam current), a magnification of 8000x, and a working distance of 10.1 mm. The deposition times used were 0.25, 0.5, 0.75, 1, 1.5, 2, 3, 4, 5, 7, 10, 15, and 25 minutes. Images of the fiber profiles were used to measure the fiber heights and base diameters. These images and measurements are shown in Appendix A.2. The results for the vertical growth rate vs. deposition time are shown in Figure 4-7. The results for the fiber base diameter growth rate vs. deposition time are shown in Figure 4-8. As before, the vertical and base diameter growth rates decrease in an exponential fashion with increasing deposition. The vertical growth rate for the higher beam current shown here is over twice as much as for the lower beam current, but the base diameter growth rates are similar for both.

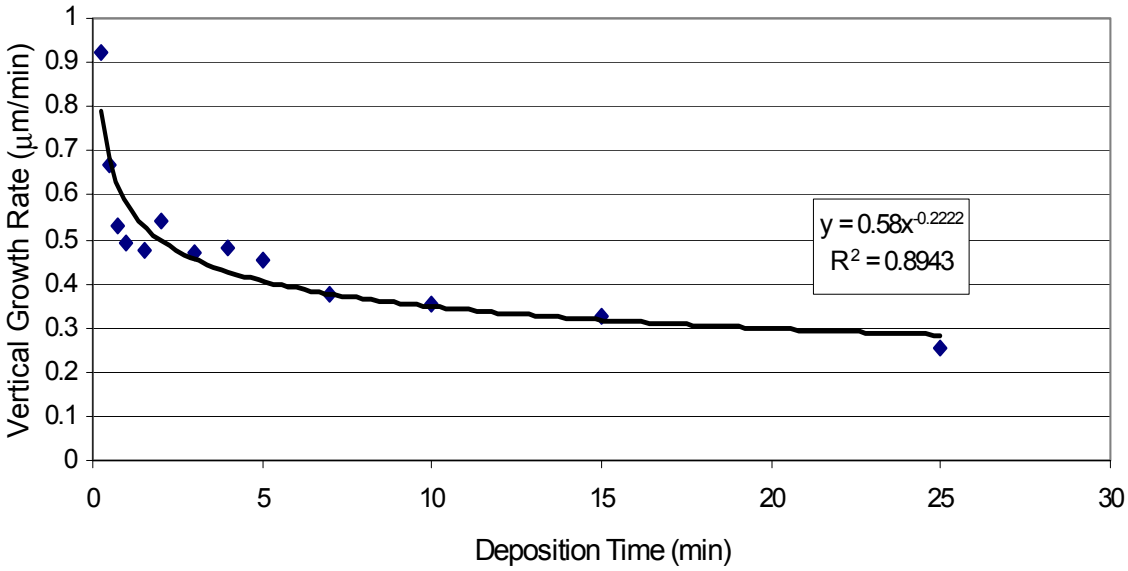

Figure 4-7. Pt Fiber Vertical Growth Rate vs. Deposition Time for 6.0 Spot Size

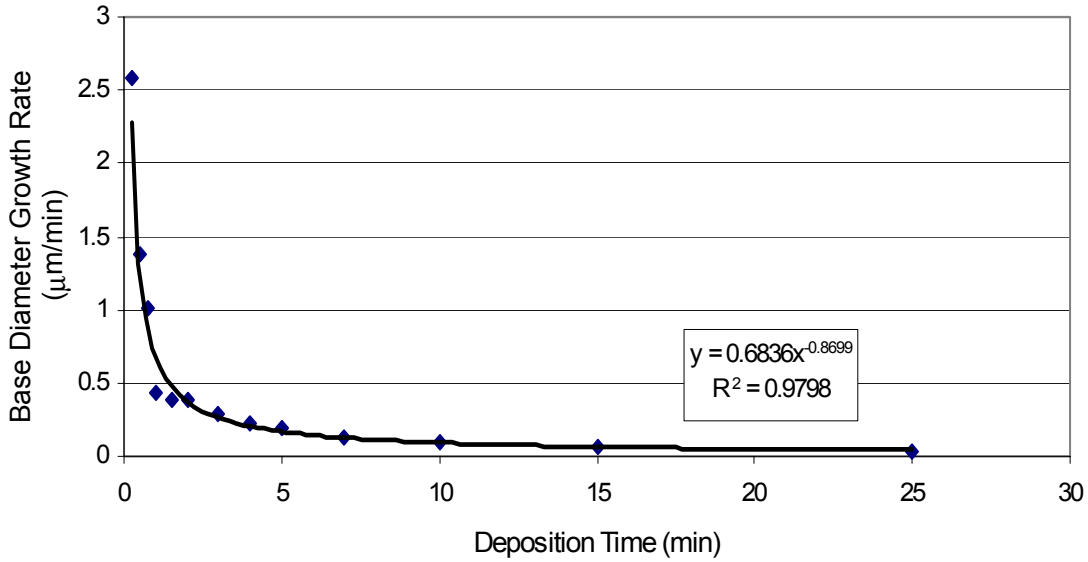

Figure 4-8. Pt Fiber Base Diameter Growth Rate vs. Deposition Time for 6.0 Spot Size

4.2.2. Platinum Fiber Current Density Study

The effects of current density on fiber growth were investigated by depositing fibers at various spot sizes for a constant voltage. Different spot sizes correspond to different current densities, as was discussed earlier. Two different voltages were used, 10 and 30

kV. These were chosen so as to provide ranges of current densities that were sufficiently different to determine any effects on deposit height and base diameter. The current density values at 30 kV are approximately 7 times greater than those at 10 kV, but the spot sizes selected also corresponded to similar values for beam current. Fixed settings for this study were a deposition time of 10 minutes, a magnification of 8000x, and a working distance of 10.1 mm. Deposits were made at five different spot sizes at both 10 kV and 30 kV. Table 4-1 lists the experimental settings and measurements that were later recorded for the deposits. Images of the fibers with measurements are shown in Appendix A.3.

Table 4-1. Experimental Settings and Measurements for Pt Fiber Current Density Study

Trial	Voltage (kV)	Spot Size	Beam Current (pA)	Current Density (A/cm^2)	Fiber Height (μm)	Base Diameter (μm)
T1	30	2	24	8.65	1.172	0.383
T2	30	3	100	7.39	1.894	0.41
T3	30	4	390	6.31	2.454	0.476
T4	30	5	1500	5.39	3.326	0.551
T5	30	6	5400	4.60	3.626	0.789
T6	10	2.3	24.6	1.15	1.031	0.416
T7	10	3.4	103.6	0.93	1.569	0.523
T8	10	4.4	383.7	0.78	1.561	0.66
T9	10	5.4	1420	0.65	2.031	0.691
T10	10	6.4	5257	0.54	2.361	0.758

The measurements for fiber height and base diameter were plotted against the current density. The plot for fiber height is shown in Figure 4-9, and the plot for fiber base diameter in Figure 4-10.

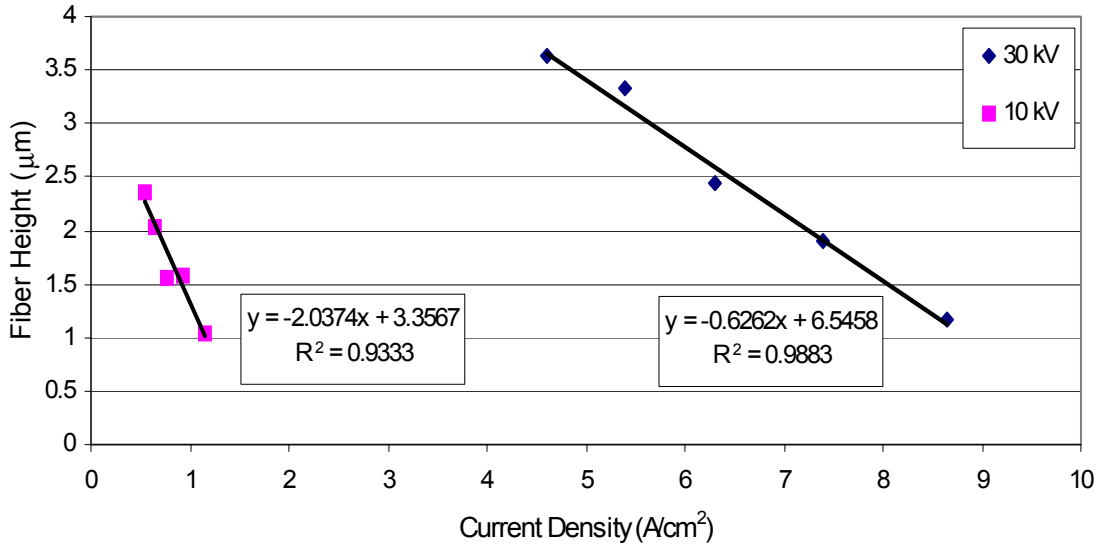

Figure 4-9. Pt Fiber Height vs. Current Density for 10 kV and 30 kV

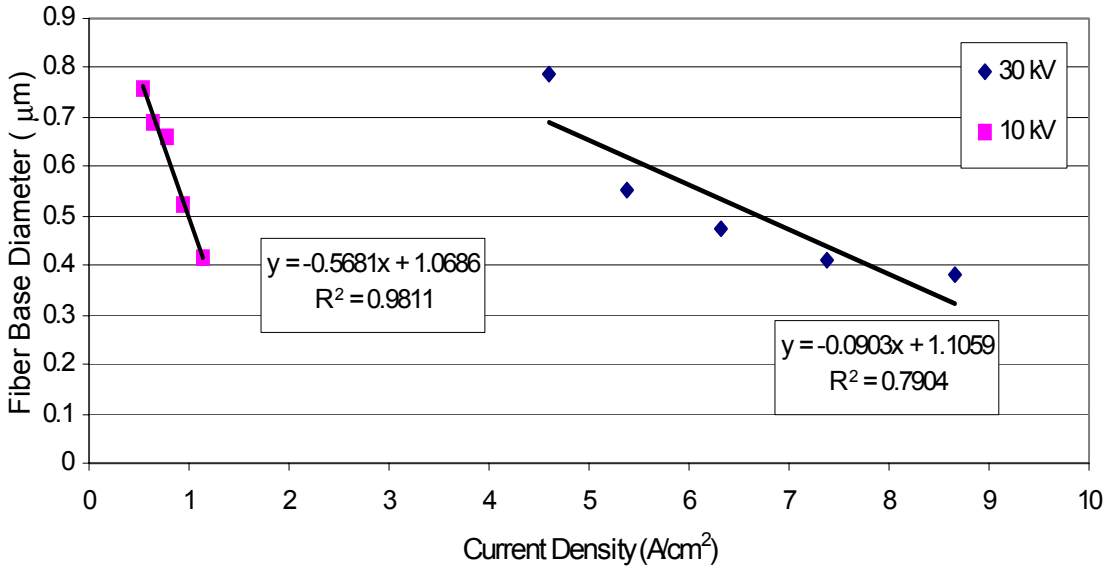

Figure 4-10. Pt Fiber Base Diameter vs. Current Density for 10 kV and 30 kV

As shown, both the fiber height and base diameter appear to decrease as current density increases for a fixed voltage. However, both the height and base diameter appear to be independent of current density, as the fiber dimensions are on the same order for both voltages. If the current density were a dominant factor, the fiber dimensions should

reflect this. The 30 kV fibers should be substantially larger than the 10 kV fibers. Higher current density corresponds to lower beam current, and the fiber dimensions have an obvious correlation to this quantity. Larger fiber dimensions correspond to higher beam current, as shown in Figures 4-11 and 4-12. Results from this study indicate that the current density is not a dominant factor. The 10 kV fibers did not exhibit growth rates that were significantly less than the 30 kV fibers, even though the current densities for the two voltages are approximately 7 times different. The Pt fiber growth rates thus appear to correspond more strongly to the beam current than to the current density.

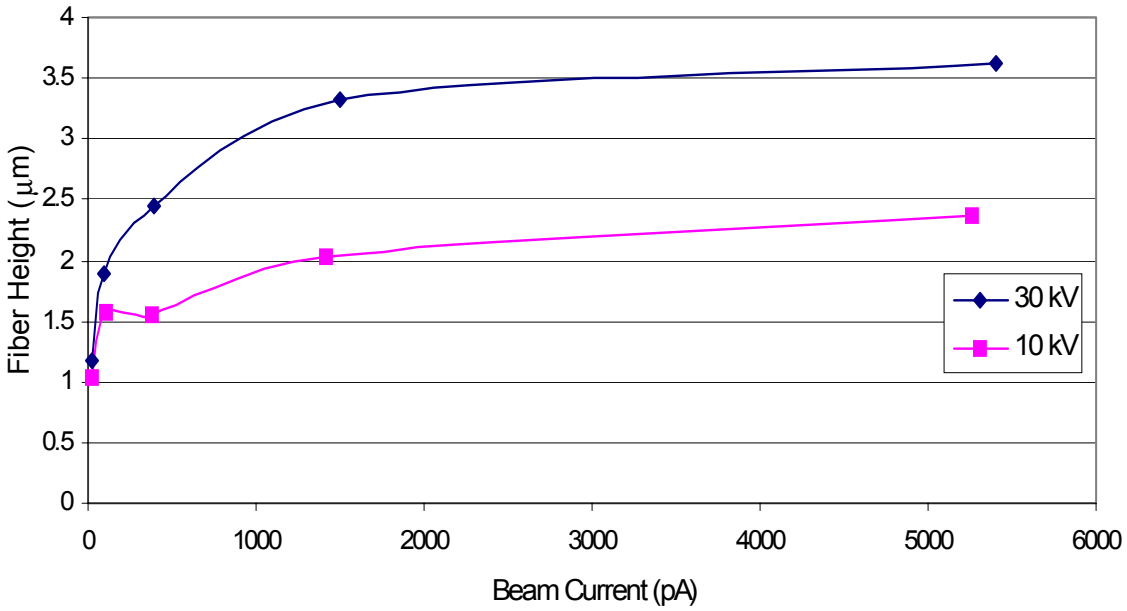

Figure 4-11. Pt Fiber Height vs. Beam Current for 10 and 30 kV

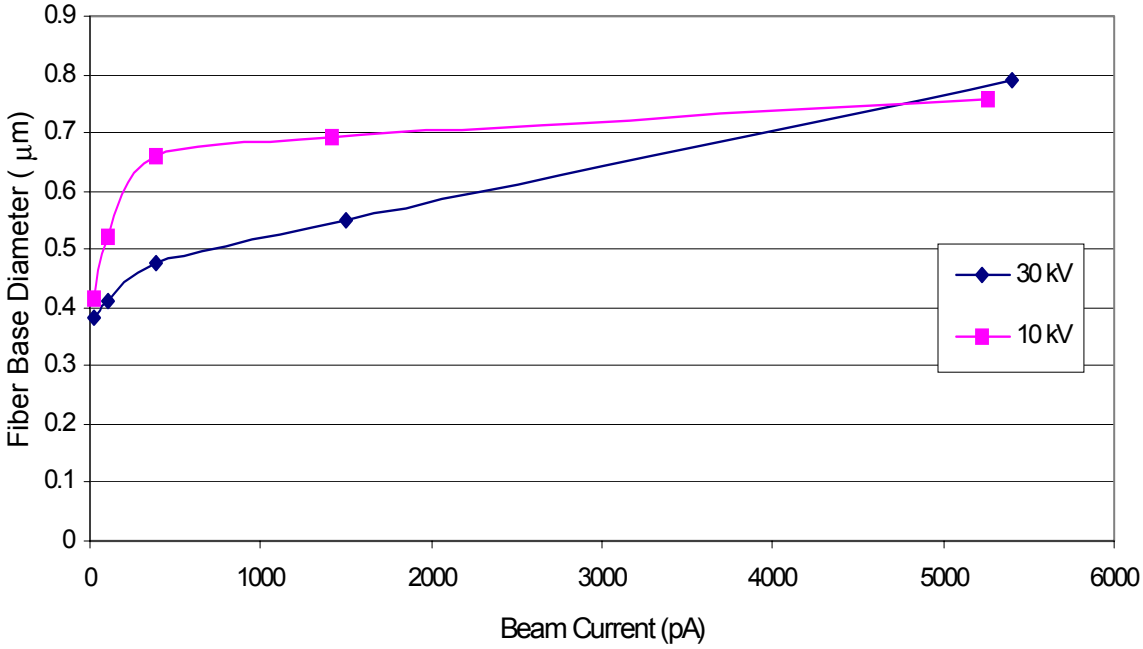

Figure 4-12. Pt Fiber Base Diameter vs. Beam Current for 10 and 30 kV

4.2.3. Platinum Fiber 2^3 Factorial Experiment

Two-level factorial trials with three variables were performed for Pt fiber deposition. The variables used for these experiments were voltage, beam current, and deposition time. The levels used for the variables were 10 and 30 kV for voltage, 100 and 5400 pA for beam current, and 5 and 15 minutes for deposition time. Fixed settings included a working distance of 10.1 mm and a magnification of 8,000x. Experimental settings and measurements of the fibers are listed in Table 4-2. Images and measurements for the fiber are shown in Appendix A.4.

Table 4-2. Experimental Settings and Measurements for Pt Fiber 2^3 Factorial Study

Trial	Voltage (kV)	Beam Current (pA)	Time (min)	Fiber Height (μm)	Fiber Base Diameter (μm)
T1	10	5400	5	2.573	1.134
T2	30	50	5	1.374	0.783
T3	10	5400	15	4.245	1.368
T4	10	50	5	0.488	0.639
T5	30	5400	5	2.958	0.704
T6	30	50	15	3.099	0.423
T7	30	5400	15	4.673	0.71
T8	10	50	15	1.756	0.657

The average vertical and base diameter growth rates were obtained by dividing the measured heights and diameters by the corresponding deposition time. Initial analysis for the fiber vertical growth rate performed using STATGRAPHICS with all interaction terms included indicated that two of the interactions had P-values that were three times greater than any other factor. As a result, these terms were therefore excluded from the final analysis. Figure 4-13 shows the final analysis results. Analysis of variance (ANOVA) results are shown in Appendix B.

As shown, the factors which had a statistically significant effect at the 95% confidence level were the beam current, deposition time, and the beam current-deposition time interaction term. The general trends indicated in the main effects plot show an increase in the vertical growth rate with increasing beam current, and a decrease with increasing deposition time. The correlation coefficient for this analysis was 97.3%.

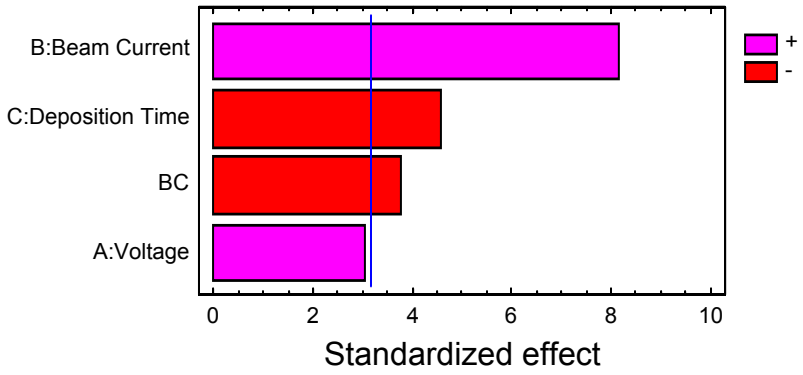

(a) Standardized Pareto Chart for Vertical Growth Rate

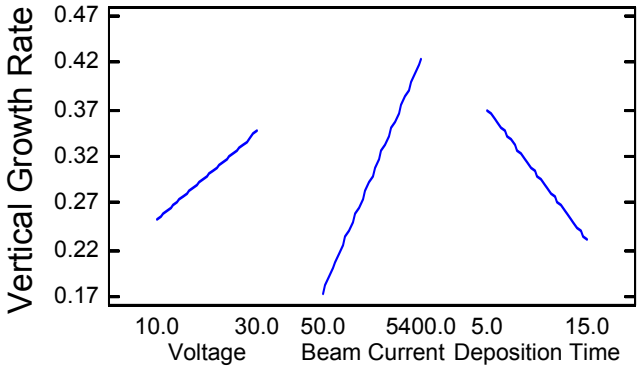

(b) Main Effects Plot for Vertical Growth Rate (μm/min)

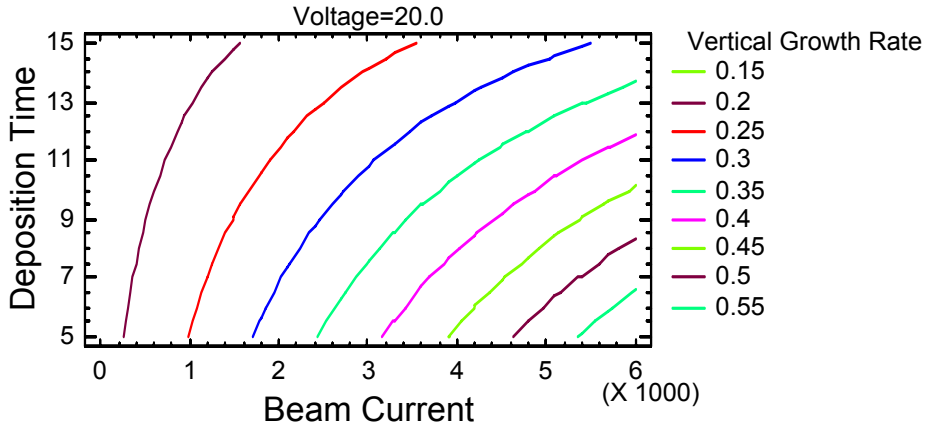

(c) Response Contours for Vertical Growth Rate (μm/min) for Constant Voltage

Figure 4-13. Analysis Results for Vertical Growth Rate from Pt Factorial Fiber Experiment: (a) Standardized Pareto Chart (b) Main Effects Plot (c) Response Contours

Initial analysis for the fiber base diameter growth rate when the interaction terms were included indicated that the interaction terms had high P-values (all were greater than 0.35). Results for the final statistical analysis for the fiber base diameter growth rate are shown in Figure 4-14. The ANOVA results are shown in Appendix B.

As shown, the deposition time was the only factor which had a statistically significant effect at the 95% confidence level. The general trends in the main effects plot show that an increase in deposition time leads to a sharp decrease in the fiber base diameter growth rate. This is an expected result, as the fibers approach a saturation base diameter as the deposition time increases. This maximum diameter results from the limited range of the secondary electron scattering for the beam when held in a fixed position. The correlation coefficient for this analysis was 89.1%.

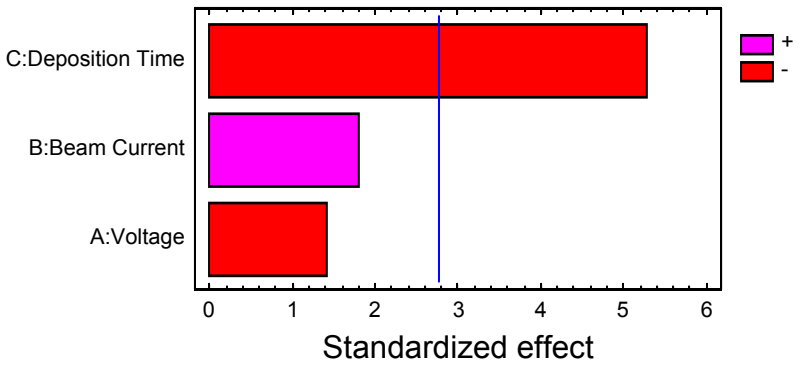

(a) Standardized Pareto Chart for Fiber Base Diameter Growth Rate

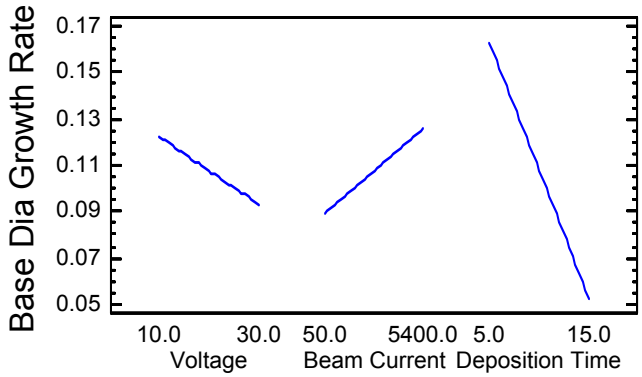

(b) Main Effects Plot for Fiber Base Diameter Growth Rate (μm/min)

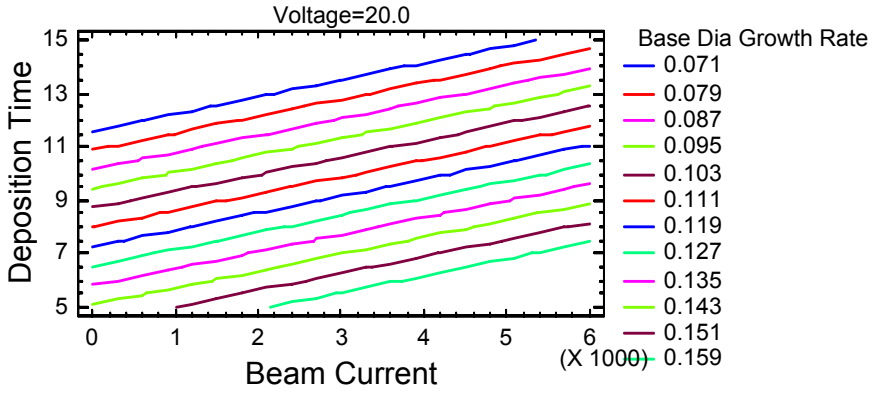

(c) Response Contours for Base Diameter Growth Rate (μm/min) for Constant Voltage

Figure 4-14. Analysis Results for Fiber Base Diameter Growth Rate for Pt Fiber Factorial Study: (a) Standardized Pareto Chart (b) Main Effects Plot (c) Response Contours

4.2.4. 2nd Platinum 2^3 Factorial Experiment

A second two level, three factor study was performed to study platinum fiber deposition. The factors were the same as for the first experiment, but the levels for the voltage and beam current were changed. The voltage values were changed so that a wider range could be investigated, and the factor levels were 5 and 30 kV. For the beam current, higher values were investigated, and the factor levels were 1,500 and 20,000 pA. The deposition time values investigated were the same as before, 5 and 15 minutes. Fixed settings were a working distance of 10.1 mm and a magnification of 6,000x. The experimental settings and measurements are listed in Table 4-3. Images of the fiber deposits with measurements are shown in Appendix A.5.

Table 4-3. Experimental Settings and Measurements for 2nd Pt Factorial Fiber Study

Trial	Voltage (kV)	Beam Current (pA)	Deposition Time (min)	Fiber Height (μm)	Fiber Base Diameter (μm)
T9	5	20000	5	2.737	2.223
T10	5	1500	5	1.327	0.798
T11	30	20000	5	2.032	0.856
T12	30	20000	15	3.937	0.847
T13	5	1500	15	3.684	0.826
T14	30	1500	5	0.916	0.297
T15	5	20000	15	5.705	1.547
T16	30	1500	15	1.772	0.457

The average fiber vertical growth rate was calculated by dividing the measured height by the deposition time. This parameter was analyzed in STATGRAPHICS, and initial results with all of the interaction terms included indicated that all of these terms had much larger P-values than the main factors. The interaction terms were therefore excluded from the final analysis. The results for the final analysis for the fiber vertical growth rate are shown in Figure 4-15. ANOVA results are shown in Appendix B.

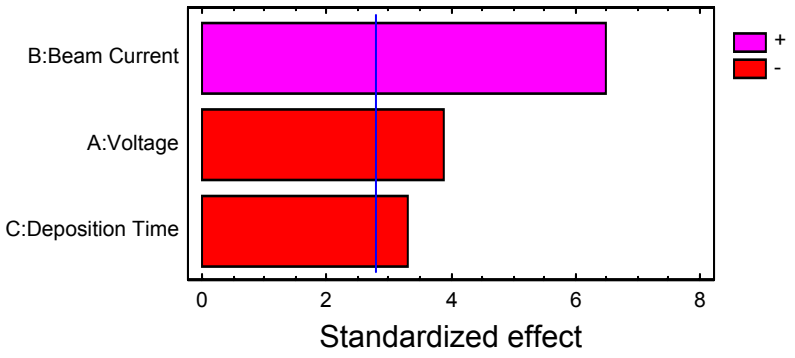

(a) Standardized Pareto Chart for Fiber Vertical Growth Rate

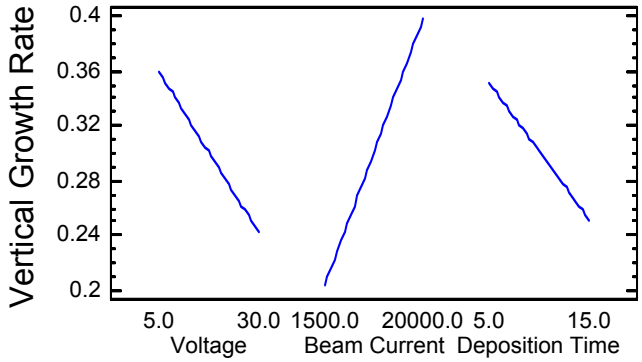

(b) Main Effects Plot for Fiber Vertical Growth Rate (μm/min)

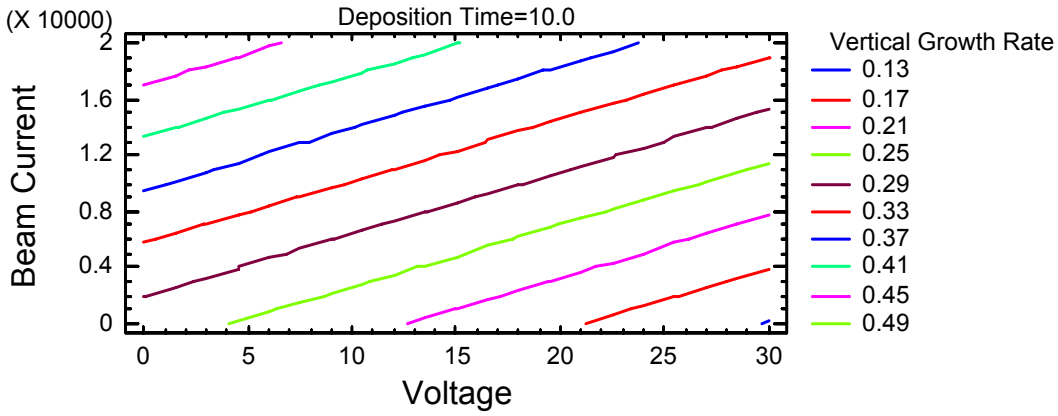

(c) Response Contours for Fiber Vertical Growth Rate (μm/min) for Constant Deposition Time

Figure 4-15. Analysis Results for Fiber Vertical Growth Rate for 2nd Pt Factorial Fiber Study: (a) Standardized Pareto Chart (b) Main Effects Plot (c) Response Contours

As shown, all three of the factors are statistically significant at the 95% confidence level. The general trends shown in the main effects plot indicate an increase in vertical growth rate with increasing beam current, and a decrease in vertical growth rate as voltage and deposition time are increased. These results again show the prominent role the beam current plays in the vertical growth rate. In contrast with the previous factorial fiber study, the deposition time was a statistically significant factor at the 95% confidence level. The decrease in vertical growth rate with increasing voltage is likely due to the fact that the secondary electron emission from (100) Si drops dramatically as voltage increases in the 1 to 10 kV range. From the 10 to 30 kV range, there is not a large difference in the secondary electron emission, meaning that the voltage effects should be harder to discern in this range. The correlation coefficient was 94.4%.

The fiber base diameter growth rate was analyzed, and initial results with all of the interaction terms included indicated that two of these terms had large P-values, so these terms were excluded from the final analysis. The results for the final analysis are shown in Figure 4-16, and the ANOVA results are shown in Appendix B.

As shown, the deposition time and voltage factors were found to be statistically significant at the 95% confidence level. The general trends are illustrated in the main effects plot, which shows a sharp decrease in base diameter growth rate as the voltage and deposition time increase. The effect of the voltage is again likely due to the decrease in secondary electron yield from the Si substrate as the voltage is increased. The effect of

the deposition time is as expected, with the base diameter growth rate decreasing as the fibers approach a saturation base diameter. The correlation coefficient was 94.7%.

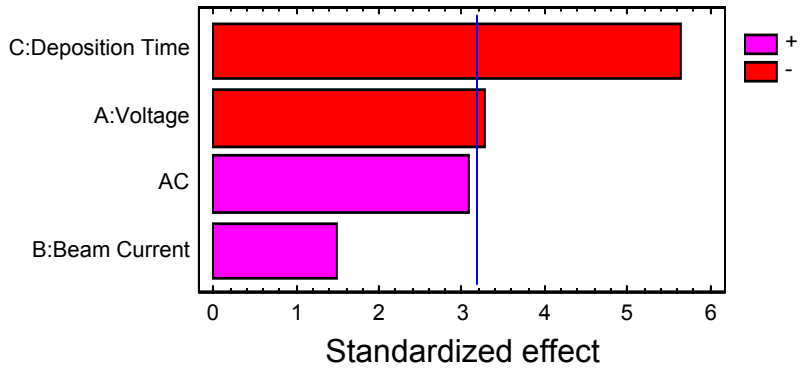

(a) Standardized Pareto Chart for Fiber Base Diameter Growth Rate

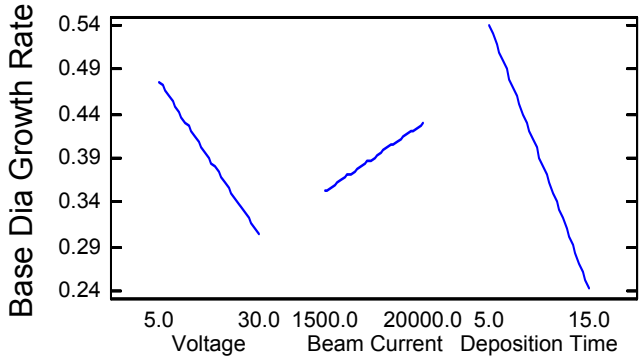

(b) Main Effects Plot for Fiber Base Diameter Growth Rate (µm/min)

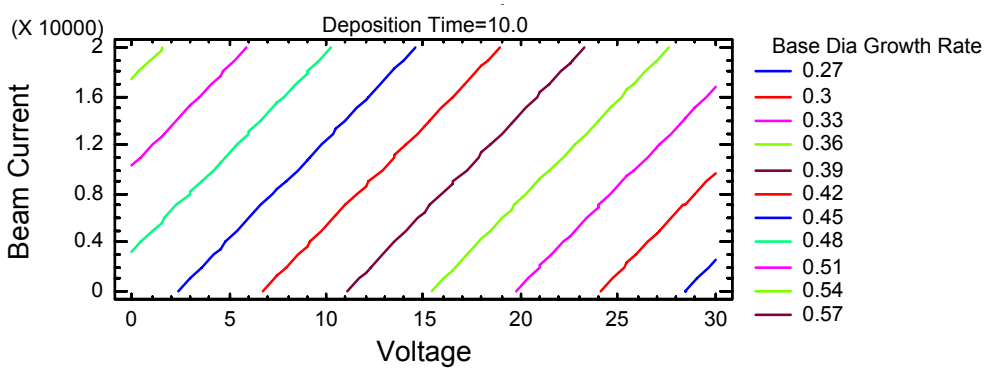

(c) Response Contours for Fiber Base Diameter Growth Rate (µm/min) for Constant Deposition Time

Figure 4-16. Analysis Results for Fiber Base Diameter Growth Rate for 2nd Pt Factorial Fiber Study: (a) Standardized Pareto Chart (b) Main Effects Plot (c) Response Contours

As shown, the deposition time and voltage factors were found to be statistically significant at the 95% confidence level. The general trends are illustrated in the main effects plot, which shows a sharp decrease in base diameter growth rate as the voltage and deposition time increase. The effect of the voltage is again likely due to the decrease in secondary electron yield from the Si substrate as the voltage is increased. The effect of the deposition time is as expected, with the base diameter growth rate decreasing as the fibers approach a saturation diameter. The correlation coefficient was 94.7%.

4.2.5. Platinum Central Composite Fiber Study

Following the two level factorial fiber trials, a set of experiments featuring a central composite design with star points was performed. In total, 16 fiber depositions were necessary for this experiment. The variables were the same as for the factorial trials, voltage, beam current, and deposition time. Upon completion of the experiments, the sample was mounted on a 90^{o} angle aluminum mount and images were taken of the profiles of the fibers. Measurements were then taken for the height and the base diameter of the fibers. Ranges for the variables were dictated by the capabilities of the microscope and the constraints of the experimental design. Fixed settings for the experiments were a working distance of 10.1 mm and a magnification of 8000x. The experimental settings and fiber measurements are detailed in Table 4-4. Images of the fibers with measurements are shown in Appendix A.6.

Table 4-4. Settings and Measurements for Pt Central Composite Fiber Experiments

Trial	Voltage (kV)	Beam Current (pA)	Time (min)	Fiber Height (μm)	Fiber Base Diameter (μm)
1	30.1	775	9	2.071	0.362
2	25	1200	14	3.75	0.394
3	17.5	1489.8	9	2.318	0.554
4	25	350	4	0.946	0.331
5	10	1200	4	1.63	0.614
6	25	350	14	1.005	0.63
7	17.5	775	0.59	0.191	0.423
8	17.5	60.2	9	0.64	0.474
9	17.5	775	9	2.089	0.665
10	17.5	775	17.4	3.013	0.706
11	17.5	775	9	1.99	0.777
12	4.9	775	9	3.012	0.571
13	10	350	4	1.083	0.485
14	10	350	14	2.582	0.502
15	25	1200	4	1.642	0.537
16	10	1200	14	3.859	0.716

The data for these experiments were analyzed in STATGRAPHICS, and the average vertical growth rate and average base diameter growth rate were used as response variables. The average growth rates were obtained by dividing the measured heights and diameters by the deposition time. Initial analysis showed that the interaction terms aside from the voltage squared term all had P-values ranging from 0.20 to 0.82. Since these values were more than four times greater than the P-values for the other factors, these terms were excluded. The results from the final analysis for vertical growth rate are shown in Figure 4-17. ANOVA results are shown in Appendix B.

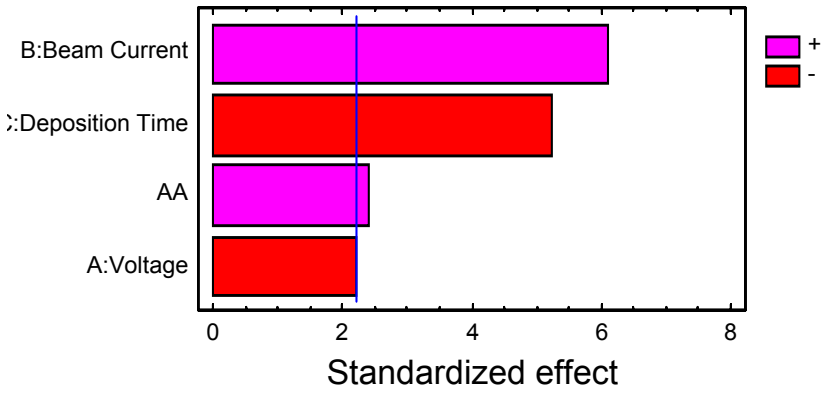

(a) Standardized Pareto Chart for Pt Fiber Vertical Growth Rate

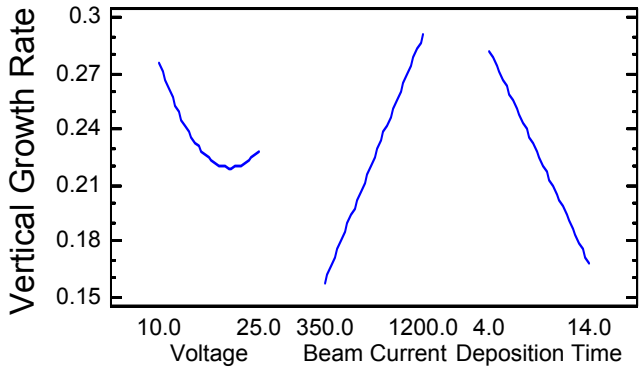

(b) Main Effects Plot for Vertical Growth Rate (µm/min)

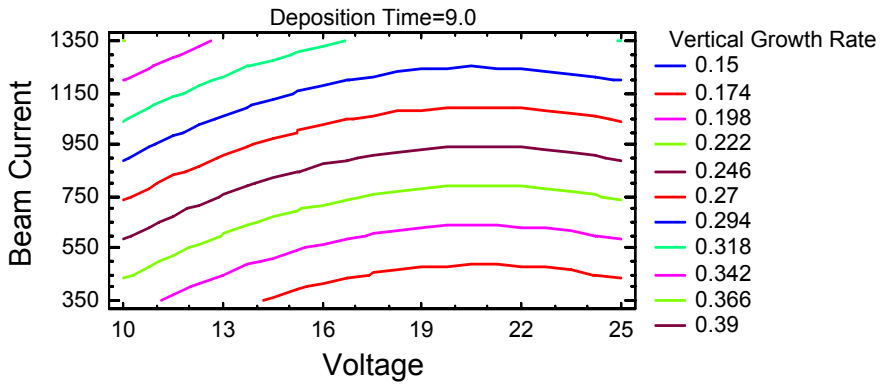

(c) Response Contours for Constant Deposition Time for Vertical Growth Rate (µm/min)

Figure 4-17. Analysis Results for Vertical Fiber Growth Rate from Pt Central Composite Fiber Study: (a) Standardized Pareto Chart (b) Main Effects Plot (c) Response Contours

As shown in the standardized Pareto chart, all three of the variables were found to be significant at a 95% confidence level. The main effects plot illustrates the influence of the variables. Increasing voltage leads to lower vertical growth rates, as does increasing deposition time. Increasing beam current leads to higher vertical growth rates. Analysis of variance (ANOVA) for the Pt fiber vertical growth rate indicated a correlation coefficient of 87.1%, indicating a good fit for the model with the experimental data.

Results for the analysis of the fiber base diameter growth rate are shown in Figure 4-18. ANOVA results are shown in Appendix B. Initial investigation indicated that all of the interaction terms aside from the deposition time squared term had P-values greater than 0.52, and these terms were therefore excluded. As shown, the only terms found to be statistically significant at the 95% confidence level were the deposition time and deposition time squared term, which had a negative effect on the base diameter growth rate. The analysis also indicates that there are no significant interactions between the variables. Analysis of variance indicates a correlation coefficient of 70.6% for the fiber base diameter growth rate data to the model. The negative effect of increasing deposition time on base diameter growth rate is expected, as the fibers reach what is referred to as a saturation diameter if given enough time.

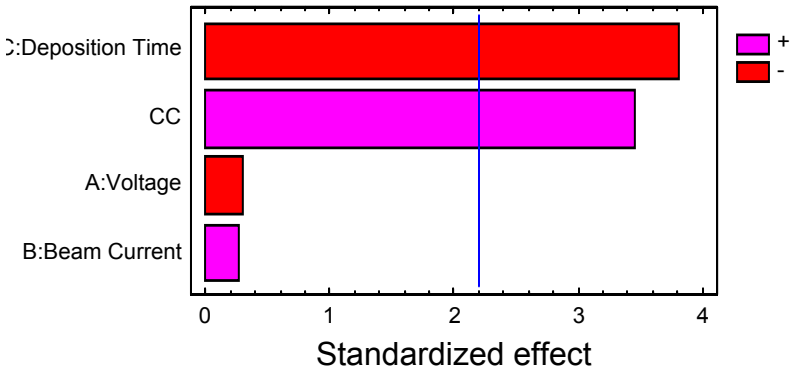

(a) Standardized Pareto Chart for Base Diameter Growth Rate

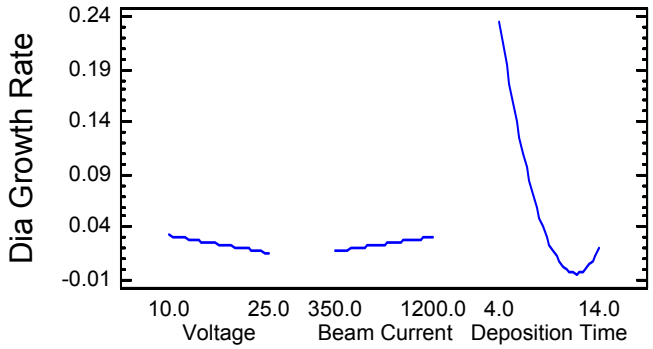

(b) Main Effects Plots for Base Diameter Growth Rate (µm/min)

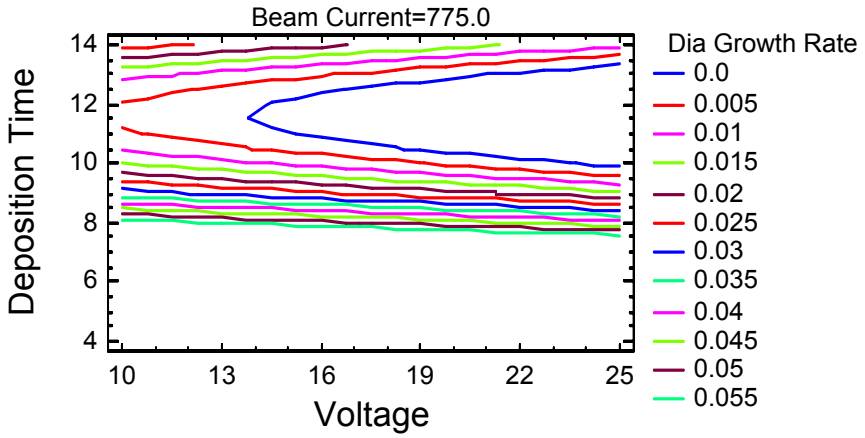

(c) Response Contours for Constant Beam Current for Base Diameter Growth Rate (µm/min)

Figure 4-18. Analysis Results for Base Diameter Growth Rate for Pt Central Composite Fiber Study: (a) Standardized Pareto Chart (b) Main Effects Plot (c) Response Contours

4.2.6. Platinum 2^3 Factorial Line Deposition Study

Two level factorial trials with three variables were performed to study platinum line deposition. The variables and levels were voltage (10 and 30 kV), beam current (50 and 5400 pA), and dwell/line time (10 and 1000 μs dwell times, 10.60 and 1060 ms line times). Varying the dwell time over such a range also necessitates varying the line time by an amount proportional to the dwell time. The effects of the line time thus can not be separated out from those of the dwell time for this set of experiments. Fixed settings for these experiments were a working distance of 10.1 mm, a magnification of 15000x, and a deposition time of 15 minutes. Experimental conditions and measurement results are listed in Table 4-5. Measurements of line widths and heights were taken at the midpoint of the deposits. This was done to provide a characteristic value for each line deposit that did not take into account the build up that occurred at the ends of the lines on some of the deposits. Images of the line deposits and measurements are shown in Appendix A.7.

Table 4-5. Experimental Settings and Measurements for Pt 2^3 Factorial Line Study

Trial	Voltage (kV)	Beam Current (pA)	Dwell Time (μs)	Line Time (ms)	Line Height (μm)	Line Width (μm)
T1	30	5400	10	10.60	0.412	0.589
T2	10	50	10	10.60	0.071	0.536
T3	30	5400	1000	1060	0.401	0.693
T4	30	50	10	10.60	0.123	0.209
T5	10	50	1000	1060	0.137	0.356
T6	30	50	1000	1060	0.141	0.346
T7	10	5400	10	10.60	0.529	0.882
T8	10	5400	1000	1060	0.471	1.034

The number of scans performed for the fixed 15 minute deposition time was calculated for both of the line times, and the heights were divided by these factors correspondingly. For example, for Trial T1 the line height of 0.412 μm was divided by 84,905 to yield the

value of 4.85 x 10^{-6} μm for the line height per scan. These height/scan values were then multiplied by 10^{6} to provide values that were capable of being properly analyzed in STATGRAPHICS, since initial analysis indicated software issues with the original magnitude of the height/scan numbers.

Initial analysis when all main effect and interaction terms were included indicated that the beam current-dwell/line time term had a P-value less than 0.08, while the other two interaction terms had P-values greater than 0.48. Two of the three interaction terms were therefore excluded for the final analysis. The final analysis for the line height/scan is shown in Figure 4-19. ANOVA results are shown in Appendix B. As shown, the general trends include a statistically significant increase with increasing beam current and dwell/line time. The correlation coefficient was 99.2%, indicating a very good fit between the data and the statistical model.

The line width was also analyzed in the same manner, and the initial results indicated no variables were significant to the 95% confidence level. Since all the interaction terms had P-values greater than 0.56, these terms were excluded and the analysis was run again. The final results are shown in Figure 4-20. ANOVA results are shown in Appendix B. The line width trends differ from those for height/scan, with both the beam current and the voltage being statistically significant at the 95% confidence level. The main effects plot illustrates the general trends of a decrease in line width corresponding to an increase in voltage, and an increase in line width corresponding to an increase in beam current. The correlation coefficient was 91.4%.

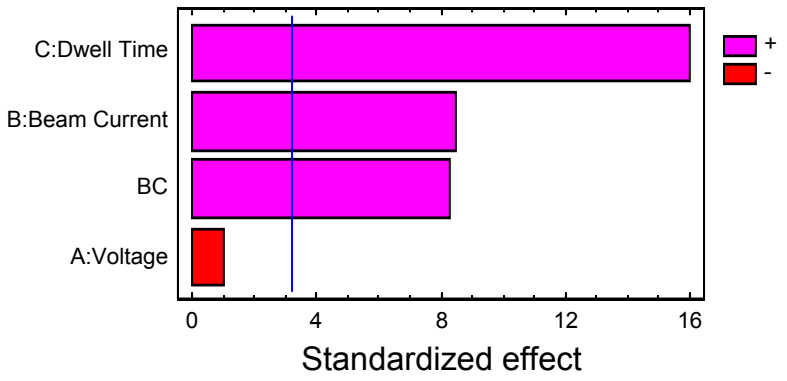

(a) Standardized Pareto Chart for Height/scan

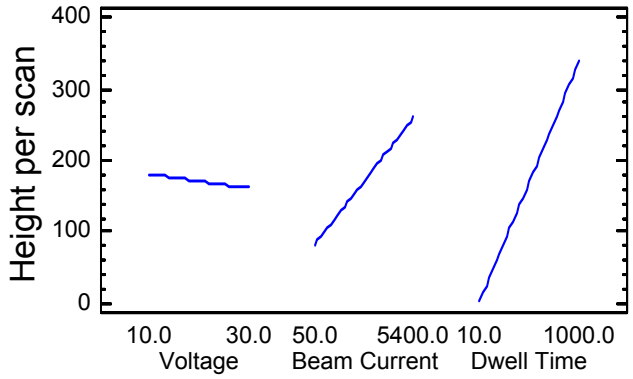

(b) Main Effects Plot for Height/scan (μm/scan) x 10^6

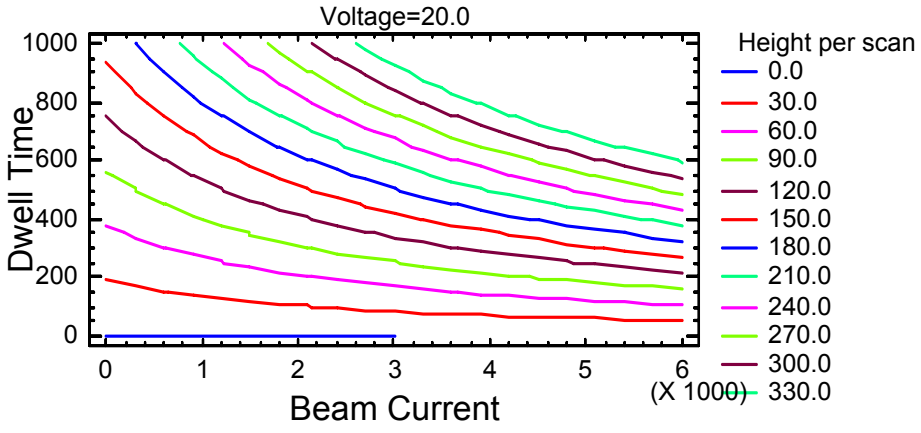

(c) Response Contours for Height/scan (μm/scan) x 10^6 for Fixed Voltage

Figure 4-19. Analysis Results for Height/scan for Pt 2^3 Line Trials: (a) Standardized Pareto Chart (b) Main Effects Plot (c) Response Contours

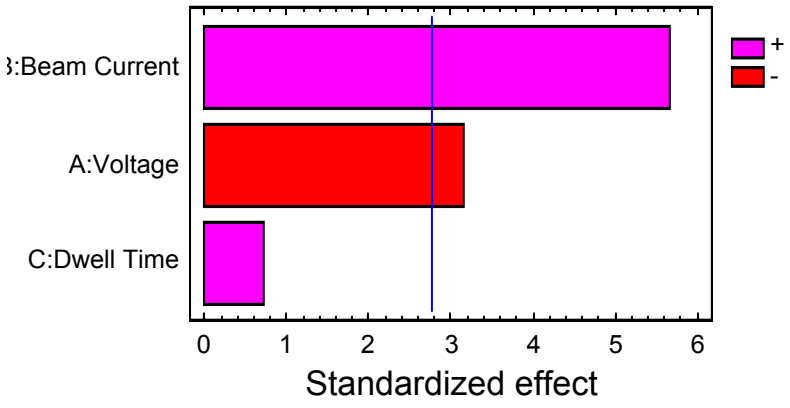

(a) Standardized Pareto Chart for Line Width

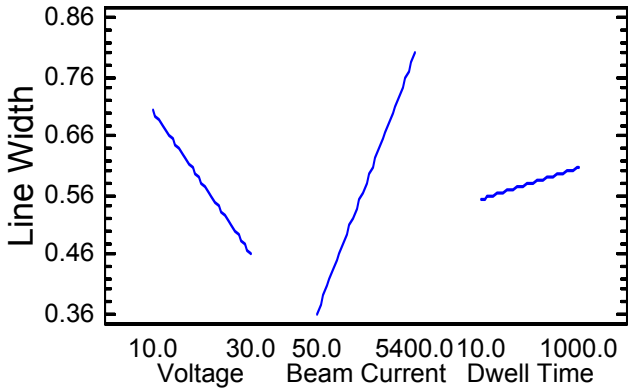

(b) Main Effects Plot for Line Width (µm)

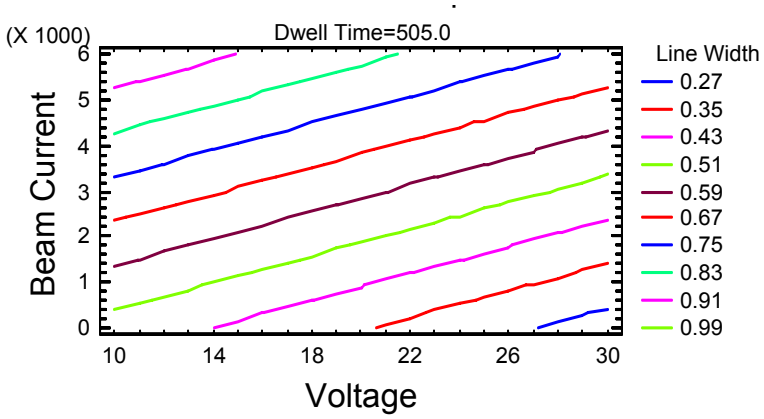

(c) Response Contours for Line Width (µm) for Fixed Voltage

Figure 4-20. Analysis Results for Line Width for Pt 2^3 Line Trials: (a) Standardized Pareto Chart (b) Main Effects Plot (c) Response Contours

4.2.7. Central Composite Platinum Line Experiment

A central composite cubic design with star points was performed for further study of platinum line deposition. The variables used for the experiments were voltage, beam current, and dwell/line time. Fixed settings for the experiments were a 20 min deposition time, a 15,000x magnification, and a working distance of 10.1 mm. As with the previously detailed 2^3 line trials, the line time varied proportionately with the dwell time. The effects of the varying line time were factored out by calculating the number of scans performed for each dwell time and then dividing the measured line heights by the corresponding quantity. The height and width were measured for each line from profile and overhead views of the deposits. The experimental settings and recorded measurements are detailed in Table 4-6. Images of the line deposits with measurements are shown in Appendix A.8.

Table 4-6. Experimental Settings and Measurements for Pt Central Composite Line Study

Trial	Voltage (kV)	Beam Current (pA)	Dwell Time (μs)	Line Time (s)	Number of Scans	Line Height (μm)	Line Width (μm)
1	25	1200	100	0.11	10909	0.266	0.352
2	10	1200	100	0.11	10909	0.21	0.44
3	17.5	1489.8	237.5	0.25	4800	0.161	0.396
4	25	350	100	0.11	10909	0.032	0.552
5	17.5	775	237.5	0.25	4800	0.105	0.383
6	10	350	100	0.11	10909	0.106	0.533
7	17.5	775	468.75	0.5	2400	0.112	0.484
8	30.1	775	237.5	0.25	4800	0.096	0.411
9	25	350	375	0.4	3000	0.064	0.304
10	17.5	775	237.5	0.25	4800	0.133	0.307
11	10	1200	375	0.4	3000	0.286	0.44
12	25	1200	375	0.4	3000	0.277	0.296
13	17.5	775	6.25	0.00662	181269	0.109	0.564
14	17.5	60.2	237.5	0.25	4800	0.081	0.267
15	4.9	775	237.5	0.25	4800	0.348	0.539
16	10	350	375	0.4	3000	0.138	0.288

Analysis of the data was performed in STATGRAPHICS, and the results for the height/scan indicated that the beam current and dwell/line time, voltage, and the beam current-dwell/line time interaction terms were all found to be statistically significant at the 95% confidence level. Results for this analysis for height/scan are shown in Figure 4-21. ANOVA results are shown in Appendix B.

Initial analysis indicated that all of the interaction terms aside from the voltage squared and the beam current-dwell/line time term had P-values greater than 0.51. As a result, these terms were excluded from the final analysis. As shown in the figures, the general trends include a decreasing line height/scan with increasing voltage, and increasing height/scan for increasing beam current and dwell/line time. The correlation coefficient for the data and statistical model was 84.6%.

The results for the final analysis with the width as the response variable are shown in Figure 4-22. ANOVA results are shown in Appendix B. Initial analysis indicated that three of the interaction terms had P-value ranging from 0.22 to 0.77, so these terms were then excluded. The final results indicate that the dwell/line time, the dwell/line time squared, and the beam current-dwell/line time interaction terms have a statistically significant effect on the line width at the 95% confidence level. The main effects plot also shows a general decrease in line width as voltage increases. No interactions were found to be significant at the 95% level. The correlation coefficient for this analysis was 74.2%.

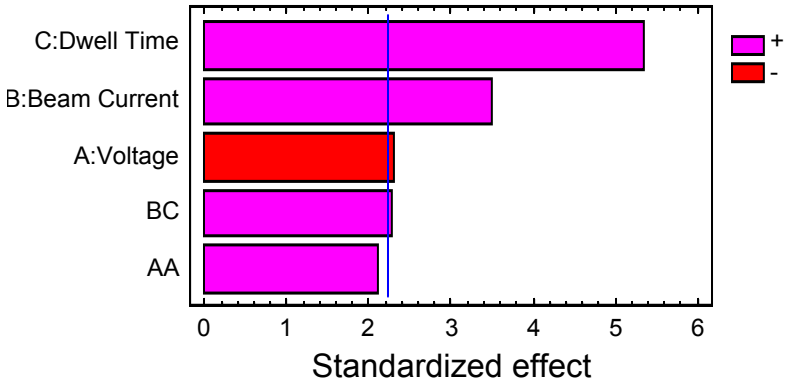

(a) Standardized Pareto Chart for Height/scan

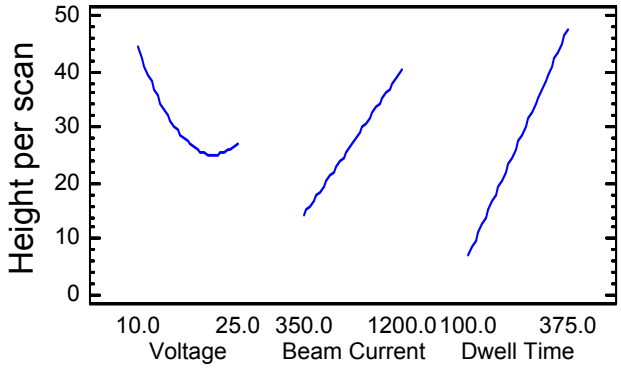

(b) Main Effects Plot for Height/scan (μm/scan) x 10^6

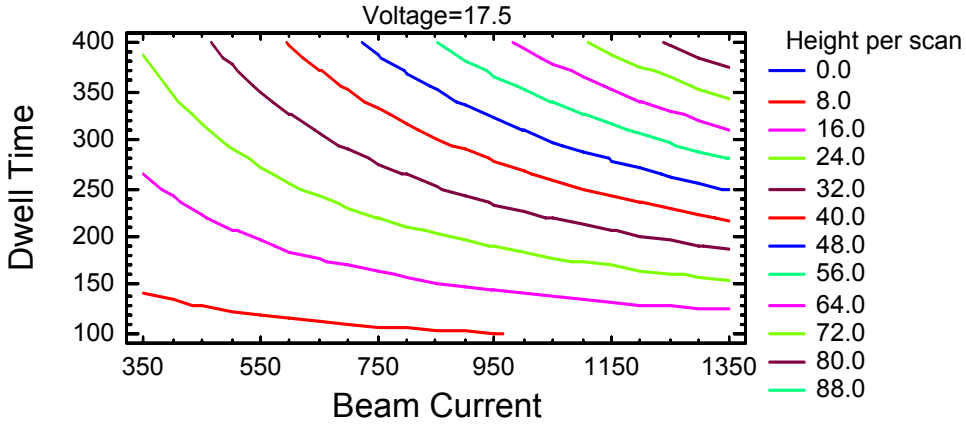

(c) Response Contours for Height/scan (μm/scan) x 10^6 for Constant Voltage

Figure 4-21. Analysis Results for Height/scan for Pt Central Composite Line Experiments: (a) Standardized Pareto Chart (b) Main Effects Plot (c) Response Contours

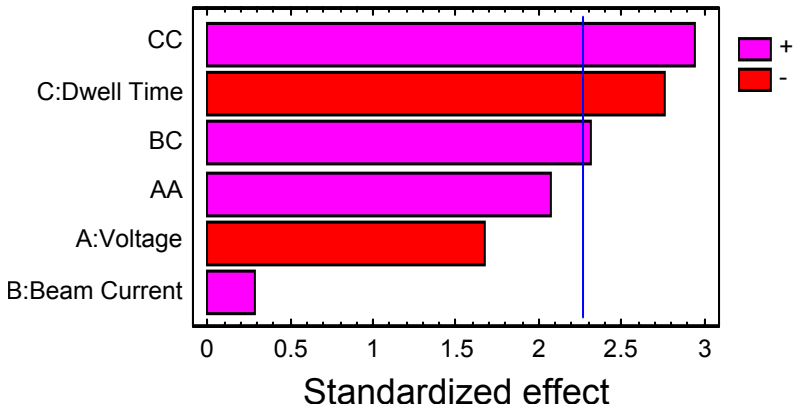

(a) Standardized Pareto Chart for Line Width

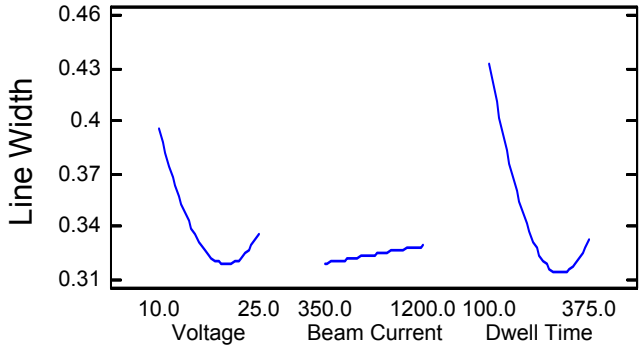

(b) Main Effects Plot for Line Width (μm)

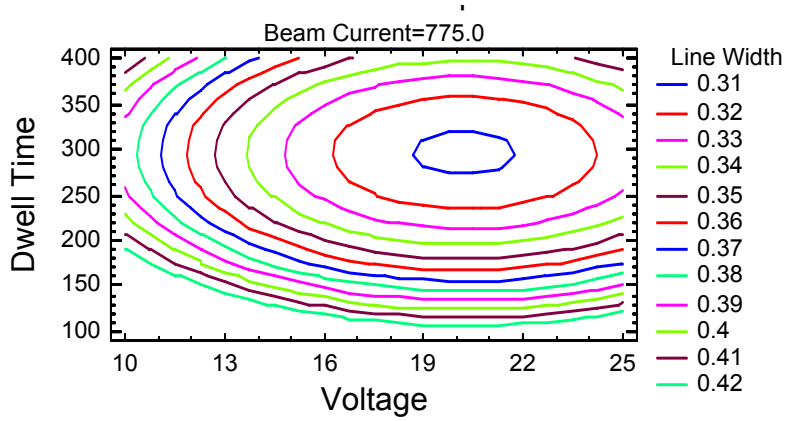

(c) Response Contours for Line Width (μm) for Constant Beam Current

Figure 4-22. Analysis Results for Line Width for Pt Central Composite Line Experiments: (a) Standardized Pareto Chart (b) Main Effects Plot (c) Response Contours

4.2.8. Platinum 2^3 Factorial Line Time Study

The effects of varying the line time were investigated as part of a two level, three variable factorial study. The line time denotes the time required for the beam to return to a specific pixel, so it is a direct way to quantify the time that reagent gas molecules have to adsorb in a specific area before the beam returns there. The variables investigated were line time, voltage, and beam current. The levels used for the variables were 10 and 30 kV for voltage, 100 and 5400 pA for beam current, and 0.53 and 2.12 ms for line time. The fixed settings for these experiments were a working distance of 10.1 mm, a deposition time of 20 min, a magnification of 15,000x, and a dwell time of 1 μs. Holding the dwell time fixed means its effects do not influence those of the line time. Holding the magnification fixed means that the beam scans along the same length for all the trials, but this also means that a specific line time has a specific number of scans associated with it for a constant deposition time. This means that a shorter line time would complete more scans than a longer line time for a constant overall deposition time. This discrepancy was factored out by dividing the measured heights and widths by the number of scans performed. For the low level setting of 0.53 ms for the line time and a 20 minute deposition time, approximately 2.18×10^6 scans were completed. For the high level line time setting of 2.12 ms, approximately 5.77×10^5 scans were completed for a 20 minute deposition time. The experimental settings and recorded measurements are shown in Table 4-7. Images of the line deposits with measurements are shown in Appendix A.9.

Table 4-7. Experimental Settings and Measurements for Pt Line Time 2^3 Factorial Study

Trial	Voltage (kV)	Beam Current (pA)	Line Time (ms)	Line Height (μm)	Line Width (μm)	Height/scan (μm/scan)
1	30	5400	0.53	0.596	0.66	2.73167E-07
2	30	100	0.53	0.187	0.647	8.57083E-08
3	10	100	0.53	0.293	0.627	1.34292E-07
4	10	5400	0.53	0.646	0.879	2.96083E-07
5	30	100	2.12	0.215	0.64	3.72667E-07
6	30	5400	2.12	0.442	0.601	7.66133E-07
7	10	100	2.12	0.309	0.476	5.356E-07
8	10	5400	2.12	0.781	0.898	1.35373E-06

The height/scan values were multiplied by 10^6 to increase their magnitude to allow for full analysis in the software. Analysis was performed in STATGRAPHICS, and the results indicated no interaction between any of the variables. Initial analysis indicated that P-values for the interaction terms were all greater than 0.30, so these terms were excluded from the final analysis. The final analysis was thus performed for just the three main variables. The results for the measured line height/scan are shown in Figure 4-23. ANOVA results are shown in Appendix B.

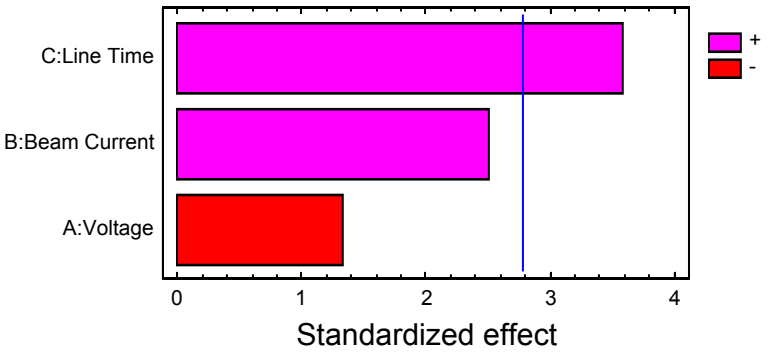

(a) Standardized Pareto Chart for Height/scan (μm/scan) x 10^6

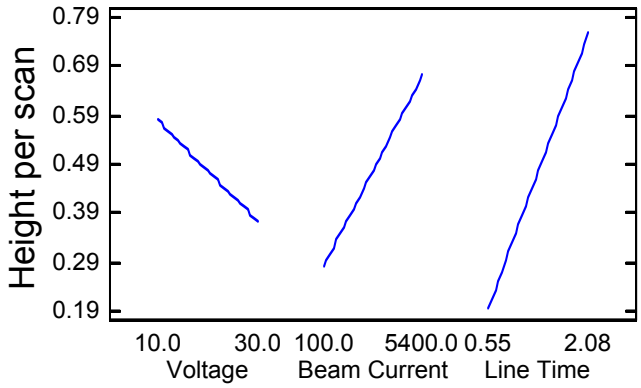

(b) Main Effects Plot for Height/scan (μm/scan) x 10^6

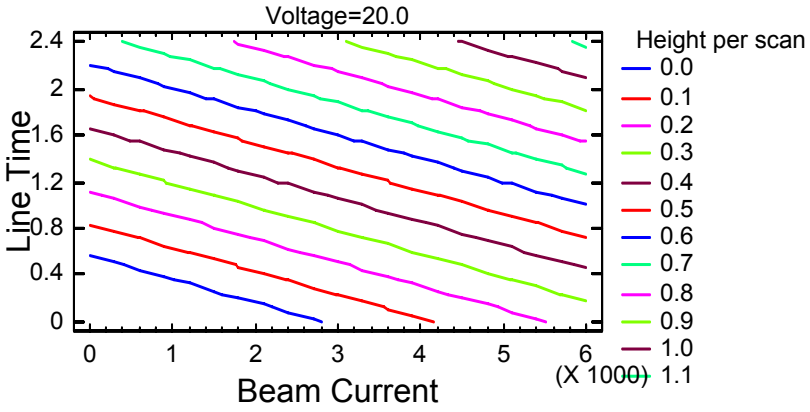

(c) Response Contours for Constant Voltage for Height/scan (μm/scan) x 10^6

Figure 4-23. Analysis Results for Height/scan for Pt 2^3 Line Time Trials: (a) Standardized Pareto Chart (b) Main Effects Plot (c) Response Contours

As shown, the line time was the only variable found to be significant at the 95% confidence level. The illustrated effects of the line time indicate that increasing the time for the reagent molecules to adsorb on the surface has a significant effect on the vertical deposition rate. The general trends in the data are indicated in the main effects plot, with the beam current possibly leading to an increase in deposited height/scan. The correlation coefficient for the model was 83.8%.

The results for the analysis with line width as the response variable are shown in Figure 4-24. ANOVA results are shown in Appendix B. Initial analysis indicated P-values in excess of 0.68 for two of the interaction terms, so these terms were excluded. The line width trends differ from those for height/scan, with both the beam current and the voltage-beam current interaction terms being statistically significant at the 95% confidence level. The main effects plot illustrates the general trends of a decrease in line width corresponding to an increase in voltage, and an increase in line width corresponding to an increase in beam current. The correlation coefficient was 94.0%.

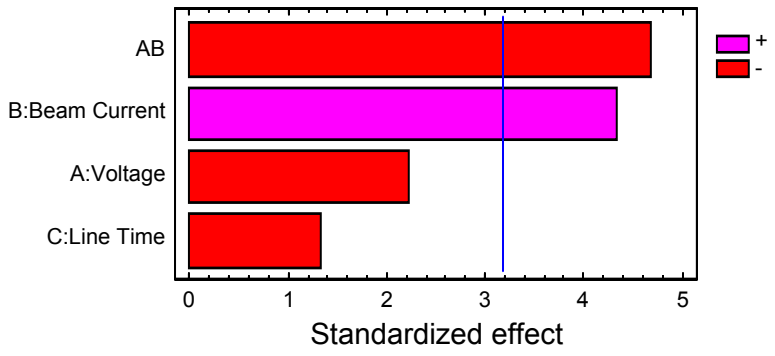

(a) Standardized Pareto Chart for Line Width

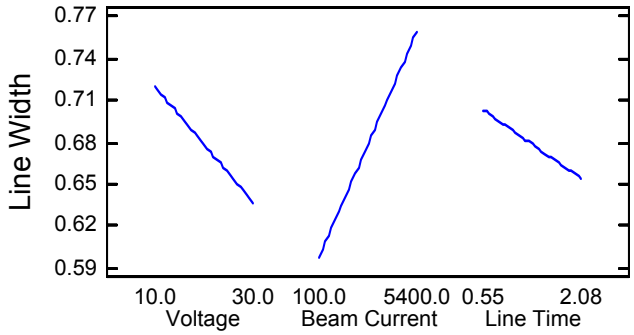

(b) Main Effects Plot for Line Width (μm)

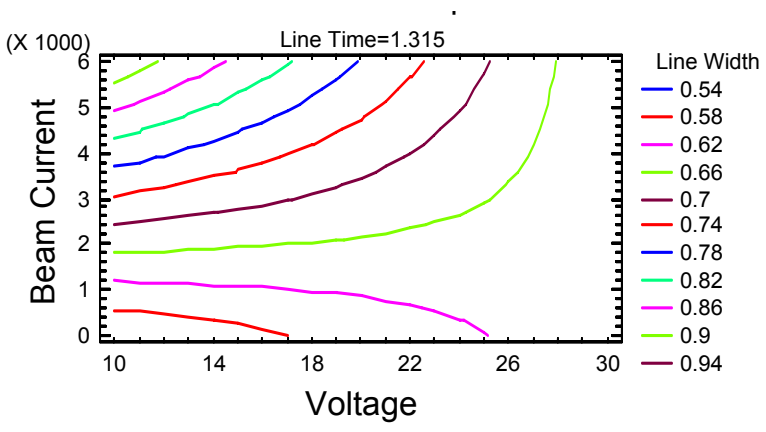

(c) Response Contours for Constant Line Time for Line Width (μm)

Figure 4-24. Analysis Results for Line Width for Pt 2^3 Line Time Trials: (a) Standardized Pareto Chart (b) Main Effects Plot (c) Response Contours

4.2.9. Platinum 2^3 Factorial Dwell Time Study

A two level, three factor study was performed to investigate the effects of varying the dwell time while holding the line time constant. The dwell time was varied by adjusting the pixel resolution settings, which means that there is only a limited range over which this variable can be investigated. The other factors studied were voltage and beam current. The factor levels were 10 and 30 kV for the voltage, 100 and 5400 pA for the beam current, and 0.25 and 1.0 ms for the dwell time. Fixed settings were a line time of 512 ms, a magnification of 15,000x, a working distance of 10.1 mm, and a deposition time of 20 minutes. The factor settings and measurements are listed in Table 4-8. Images of the deposits with measurements are shown in Appendix A.10.

Table 4-8. Experimental Settings and Measurements for Pt Factorial Dwell Time Study

Trial	Voltage (kV)	Beam Current (pA)	Dwell Time (ms)	Line Height (μm)	Line Width (μm)
T1	30	5400	.25	0.271	0.321
T2	10	100	1.0	0.126	0.203
T3	30	100	1.0	0.148	0.250
T4	10	5400	.25	0.304	0.490
T5	10	100	.25	0.086	0.264
T6	30	5400	1.0	0.179	0.396
T7	30	100	.25	0.095	0.236
T8	10	5400	1.0	0.244	0.371

Since the line time was held constant throughout this experiment, the same number of scans were performed for each deposition. The height/scan parameter was therefore not needed, and the line height was analyzed in STATGRAPHICS. Initial analysis with all interaction terms indicated that two of the interaction terms had P-values greater than 0.42. These terms were excluded for the final analysis. Results for the final analysis for the line height are shown in Figure 4-25. ANOVA results for this analysis are shown in Appendix B.

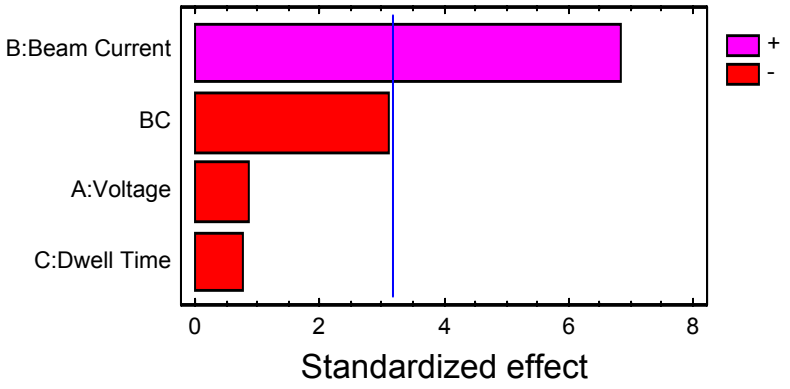

(a) Standardized Pareto Chart for Line Height

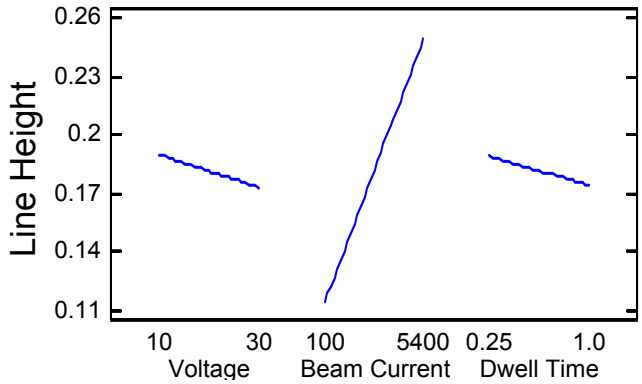

(b) Main Effects Plot for Line Height (µm)

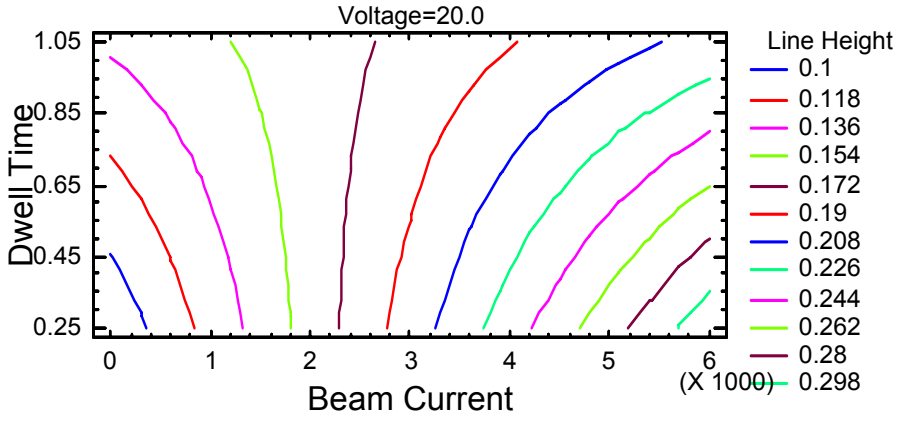

(d) Response Contours for Line Height (µm) for Constant Dwell Time

Figure 4-25. Analysis Results for Line Height for Pt Factorial Dwell Time Study: (a) Standardized Pareto Chart (b) Main Effects Plot (c) Response Contours

As shown, only the beam current was found to be statistically significant at the 95% confidence level. The dwell time appears to have the least effect of all of the factors, with a P-value of 0.513. The factor of interest for this study, the dwell time, was not shown to have a significant effect on the line height. The correlation coefficient was 95.0%.

The line width was also analyzed as a response variable, and initial results with all of the interaction terms indicated that two of these terms had P-values greater than 0.40, so these terms were excluded from the final analysis. The results for the final analysis for the line width are shown in Figure 4-26. ANOVA results are shown in Appendix B. As shown, the beam current was the only process variable to have a statistically significant effect at the 95% confidence level for the line width. An increase in beam current corresponded to an increase in line width. These results are logical, since a high beam current corresponds to a larger beam diameter, which would lead to a wider deposit. The dwell time was not shown to have a statistically significant effect on the line width, and it appeared to be the least influential factor, as it had the largest P-value of all of the factors (0.492). The correlation coefficient for this analysis was 92.3%.

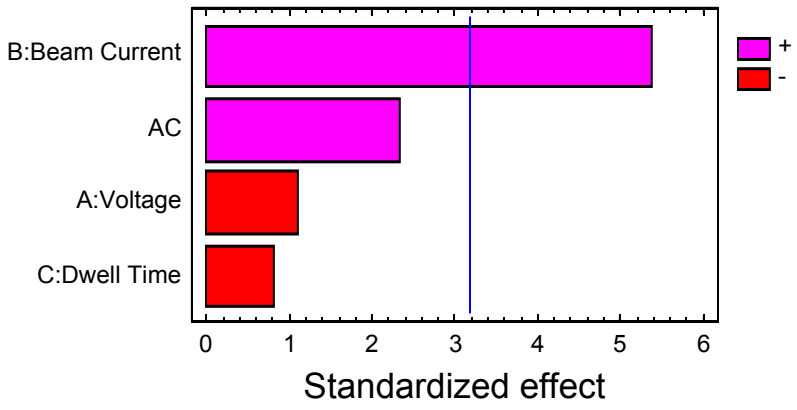

(a) Standardized Pareto Chart for Line Width

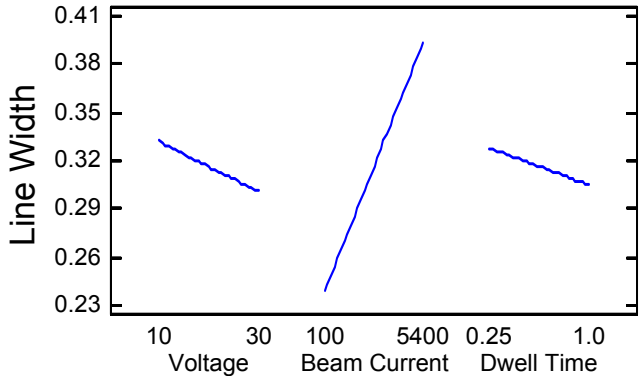

(b) Main Effects Plot for Line Width (µm)

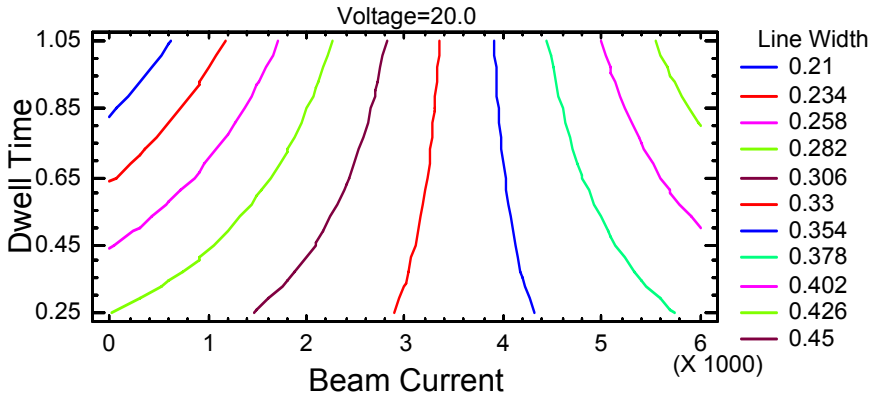

(b) Response Contours for Line Width (µm) for Constant Dwell Time

Figure 4-26. Analysis Results for Line Width for Pt Factorial Dwell Time Study: (a) Standardized Pareto Chart (b) Main Effects Plot (c) Response Contours

4.2.10. Optimization of Platinum Lines and Fiber Deposition

Optimization analysis was performed using STATGRAPHICS for several parameters. That is, STATGRAPHICS was used to predict process variable settings which should yield optimum results. The aspect ratios of both platinum line and fiber deposits were optimized by running a multiple response optimization to maximize deposit height and minimize width/base diameter. Optimization analyses were also performed for the fiber deposition rate (through maximizing both vertical and base diameter growth rates) and minimum line width parameters. One of the objectives of this optimization was to give insight into better control of deposit geometry. Certain geometric characteristics are preferable for specific applications. High aspect ratio line or fiber deposits may be preferable, an example of which are fibers deposited on AFM tips to improve resolution.[38] The central composite design fiber and line experiments were used for the optimization analyses, as they provided the most accurate illustration of the factor effects. The disadvantage of using the central composite experiments in this manner is that they covered a smaller range of values for the factors, especially the beam current. Analysis for optimization of the platinum fiber aspect ratio provided settings of 29 kV for voltage, 1378 pA for beam current, and 15.1 minutes for deposition time to maximize height and minimize base diameter. The beam current suggested is near the higher end (1490 pA) of the values used for the original experiment. For comparison, more depositions were made with a higher beam current (5400 pA), but with the other settings identical. The settings suggested to maximize line height and minimize line width at the same time were 30 kV, 1484 pA, and 177 μs dwell time (181 ms line time). The voltage and beam current suggested for optimization were virtually the upper limits for the analysis, so the

beam current was increased to 5400 pA and more depositions were made for comparison. For single parameter optimization, the minimum line width was investigated. Optimization analysis suggested settings of 15.8 kV, 60.2 pA, and 423 μs dwell time (433 ms line time). Experiments were conducted at these settings, and the beam current was lowered (while keeping the other factors the same) and two more lines were deposited. These were done at a beam current of approximately 20 pA, since the value recommended by the optimization analysis was the minimal value used for the central composite experiment. The fiber deposition rate was also analyzed, and the suggested settings from the central composite experiment were 14.5 kV, 1100 pA, and 0.59 minutes for the deposition time. The short deposition time suggested indicates the prominent role this factor plays in the deposition rates. Since the effects of the deposition time are known and have already been investigated in detail, it was determined that the deposition time used for the optimization experiments should be increased to allow for larger deposit size. Optimization analyses were therefore performed on the two factorial platinum fiber experiments, and results for both indicated suggested settings of minimum voltage, maximum beam current, and minimum deposition time (5 minutes). Depositions were thus performed at the optimal settings given by the factorial experiments, since these had a larger minimum time value. Fixed settings used for all of the fiber optimization experiments were a working distance of 10.1 mm and a magnification of 6,000x. Fixed settings for all of the line optimization experiments were a working distance of 10.1 mm, a magnification of 15,000x, and a deposition time of 20 minutes. The optimization experimental settings and measurements are detailed in Table 4-9 for line optimization

and in Table 4-10 for fiber optimization. Images with measurements are shown in Appendix A.11.

Table 4-9. Experimental Settings and Measurements for Pt Line Optimization

Trial	Voltage (kV)	Beam Current (pA)	Line Time (ms)	Dwell Time (μs)	Line Height (μm)	Line Width (μm)	Aspect Ratio
TLAR1	30	1485	0.363	177.2	0.16	0.495	0.323
TLAR2	30	1485	0.363	177.2	0.185	0.456	0.406
TLAR3	30	5400	0.363	177.2	0.637	0.409	1.557
TLAR4	30	5400	0.363	177.2	0.551	0.370	1.489
TLW1	15.8	60.2	0.867	423.2	----	0.203	----
TLW2	15.8	60.2	0.867	423.2	----	0.196	----
TLW3	15.8	20	0.867	423.2	----	0.177	----
TLW4	15.8	20	0.867	423.2	----	0.182	----

Table 4-10. Experimental Settings and Measurements for Pt Fiber Optimization

Trial	Voltage (kV)	Beam Current (pA)	Dep. Time (min)	Fiber Height (μm)	Fiber Base Dia. (μm)	Aspect Ratio	VGR (μm/min)	BDGR (μm/min)
TFAR1	29	1378	15.1	0.766	0.971	0.789	----	----
TFAR2	29	1378	15.1	1.422	0.628	2.264	----	----
TFAR3	29	5400	15.1	2.219	0.713	3.112	----	----
TFAR4	29	5400	15.1	2.065	0.611	3.380	----	----
TFGR3	10	5400	5	1.440	0.714	----	0.288	0.143
TFGR4	10	5400	5	1.477	0.735	----	0.295	0.147
TFGR5	5	20000	5	2.399	2.077	----	0.480	0.415
TFGR6	5	20000	5	2.669	1.871	----	0.534	0.374
Note: VGR = Fiber Vertical Growth Rate; BDGR = Fiber Base Diameter Growth Rate								

The results listed in Table 4-9 for the line optimization experiments show that increasing the beam current leads to a considerable increase in the aspect ratio for the lines (shown in trials TLAR1 to TLAR4). The minimum line width experiments (trials TLW1 to TLW4) show that the line width was approximately 200 nm for the two experiments performed at the suggested optimization settings, and under 185 nm for the experiments performed at the lower beam current.

The results listed in Table 4-10 for the fiber optimization experiments show that increasing the beam current leads to an increase in the fiber aspect ratio (shown in trials TFAR1 to TFAR4). This is in agreement with the previously discussed line optimization experiments, with high voltage and high beam current leading to higher aspect ratios. The fiber growth rate optimization experiments, listed in trials TFGR3 through TFGR6, show that the highest growth rates were obtained for low voltage and high beam current. At the current levels investigated, it is not possible to obtain sub-micron feature sizes when at the 5 kV voltage level, since the beam diameter is greater than 1 μm at these settings.

4.2.11. Platinum Deposit TEM Analysis and Results

Platinum fibers were deposited on a copper TEM grid in a 2^2 factorial design with the variables being the voltage and beam current. The voltage values used were 10 and 30 kV, and the beam current values were 10 and 1000 pA. The deposits were made by tilting the copper grid to a 40^o angle so that the inner walls of the grid were visible (i.e., deposits were made on the approximately 20 μm thickness dimension of the grids). The fibers were thus deposited in such a manner that when the grid was mounted for analysis in the TEM, the fiber extended into open space, as illustrated in Figure 4-27. Views of the individual fibers are shown in Figure 4-28.

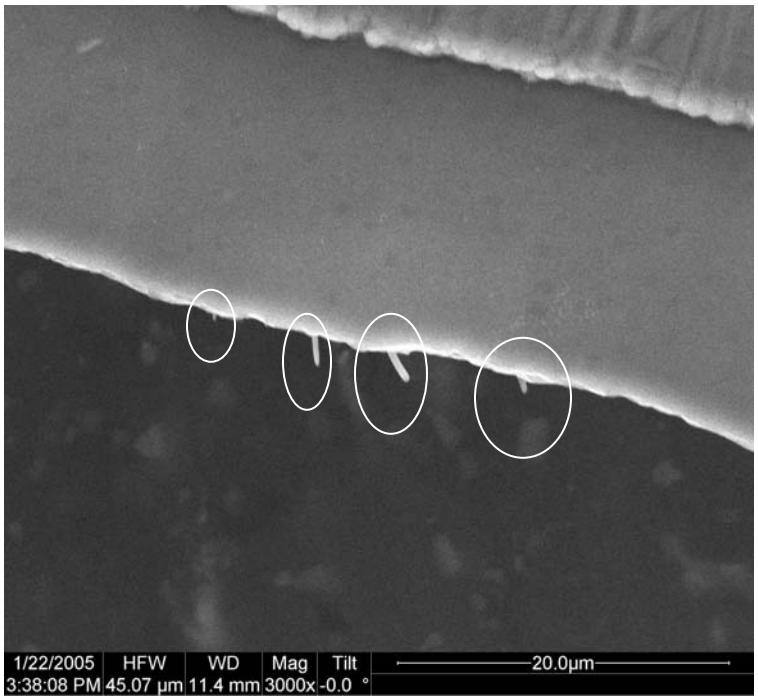

Figure 4-27. Overhead View of Pt Fiber Deposits on Inner Wall of Cu TEM Grid

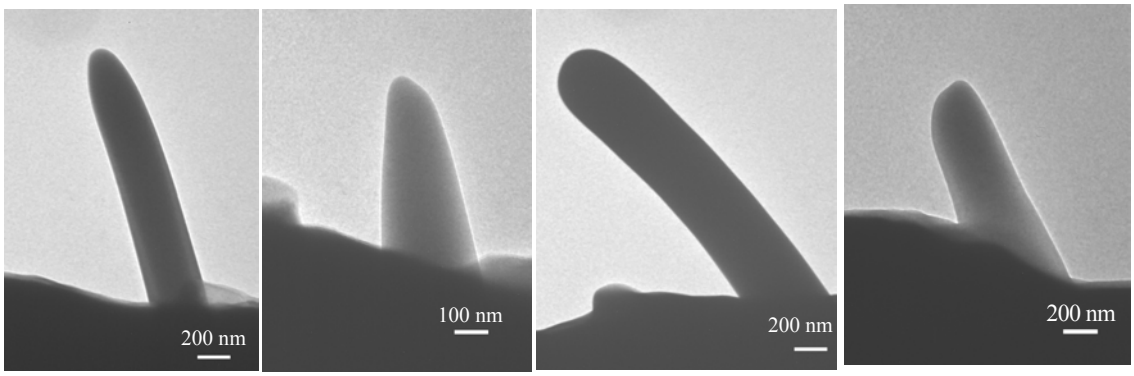

Figure 4-28. Platinum Fiber Deposits used for TEM Analysis

Electron Dispersive Spectroscopy (EDS) was performed on each of the platinum fibers. Results indicated 100% Pt content with no discernable carbon content for each fiber. This result differs from previously reported results using similar reagents, which found the Pt content to be on the order of 20%, with more than 70% C content.[16,26-28] The reagent used for the previously reported depositions was $(CH_3)_3Pt(Cp)$, while the one used for the experiments performed here was $(CH_3)_3Pt(CpCH_3)$. The previously reported

deposits were found to consist of Pt nanocrystals (of approximately 2 nm size) in an amorphous C matrix. TEM analysis of the Pt deposits made in the Georgia Tech EBCVD system were found to be amorphous, also differing from previously reported results for Pt deposition. EDS results for a single fiber are shown in Figure 4-29. A TEM image of the amorphous Pt for a single fiber is shown in Figure 4-30. The results for content and structure were the same for every fiber.

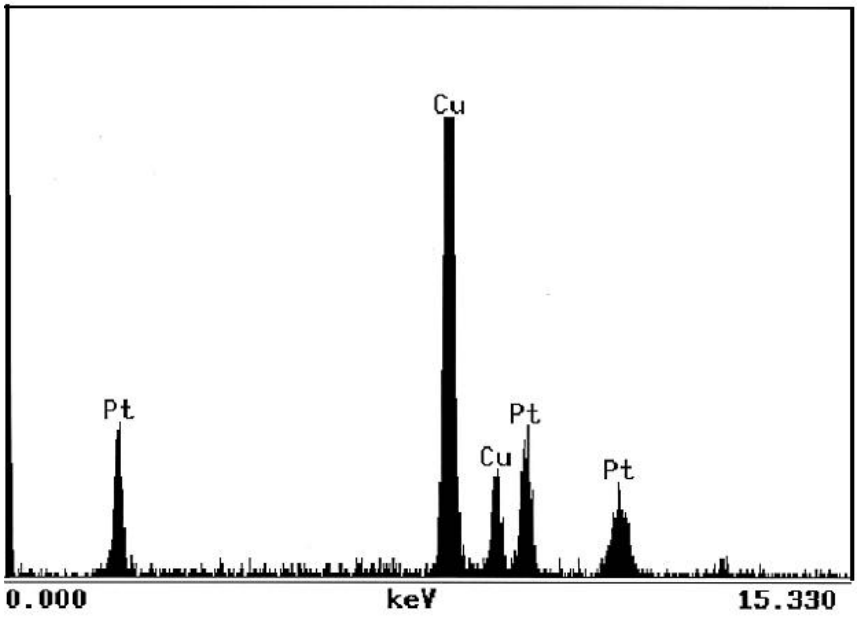

Figure 4-29. EDS of a Platinum Fiber Deposited on a Cu TEM grid

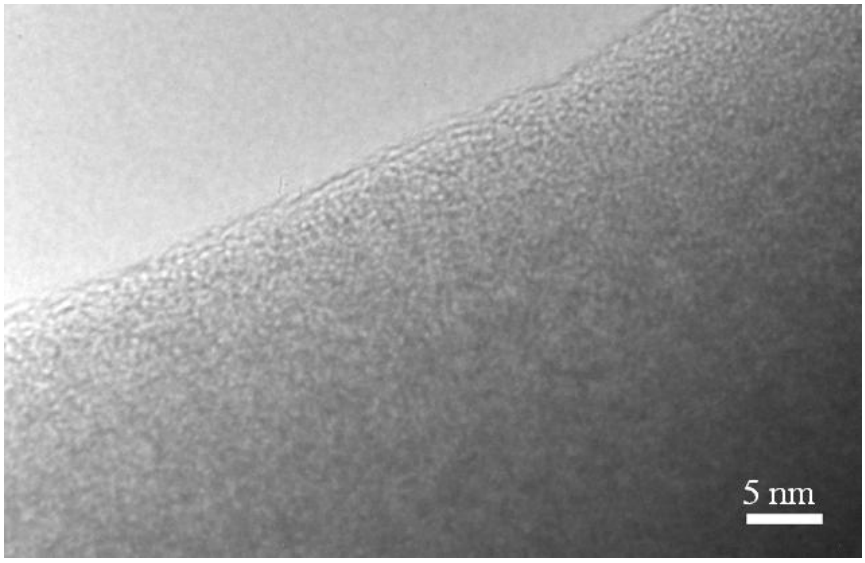

Figure 4-30. TEM Image of Amorphous Platinum Fiber Deposit

Four more platinum fiber deposits were made in a similar fashion as was described earlier, with a 2^2 factorial design. This time, however, voltage settings were 5 and 30 kV and beam current settings were 100 and 5400 pA. Electron Energy Loss Spectroscopy (EELS) was performed on these deposits, and the results are shown in Figure 4-31. As shown, there was a very weak peak for carbon around 284 eV which was attributed to carbon contamination at the surface of the fiber that occurred during when the spectra was acquired. The platinum deposits were again found to be composed only of Pt and were amorphous. Figure 4-32 shows the electron diffraction patterns that were recorded. Discrepancies from previously reported results could be due to the inadvertent presence of water vapor in the chamber, but this is speculation. Operating in the Environmental mode with water vapor in the chamber during Au deposition has been shown to greatly improve the metal content.[14,35,36]

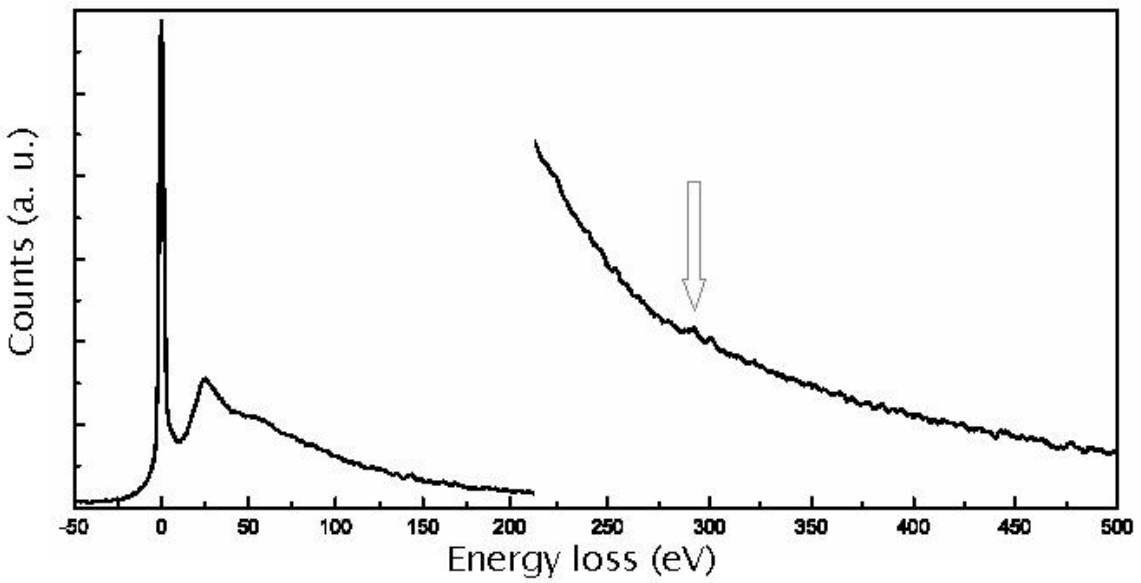

Figure 4-31. EELS for Platinum Fiber Deposit (Arrow Indicates Weak Carbon Peak)

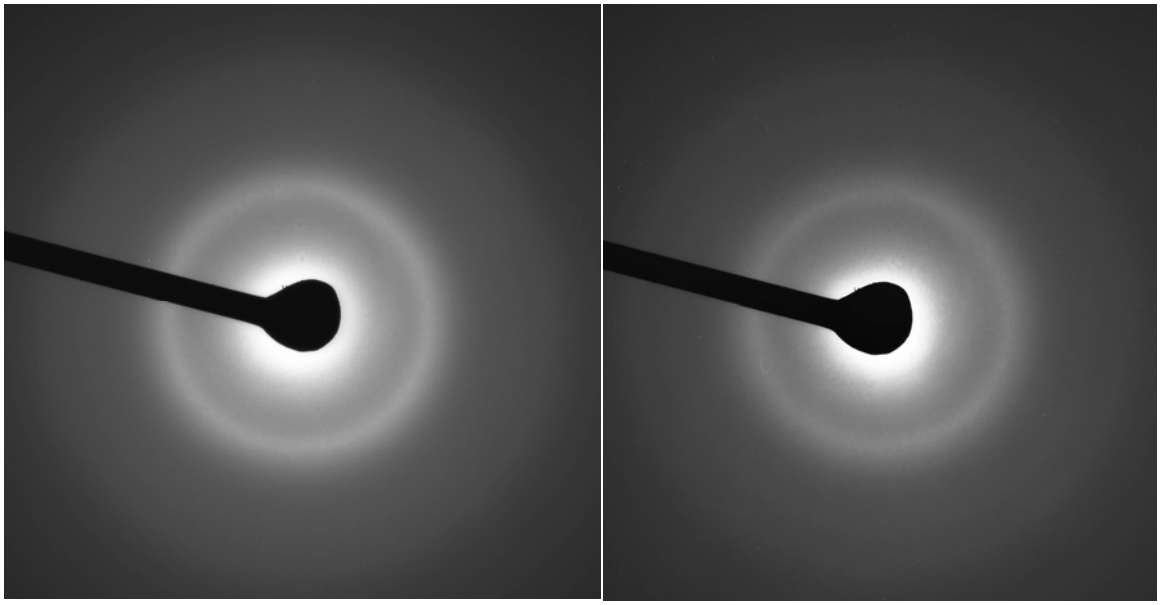

Figure 4-32. Electron Diffraction Patterns Recorded for Platinum Fibers

4.2.12. 3D Platinum Fiber Structure

Two platinum fibers were deposited to from a three-dimensional structure. Both fibers were deposited with a 30 kV beam with a spot size of 3.0 (corresponding to a beam

current of approximately 100 pA). The base fiber was deposited in the normal manner, with the substrate surface being perpendicular to the electron beam (i.e., 0^o tilt). The deposition time used was 10 minutes. The second fiber was grown by tilting the substrate to a 40^o angle and focusing the electron beam on the tip of the now tilted fiber. A 40 minute deposition time was used, and a second angled fiber was grown from the tip location of the original vertical fiber. The results are shown in Figure 4-33. As shown, the growth rate for the second fiber was significantly slower than that for the original fiber. This discrepancy is attributable to the difference in secondary electron emission with regards to the two depositions. The original fiber was deposited with the electron beam impinging directly upon the Si substrate, while the second fiber had the electron beam focused only on the original fiber. This experiment further illustrates the importance of secondary electron emission on the deposition process.

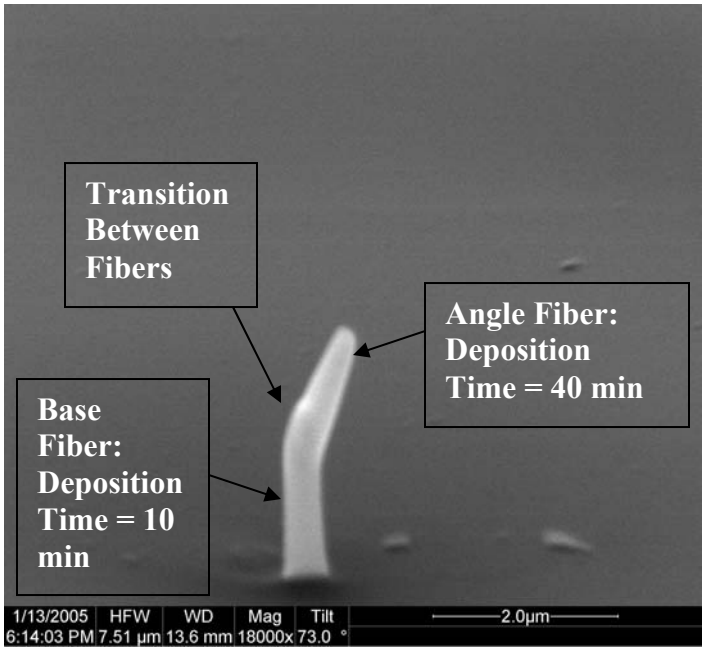

Figure 4-33. Two-Fiber Platinum Structure

4.3. Carbon Deposition Experiments

4.3.1. Carbon Deposition Rate Study

The deposition rate for carbon fibers from the methane-argon mixture was studied by holding the voltage and spot size fixed and varying the deposition time. Fibers were chosen for the study of deposition rate due to the shorter deposition times required in comparison with line deposits. A voltage of 30 kV and a spot size of 3.0 were used, along with deposition times of 1, 2, 3, 4, 5, 7, 10, 12, and 15 minutes. The resulting fibers were examined, and measurements were taken from images of the profiles of the fibers for the base diameter and the height. Images of the fibers with measurements are shown in Appendix A.12. The values for vertical growth rate vs. deposition time are shown in Figure 4-34. Figure 4-35 shows the fiber bottom diameter growth rate vs. deposition time. The deposition rates for carbon, especially the vertical growth rate, were noticeably less than those for the Pt fiber experiments.

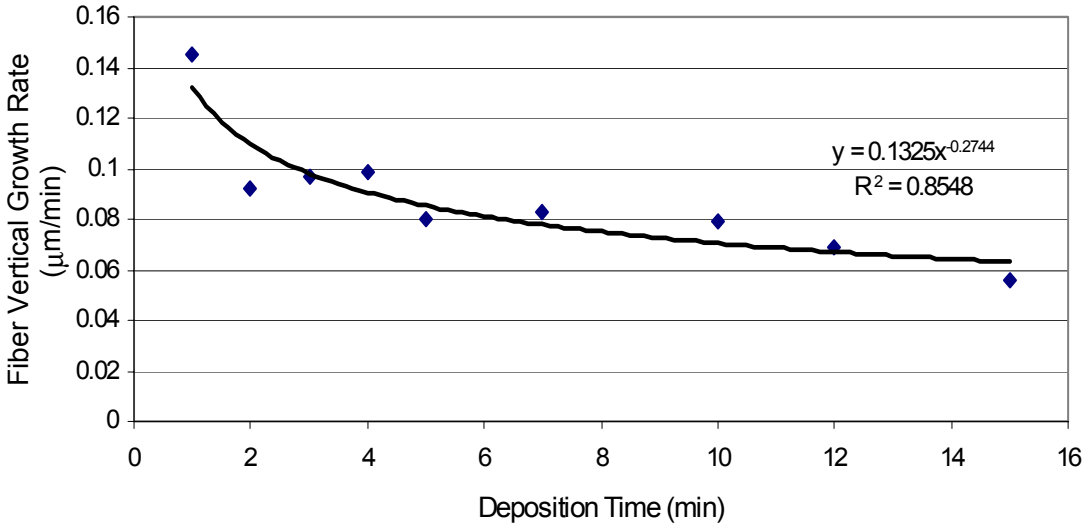

Figure 4-34. Carbon Fiber Vertical Growth Rate vs. Deposition Time

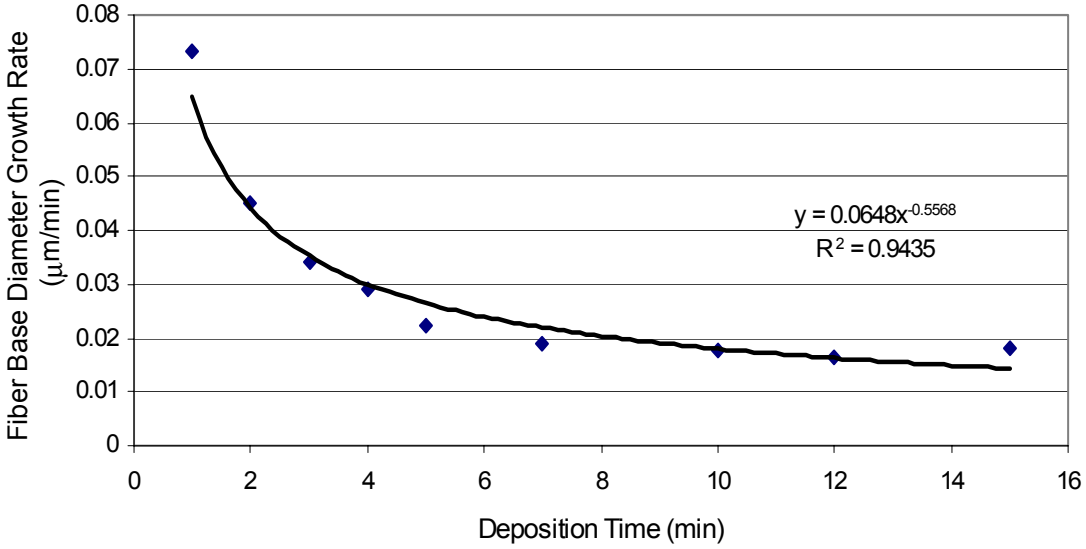

Figure 4-35. Carbon Fiber Base Diameter Growth Rate vs. Deposition Time

4.3.2. Carbon Fiber Exploratory Trials

Exploratory experiments were performed for carbon fiber deposition from the methane-argon mixture. These experiments consisted of two separate two factor, two level studies, with the beam current and chamber pressure being the factors of interest. One study was performed for a voltage of 30 kV, and the beam current levels were 100 and 1500 pA. The second study was performed at 10 kV, and the beam current levels were 16.4 and 240 pA. The chamber pressure factor levels for both studies were 0.1 and 1.0 Torr. Fixed settings were a working distance of 10.0 mm, a magnification of 6,000x, and a deposition time of 20 minutes. All eight depositions were performed in a random order in the same sitting. The experimental settings and fiber measurements are listed in Table 4-11. Images of the fibers with measurements are shown in Appendix A.13.

Table 4-11. Settings and Measurements for Exploratory Carbon Fiber Deposition Trials

Trial	Voltage (kV)	Beam Current (pA)	Chamber Pressure (Torr)	Fiber Height (μm)	Fiber Base Diameter (μm)
T1	10	16.4	0.1	1.208	0.290
T2	30	100	0.1	0.987	0.484
T3	30	1500	1.0	0.637	0.488
T4	10	240	1.0	1.036	0.361
T5	30	1500	0.1	0.234	0.314
T6	10	240	0.1	0.484	0.441
T7	30	100	1.0	1.04	0.340
T8	10	16.4	1.0	0.209	0.104

Analysis results for the fiber height for the 30 kV exploratory study are shown in Figure 4-36. As shown, the beam current appears to have the largest effect, with an increase in beam current corresponding to a decrease in fiber height. The chamber pressure appeared to correspond to an increase in fiber height.

Analysis results for the fiber base diameter for the 30 kV, exploratory study are shown in Figure 4-37. The beam current-chamber pressure interaction term appears to have the largest effect from the Pareto Chart. As shown in the main effects plot, the base diameter appears to decrease with increasing beam current and increase with increasing chamber pressure.

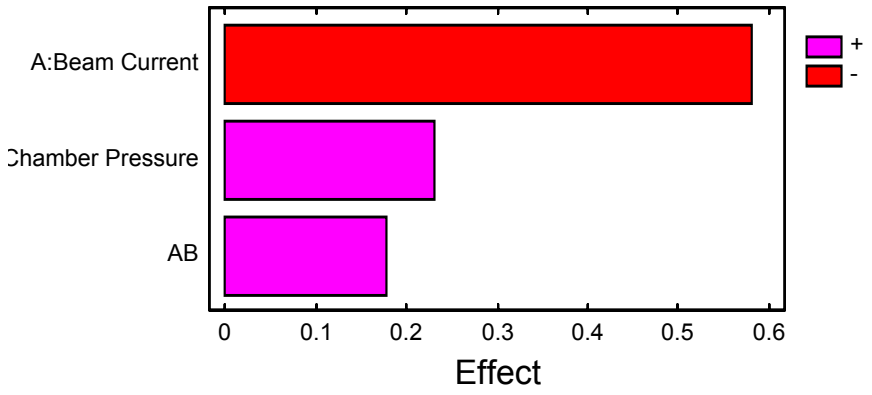

(a) Pareto Chart for Carbon Fiber Height

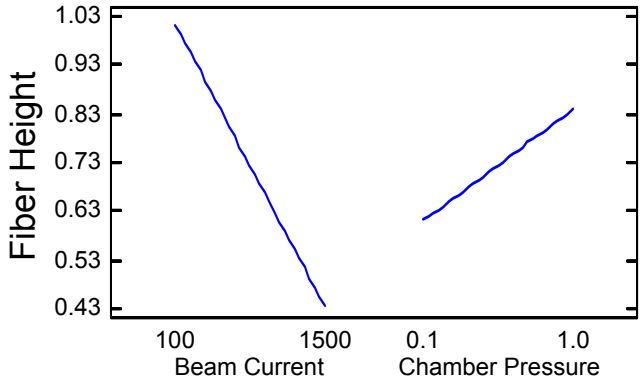

(b) Main Effects Plot for Carbon Fiber Height (μm)

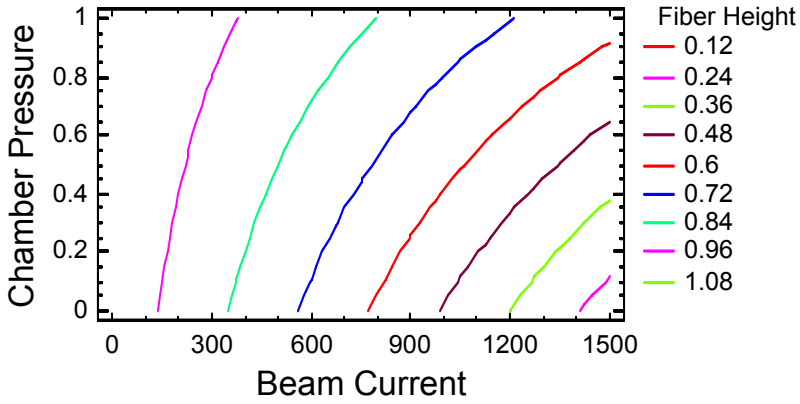

(c) Response Contours for Carbon Fiber Height (μm)

Figure 4-36. Analysis Results for Carbon Fiber Height for 30 kV 2^2 Exploratory Study: (a) Pareto Chart (b) Main Effects Plot (c) Response Contours

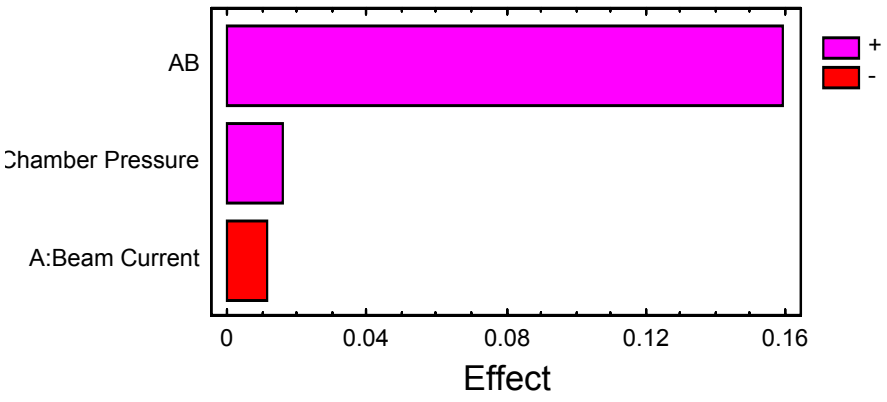

(a) Pareto Chart for Carbon Fiber Base Diameter

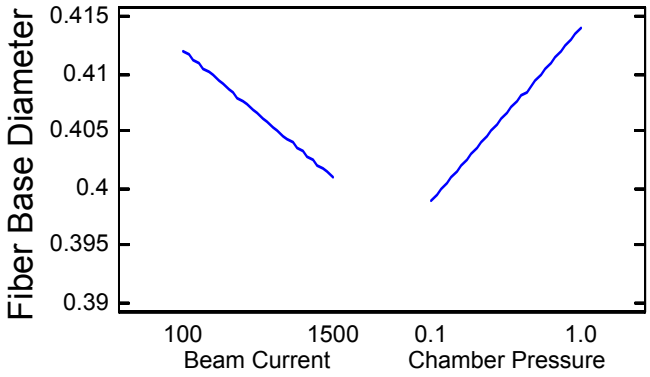

(b) Main Effects Plot for Carbon Fiber Base Diameter (µm)

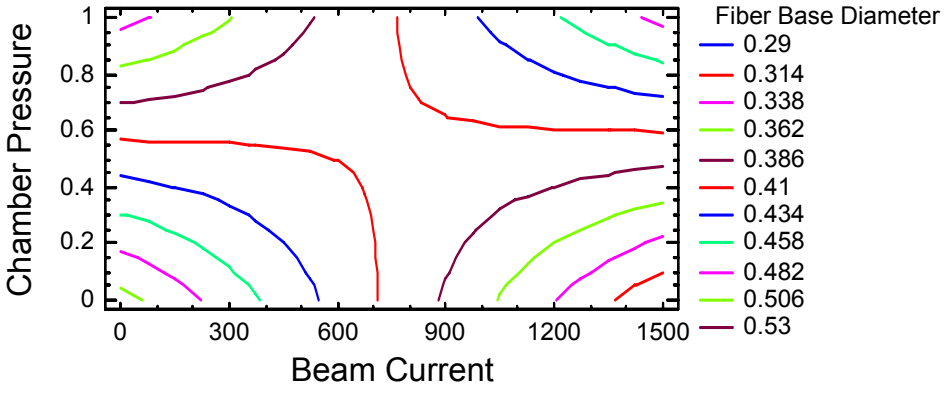

(c) Response Contours for Carbon Fiber Base Diameter (µm)

Figure 4-37. Analysis Results for Carbon Fiber Base Diameter for 30 kV 2^2 Exploratory Study: (a) Pareto Chart (b) Main Effects Plot (c) Response Contours

Analysis results for the fiber height for the 10 kV exploratory study are shown in Figure 4-38. As shown, the beam current-chamber pressure interaction term again appears to be the most important factor. As shown in the main effects plot, the fiber height appears to increase slightly with increasing beam current and decrease sharply with increasing chamber pressure. These general trends seem to be opposite those for the 30 kV study, although the range of beam currents investigated was smaller here.

Analysis results for the fiber base diameter for the 10 kV exploratory study are shown in Figure 4-39. As shown, the beam current appears to have the largest effect. The general trends in the data appear to be an increase in base diameter with increasing beam current and a decrease in base diameter with increasing chamber pressure. These trends seem to be opposite those for the 30 kV study, although there was a smaller current range studied here.

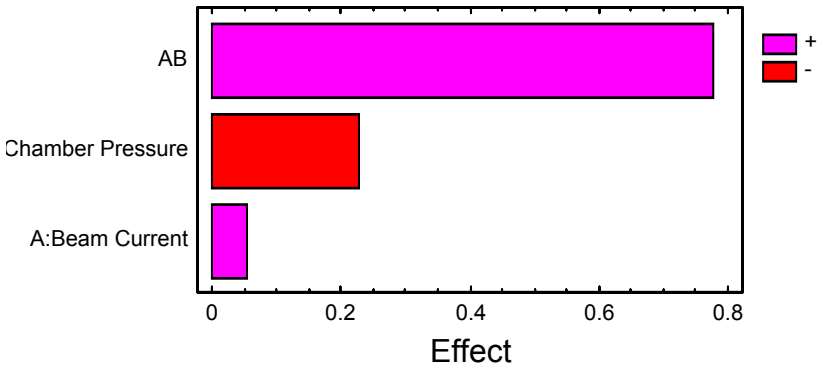

(a) Pareto Chart for Carbon Fiber Height

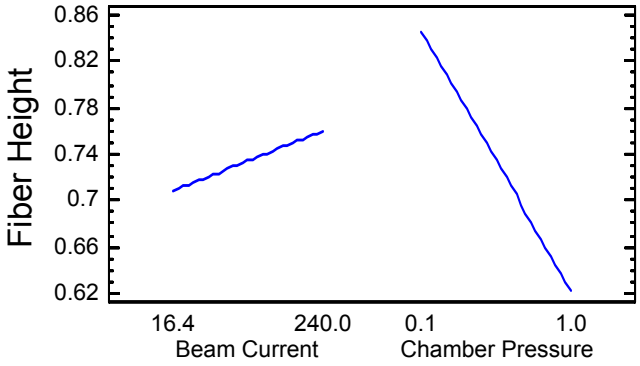

(b) Main Effects Plot for Carbon Fiber Height (μm)

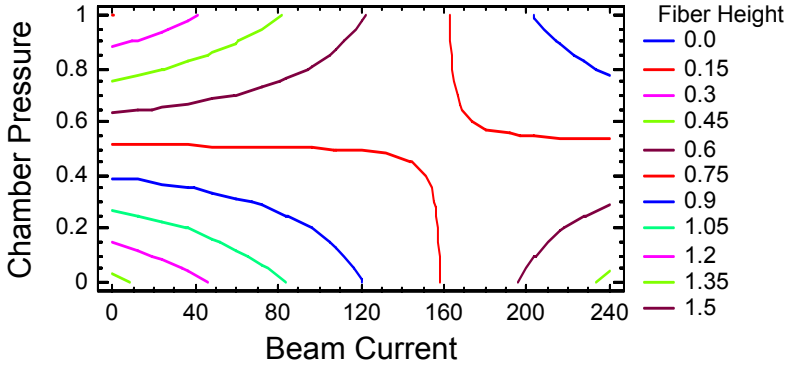

(c) Response Contours for Carbon Fiber Height (μm)

Figure 4-38. Analysis Results for Carbon Fiber Height for 10 kV 2^2 Exploratory Study: (a) Pareto Chart (b) Main Effects Plot (c) Response Contours

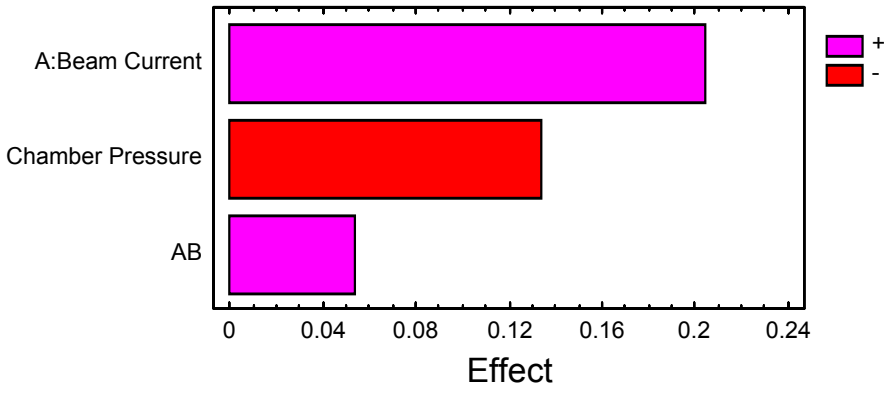

(a) Pareto Chart for Carbon Fiber Base Diameter

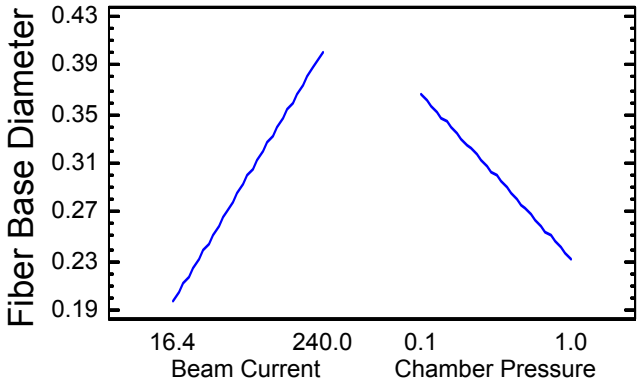

(b) Main Effects Plot for Carbon Fiber Base Diameter (µm)

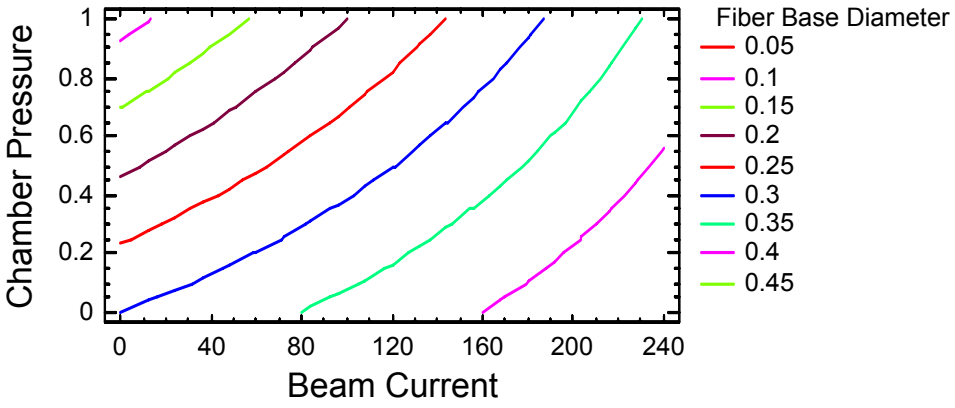

(c) Response Contours for Carbon Fiber Base Diameter (µm)

Figure 4-39. Analysis Results for Carbon Fiber Base Diameter for 10 kV 2^2 Exploratory Study: (a) Pareto Chart (b) Main Effects Plot (c) Response Contours

4.3.3. Carbon 2^3 Factorial Line Deposition Study

Two level, three factor trials were completed for carbon deposition from the methane-argon mixture. The variables used were the same as for the Pt line trials: voltage, beam current, and the dwell/line time. The high and low settings for each variable were 10 and 30 kV for voltage, 50 and 5400 pA for beam current, and 10 and 1000 μs for dwell time (with corresponding 10.60 and 1060 ms line times). Fixed settings for the trials were a chamber pressure of 1.0 Torr, a magnification of 40,000x, a working distance of 10.0 mm, and a deposition time of 45 minutes. Initial experiments were attempted at 5 kV, but these were very unsuccessful due to the difficulty in adequately focusing the beam for this lower voltage at the high magnification required to produce sizable deposits. The experimental settings and subsequent deposit measurements recorded are listed in Table 4-12. Images of the lines with measurements are shown in Appendix A.14.

Table 4-12. Experimental Settings and Measurements for Carbon 2^3 Line Deposition Study

Trial	Voltage (kV)	Beam Current (pA)	Dwell Time (μs)	Line Time (ms)	Line Height (μm)	Line Width (μm)
T1	10	5400	1000	1060	0.15	0.576
T2	10	50	10	10.60	0.076	0.227
T3	30	50	10	10.60	0.125	0.165
T4	30	5400	1000	1060	0.112	0.368
T5	30	50	1000	1060	0.227	0.209
T6	10	50	1000	1060	0.081	0.244
T7	10	5400	10	10.60	0.154	0.464
T8	30	5400	10	10.60	0.106	0.341

The total number of scans completed for each line deposition were calculated, using the line time values, to be approximately 255,000 and 2,550 for the 10.60 ms and 1060 ms line times, respectively. The measured heights were then divided by the corresponding

number of scans performed to give values for the height/scan. These values, along with the recorded line widths, were analyzed using STATGRAPHICS.

The only variable found to be statistically significant at the 95% confidence level was the dwell/line time. Initial analysis indicated the interaction terms had P-values of 0.50, 0.66, and 0.84, indicating they were not statistically significant. As such, these terms were excluded from the final analysis. Final analysis results are shown in Figure 4-40. ANOVA results are shown in Appendix B. The general trends are indicated in the main effects plot, with the dwell/line time being the only variable that has a significant effect on the vertical deposition rate. The correlation coefficient was 80.3%.

Final analysis results for the line width as the response variable are shown in Figure 4-41. ANOVA results are shown in Appendix B. As shown, the variables that have the largest influence on the deposit width are the beam current and the voltage, both of which are significant to a 95% confidence level. The interaction terms were excluded, as initial analysis revealed P-values of 0.28, 0.70, and 0.61 for these terms. The exclusion of these terms also had a very small effect on the correlation coefficient. General trends in the data are illustrated in the main effects plot, with increasing voltage leading to a decrease in line width. Increasing the beam current and dwell/line time correspond to an increase in width. The correlation coefficient for this analysis was 93.1%.

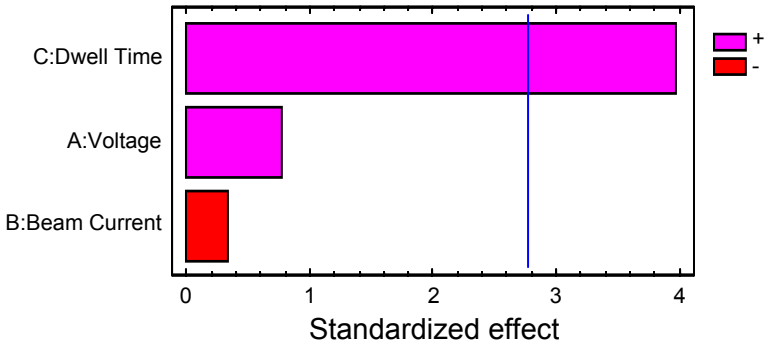

(a) Standardized Pareto Chart for Height/scan

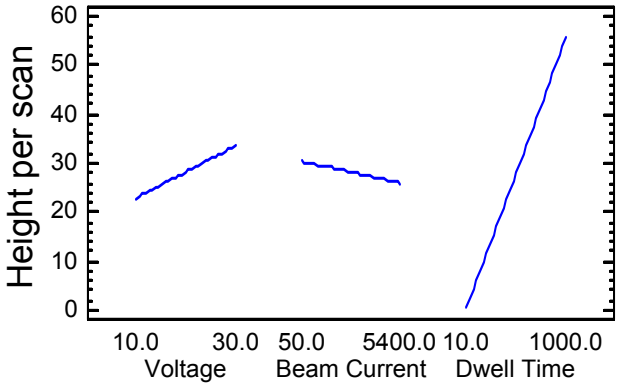

(b) Main Effects Plot for Height/scan (μm/scan) x 10^6

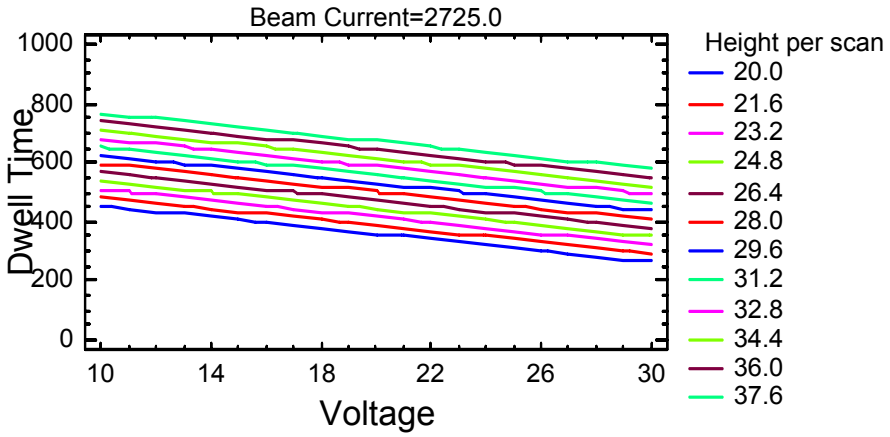

(c) Response Contours for Height/scan (μm/scan) x 10^6 for Constant Beam Current

Figure 4-40. Analysis Results for 2^3 Carbon Line Study for Height/scan:
(a) Standardized Pareto Chart (b) Main Effects Plot (c) Response Contours

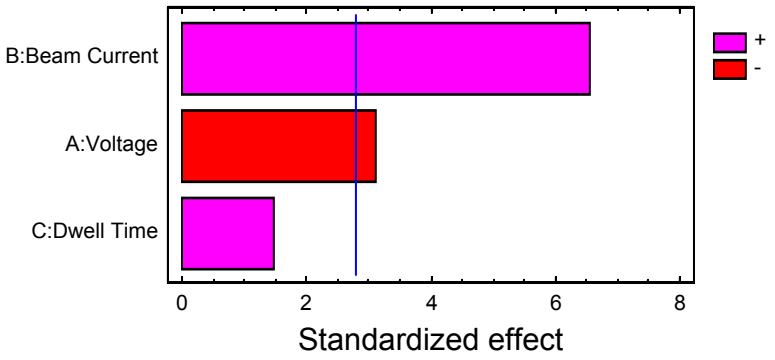

(a) Standardized Pareto Chart for Line Width

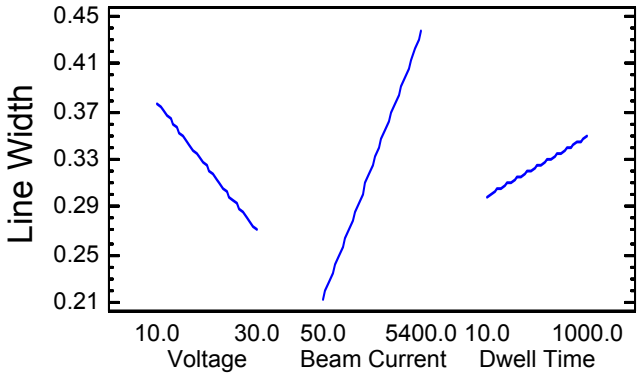

(b) Main Effects Plot for Line Width (μm)

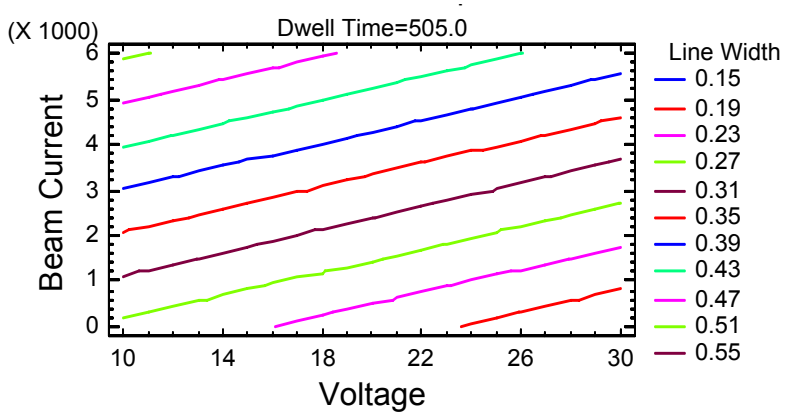

(c) Response Contours for Line Width (μm) for Constant Dwell Time

Figure 4-41. Analysis Results for Line Width for Carbon Line 2^3 Trials: (a) Standardized Pareto Chart (b) Main Effects Plot (c) Response Contours

4.3.4. Carbon 2^3 Factorial Line Time Study

A two level, three factor study was conducted for carbon line deposition from the methane-argon mixture, with the dwell time held constant. The variables used were voltage, beam current, and line time. The levels used for the variables were 10 and 30 kV for voltage, 100 and 5400 pA for beam current, and 1.06 and 2.12 ms for line time. Fixed settings were a chamber pressure of 1.0 Torr, a magnification of 30,000x, a working distance of 10.0 mm, and a deposition time of 45 minutes. The dwell time, in this case 1 μs, was also held constant for all trials to determine the effects of line time. Upon completion of the trials, images and measurements were taken for the line height and width dimensions. Table 4-13 summarizes the experimental settings and measurements that were recorded. Images of the line deposits with measurements are shown in Appendix A.15.

Table 4-13. Experimental Settings and Measurements for Carbon Line Time Study

Trial	Voltage (kV)	Beam Current (pA)	Line Time (ms)	Line Height (μm)	Line Width (μm)
T1	30	5400	1.06	0.331	0.433
T2	10	100	2.12	0.249	0.398
T3	30	100	2.12	0.306	0.561
T4	10	5400	2.12	0.212	1.053
T5	30	100	1.06	0.352	0.304
T6	30	5400	2.12	0.213	0.294
T7	10	5400	1.06	0.219	0.809
T8	10	100	1.06	0.269	0.31

The total number of scans completed for both of the line time settings was calculated using the overall deposition time to be 2.55×10^6 and 1.27×10^6 for line times of 1.06 ms and 2.12 ms, respectively. The total number of scans performed were then divided out from the measured height to give height/scan values. These values, along with the

measured line widths, were analyzed as response variables in STATGRAPHICS. Analysis results for height/scan as a response variable are shown in Figure 4-42. ANOVA results are shown in Appendix B.

Initial analysis indicated that the interaction terms had P-values significantly higher than the other factors, so these terms were excluded. As shown, the line time was the only factor found to be significant with 95% confidence for the height/scan analysis. The general trends indicated in the main effects plot are an increase in height/scan with increasing line time and voltage, and conversely a decrease in height/scan with increasing beam current. The correlation coefficient was 92.3%.

Analytical results determined using the line width as the response variable are shown in Figure 4-43. Initial results indicated that the beam current-line time and voltage-line time interaction terms had P-values greater than 0.73, so these terms were excluded from the final analysis. ANOVA results are shown in Appendix B.

The results for the analysis for line width indicate that the only variable that is statistically significant at the 95% confidence level is the voltage-beam current interaction term. The main effects plot illustrates the general trends in the data. A decrease in line width correlates to an increase in voltage, while an increase in line width results from increasing beam current and line time. The correlation coefficient for this analysis was 90.4%.

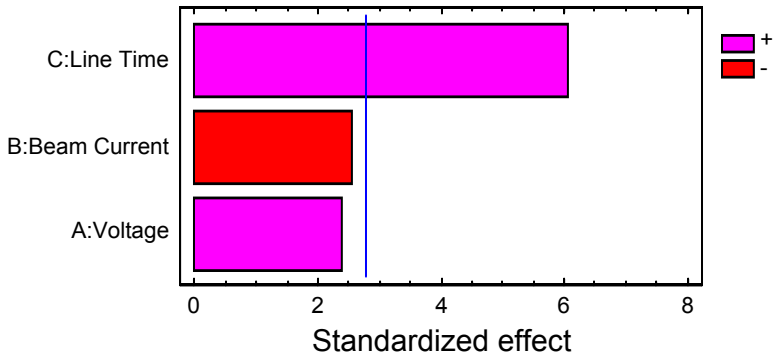

(a) Standardized Pareto Chart for Height/scan

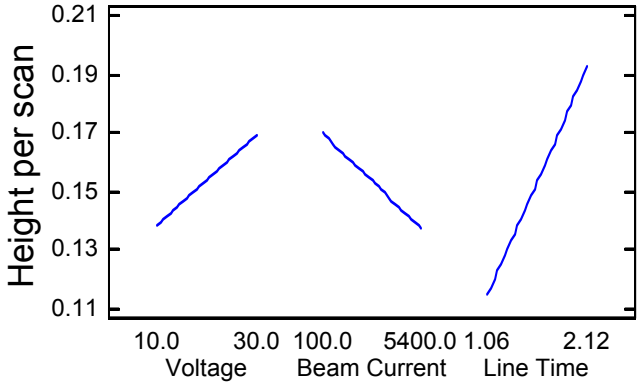

(b) Main Effects Plot for Height/scan (μm/scan) x 10^6

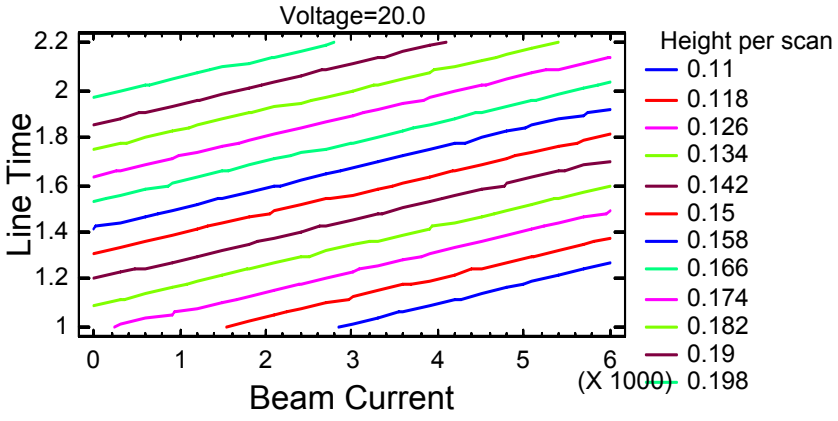

(c) Response Contours for Height/scan (μm/scan) x 10^6 for Constant Voltage

Figure 4-42. Analysis Results for Height/scan for Carbon Line Time Study: (a) Standardized Pareto Chart (b) Main Effects Plot (c) Response Contours

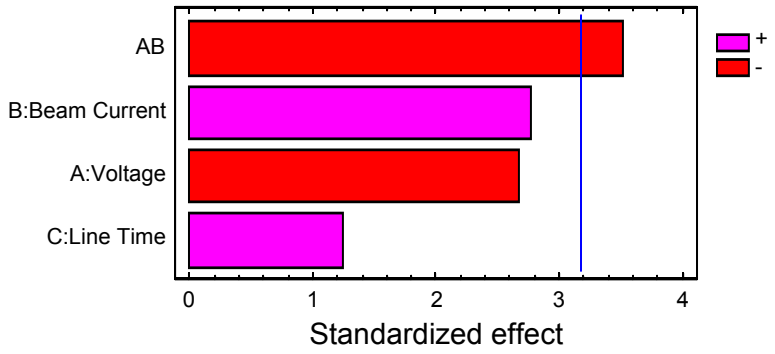

(a) Standardized Pareto Chart for Line Width

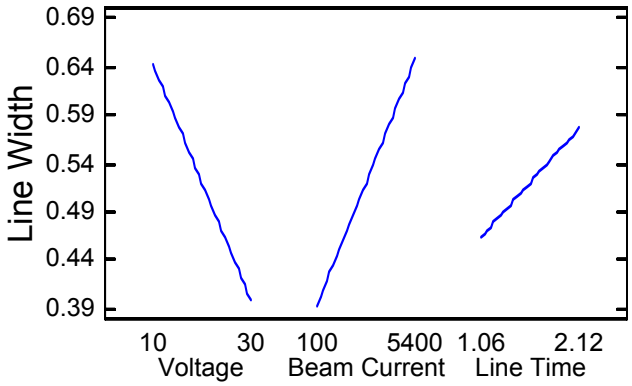

(b) Main Effects Plot for Line Width (µm)

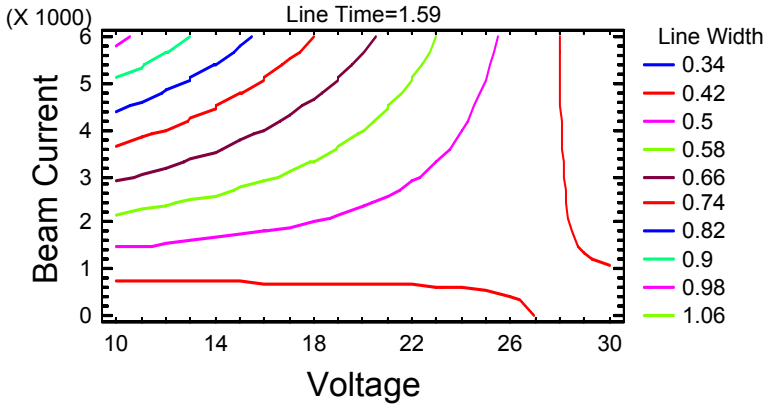

(c) Response Contours for Line Width (µm) for Constant Line Time

Figure 4-43. Analysis Results for Line Width for Carbon Line Time Study: (a) Standardized Pareto Chart (b) Main Effects Plot (c) Response Contours

4.3.5. Carbon Deposit TEM Analysis and Results

Carbon fibers were deposited on a copper TEM grid by tilting the grid to a 45^{o} angle and focusing the electron beam on the thickness of the grid, in the same fashion as for the Pt fibers. The fibers are shown in Figure 4-44. Only two fibers were deposited, and Electron Energy Loss Spectroscopy (EELS) was performed. Results indicated that only carbon was detected, as indicated in Figure 4-45. TEM images taken of the fibers showed that the deposits were mostly amorphous. This is in agreement with previously published results.[38,39] Some crystallinity is apparent in the first carbon deposited, i.e., adjacent to the Cu substrate. A TEM image from one of the fibers is shown in Figure 4-46.

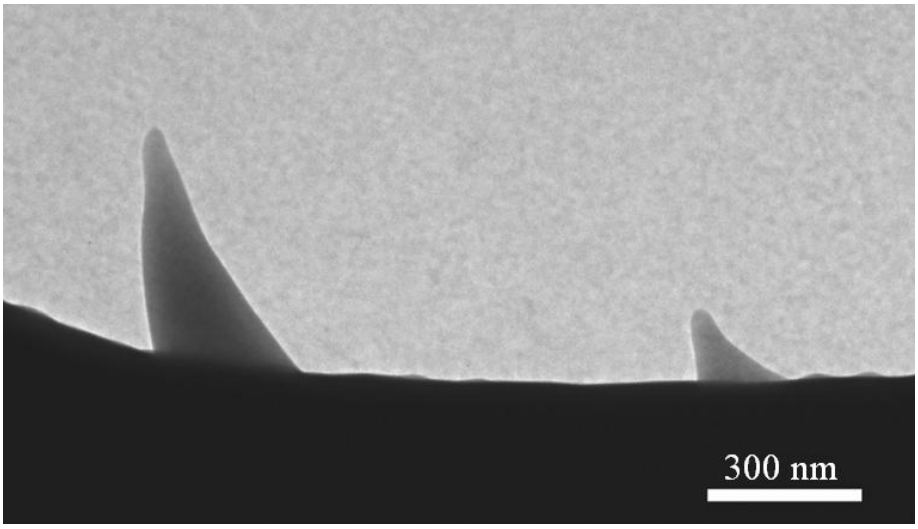

Figure 4-44. Carbon Fibers Deposited on Cu TEM Grid

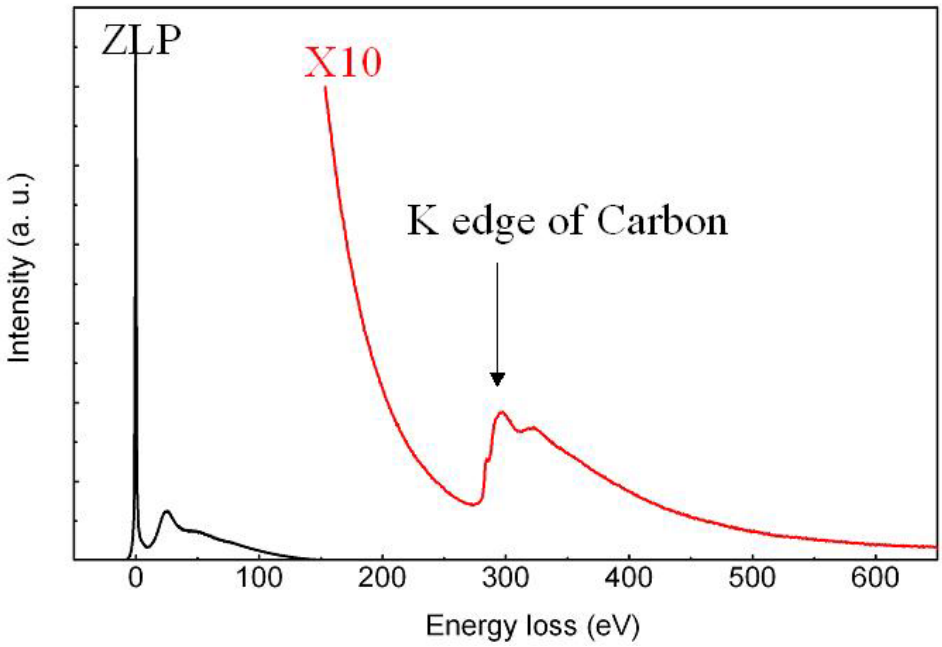

Figure 4-45. EELS for Carbon Fiber Deposit

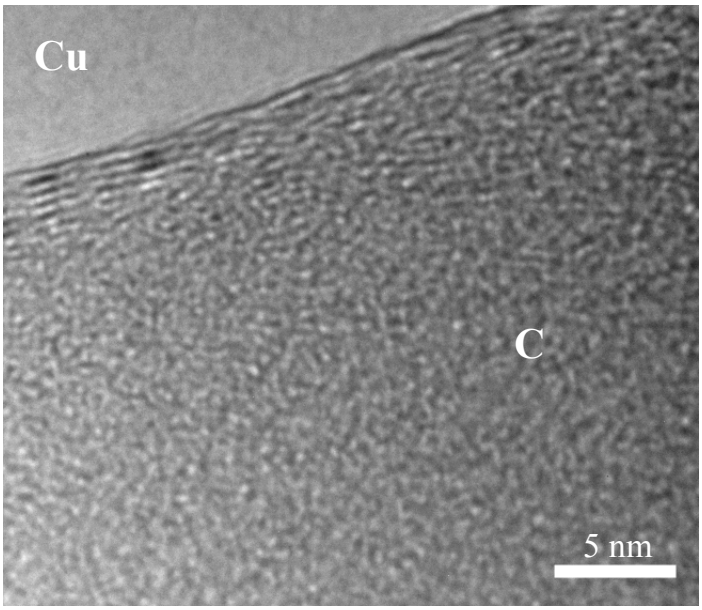

Figure 4-46. TEM Image of Carbon Fiber Deposit Showing Amorphous Structure

4.3.6. Problems with Carbon Deposition Using the Environmental Mode

Persistent problems were encountered with depositing carbon from the methane/argon mixture using the Environmental mode of the microscope. Initial exploratory experiments for carbon fiber and line deposition were successful, but some amount of inconsistency was observed. As experimentation continued, this unpredictability was exacerbated to the point that it was no longer possible to deposit fibers in a consistent manner. Sometimes carbon deposits were obtained while other trials failed to yield any deposit. Attempts to address this problem were made through the use of other reagent gases in the Environmental mode. Benzene and acetylene were used, but results were worse than for the methane argon mixture. Exploratory attempts resulted in only a single line deposition from benzene, and nothing from acetylene. Attempts were also made to deposit boron nitride from borazine ($B_3N_3H_6$), and these were unsuccessful as well. The reason(s) for the inconsistent behavior are unknown.

CHAPTER V

DISCUSSION OF RESULTS

For the platinum deposition that will be discussed in this chapter, the gas injection system used in the Georgia Tech EBCVD system utilized the reagent $(CH_3)_3Pt((C_5H_5)CH_3)$. The experimental results are compared to literature results where a slightly different reagent, $C_5H_5Pt(CH_3)_3$, was used. The carbon deposits made using the Georgia Tech EBCVD systems used a methane-argon gas mixture that was fed in through an auxiliary port while the microscope was operated in the Environmental mode. For the carbon deposition references mentioned, all deposition was performed using hydrocarbon contamination present in the chamber.

5.1. Variable Effects: Fiber Deposition

5.1.1. Voltage

For platinum fiber deposition, an increase in voltage leads to a decrease in vertical growth rate. The analysis for the central composite experiment (which covered the 5 to 30 kV range) indicated an effect of the square of the voltage as well (both were statistically significant at the 95% confidence level). The base diameter growth rate appeared to exhibit a slight decrease as voltage was increased, but this was not statistically significant. Figure 5-1 illustrates the effect of the voltage for two fibers

deposited with a 1,500 pA beam current and 15 minute deposition time. Takai et al.[28] reported volumetric deposition rates for platinum of 0.6 μm^3/min that decreased to less than .06 μm^3/min as voltage was increased from 1 to 30 kV. Virtually all of the decrease occurred in the 1 to 10 kV range. It was noted that this decrease appeared to mirror the decrease in secondary electron yield from (100) Si over this voltage range. The experimental data for this thesis corresponds to this trend, as the vertical growth rate showed a distinct decrease with increasing voltage, while there appeared to be minimal effects on the base diameter growth rate. Hübner et al.[49] reported that for small dot deposition the base diameter increased when the voltage was decreased from 15 to 2.5 kV.

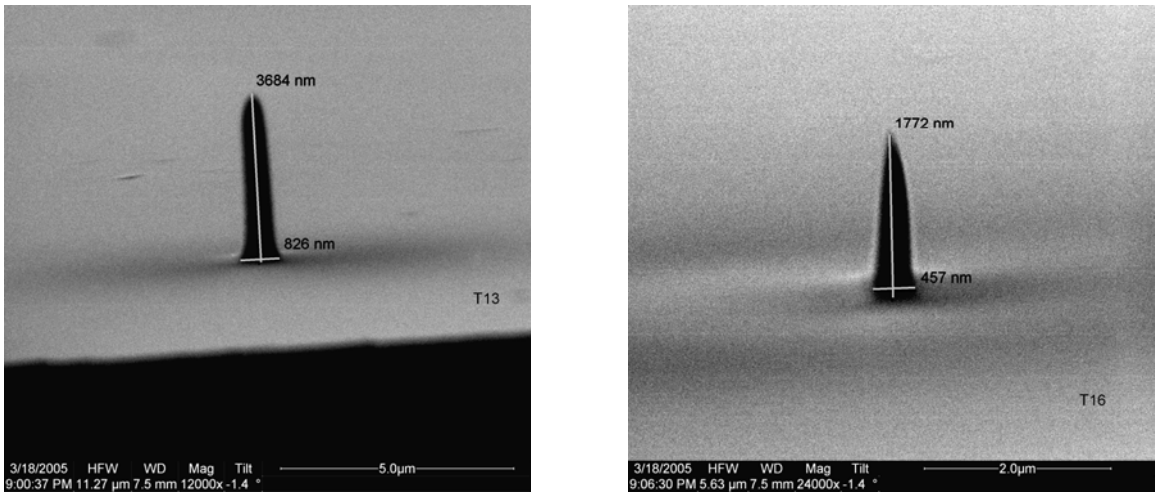

Figure 5-1. Pt Fibers Deposited at 5 kV (Left) and 30 kV (Right) (Fixed Settings: Beam Current=1,500 pA, Deposition Time=15 minutes)

For carbon fiber deposition, Schiffmann[39] reported that increasing the voltage from 1 to 30 kV led to a general increase in carbon fiber height, but had little effect on the fiber base diameter. The authors noted a significant increase in the fiber height when the

voltage was increased over the 1 to 10 kV range. From the 10 to 30 kV range, the fiber heights increased slightly. Wendel et al.[46] reported a steady, significant increase in carbon fiber height as voltage was increased from 2 to 40 kV (for a fixed 5 minute deposition time and 2-3 pA beam current). Since only exploratory studies were able to be performed due to persistent problems with fiber deposition when in the Environmental mode, there is little data to provide a valid comparison with previously reported results.

5.1.2. Beam Current

The beam current appeared to be the dominant factor for platinum fiber vertical deposition rate. An increase in beam current corresponds to a distinct increase in the vertical growth rate, and this factor was statistically significant at the 95% confidence level. The beam current has a much less significant effect on the fiber base diameter growth rate, and it was not found to be statistically significant. An increase in beam current corresponds only to a slight increase in growth rate for the base diameter. For fixed voltage settings (30 kV), changing the beam current from 100 to 5400 pA leads to a vertical growth rate that is more three times greater. The beam current appears to be a much more significant factor than the current density for platinum deposition based on the experiments performed for this investigation. The effect of the current density was studied for constant voltages, and it did not appear to be a driving factor for deposition. Values for the platinum fiber vertical growth rates for this investigation ranged from approximately 0.15 to 0.3 μm/min for the central composite experiment (with a beam current range of approximately 60 to 1500 pA), and from approximately 0.17 to 0.42 μm/min for the factorial fiber study performed with a larger disparity between beam

currents (50 and 5400 pA). The maximum vertical growth rate observed was approximately 0.90 μm/min, and it was observed for the maximum beam current tested (5400 pA) and for shortest deposition times (less than 1 minute). The effect of the beam current is illustrated in Figure 5-2 for two fibers deposited with a voltage of 30 kV and a deposition time of 5 minutes.

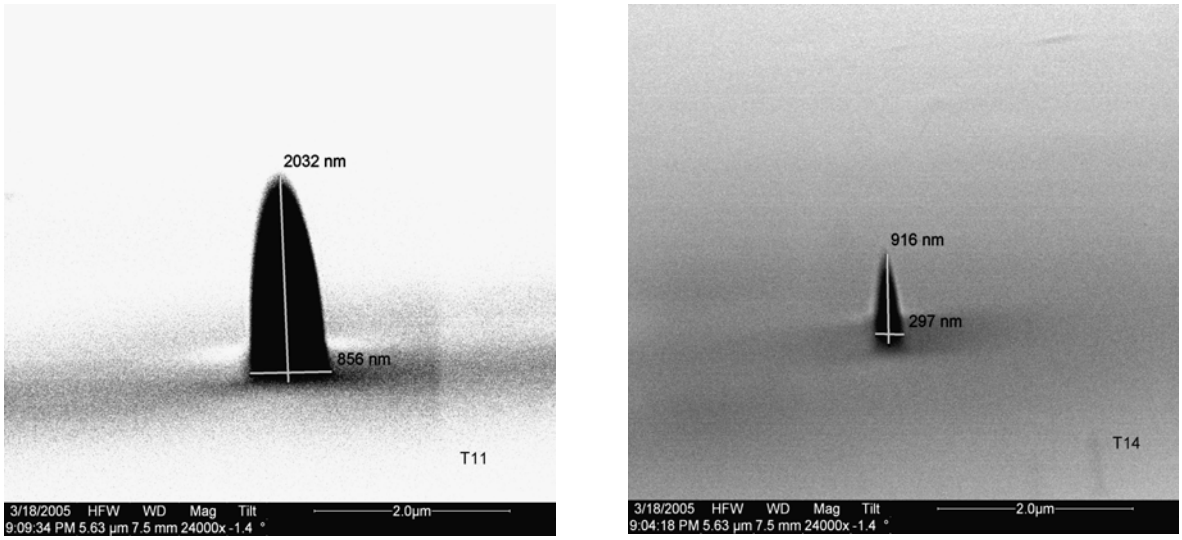

Figure 5-2. Pt Fibers Deposited at 20,000 pA Beam Current (Left) and 1,500 pA Beam Current (Right) (Fixed Settings: Voltage=30 kV, Deposition Time=5 minutes)

Koops et al.[27] reported vertical growth rates for platinum fibers as high as 9 μm/min, but did not detail the deposition conditions used to achieve this rate. Growth rates were in excess of 10^{12} nm/C at 20 kV. The authors also reported that the platinum content increased from 4 to 14 atomic % as beam current was increased from 10 to 1200 pA. Koops et al.[9] describe a theoretical model for which the deposition rate is proportional to the current density of the electron beam if there is a sufficient surface density of adsorbed molecules. Scheuer et al.[8] make a distinction between two cases concerning the limiting of deposition rates. At high adsorbate densities, growth rates are limited by the beam

current, while at high beam currents, growth rates are limited by the reagent gas flux. The deposition rates obtained in this thesis (vertical growth rates) ranged from 10^9 to 10^{11} nm/C.

The platinum content in the deposits was distinctly different from what has been reported thus far, as all of the deposits were found to be amorphous platinum and no carbon content was detected (using EDS). EELS was also performed on platinum fiber deposits, and the results from the EDS analysis were confirmed. A very weak peak for carbon was observed, but this was attributed to contamination of the fiber surface that occurred during acquisition of the spectra. This result differs from previously reported results using similar reagents, which found the Pt content to be on the order of 20%, with more than 70% C content.[16,26-28] A speculative reason for this is the inadvertent presence of water vapor in the chamber, possibly simply from the air when the chamber was opened to insert the sample. This has not been reported elsewhere, however. Operating in the Environmental mode with water vapor in the chamber during Au deposition has been shown to greatly improve the metal content.[14,35,36] The reasons postulated for this effect are that the carbon in the deposits was desorbed in the form of CO or CO_2 molecules as the deposition occurred. This effect has not been shown for platinum deposition in any known literature.

In the exploratory carbon fiber depositions, when a wide range of beam currents was used (100 and 1500 pA at 30 kV), a significant decrease in vertical deposition rate was observed for increasing current. A slight increase was observed when a smaller range of

currents (16.4 and 240 pA) was used at 10 kV. Schiffmann[39] observed a decrease in carbon fiber deposition rate that correlated to increasing beam current, not current density. Schiffmann[39] noted a sharp decrease in carbon fiber height (from over 2 μm to less than 0.25 μm) and a slowly increasing of fiber base diameter (from 0.1 to 0.5 μm) as beam current was increased over a range of 3 to 300 pA. This was performed using a microscope with a field emission gun, and it was noted that increasing the beam current is almost proportional to the resulting increase in the current density for this type of system, since the beam diameter only increases slightly over the range of beam currents studied. It was speculated that an increase in current density could lead to increased heating, which could alter sticking coefficients and adsorbate lifetimes, leading to a decrease in deposition rate. Bøggild et al.[50] noted that higher beam current reduces the carbon fiber growth rate, possibly due to increased charging which leads to beam deflection.

5.1.3. Deposition Time

The vertical growth rate for platinum fiber deposition decreased considerably as the deposition time increased. This is to be expected as the secondary electron emission from the substrate decreases as the deposit size increases. The initial average vertical growth rates (for 30 second deposition time) at 30 kV were on the order 0.3 and 0.9 μm/min for 100 and 5400 pA beam currents, respectively. As the deposition time was increased to 15 minutes, these rates dropped to approximately 0.06 and 0.3 μm/min, respectively. Hübner et al.[49] reported a linear increase in platinum fiber height corresponding to an average vertical growth rate of 8.4 nm/s (0.50 μm/min) for deposition time over the range of 0.30 to 104 sec. These results differ from the trends

observed for this thesis, but this could be due to the fact that they only cover a relatively short deposition time. Beam settings were a voltage of 15 kV and beam current of 170 pA. Takai et al.[28] reported a vertical deposition rate of approximately 2 μm/min for a deposition time of 0.5 minutes and a voltage of 30 kV (the beam current was not reported). These values are on the order of the values observed in this thesis for larger beam currents and short deposition times. Figure 5-3 illustrates the effect of the deposition time for two fibers deposited at a voltage of 30 kV and a beam current of 5,400 pA.

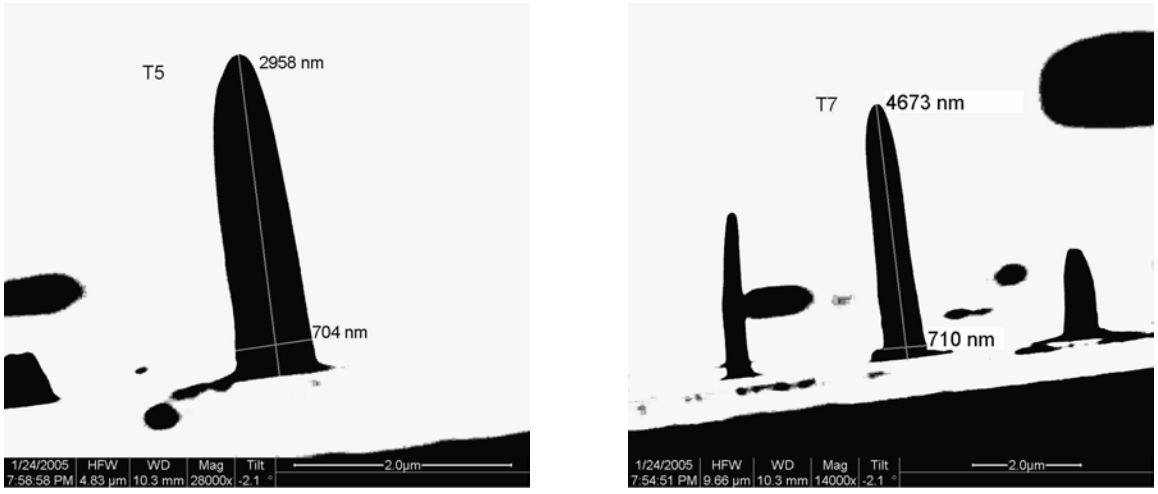

Figure 5-3. Pt Fibers Deposited for 5 Minute Deposition Time (Left) and 15 Minute Deposition Time (Right) (Fixed Settings: Voltage=30 kV, Beam Current=5,400 pA)

The platinum fiber base diameter growth was dependent primarily upon the deposition time and the deposition time squared according to the central composite analysis. Both of these factors were significant at the 95% confidence level. The base diameter growth rate decreases sharply as the deposition time increases. This is expected as the fibers reach a saturation diameter as the deposition time increases. This maximum (or

saturation) diameter is representative of the limiting range over which the secondary electrons can dissociate adsorbed molecules when the electron beam is held in a fixed position. The saturation effect concerning the maximum size (fiber diameter or line width) for a deposit is described by Schiffmann[39] as follows. When primary electrons from the beam penetrate the top of the growing fiber, they first dissociate molecules that are adsorbed at the top, leading to vertical fiber growth. Once they enter the body of the fiber, the primary electrons are scattered and leave the fiber from the sides. If they are able to escape the sides of the fiber, they can dissociate molecules that have adsorbed on these sidewalls of the deposit, which would lead to an increase in the fiber diameter. The diameter growth is thus defined by the mean maximum electron path length inside the fiber, and molecules that are adsorbed outside of this path length will not be dissociated. Silvis-Cividjian et al.[44] further describe this effect by suggesting that as the primary electrons scatter in the growing fiber, they generate secondary electrons that can exit the side walls of the deposit. Under this modified model, saturation occurs when the secondary electrons can no longer exit the side walls of the deposit, and Reimer[45] gives a general value for the inelastic mean free path of the secondary electrons in the deposit in the 5-15 nm range. This model was found to have a strong correlation to empirical results. This effect was also evident in the depositions made for this investigation.

For carbon fiber deposition, the deposition time had very similar effects as those described for the platinum fibers. The vertical and base diameter growth rates decreased significantly as the deposition time increased. For fixed deposition settings (30 kV, 100 pA beam current), the vertical growth rate decreased from approximately 0.14 μm/min to

0.06 μm/min as deposition time increased from 1 minute to 15 minutes. Available literature regarding deposition rates primarily concerns deposition of carbon from hydrocarbon contamination. Akama et al.[38] reported an average vertical growth rate of approximately 0.27 μm/min for a 15 minute deposition time for carbon fibers deposited from hydrocarbon contamination. It was noted that after an initial transient period, the growth rate was approximately constant at a value of 0.1 μm/min as deposition time was increased. Schiffmann[39] noted that the carbon fiber vertical growth rate decreased from approximately 2 μm/min to 0.25 μm/min as deposition time was increased from 0.5 to 8 minutes. Wendel et al.[46] also noted a distinct decrease in vertical growth rate with increasing deposition time. Values observed in the investigation performed here using a methane-argon mixture were somewhat lower. This could be due to lack of consistent reagent supply to the deposition site or poor adsorption of methane molecules to the substrate.

5.1.4. Chamber Pressure

The effect of the chamber pressure on carbon fiber deposition in the Environmental mode was not able to be fully investigated due to inconsistencies in the process. Exploratory carbon fiber experiments only varied the chamber pressure over a small range, 0.1 to 1.0 Torr. The results from these exploratory experiments did not indicate consistent trends in the deposition rates with regards to the chamber pressure in the 0.1 to 1.0 Torr range.

5.2. Variable Effects: Line Deposition

5.2.1. Voltage

The voltage appeared to be the least significant variable for platinum line deposition with regards to the height/scan. Both of the factorial experiments indicated that the line height/scan decreased as the voltage increased, but this factor was not found to be statistically significant at the 95% confidence level for these experiments. The central composite experiment exhibited a stronger inverse correlation for the voltage and height/scan, and the square of the voltage also appeared to have an effect. The voltage was statistically significant at the 95% confidence level for the central composite experiment, and the voltage squared term fell just short of this confidence level. The voltage exhibits a similar effect on the line width for the platinum deposits. An increase in voltage leads to a decrease in line width, and the central composite experiment also appeared to indicate some influence of the voltage squared as a factor. The decrease in line width with increasing voltage is a logical result, since the higher voltages also corresponded to smaller beam diameters for these experiments. It is also easier to manually focus the beam at higher voltages. The smaller line widths at higher voltages would also correlate with lower secondary electron emission from the substrate as described earlier for platinum fibers. Since the secondary electrons play a dominant role in determining deposit size, this is also a logical result. Figure 5-4 illustrates the effect of the voltage for two lines deposited with a beam current of 5,400 pA, a dwell time of 1000 μs, and a line time of 1,060 ms.

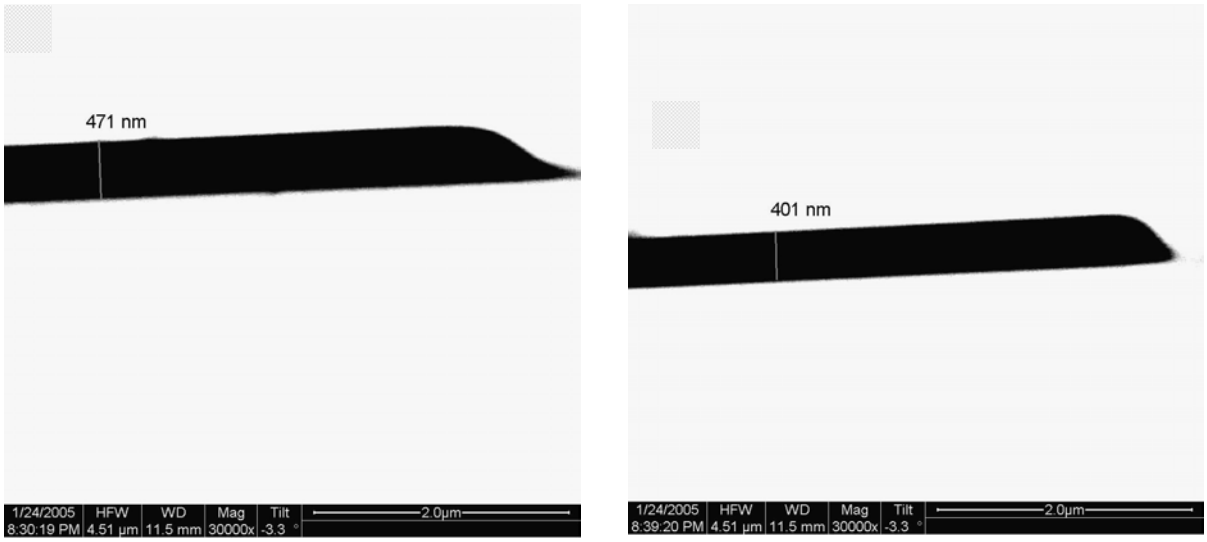

Figure 5-4. Pt Lines Deposited at10 kV (Left) and 30 kV (Right) (Fixed Settings: Beam Current=5,400 pA, Dwell Time=1,000 µs, Line Time=1,060 ms)

For carbon line deposition, the voltage exhibited the opposite trends from those for the platinum line deposition with regards to height/scan. As the voltage increased, the height/scan also increased, but this factor was not found to be statistically significant at the 95% confidence level. This response could be due to the higher current density associated with higher voltages. For line width, the voltage factor was found to be statistically significant at the 95% confidence level for one factorial experiment, but fell just short of this level for another (the voltage-beam current interaction term was found to be statistically significant, however). The line width decreased as the voltage was increased, in a similar fashion as was discussed previously for the platinum line deposition. This response is likely attributable to the smaller beam diameters at higher voltages and lower secondary electron emission. The lower voltages (under 10 kV) that have been shown to have greater effects on the process as described previously were not able to be investigated due to the inability to adequately focus the beam at the high magnification required (40,000x) for these experiments. 10 kV was determined from

exploratory experimentation to be the minimal beam voltage necessary to consistently focus the beam properly. Miura et al.[17] studied carbon line deposition from hydrocarbon contamination. They noted that a high acceleration voltage (along with high magnification) were optimal for making line deposits with high aspect ratios. This correlation between higher voltage and smaller line width agrees with observations made for this investigation.

5.2.2. Beam Current

The beam current appears to have a considerable effect on the height/scan with regards to platinum line deposition. This factor was found to be significant at the 95% confidence level. An increase in beam current corresponds to an increase in height/scan. This would correspond with the observations regarding beam current that were discussed earlier for platinum fiber deposition. This factor appeared to have the second largest effect of the variables studied. The platinum line width also appears to have a positive correlation with the beam current. This effect was considerably greater in the factorial experiments (where this factor was statistically significant at the 95% confidence level) that were performed than in the central composite experiment (where the beam current was not statistically significant). This result is likely attributable to the fact that higher beam currents are associated with larger spot sizes and thus larger beam diameters. Reported observations for platinum fiber vertical growth rate also correspond to these observed responses. Figure 5-5 illustrates the effect of the beam current for two lines deposited at voltage of 30 kV and a line time of 2.12 ms.

The beam current appeared to affect carbon line deposition in a different manner. The height/scan decreased when the beam current was increased (although this effect was not found to be statistically significant at the 95% confidence level). The carbon line width increased with increasing beam current, in a similar fashion as was described for the platinum lines. The larger beam diameter associated with the larger beam currents is a likely explanation for this occurrence. Miura et al.[17] noted a decrease in line height with increasing beam current, while the width of the line increased. The authors surmised that the increase in beam current caused local heating and re-evaporation of the carbon, thereby hindering the vertical growth rate. It was also suggested that the increase in beam current would cause electron scattering at the surface, resulting in lateral deposition. This would indicate that a lower beam current would be preferential for high aspect ratio line deposits.

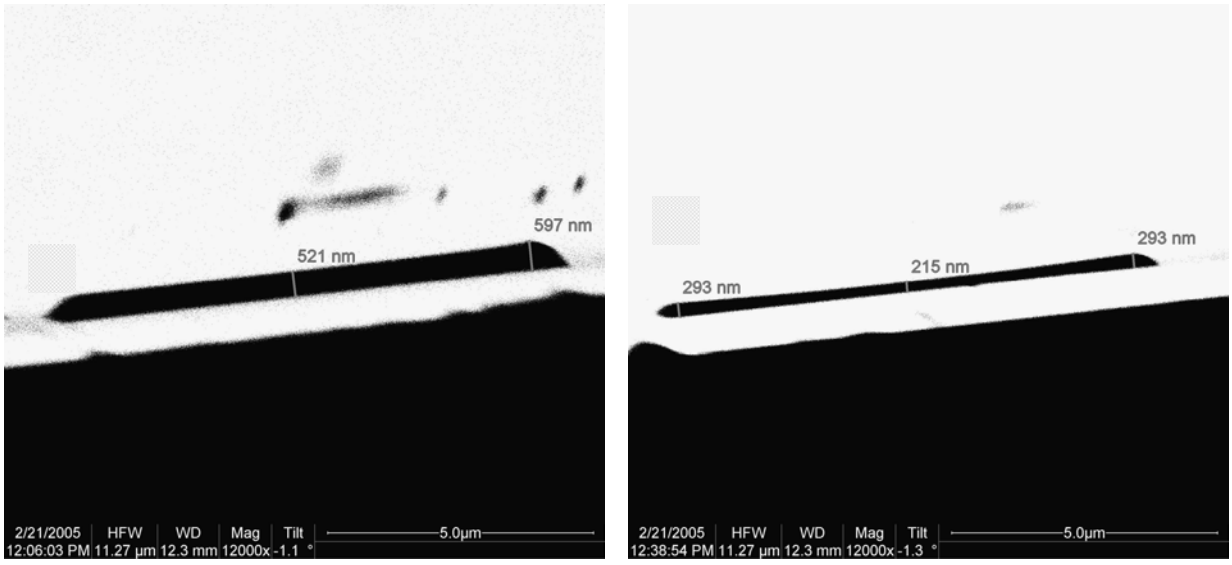

Figure 5-5. Pt Lines Deposited with 5,400 pA Beam Current (Left) and 100 pA Beam Current (Right) (Fixed Settings: Voltage=30 kV, Line Time=2.12 ms)

5.2.3. Dwell/Line Time Combined Effect

The central composite platinum line experiment varied the dwell time in conjunction with the line time. This was also done in a factorial study for platinum line deposition. The results for both of these experiments indicated that the combined effects of increasing both the dwell and line times was a significant increase in the height/scan. The dwell/line time term appeared to be the predominant factor in influencing the height/scan, as it was statistically significant at the 95% confidence level for both studies. The line width increased slightly as the dwell/line time was increased during the factorial study which featured a large range between the levels used for this factor (10 and 1000 μs for the dwell time, 10.60 and 1060 ms for the line time). This was not a statistically significant effect for the factorial study, however. The central composite platinum line experiment investigated a smaller range of values (from 6 to 470 μs for the dwell time and 6.6 and 500 ms for the line time), and it showed a definite decrease in line width as dwell/line time was increased. The square of the dwell/line time factor also appeared to have a significant effect. Both of these factors were found to be statistically significant at the 95% confidence level for the central composite experiment. The dwell time and line time effects were studied by Kohlmann-von Platen et al.[47] for W fiber deposition with a specialized system featuring an electrostatic beam blanker. Reported observations were that holding the loop (i.e., line) time constant and increasing the dwell time led to a decreasing deposition yield due to progressing consumption of the adsorbate layer. Holding the dwell time constant and increasing the loop (line) time led to an increase in deposition yield to a saturation level due to a longer time for replenishment of the adsorbate layer. The combined dwell/line time effects studied here indicate that the

adsorbate replenishment associated with the increasing line time is a more important factor than the adsorbate consumption resulting from increasing dwell time.

The dwell/line time combined factor was also the dominant factor for carbon line deposition with regards to the height/scan parameter. An increase in this factor led to a substantial increase in the height/scan. It was the only variable found to be statistically significant at the 95% confidence level. The dwell/line time factor had much less of an effect on the carbon line width. The line width increased very slightly as the dwell/line time increased, but it appeared to have the least effect of all the variables on the line width, and it was not statistically significant at the 95% confidence level.

5.2.4. Line Time

The line time appeared to be the dominant factor in height/scan for platinum line deposition based on the factorial experiment that was performed for constant dwell time, and it was found to be significant at the 95% confidence level. Although the range over which this variable could be investigated was limited, there was still a considerable effect. Increasing the line time by a factor of 4 led to an almost 4-fold increase in the height/scan values. Increasing the line time means that the time for molecules to readsorb on the newly deposited surface is greater. This is obviously a very important factor for the deposition rate. The increase in deposition rate described by Kohlmann-von Platen et al.[47] appears to agree with observations made for this investigation. The platinum line width appeared to decrease in response to increasing line time, although this effect was much less pronounced than that for the height/scan, and it was not

statistically significant at the 95% confidence level. Figure 5-6 illustrates the effect of the line time for two lines deposited with a voltage of 10 kV and a beam current of 5,400 pA.

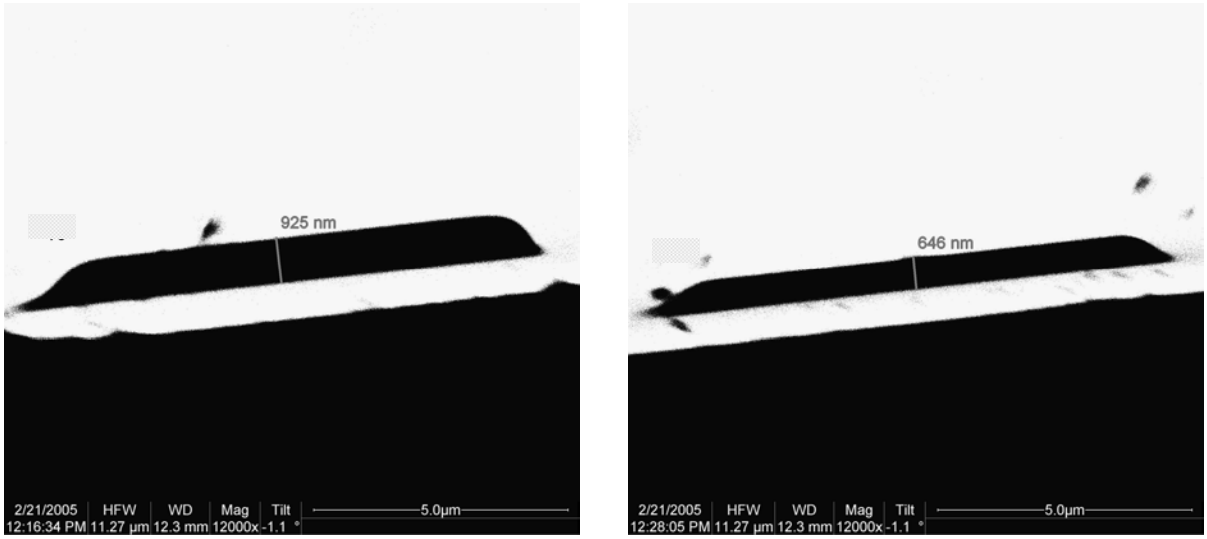

Figure 5-6. Pt Lines Deposited with 2.12 ms Line Time (Left) and 0.53 ms Line Time (Right) (Fixed Settings: Voltage=10 kV, Beam Current=5,400 pA)

The line time also appeared to have a similar effect for height/scan for carbon line deposition. An increase in line time led to a considerable increase in height/scan, and this was the dominant factor as determined from the factorial study with dwell time held constant. The line time was the only statistically significant factor at the 95% confidence level for the height/scan parameter. The line width appeared to increase with increasing line time, and this effect was not as pronounced as that for the height/scan, nor was it statistically significant at the 95% confidence level. This response for the carbon line width is opposite of that for the platinum line width. This could indicate different adsorption properties for the reagent molecules used for platinum and carbon deposition.

5.2.5. Dwell Time

The dwell time was studied independently of the line time in a platinum fiber factorial study. The range over which this variable could be tested was limited, since the only way to alter this factor separately from the line time was to change the pixel resolution. The results of this experiment did not show a statistically significant effect at the 95% confidence level for either the line height or the line width. In fact, this parameter was found to have the least effect of all the variables studied for this experiment. This indicates that the combined effects of altering the dwell/line time as described earlier are due primarily to the line time.

V.3. Platinum Optimization Results

Optimization analyses were performed for several parameters, including the aspect ratio for line and fiber deposits and the minimum line deposit width. Maximizing the fiber deposition rate was also investigated. The results for the aspect ratio optimization for both line and fiber deposition indicated that high voltage (30 kV) and high beam current (5,400 pA) were favorable for maximizing this parameter. For the minimum line width, medium voltage (15.8 kV) and low beam current (60 pA) were recommended, and results indicated that the low beam current, which corresponds to a smaller beam diameter, was a very important parameter. A long dwell time (420 μs) was also found to be preferable. The minimum line width obtained for a substantial deposition time (20 minutes) was under 200 nm. For the fiber deposition rates, low voltage (5 kV) and high beam current (20,000 pA) led to the maximum rates. A shorter deposition time also corresponds to a higher deposition rate. For a tungsten filament microscope, such as the SEM used for

this investigation, very high beam currents also correspond to substantially larger beam diameters, which means that it is difficult to achieve sub-micron features at the maximum deposition rates. Hübner et al.[49] reported that the platinum fiber diameter reached a saturation value of approximately 200 nm after a short deposition time. Minimum feature sizes (obtained for deposition times less than 1 sec) were in the 25 to 30 nm range. Optimal settings for a specific application would be determined by the sizes required for that application. If size is a critical parameter, then lower beam currents would be necessary, but this would slow down the process. If speed is the most critical parameter, then higher beam currents would be used, but this would lead to less control over deposit size and geometry. If size and speed are equally important, the optimal beam settings may be somewhere in the middle (i.e., 15-20 kV, 1,500 pA), depending on the specific requirements.

CHAPTER VI

CONCLUSIONS

- Results from factorial and central composite design platinum fiber experiments indicated that the beam current was a prominent factor in determining the deposition rates for fibers, with higher beam current leading to higher platinum deposition rates.

- The deposition time displayed the effect of approaching a saturation diameter that is dictated by the range over which the secondary electrons scatter.

- The maximum vertical growth rate observed for platinum fibers was approximately 0.90 μm/min.

- The voltage also has a significant effect on the platinum line deposition rate, and this effect is likely attributable to the increase in secondary electron yield from Si in the 1 to 10 kV range.

- The voltage and beam current had similar effects on platinum line and fiber deposition.

- The line time had a significant effect on the line deposition rate, and this was attributed to the increased time for reagent molecules to adsorb onto the surface between scans.

- The dwell time did not appear to have a statistically significant effect for platinum line deposition.

- Optimization analysis indicated that high voltage and high beam current values (30 kV, 5400 pA) were most favorable for producing high aspect ratio line and fiber deposits.

- Optimization analysis indicated that medium voltage, low beam current, and longer dwell times (15.8 kV, 60 pA or less, 420 μs) were most favorable for producing minimum width line deposits, and this effect was attributed to the smaller beam diameter associated with the lower beam current.

- Low voltage and high beam current (5 kV, 20,000 pA) correspond to maximum deposition rates, but very high beam currents (where beam diameters approach 1 μm) make it difficult to obtain sub-micron features; a trade-off must thus be made between desired feature size and maximum deposition rate.

- Optimal beam settings would depend on the requirements of the specific application. If speed is the most critical parameter, then higher beam currents

would be used, but this would lead to less control over deposit size and geometry. If size and speed are equally important, the optimal beam settings may be somewhere in the middle (i.e., 15-20 kV, 1,500 pA).

- TEM analysis, EDS, and EELS indicated that the platinum deposits were amorphous and contained no carbon, which differs from previously reported results.

- Factorial experiments were conducted for carbon line deposition, and results indicated that lower beam current appeared to be more favorable for higher deposition rates, although these results were not found to be significant at the 95% confidence level.

- The line time appeared to effect the carbon line deposition in the same manner as for the platinum lines.

- The maximum vertical growth rate observed for carbon fibers were approximately 0.14 μm/min. This is almost a factor of 10 slower than platinum deposition.

- TEM analysis and EELS indicated that the carbon deposits were mostly amorphous and only carbon was detected.

- Carbon deposits were made in the Environmental mode from a methane/argon mixture, and results from this method were found to be inconsistent. In contrast, the constant supply of reagent gas from the Gas Injection System used for platinum deposition was found to be extremely reliable.

APPENDIX A: IMAGES AND MEASUREMENTS

Appendix A.1. 1st Platinum Fiber Growth Rate Study Measurements

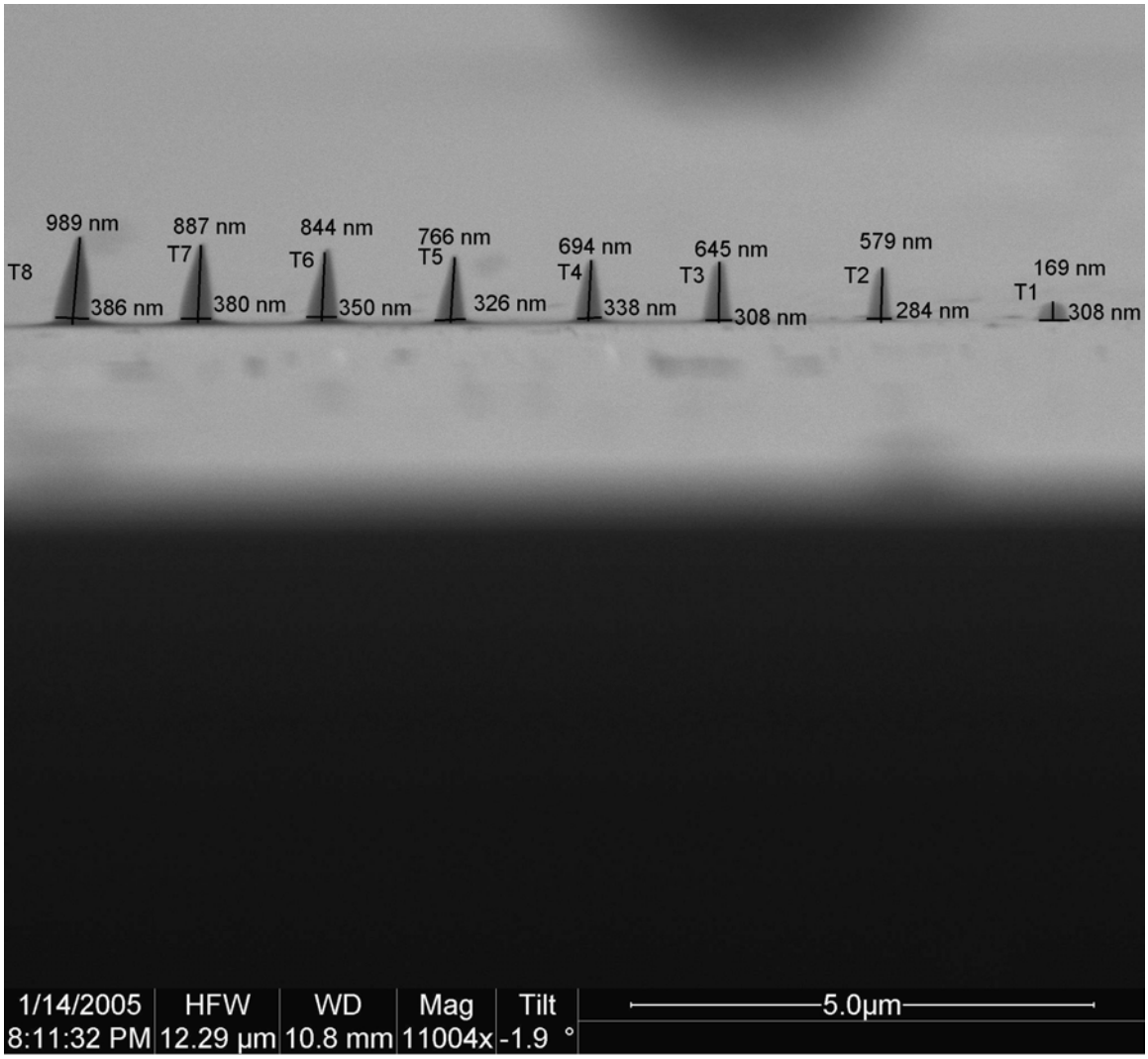

Fibers and Measurements for 1st Pt Growth Rate Study

Appendix A.2: 2nd Platinum Fiber Growth Rate Study Measurements

Note: T = Deposition Time

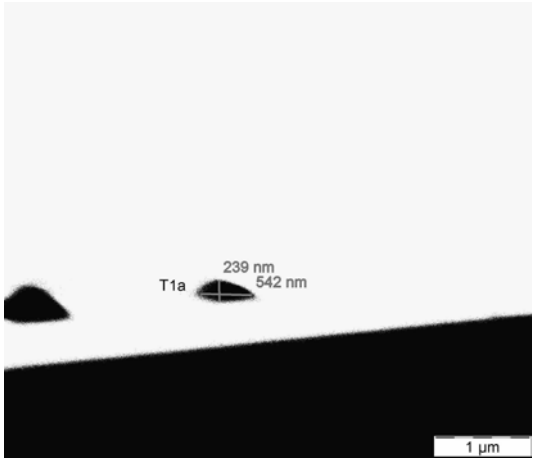

T1a Measurements (Settings: T=0.25 min)

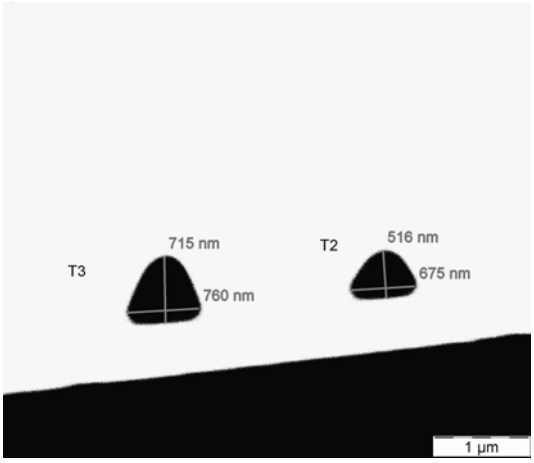

T2 Measurements (Settings: T=1 min); T3 Measurements (Settings: T=1.5 min)

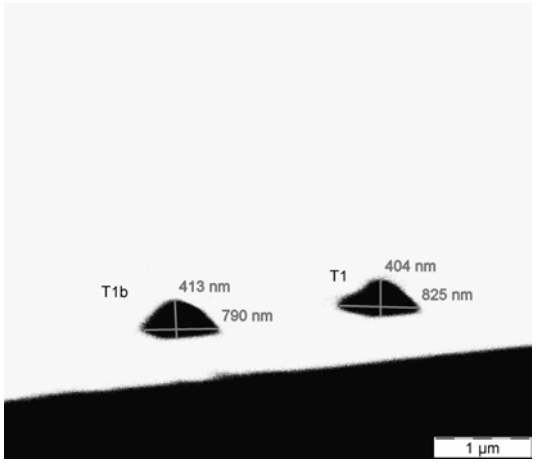

T1 Measurements (Settings: T=0.50 min); T1b Measurements (Settings: T=0.75 min)

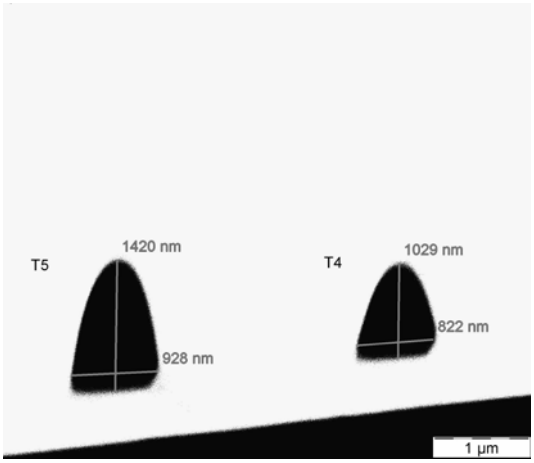

T4 Measurements (Settings: T=2 min); T5 Measurements (Settings: T=3 min)

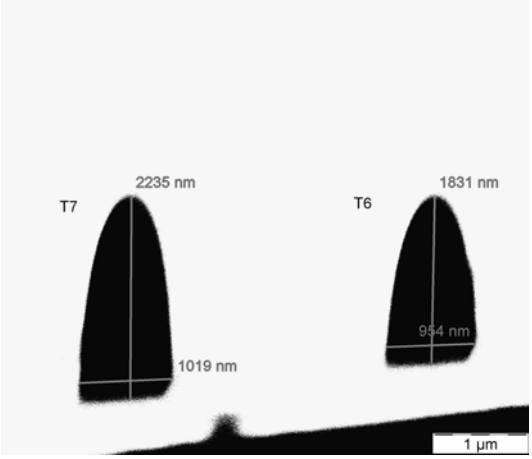

T6 Measurements (T=4 min);
T7 Measurements (T=5 min)

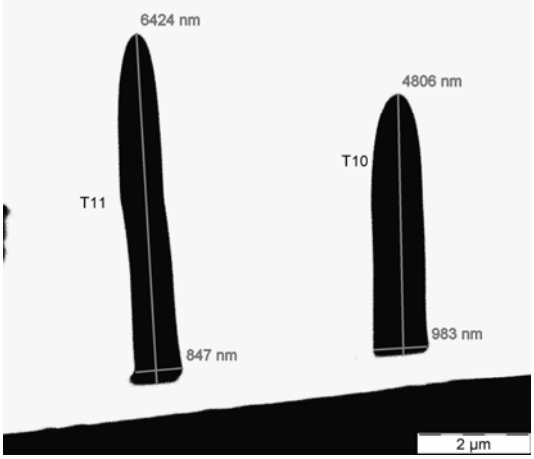

T10 Measurements (T=15 min);
T11 Measurements (T=25 min)

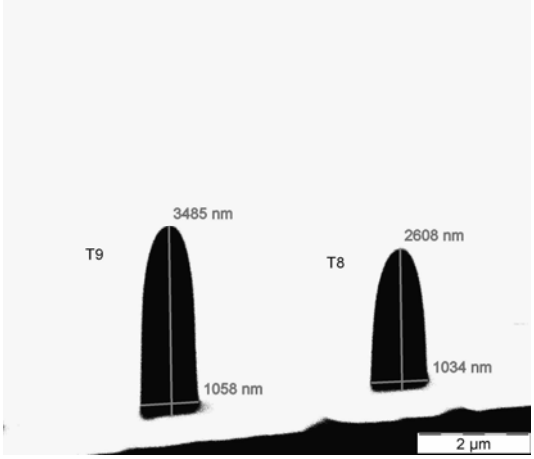

T8 Measurements (T=7 min); T9
Measurements (T=10 min)

Appendix A.3: Platinum Fiber Current Density Study Measurements

Note: HV = High Voltage, BC = Beam Current

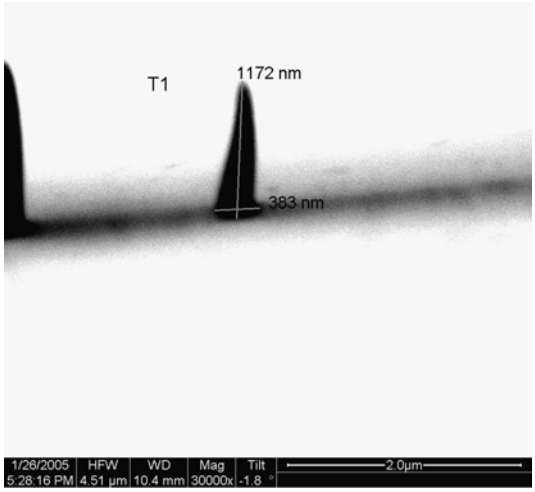

T1 Measurements (HV=30 kV, BC=24 pA)

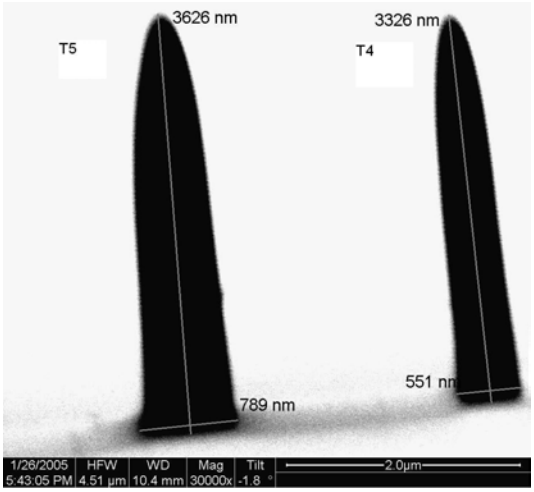

T4 Measurements (HV=30 kV, BC=1500 pA); T5 Measurements (HV=30 kV, BC=5400 pA)

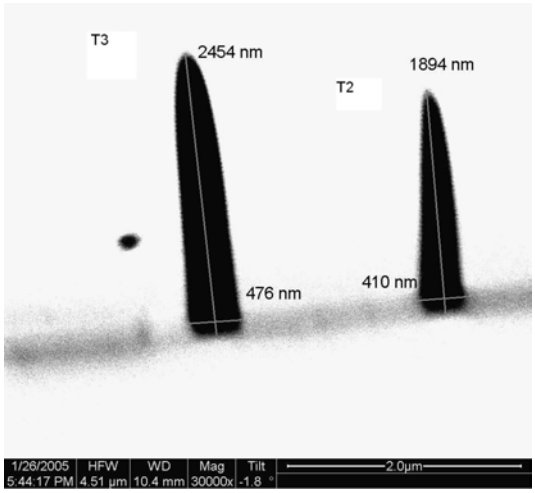

T2 Measurements (HV=30 kV, BC=100 pA); T3 Measurements (HV=30 kV, BC=390 pA)

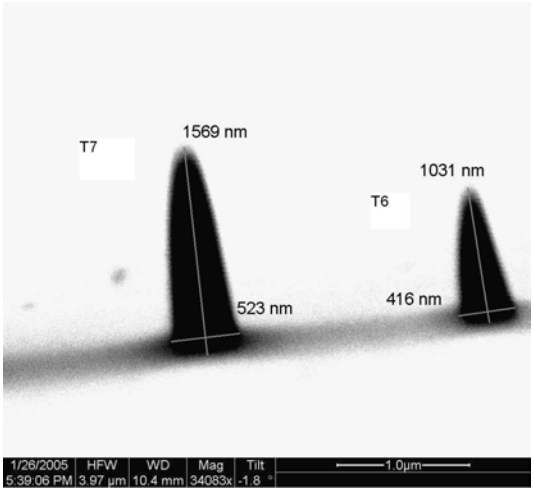

T6 Measurements (HV=10 kV, BC=24.6 pA); T7 Measurements (HV=10 kV, BC=103.6 pA)

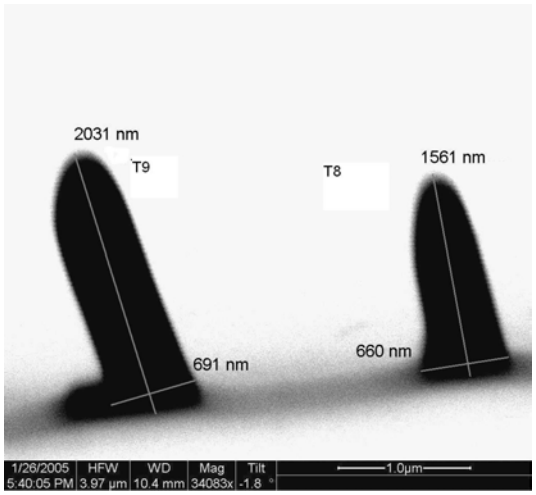

T8 Measurements (HV=10 kV, BC=383.7 pA); T9 Measurements (HV=10 kV, BC=1420 pA)

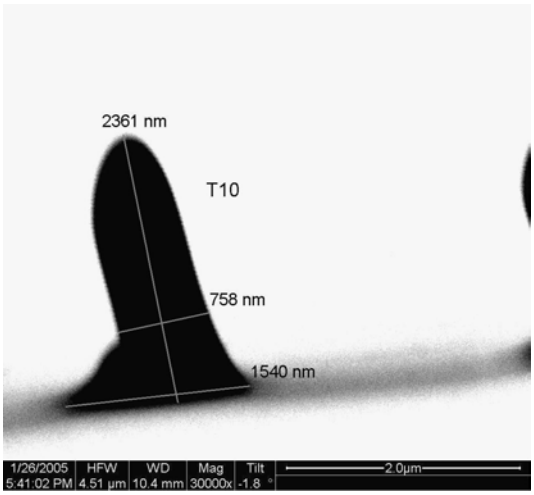

T10 Measurements (HV=10 kV, BC=5257 pA)

Appendix A.4: Platinum Fiber 2^3 Factorial Experiment Measurements

Note: HV = High Voltage, BC = Beam Current, T = Deposition Time

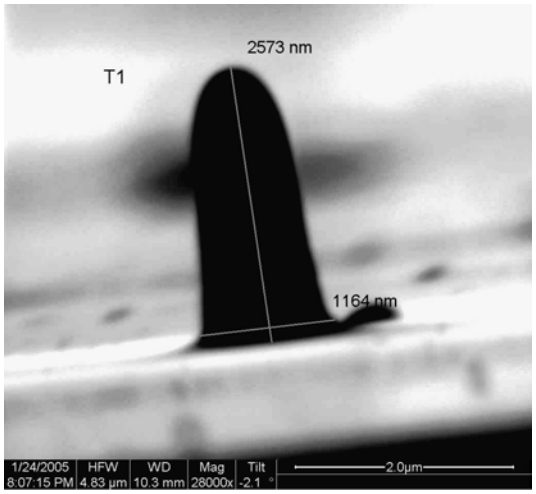

T1 Measurements (Settings: HV=10 kV, BC=5400 pA, T=5 min)

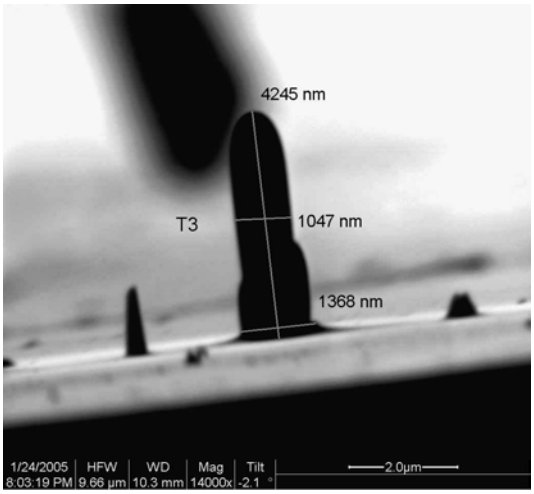

T3 Measurements (Settings: HV=10 kV, BC=5400 pA, T=15 min)

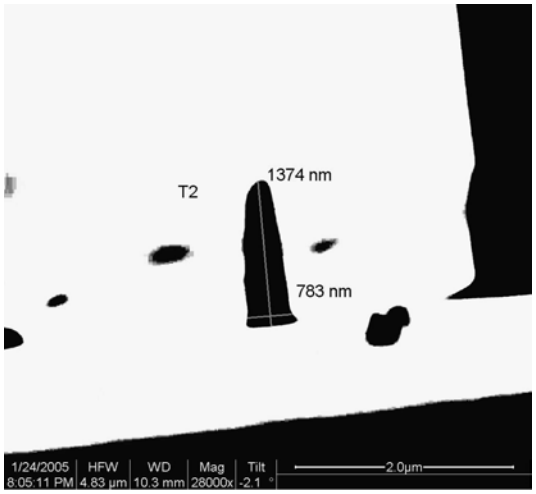

T2 Measurements (Settings: HV=30 kV, BC=50 pA, T=5 min)

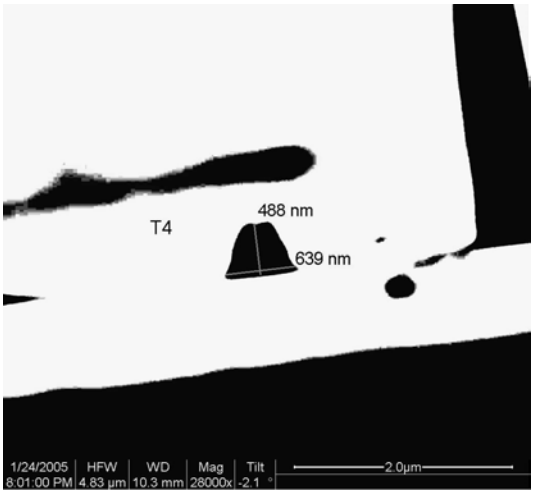

T4 Measurements (Settings: HV=10 kV, BC=50 pA, T=5 min)

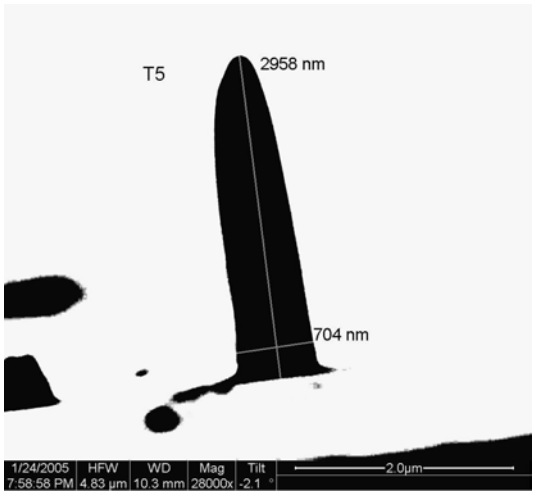

T5 Measurements (Settings: HV=30 kV, BC=5400 pA, T=5 min)

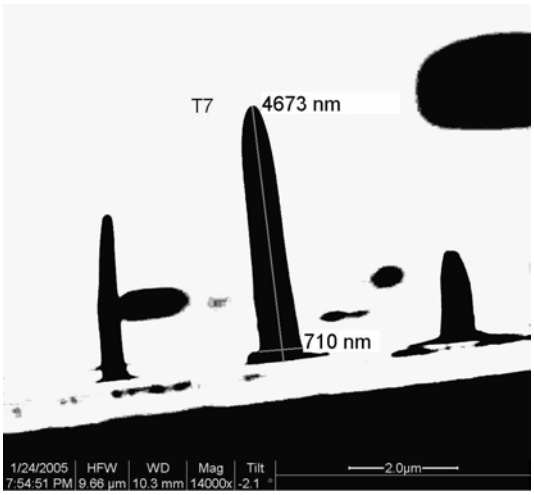

T7 Measurements (Settings: HV=30 kV, BC=5400 pA, T= 15 min)

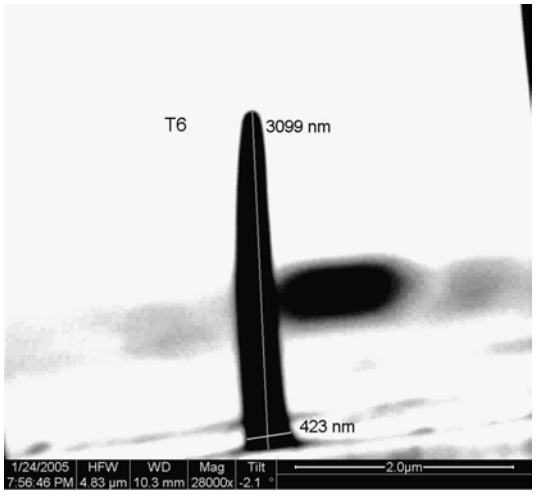

T6 Measurements (Settings: HV= 30 kV, BC=50 pA, T=15 min)

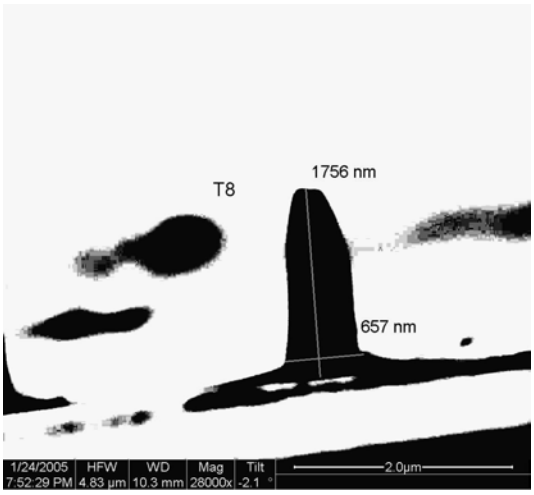

T8 Measurements (Settings: HV=10 kV, BC=50 pA, T=15 min)

Appendix A.5: 2nd Platinum Fiber Factorial Study

Note: HV = High Voltage, BC = Beam Current, T = Deposition Time

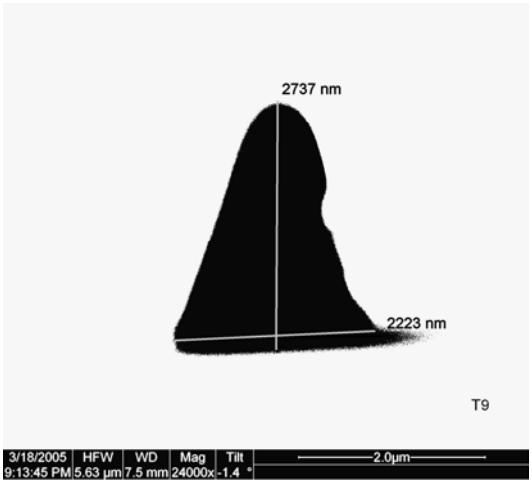

T9 Measurements (HV=5 kV, BC=20,000 pA, T=5 min)

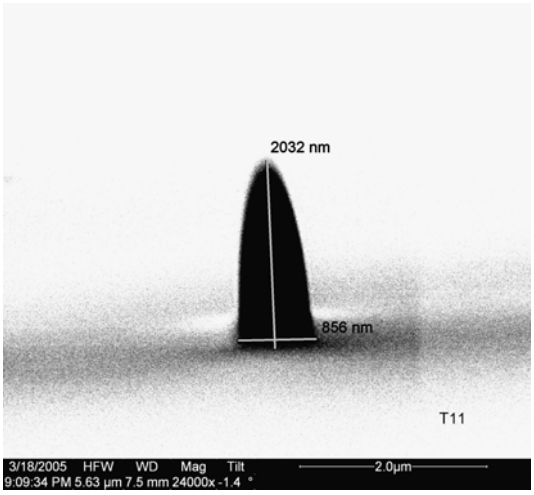

T11 Measurements (HV=30 kV, BC=20,000 pA, T=5 min)

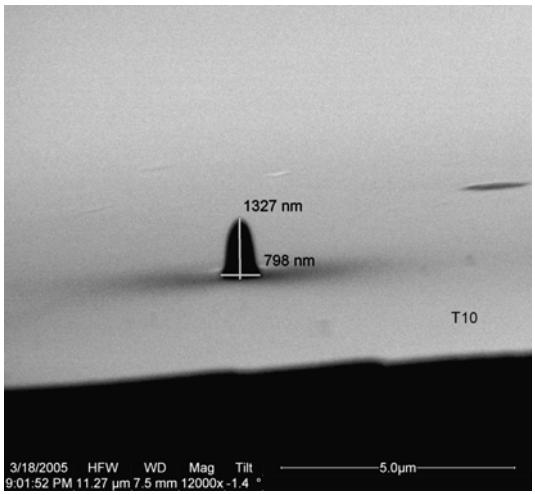

T10 Measurements (HV=5 kV, BC=1,500 pA, T=5 min)

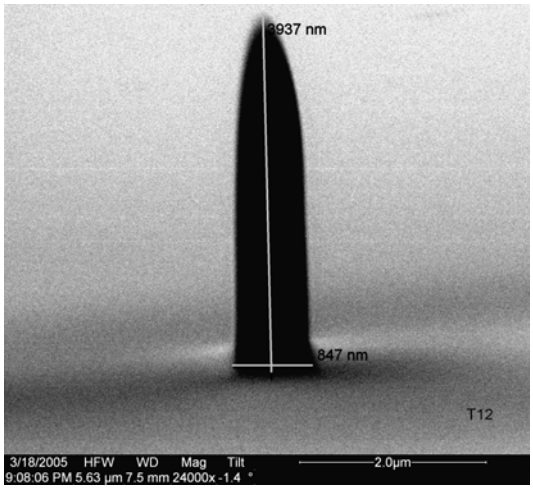

T12 Measurements (HV=30 kV, BC=20,000 pA, T=15 min)

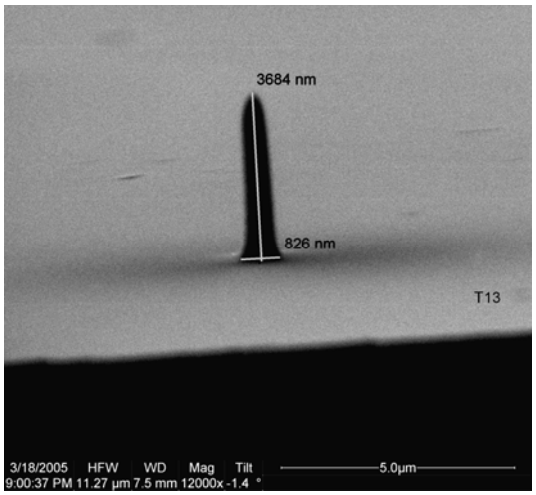

T13 Measurements (HV=5 kV, BC=1,500 pA, T=15 min)

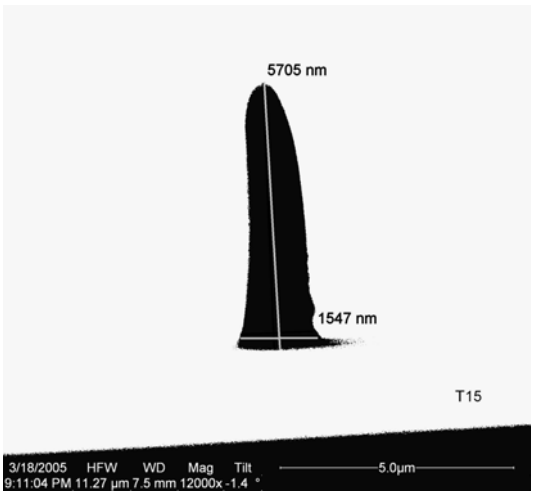

T15 Measurements (HV=5 kV, BC=20,000 pA, T=15 min)

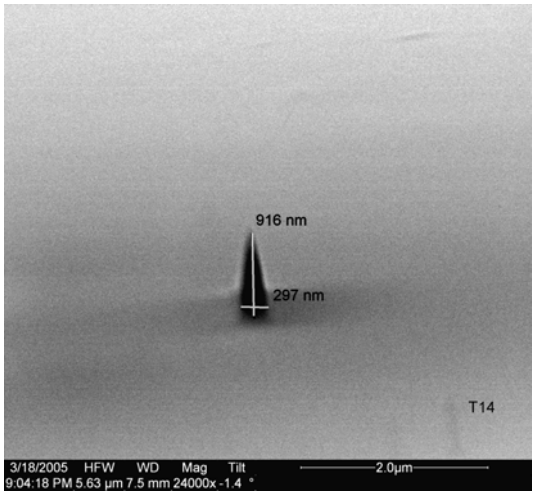

T14 Measurements (HV=30 kV, BC=1,500 pA, T=5 min)

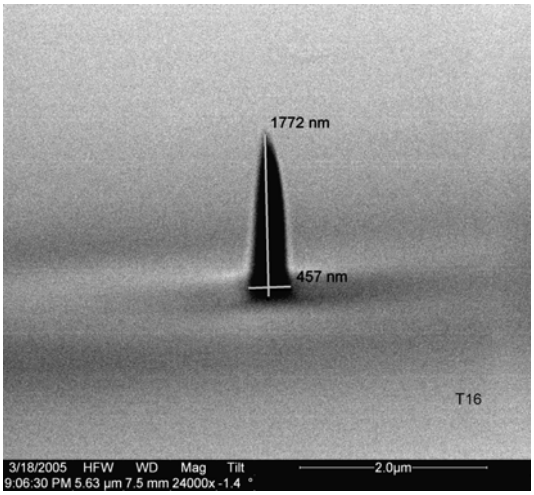

T16 Measurements (HV=30 kV, BC=1,500 pA, T=15 min)

Appendix A.6: Platinum Fiber Central Composite Experiment Measurements

Note: HV = High Voltage, BC = Beam Current, T = Deposition Time

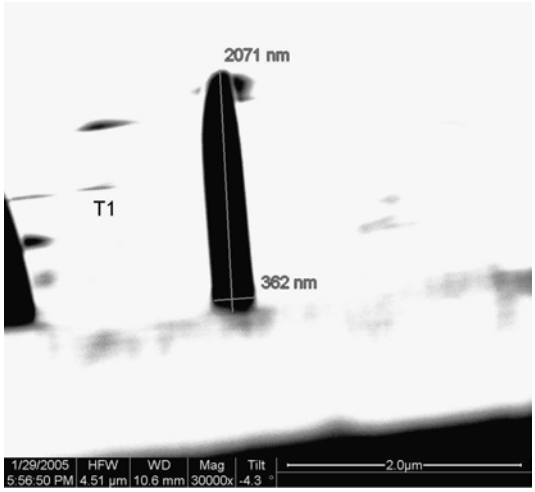

T1 Measurements (Settings: HV=30.1 kV, BC=1200 pA, T=9 min)

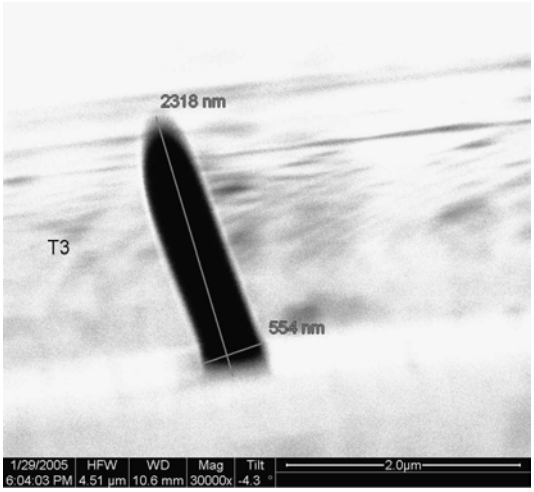

T3 Measurements (Settings: HV=17.5 kV, BC=1490 pA, T=9 min)

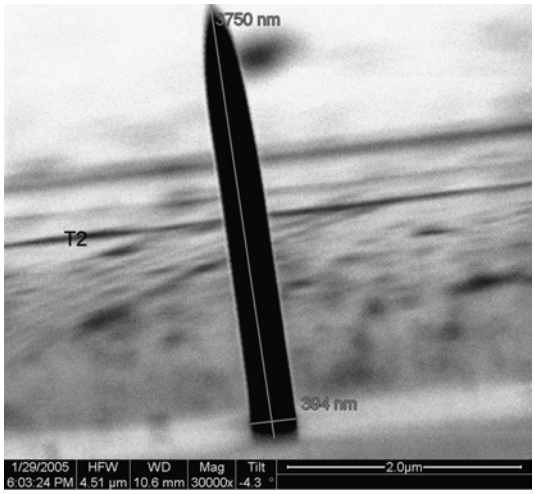

T2 Measurements (Settings: HV=25 kV, BC=1200 pA, T=14 min)

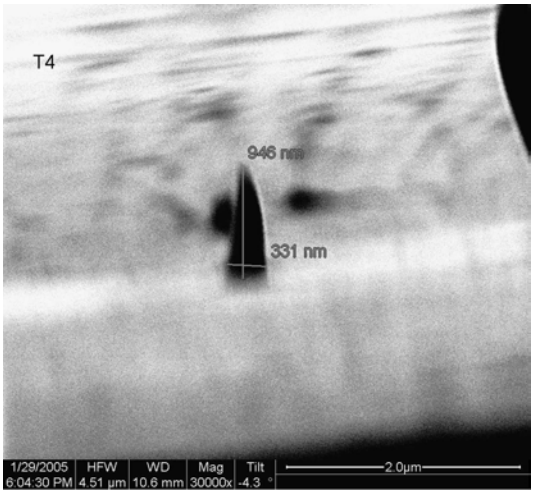

T4 Measurements (Settings: HV=25 kV, BC=3650 pA, T=4 min)

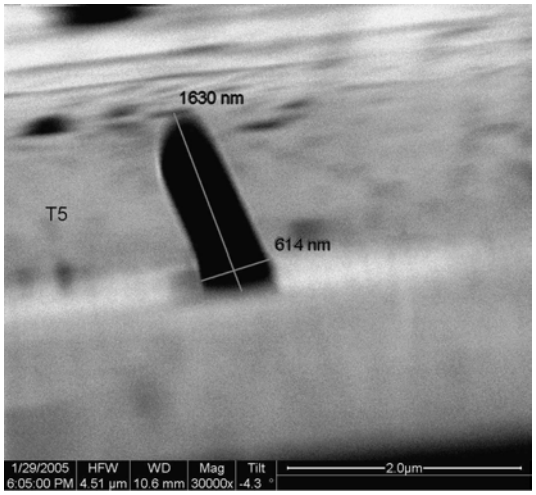

T5 Measurements (HV=10 kV, BC=1200 pA, T=4 min)

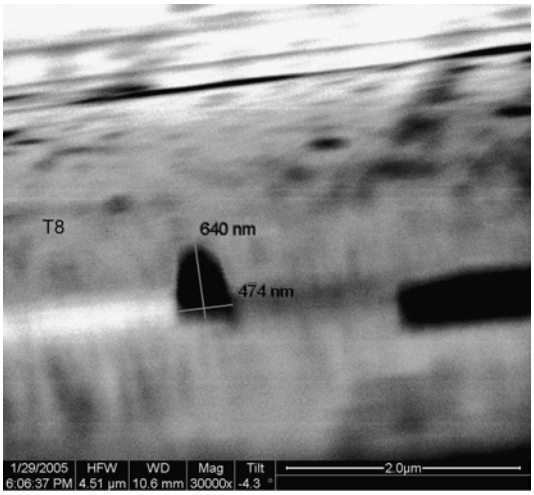

T8 Measurements (HV=17.5 kV, BC=60 pA, T=9 min)

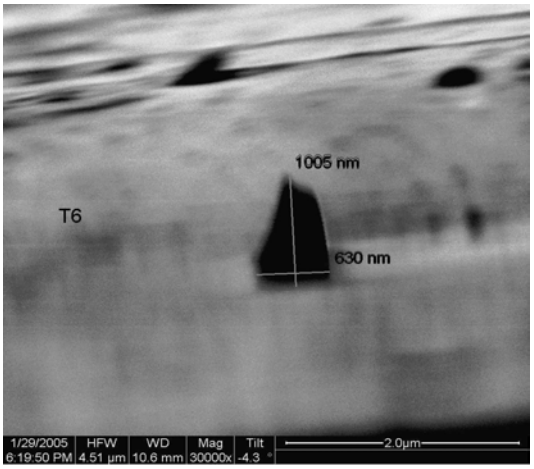

T6 Measurements (HV=25 kV, BC=350 pA, T=14 min)

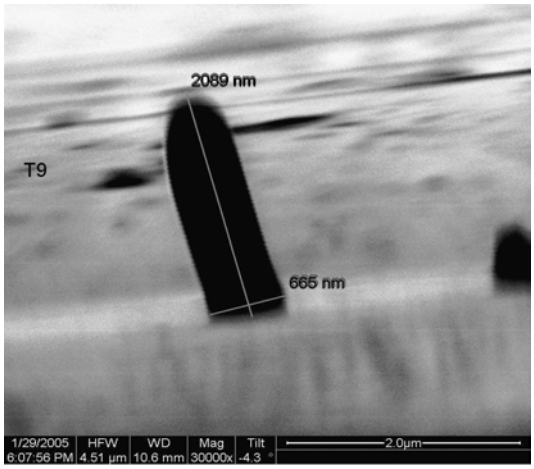

T9 Measurements (HV=17.5 kV, BC=775 pA, T=9 min)

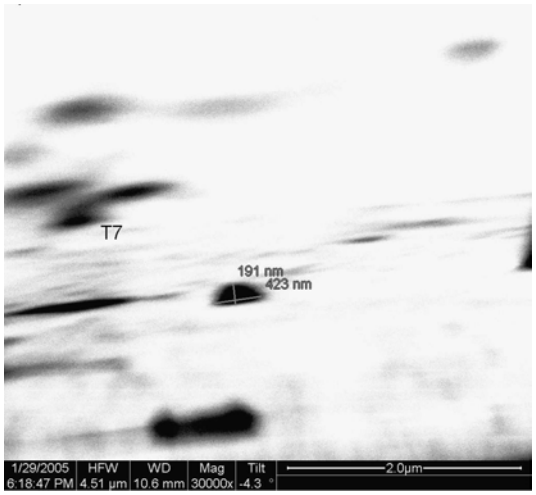

T7 Measurements (HV=17.5 kV, BC=775 pA, T=0.59 min)

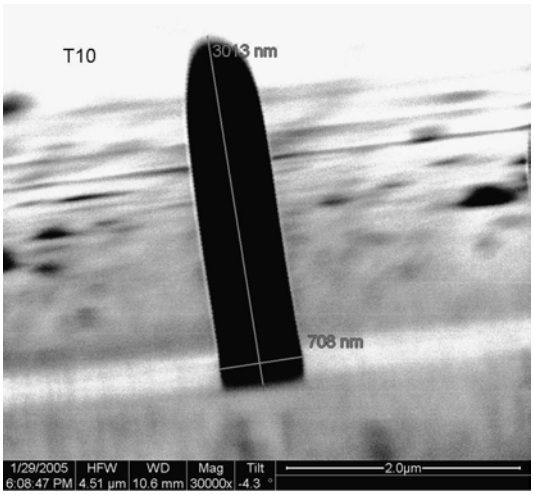

T10 Measurements (HV=17.5 kV, BC=775 pA, T=17.4 min)

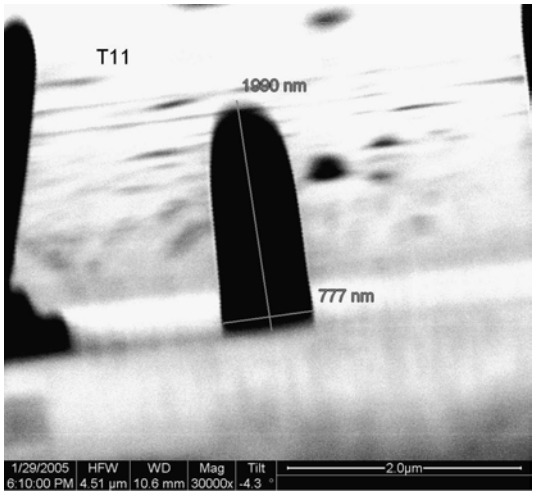

T11 Measurements (HV=17.5 kV, BC=775 pA, T=9 min)

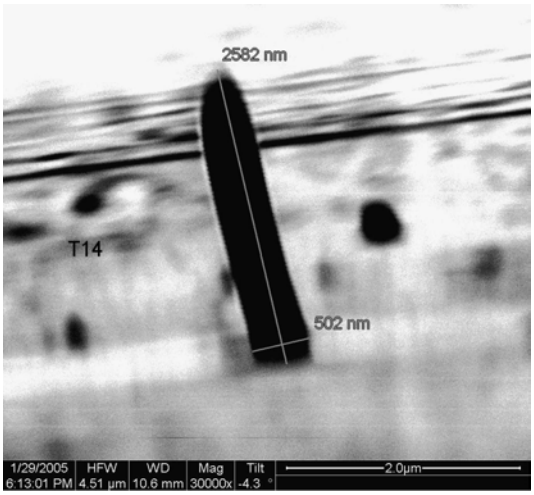

T14 Measurements (HV=10 kV, BC=350 pA, T=14 min)

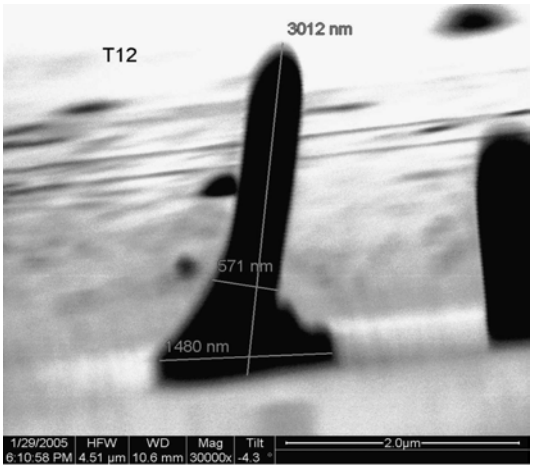

T12 Measurements (HV=4.9 kV, BC=775 pA, T=9 min)

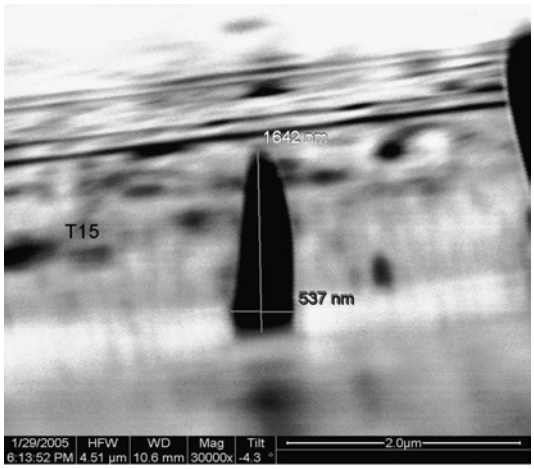

T15 Measurements (HV=25 kV, BC=1200 pA, T=4 min)

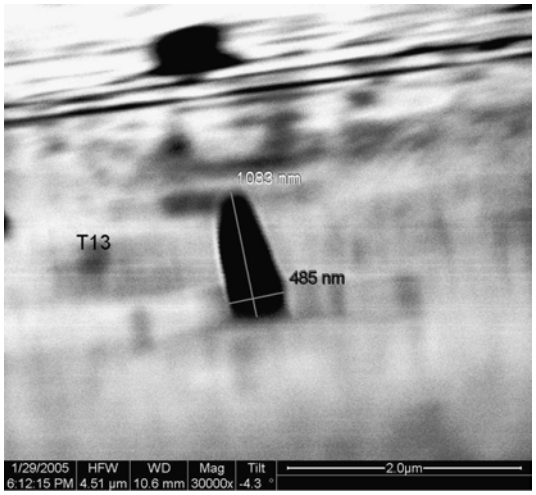

T13 Measurements (HV=10 kV, BC=350 pA, T=4 min)

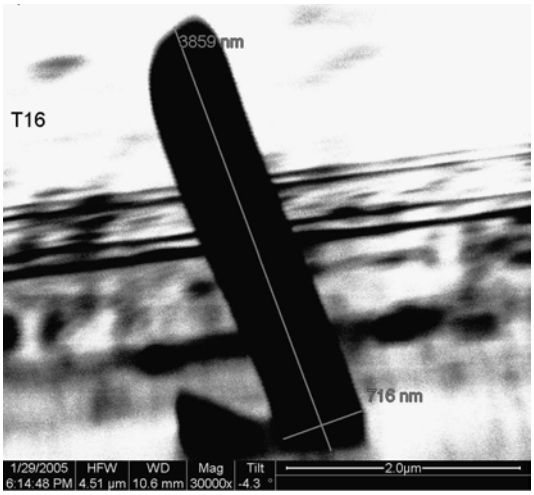

T16 Measurements (HV=10 kV, BC=1200 pA, T=14 min)

Appendix A.7: Platinum Line 2^3 Factorial Experiment Measurements

Note: HV = High Voltage, BC = Beam Current, DT = Dwell Time, LT = Line Time

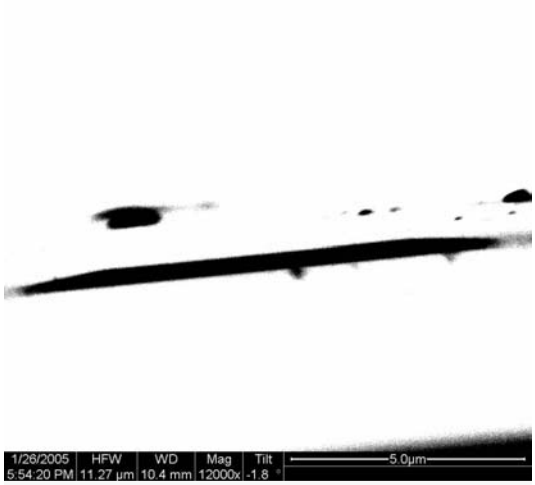

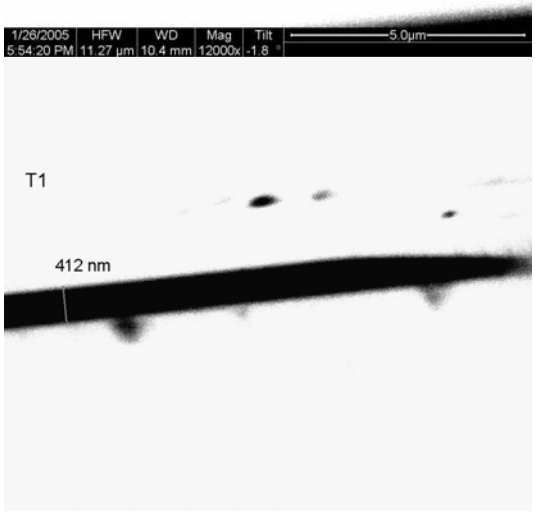

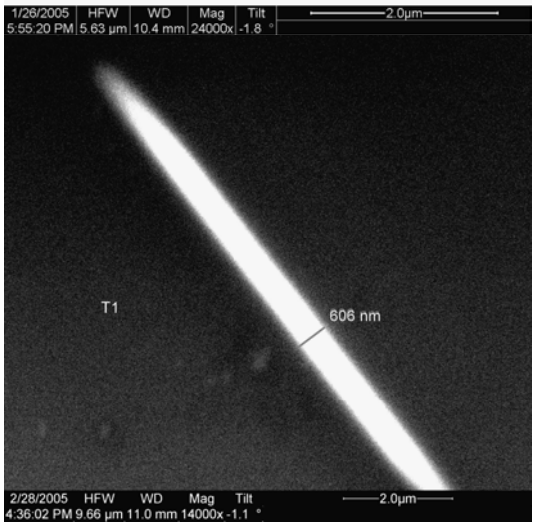

T1 Measurements (Settings: HV=30 kV, BC=5400 pA, DT= 10 µs, LT=10.60 ms)

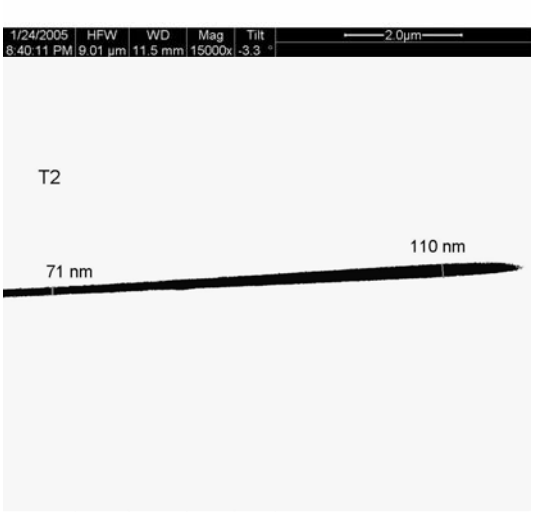

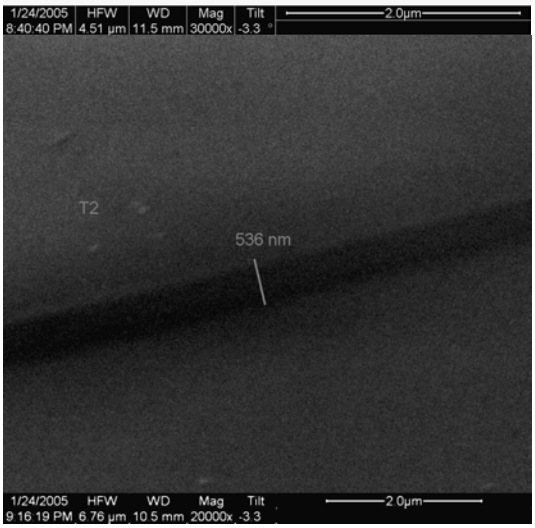

T2 Measurements (Settings: HV=10 kV, BC=50 pA, DT=10 µs, LT=10.60 ms)

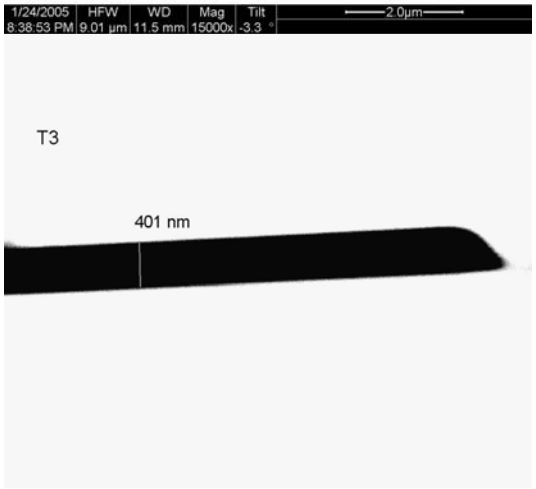

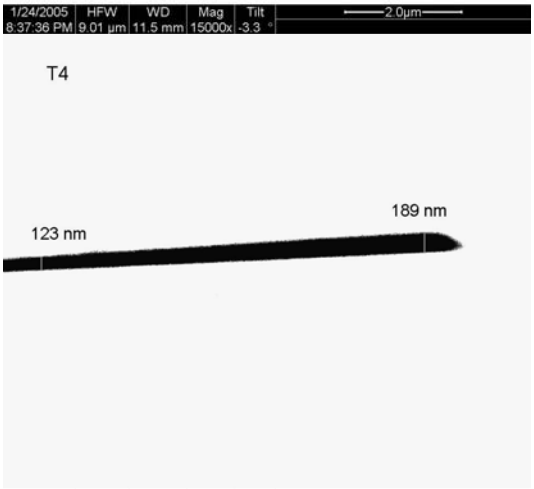

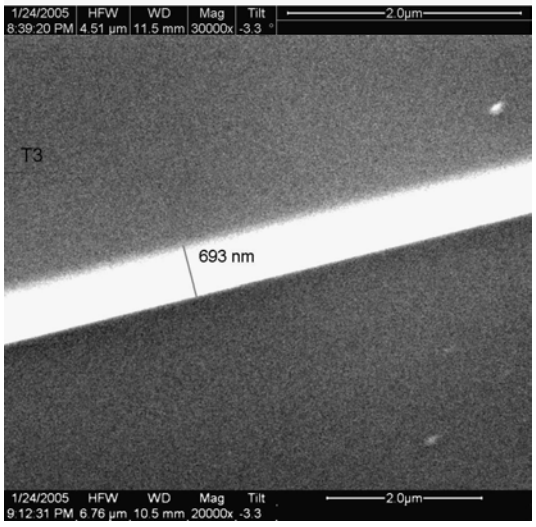

T3 Measurements (Settings: HV=30 kV, BC=5400 pA, DT=1000 µs, LT=1060 ms)

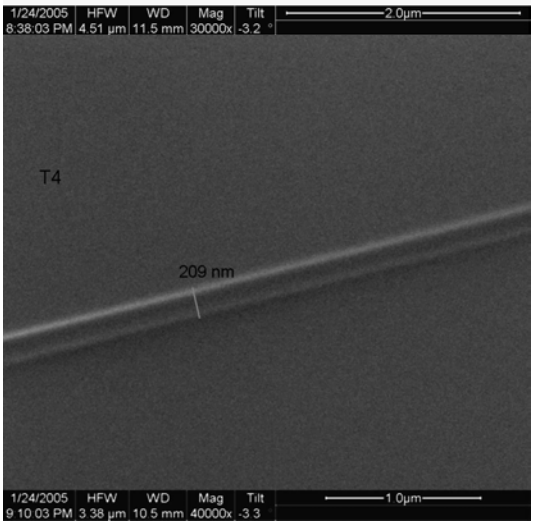

T4 Measurements (Settings: HV=30 kV, BC=50 pA, DT=10 µs, LT=10.60 ms)

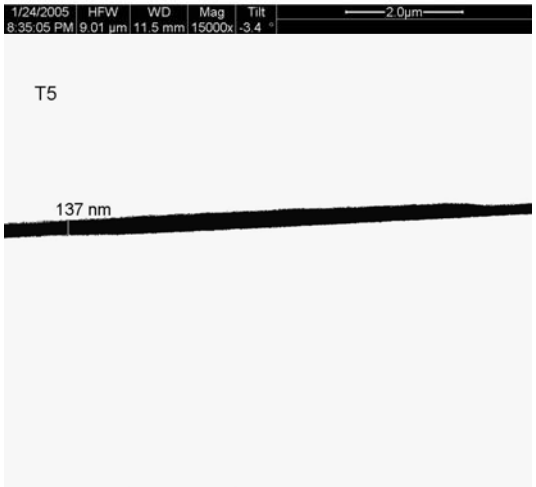

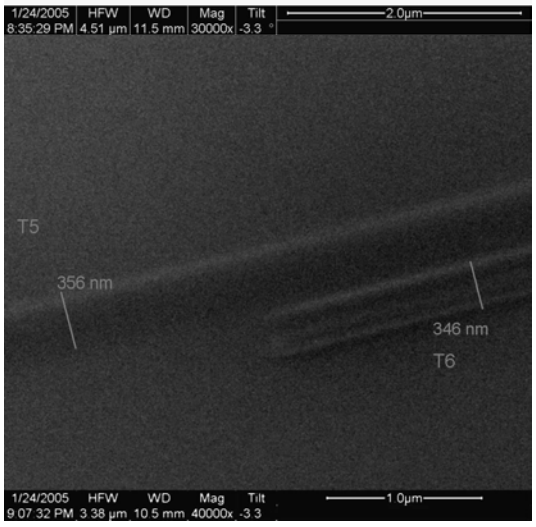

T5 Measurements (Settings: HV=10 kV, BC=50 pA, DT=1000 µs, LT=1060 ms)

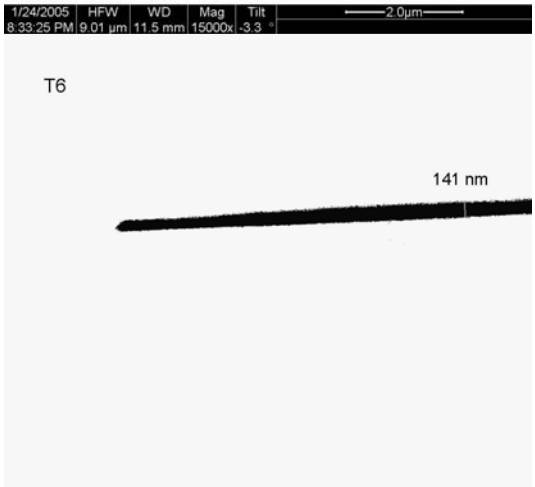

T6 Measurements (Settings: HV=30 kV, BC=50 pA, DT=1000 µs, LT=1060 ms)

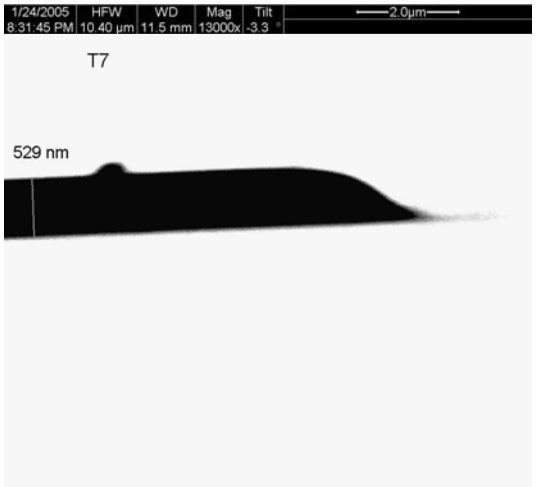

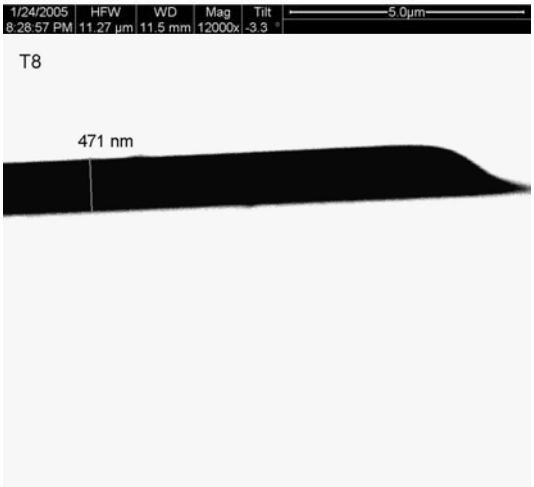

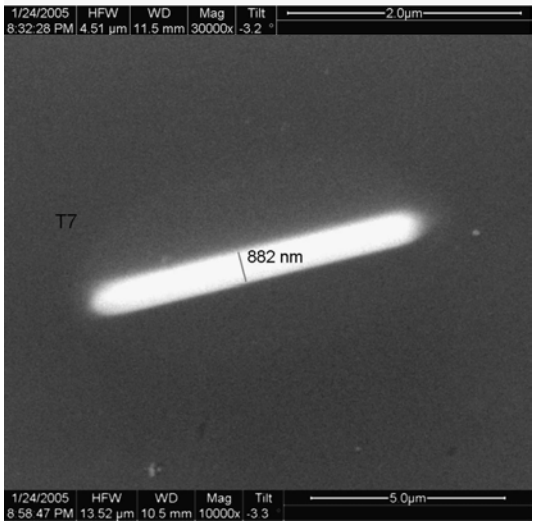

T7 Measurements (Settings: HV=10 kV, BC=5400 pA, DT=10 µs, LT=10.60 ms)

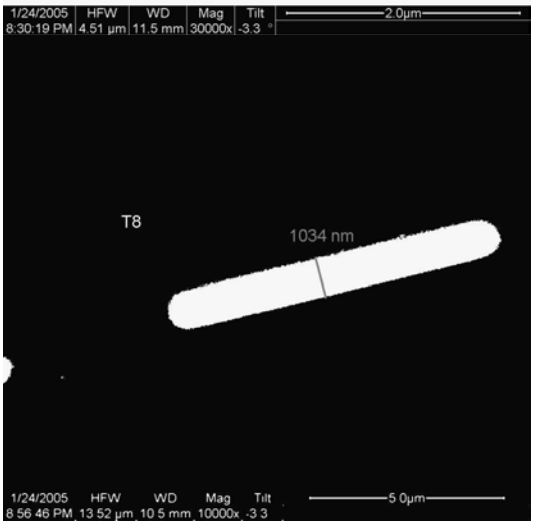

T8 Measurements (Settings: HV=10 kV, BC=5400 pA, DT=1000 µs, LT=1060 ms)

Appendix A.8: Platinum Line Central Composite Experiment Measurements

Note: HV= High Voltage, BC= Beam Current, DT= Dwell Time, LT= Line Time

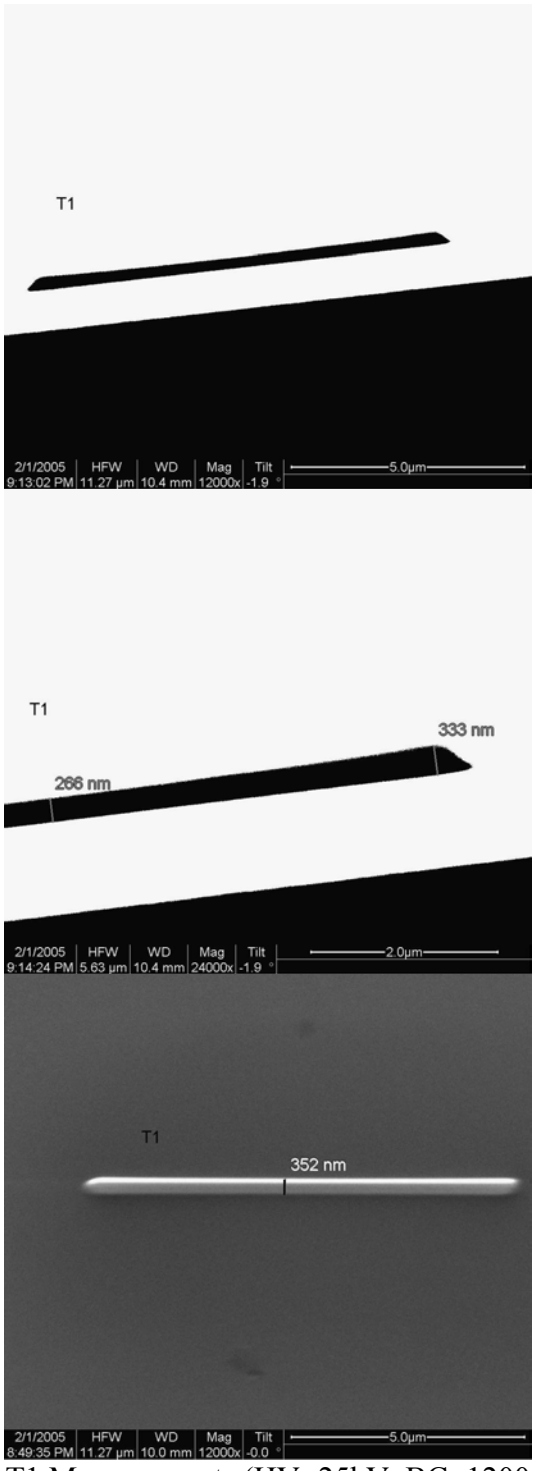

T1 Measurements (HV=25kV, BC=1200 pA, DT=100 µs, LT=0.11 s)

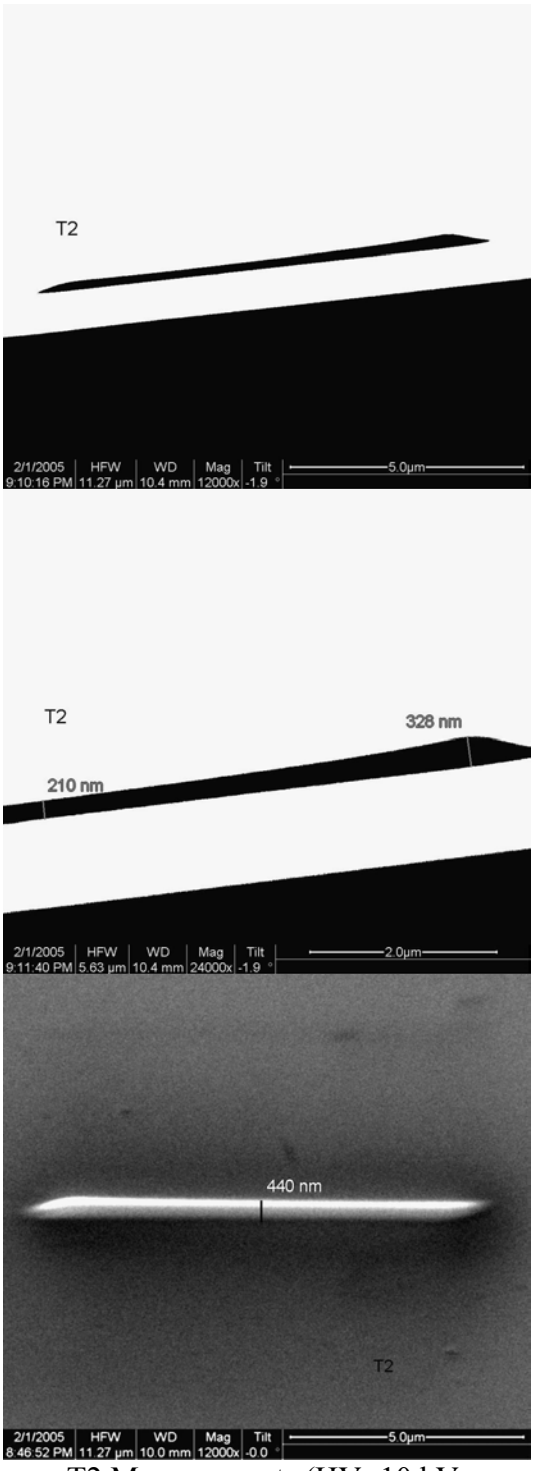

T2 Measurements (HV=10 kV, BC=1200 pA, DT=100 µs, LT=0.11 s)

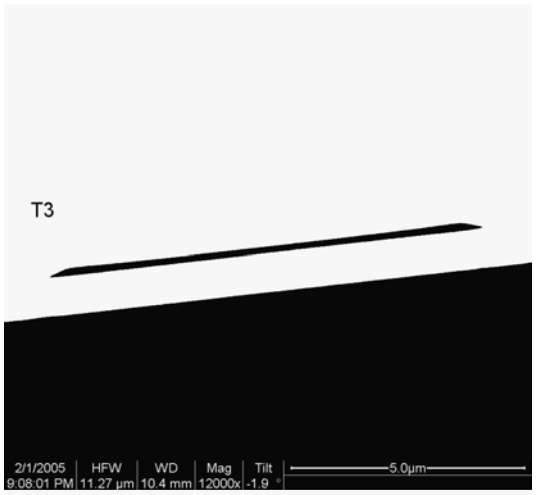

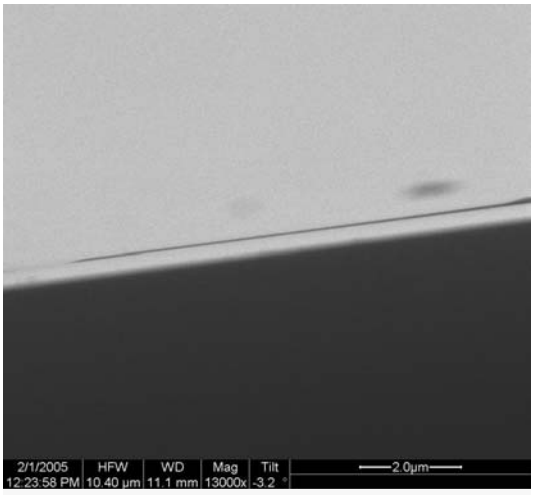

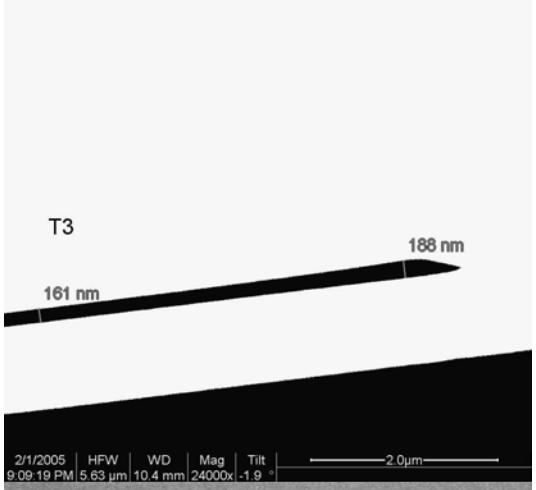

T3 Measurements (HV=17.5 kV, BC=1490 pA, DT=237.5 µs, LT=0.25 s)

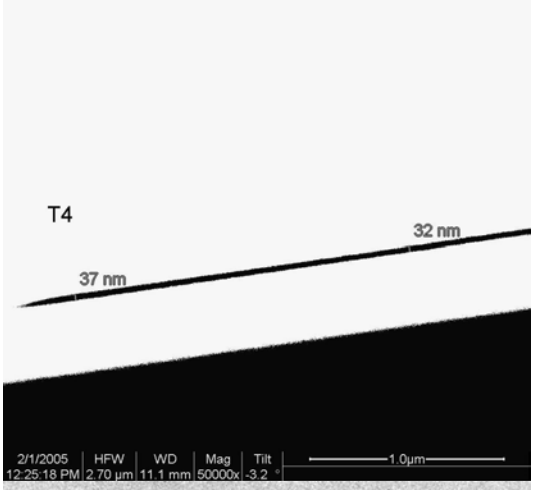

T4 Measurements (HV=25 kV, BC=350 pA, DT=100 µs, LT=0.11 s)

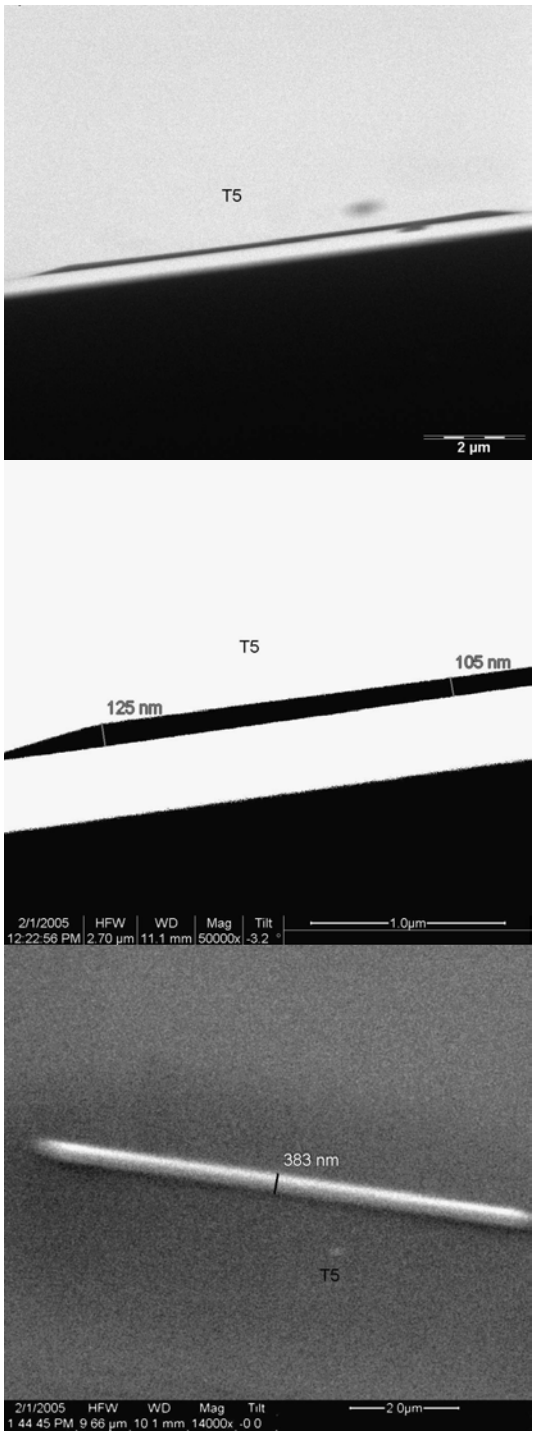

T5 Measurements (HV=17.5 kV, BC=775 pA, DT=237.5 µs, LT=0.25 s)

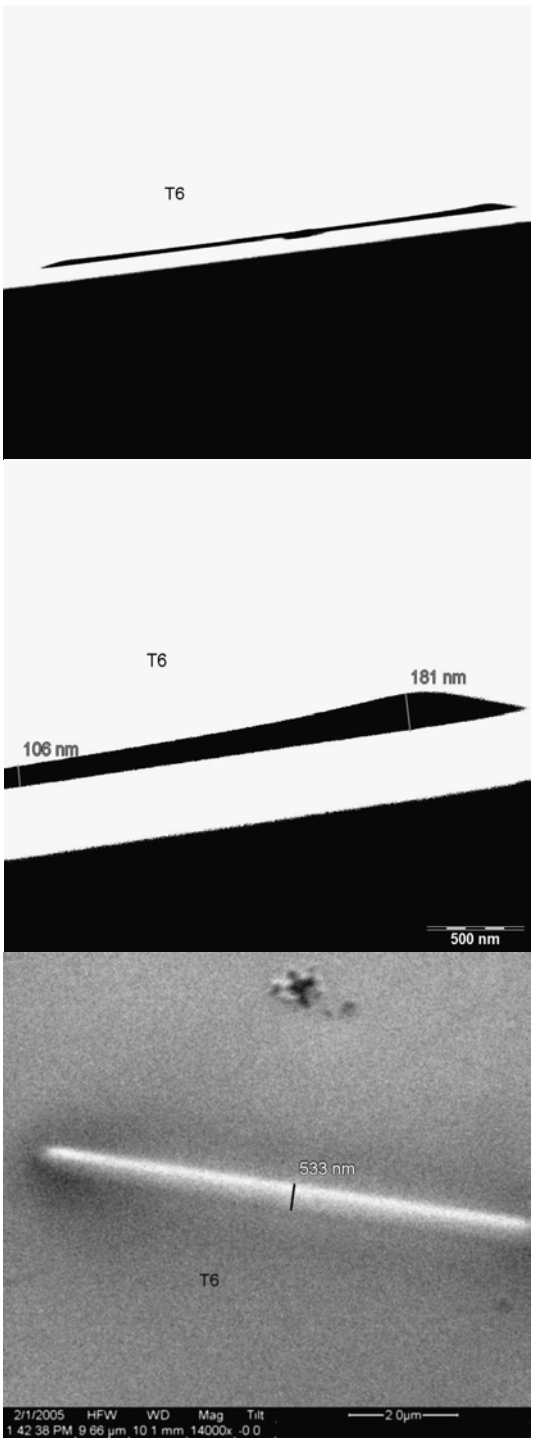

T6 Measurements (HV=10 kV, BC=350 pA, DT=100 µs, LT=0.11 s)

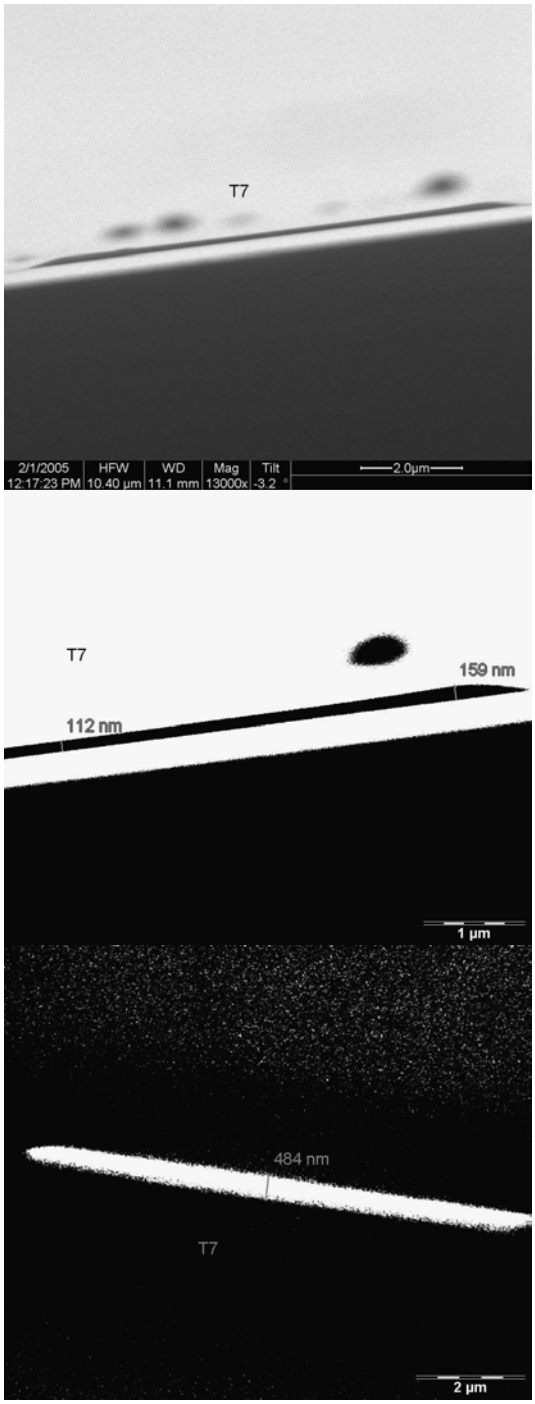

T7 Measurements (HV=17.5 kV, BC=775 pA, DT=468.75 µs, LT=0.50 s)

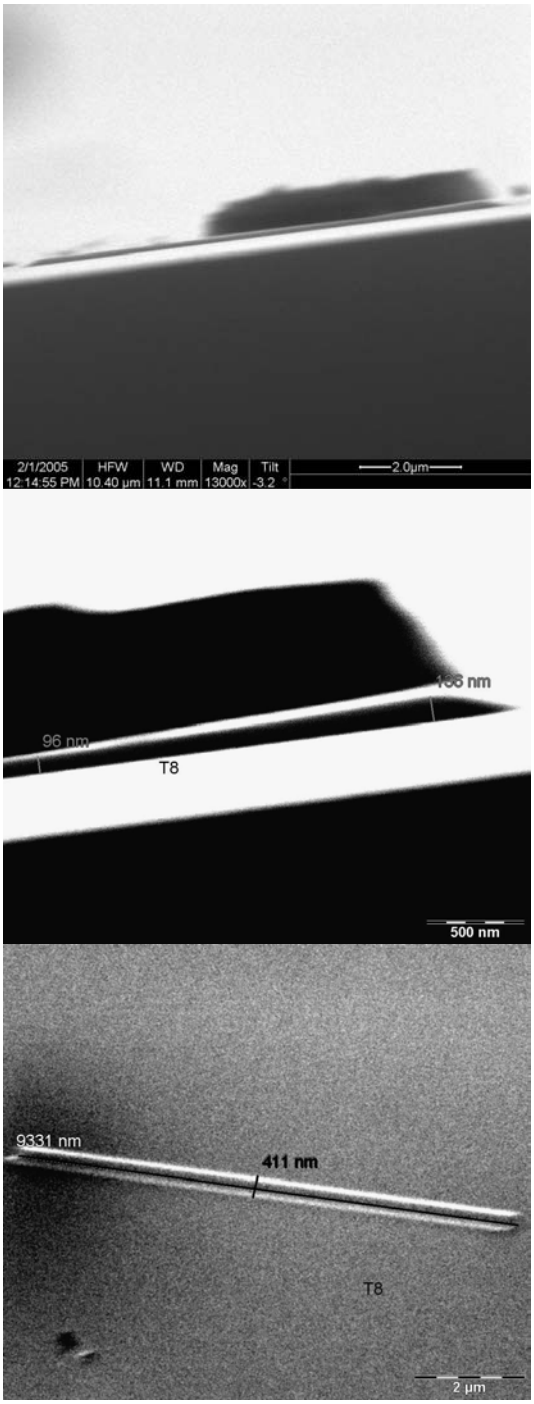

T8 Measurements (HV=30.1 kV, BC=775 pA, DT=237.5 µs, LT=0.25 s)

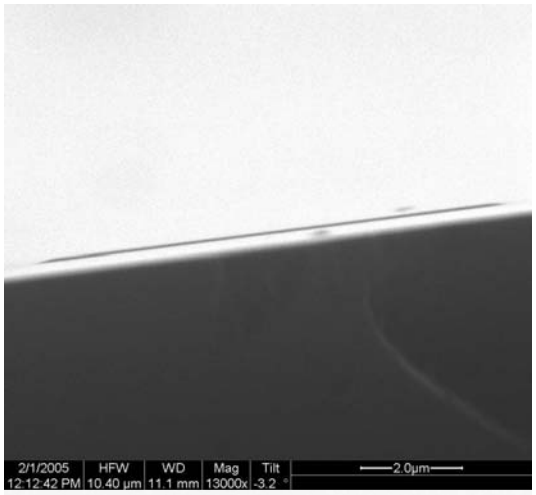

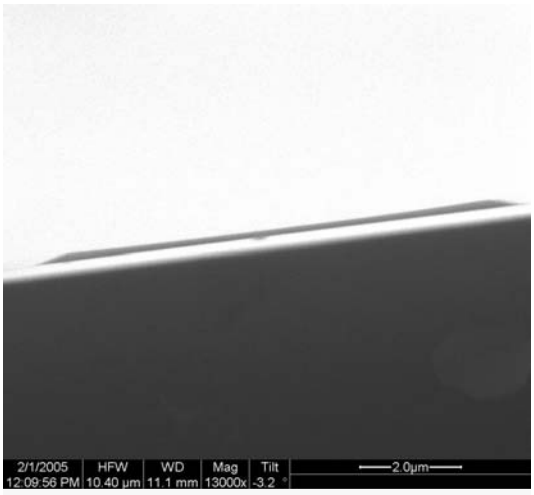

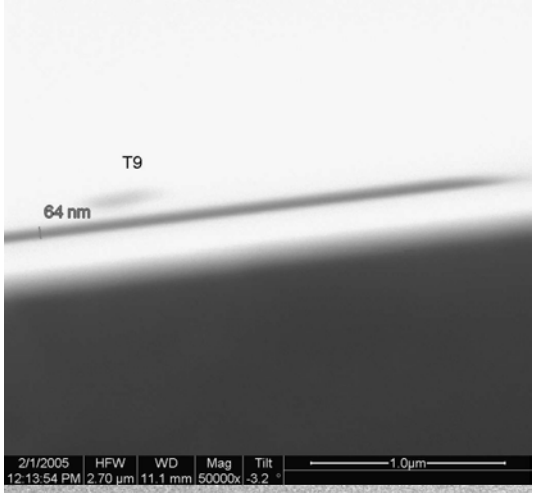

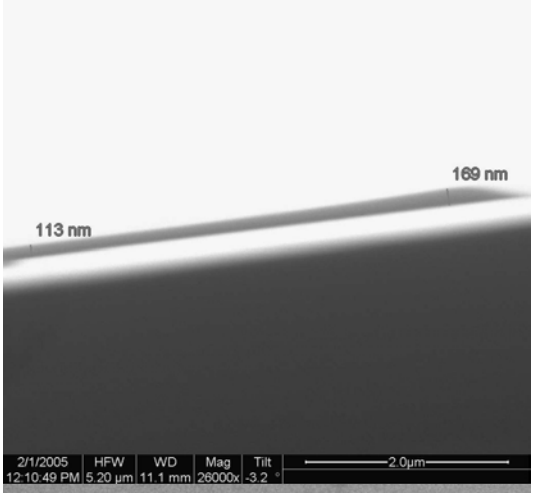

T9 Measurements (HV=25 kV, BC=350 pA, DT=375 µs, LT=0.40 s)

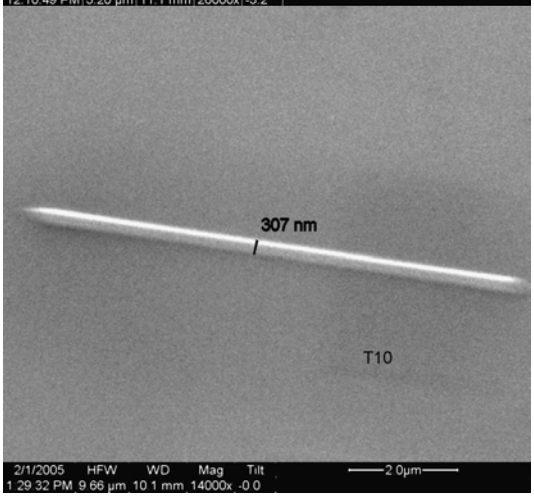

T10 Measurements (HV=17.5 kV, BC=775 pA, DT=237.5 µs, LT=0.25 s)

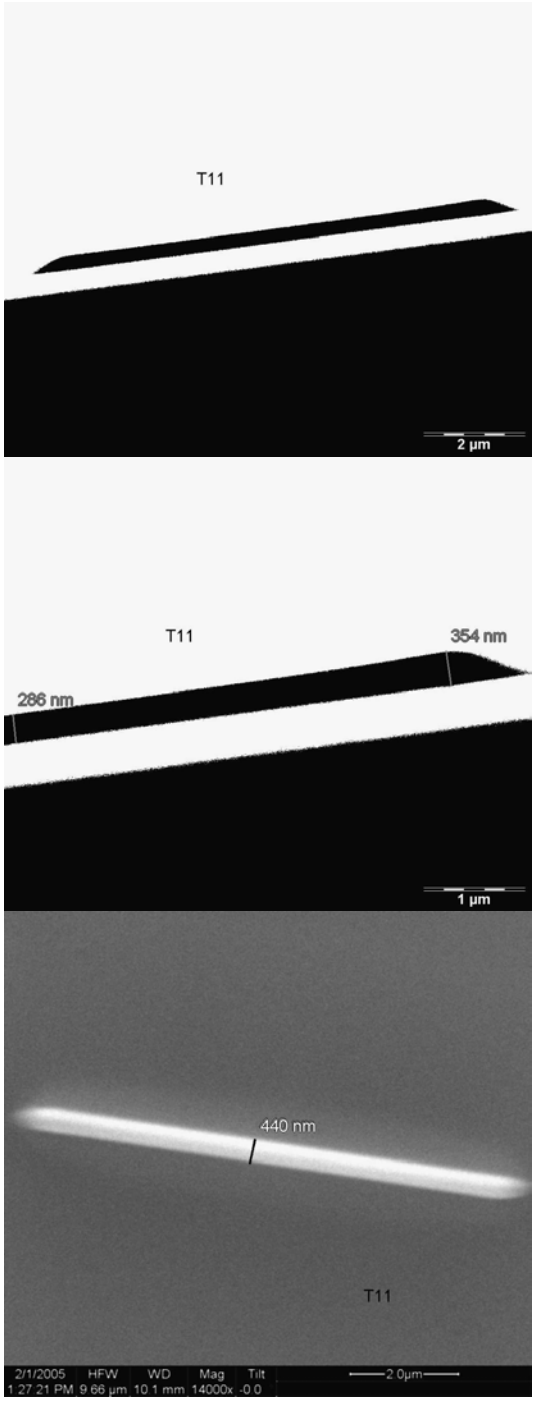

T11 Measurements (HV=10 kV, BC=1200 pA, DT=375 µs, LT=0.40 s)

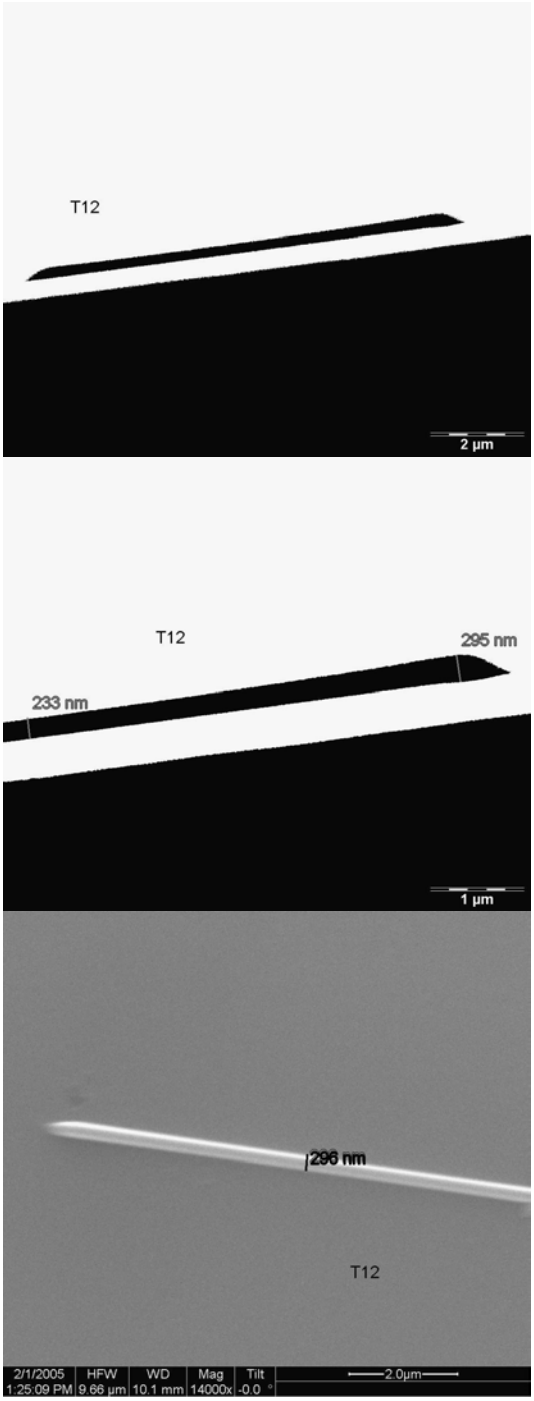

T12 Measurements (HV=25 kV, BC=1200 pA, DT=375 µs, LT=0.40 s)

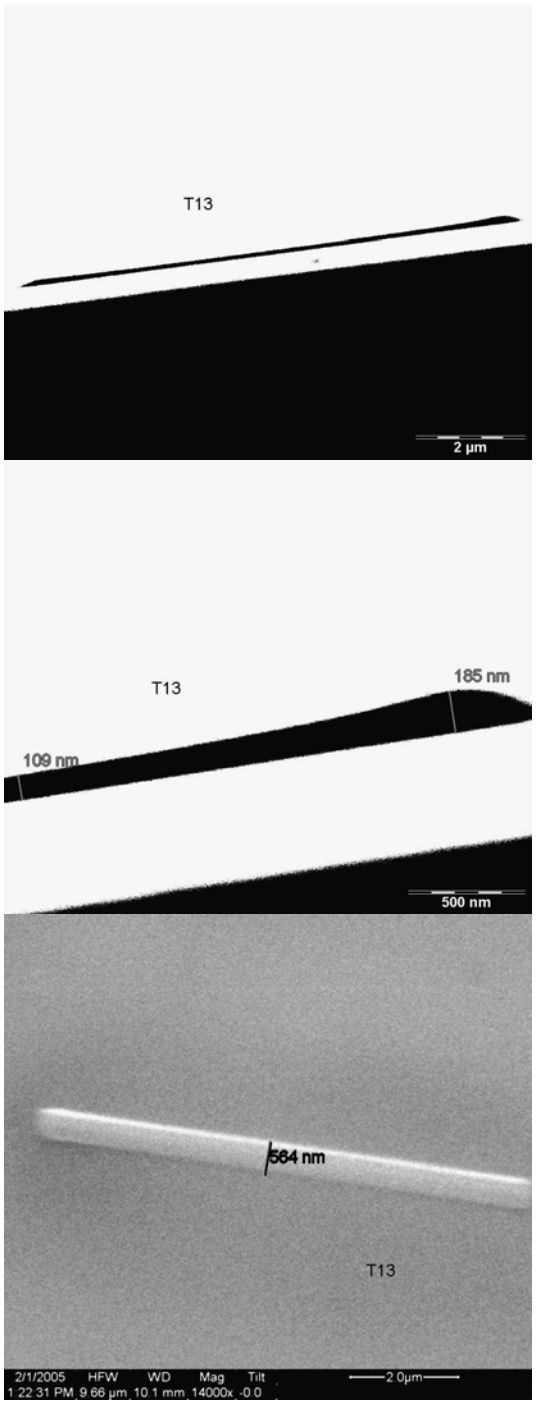

T13 Measurements (HV=17.5 kV, BC=775 pA, DT=6.25 µs, LT=.00662 s)

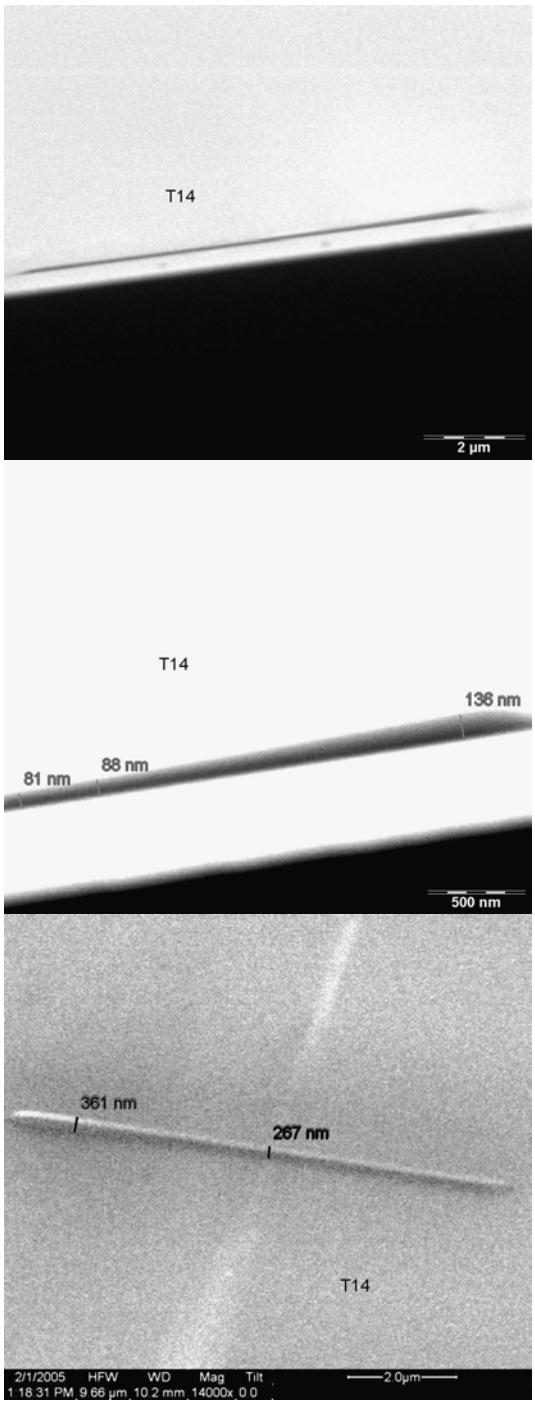

T14 Measurements (HV=17.5 kV, BC=60.2 pA, DT=237.5 µs, LT=0.25 s)

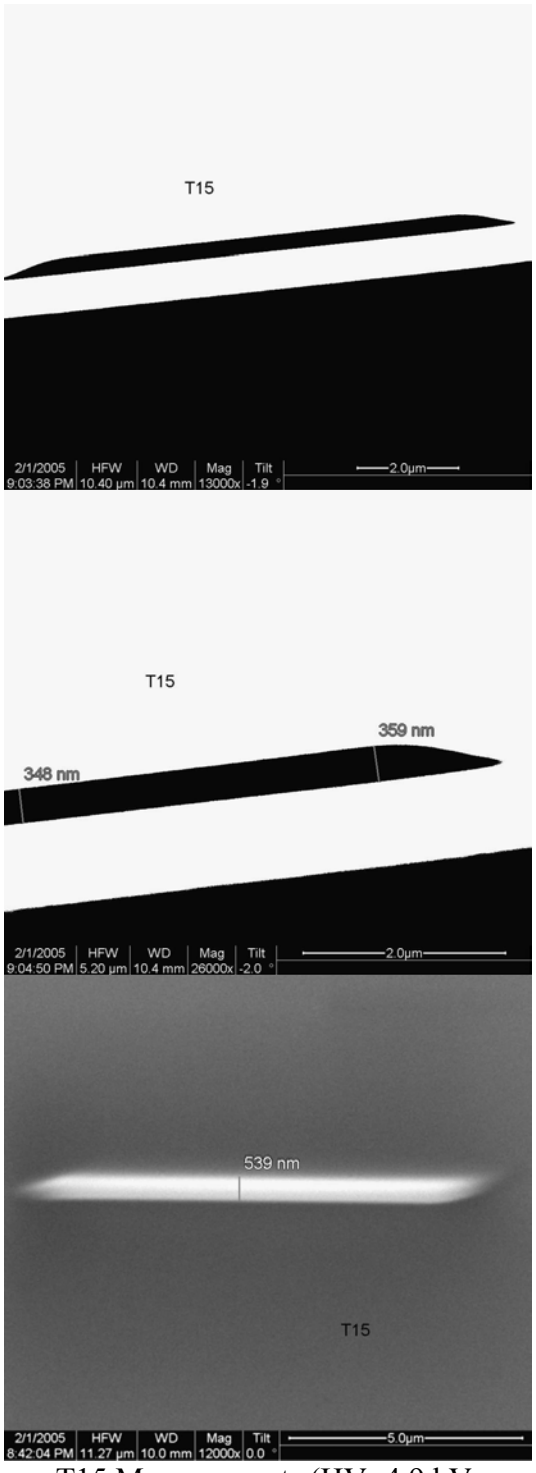

T15 Measurements (HV=4.9 kV, BC=775 pA, DT=237.5 µs, LT=0.25 s)

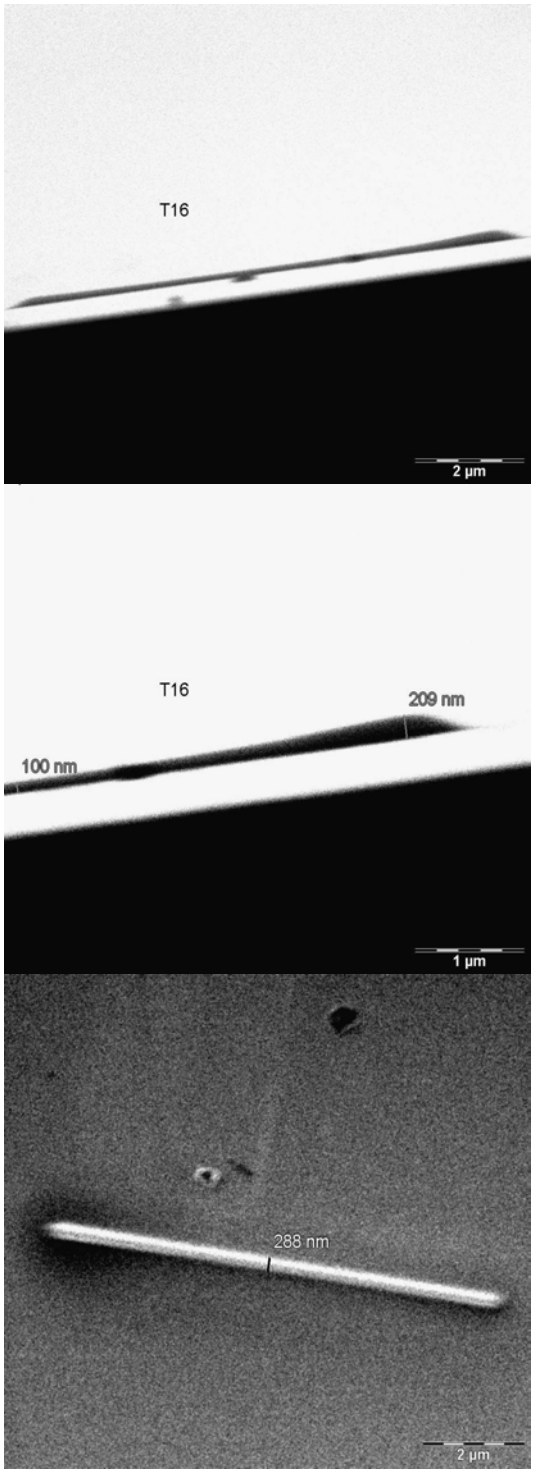

T16 Measurements (HV=10 kV, BC=350 pA, DT=375 µs, LT=0.40 s)

Appendix A.9: Platinum 2^3 Factorial Line Time Study Measurements

Note: HV = High Voltage, BC = Beam Current, LT = Line Time

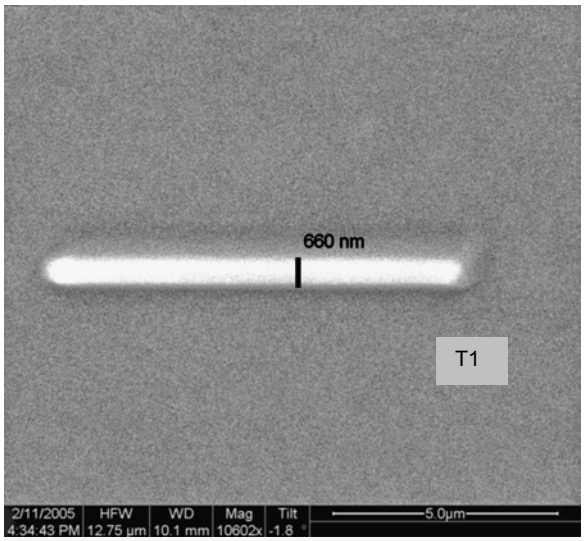

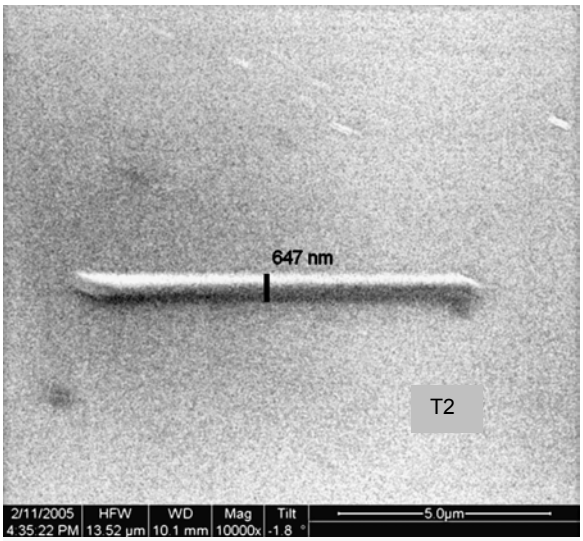

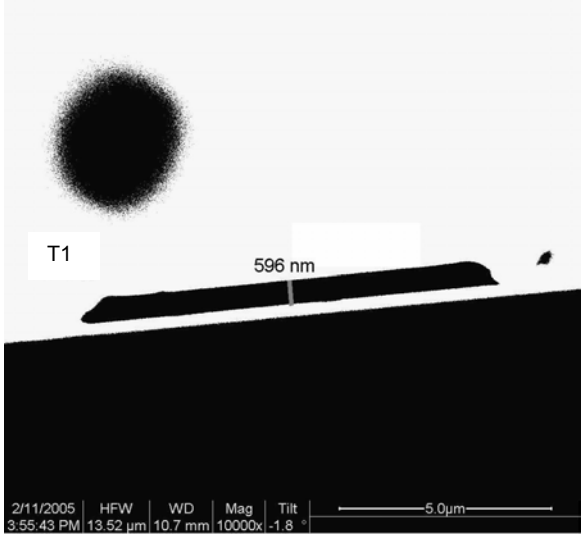

T1 Measurements (Settings: HV=30 kV, BC=5400 pA, LT=0.53 ms)

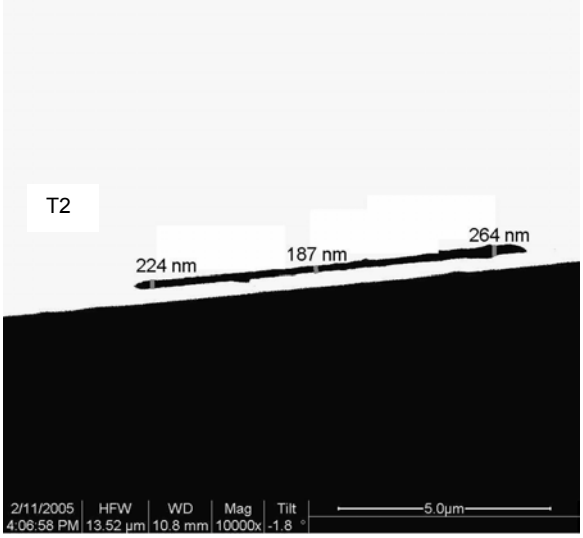

T2 Measurements (Settings: HV=30 kV, BC=100 pA, LT=0.53 ms)

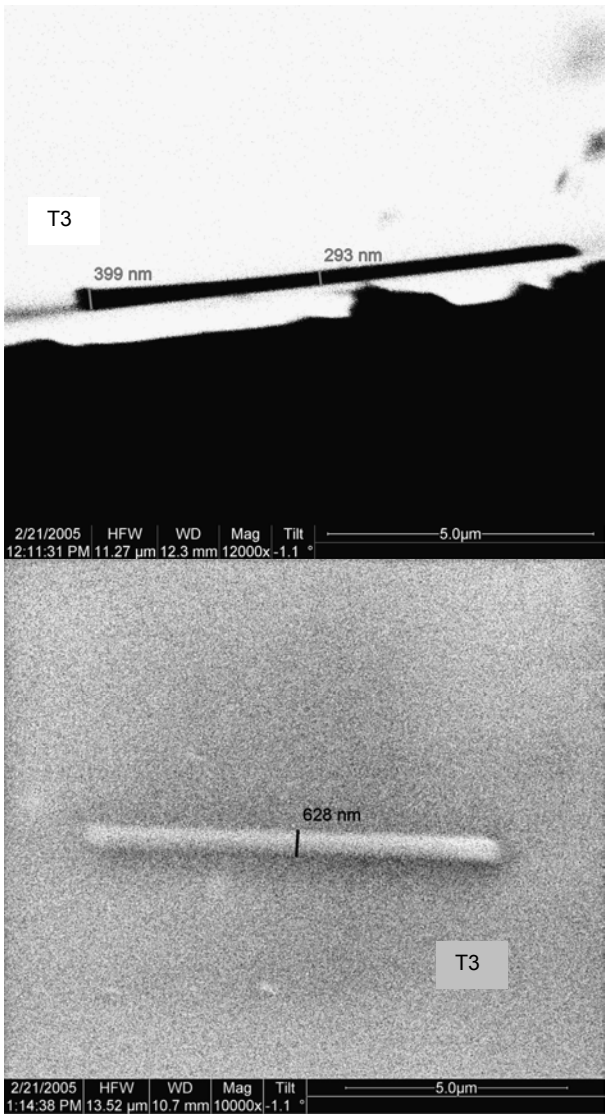

T3 Measurements (Settings: HV=10 kV, BC=100 pA, LT=0.53 ms)

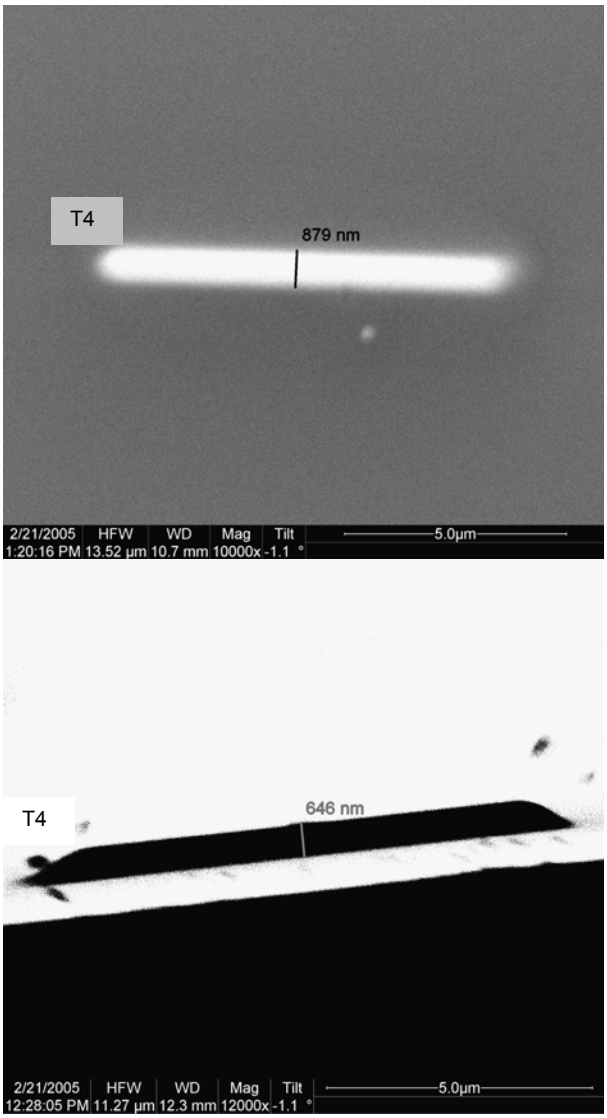

T4 Measurements (Settings: HV=10 kV, BC=5400 pA, LT=0.53 ms)

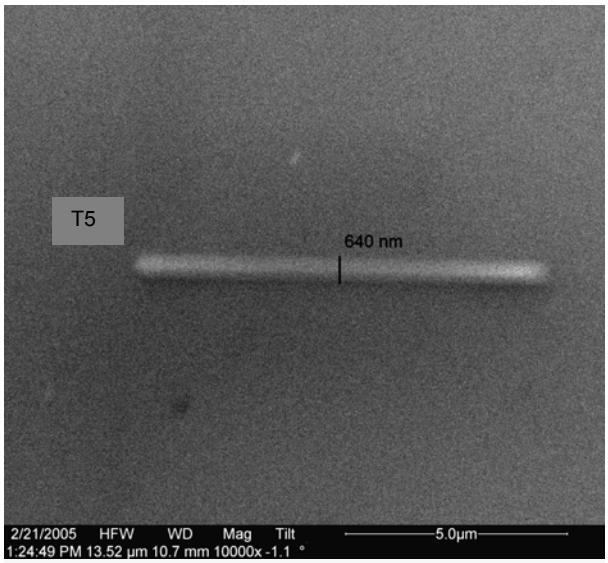

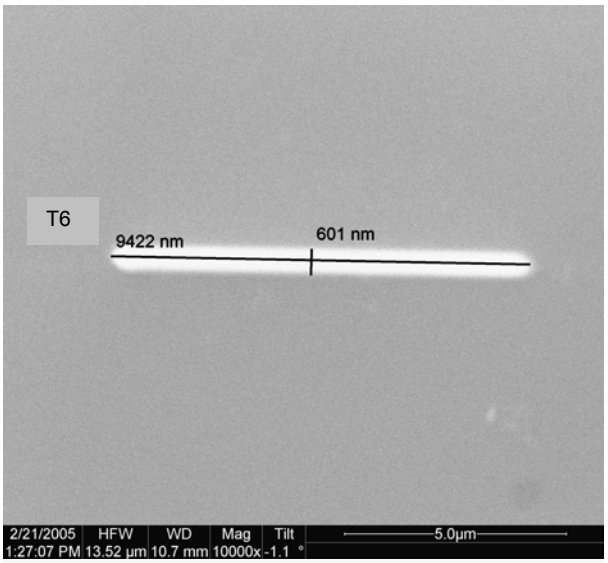

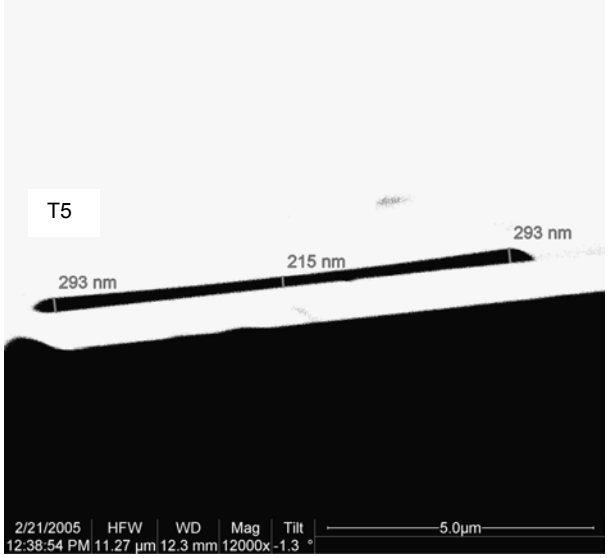

T5 Measurements (Settings: HV=30 kV, BC=100 pA, LT=2.12 ms)

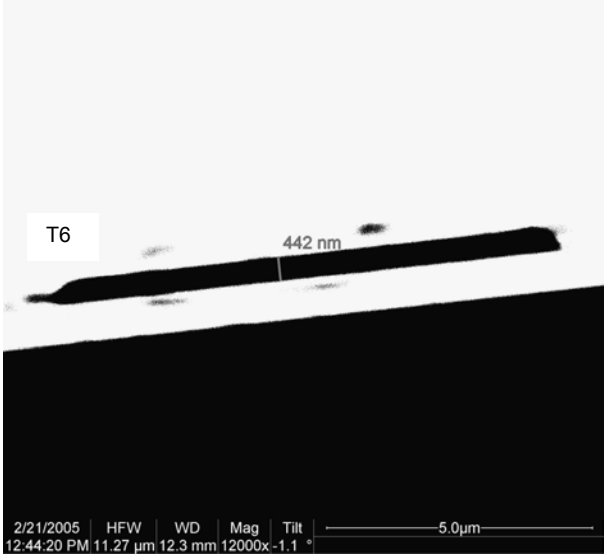

T6 Measurements (Settings: HV=30 kV, BC=5400 pA, LT=2.12 ms)

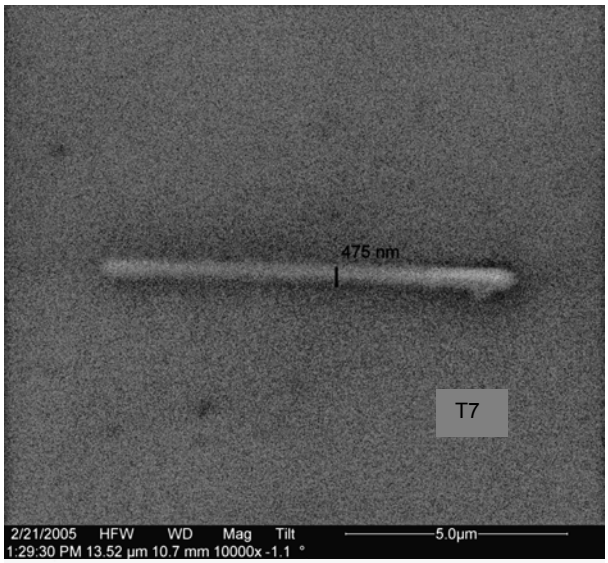

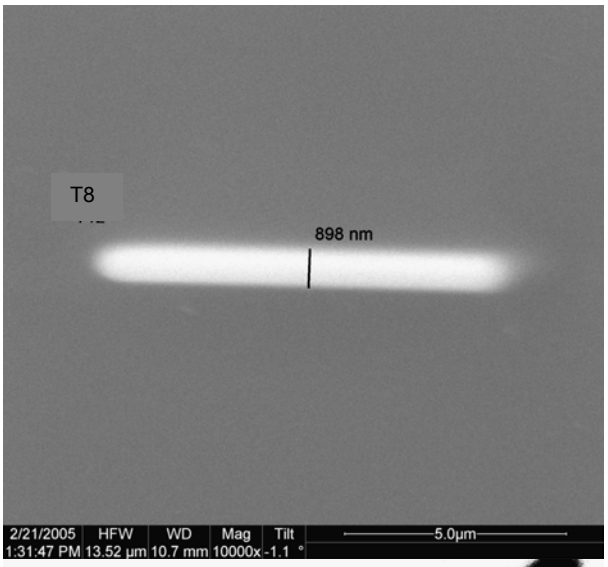

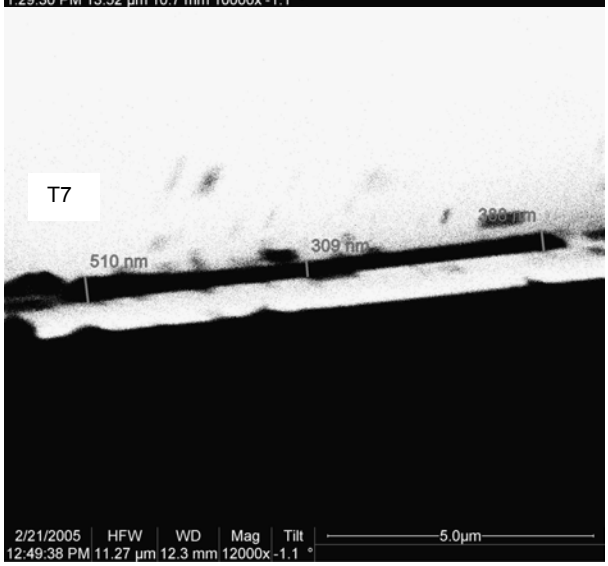

T7 Measurements (Settings: HV=10 kV, BC=100 pA, LT=2.12 ms)

T8 Measurements (Settings: HV=10 kV, BC=5400 pA, LT=2.12 ms)

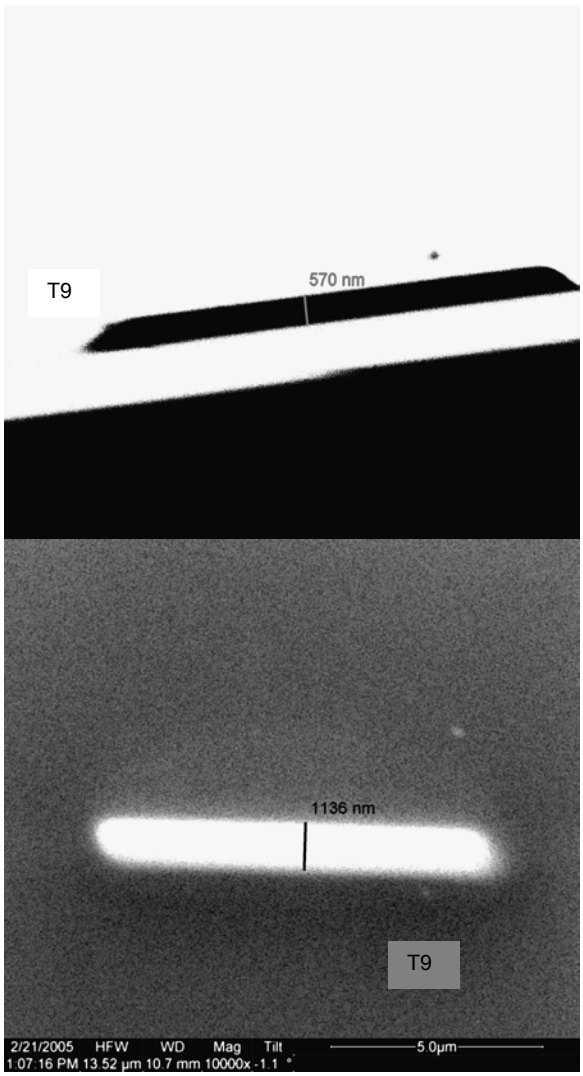

T9 Measurements (Settings: HV=10 kV, BC=5400 pA, LT=1.06 ms)

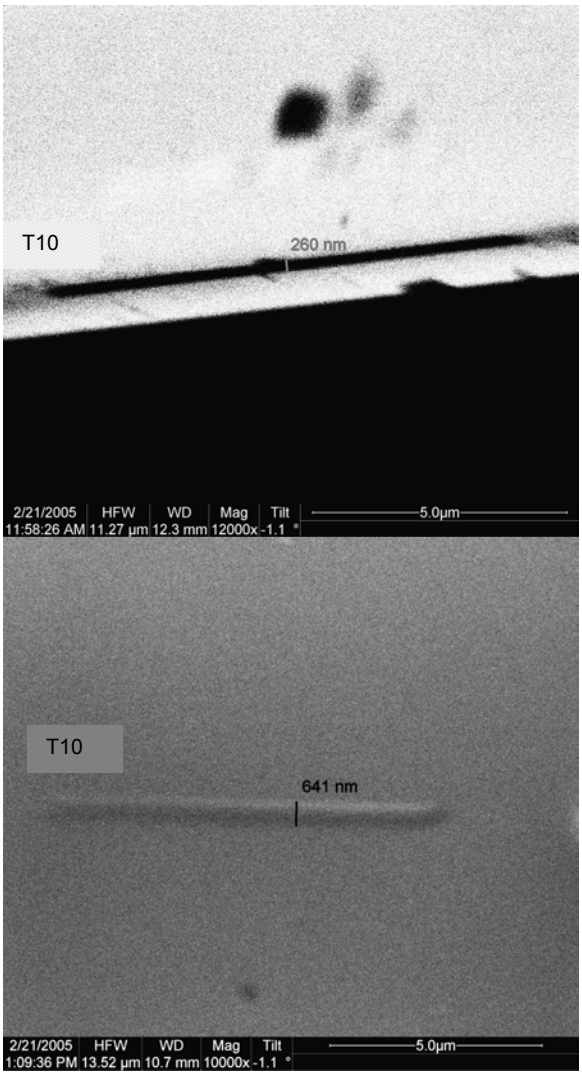

T10 Measurements (Settings HV=30 kV, BC=100 pA, LT=2.12 ms)

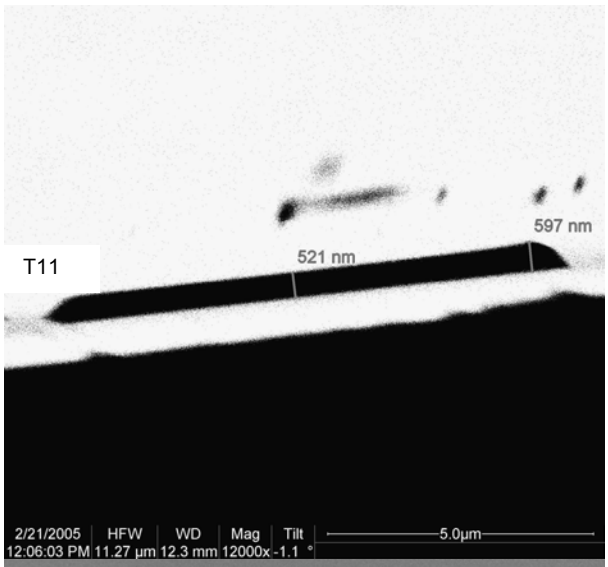

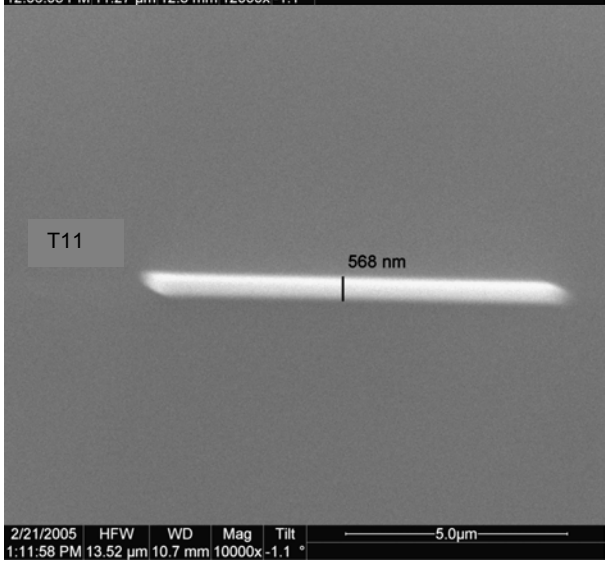

T11 Measurements (Settings: HV=30 kV, BC=5400 pA, LT=2.12 ms)

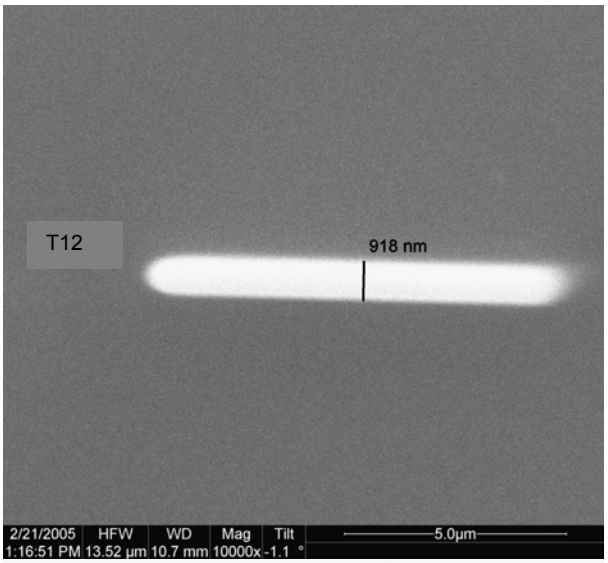

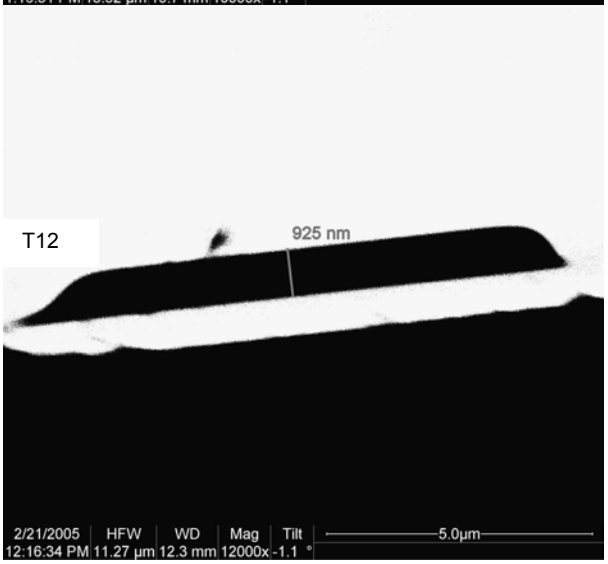

T12 Measurements (Settings: HV=10 kV, BC=5400 pA, LT=2.12 ms)

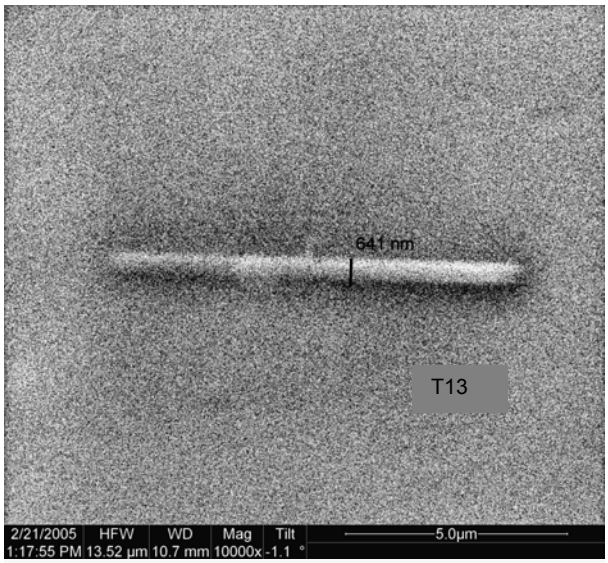

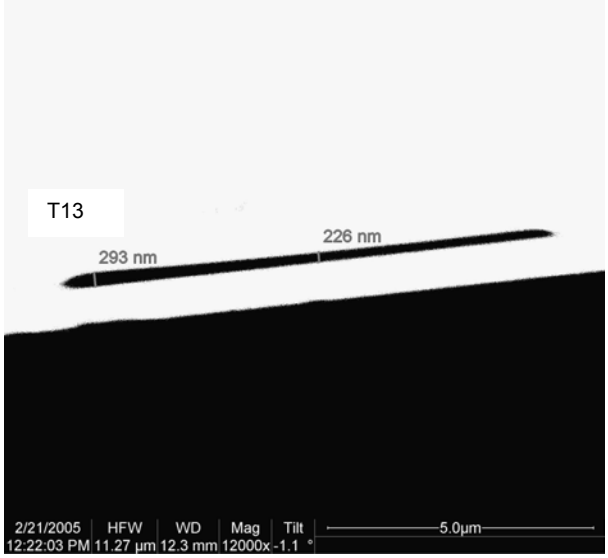

T13 Measurements (Settings: HV=10 kV, BC=100 pA, LT=2.12 ms)

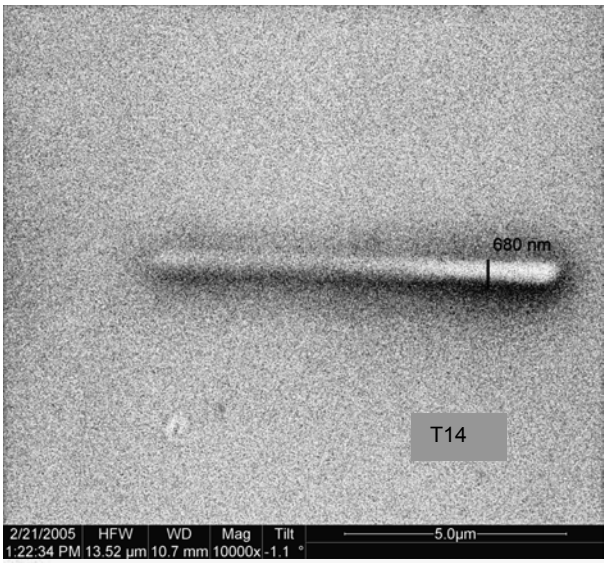

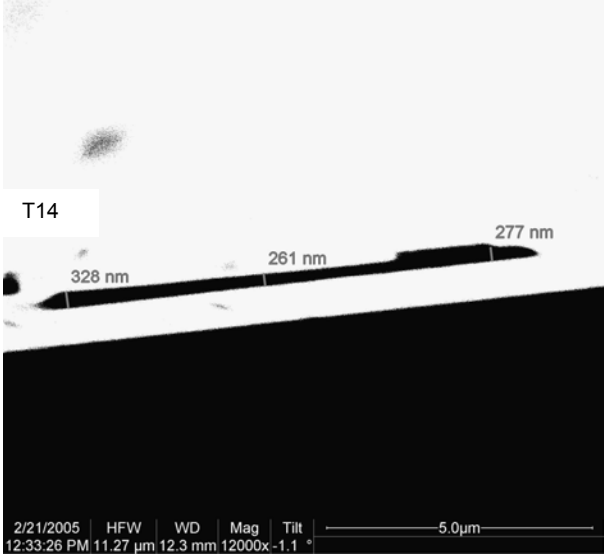

T14 Measurements (Settings: HV=10 kV, BC=100 pA, LT=1.06 ms)

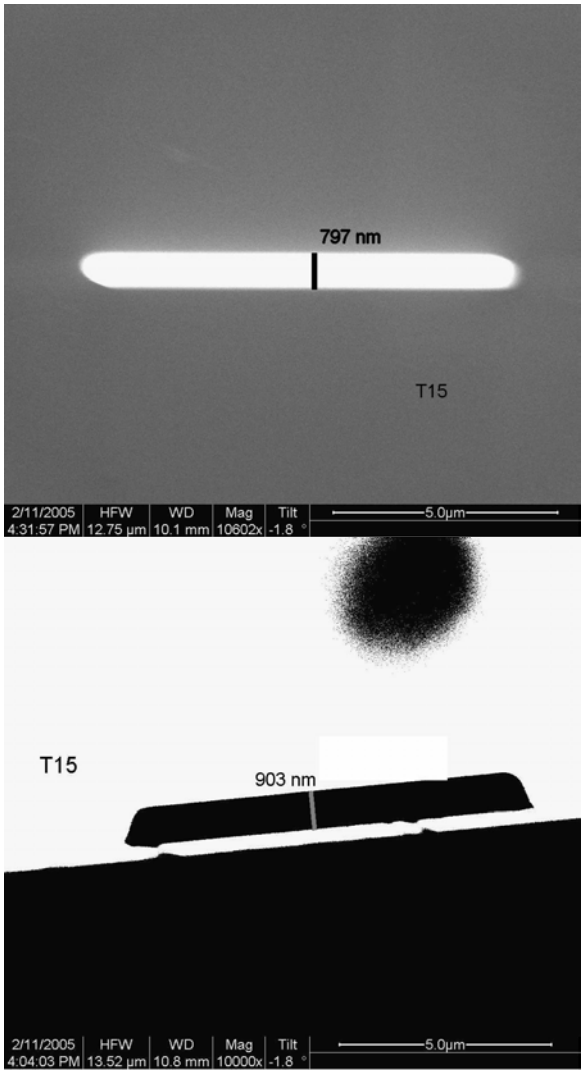

T15 Measurements (Settings: HV=30 kV, BC=5400 pA, LT=1.06 ms)

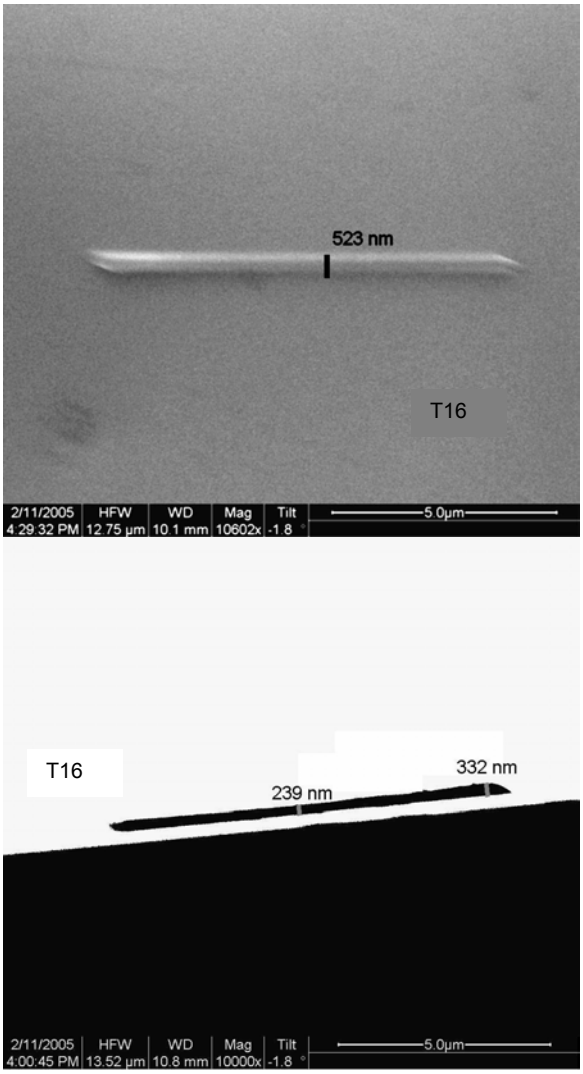

T16 Measurements (Settings: HV=30 kV, BC=100 pA, LT=1.06 ms)

Appendix A.10. Platinum Line 2^3 Factorial Dwell Time Study Measurements

Note: HV=High Voltage, BC=Beam Current, DT=Dwell Time

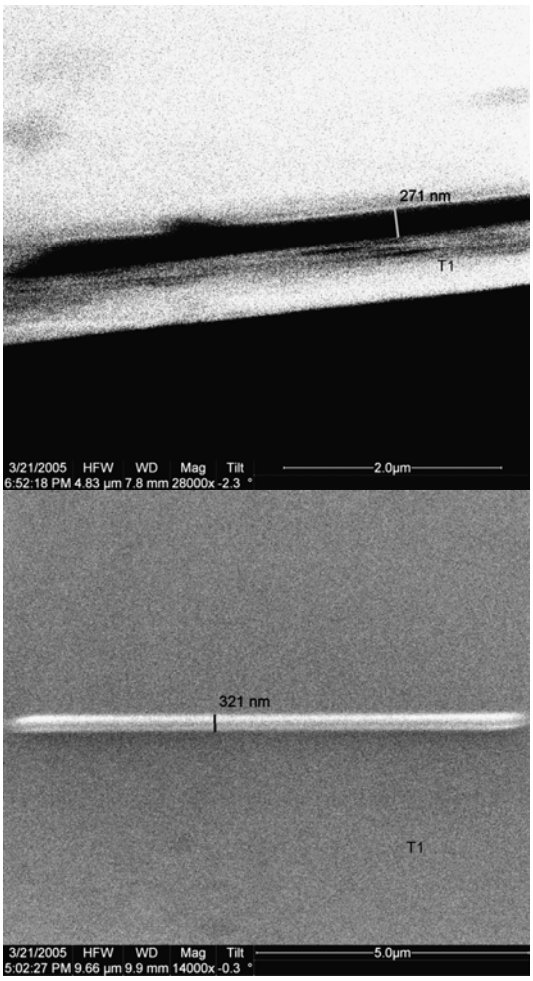

T1 Measurements (HV=30 kV, BC=5400 pA, DT=.25 ms)

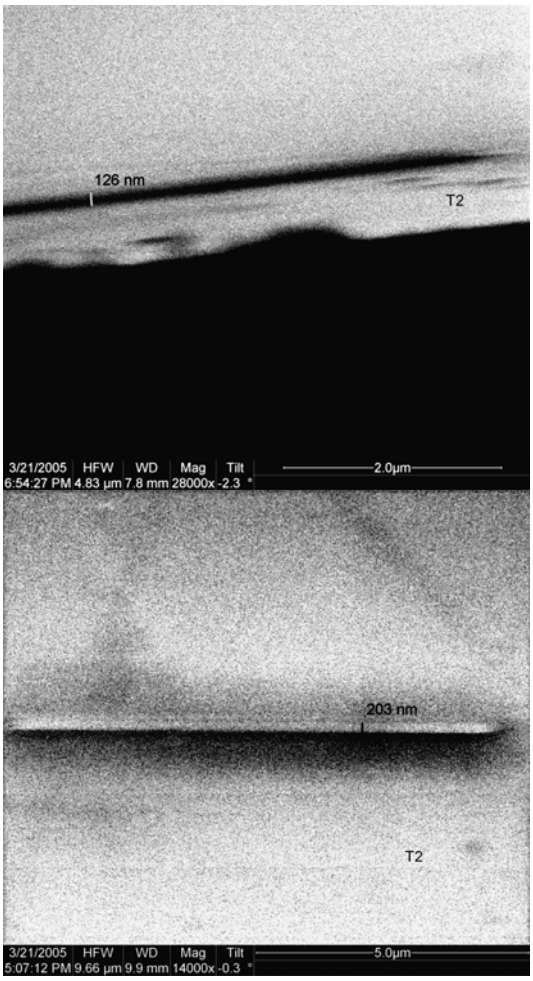

T2 Measurements (HV=10 kV, BC=100 pA, DT=1.0 ms)

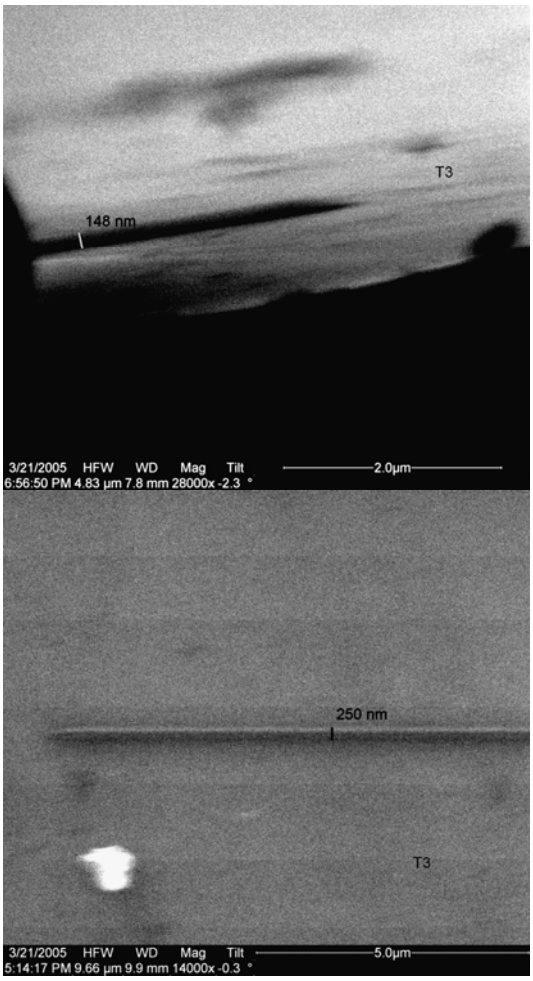

T3 Measurements (HV=30 kV, BC=100 pA, DT=1.0 ms)

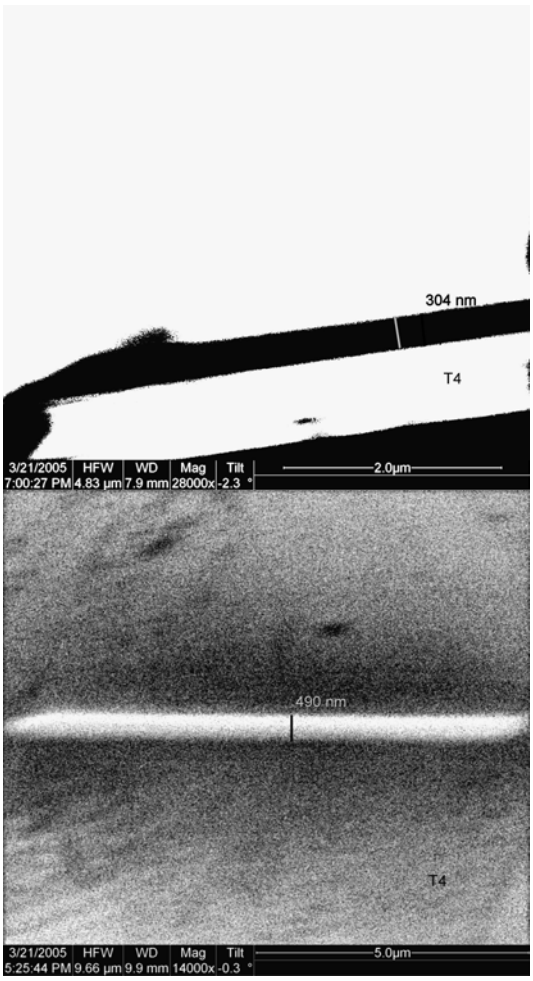

T4 Measurements (HV=10 kV, BC=5400 pA, DT=.25 ms)

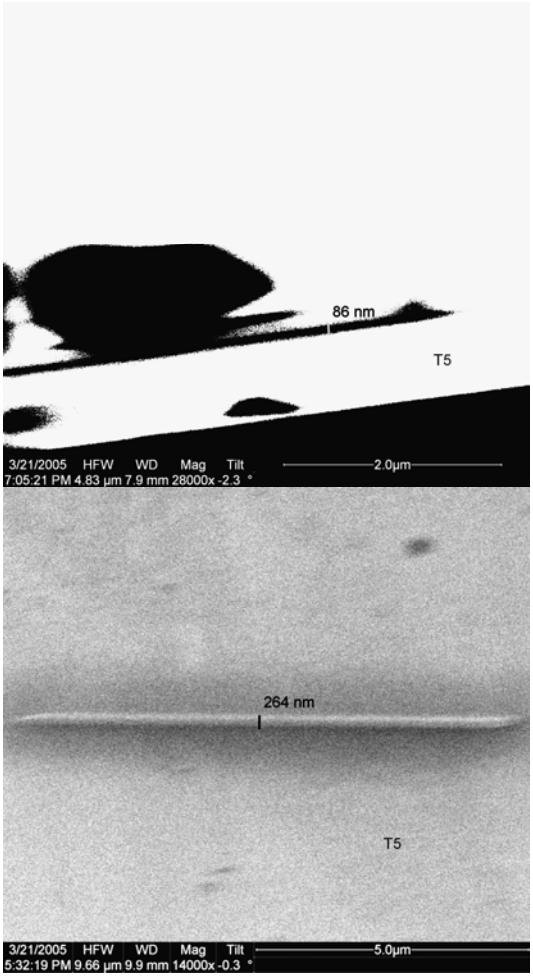

T5 Measurements (HV=10 kV, BC=100 pA, DT=.25 ms)

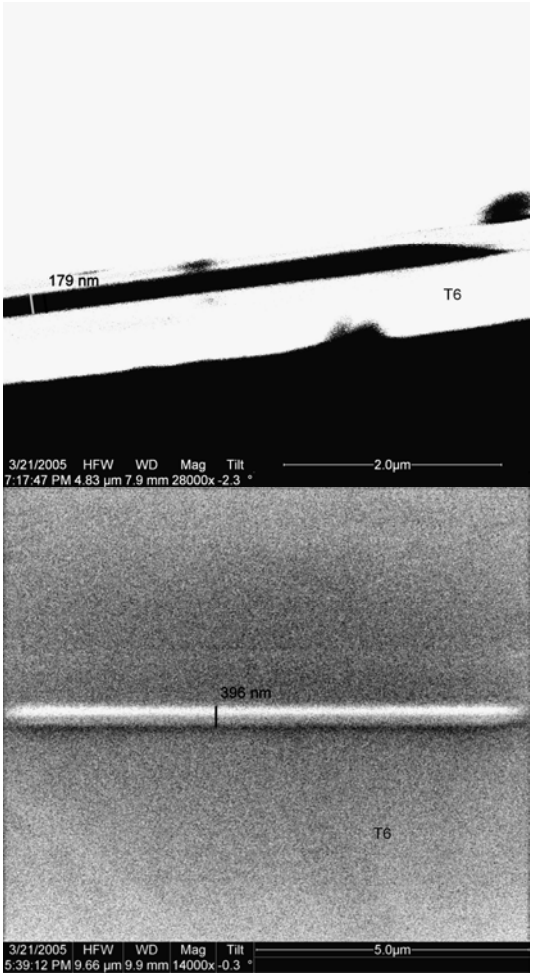

T6 Measurements (HV=30 kV, BC=5400 pA, DT=1.0 ms)

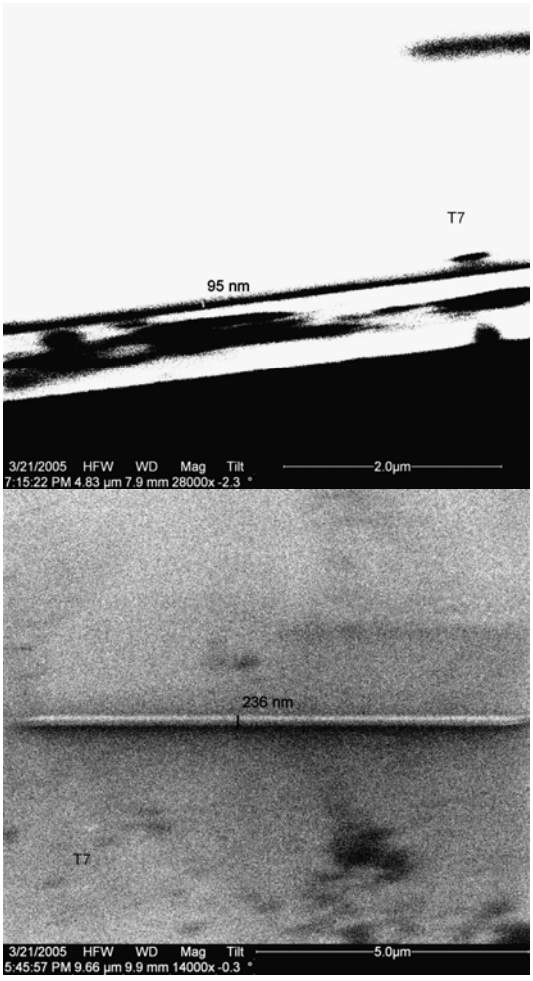

T7 Measurements (HV=30 kV, BC=100 pA, DT=.25 ms)

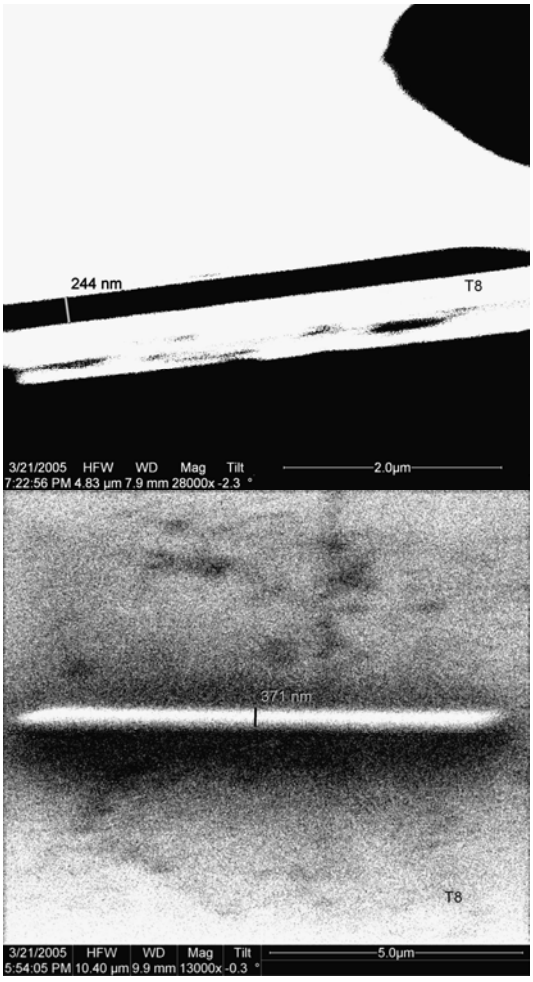

T8 Measurements (HV=10 kV, BC=5400 pA, DT=1.0 ms)

Appendix A.11: Pt Line and Fiber Optimization Measurements

Note: HV=High Voltage, BC=Beam Current, DT=Dwell Time, LT=Line Time, T=Deposition Time

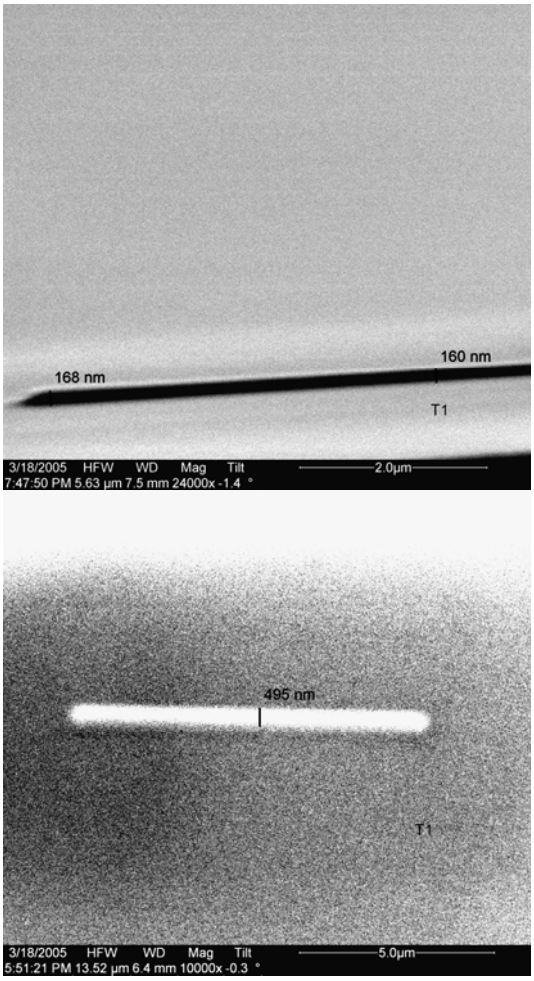

TLAR1 Measurements (HV=30 kV, BC=1485 pA, DT=177.2 µs, LT=.363ms)

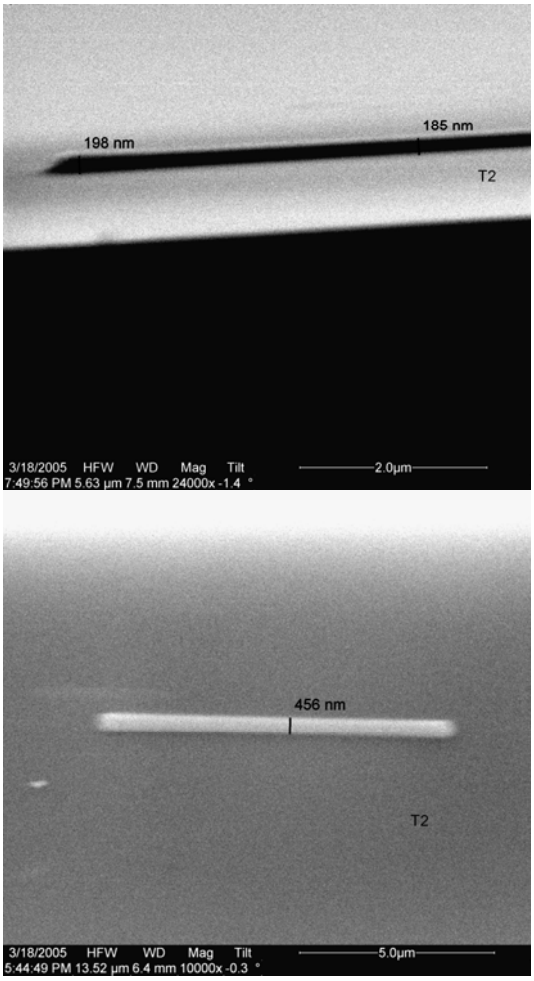

TLAR2 Measurements (HV=30 kV, BC=1485 pA, DT=177.2 µs, LT=.363ms)

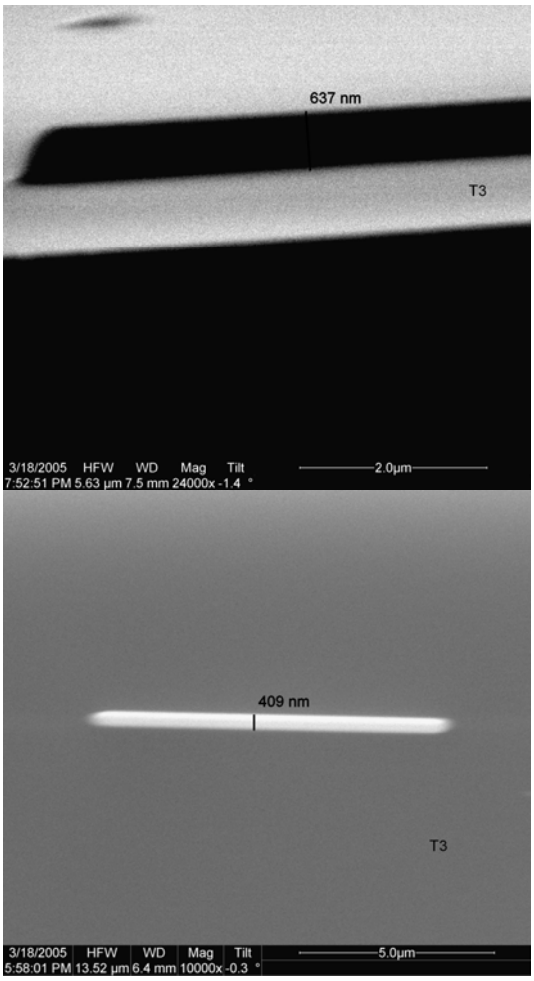

TLAR3 Measurements (HV=30 kV, BC=5400 pA, DT=177 µs, LT=.363 ms)

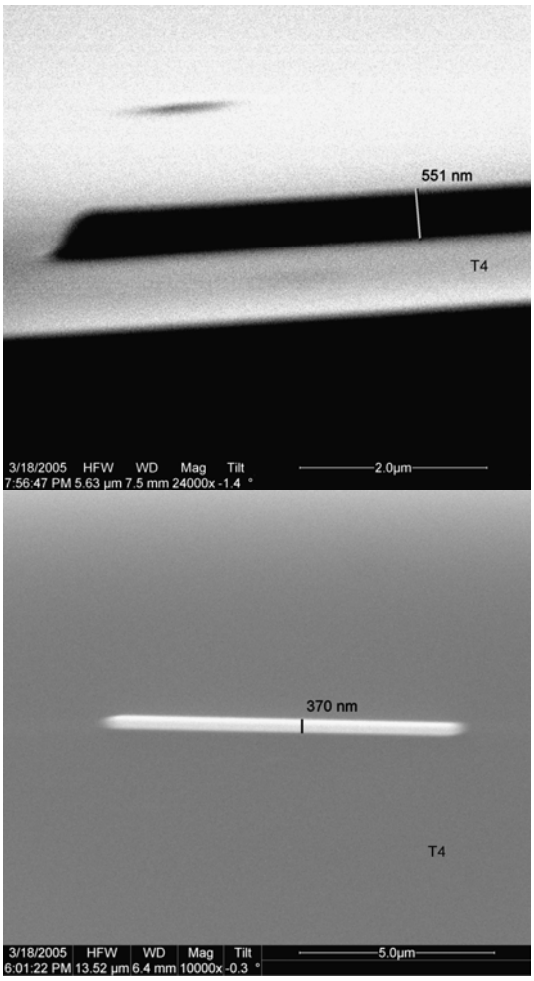

TLAR4 Measurements (HV=30 kV, BC=5400 pA, DT=177 µs, LT=.363 ms)

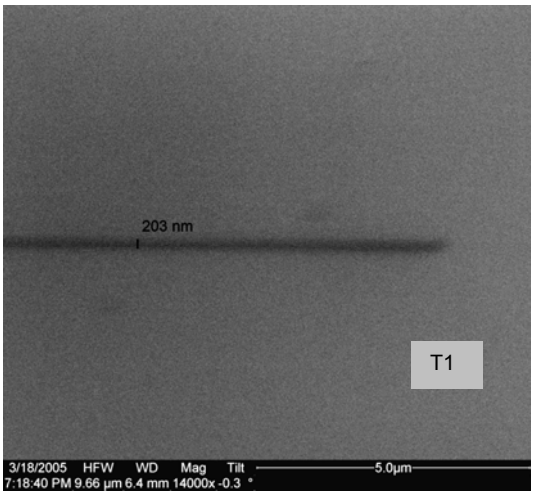

TLW1 Measurements (HV=15.8 kV, BC=60.2 pA, DT=423.2 µs, LT=.867 ms)

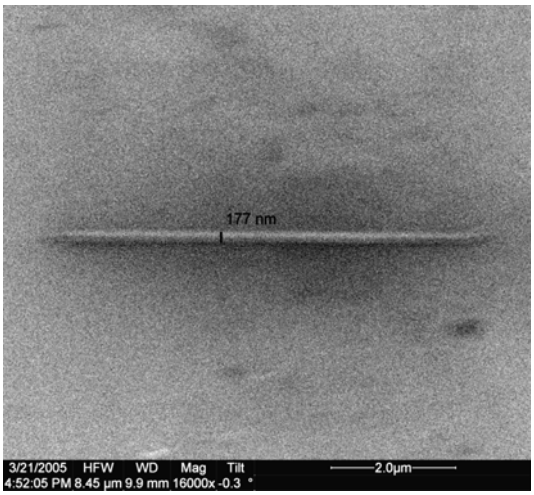

TLW3 Measurements (HV=15.8 kV, BC=20 pA, DT=423.2 s, LT=.867 ms)

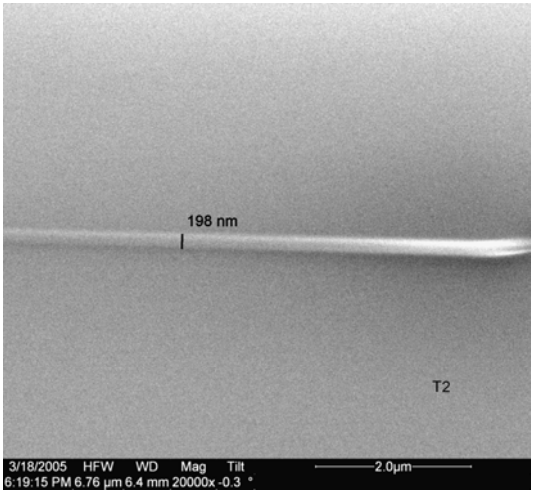

TLW2 Measurements (HV=15.8 kV, BC=60.2 pA, DT=423.2 µs, LT=.867 ms)

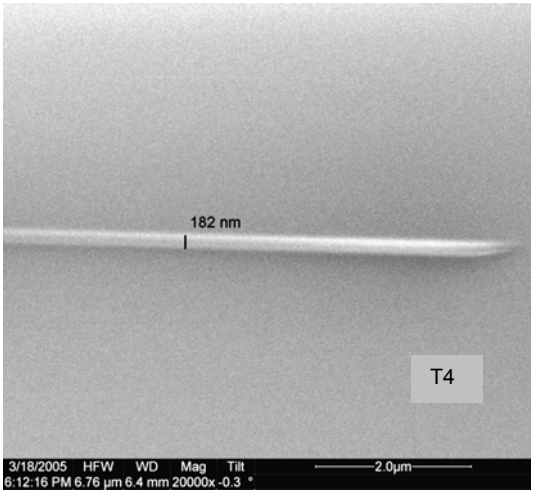

TLW4 Measurements (HV=15.8 kV, BC=20 pA, DT=423.2 s, LT=.867 ms)

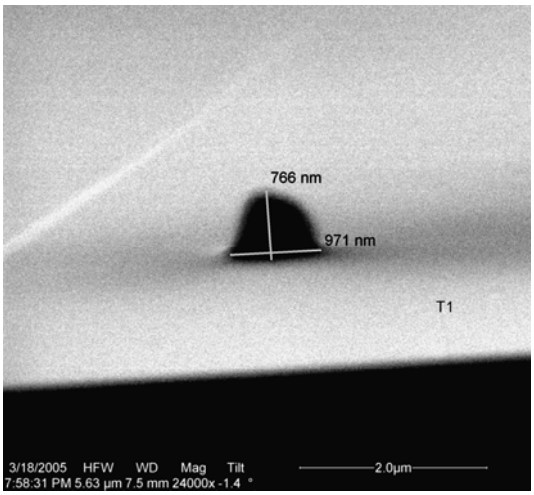

TFAR1 Measurements (HV=29 kV, BC=1378 pA, T=15.1 min)

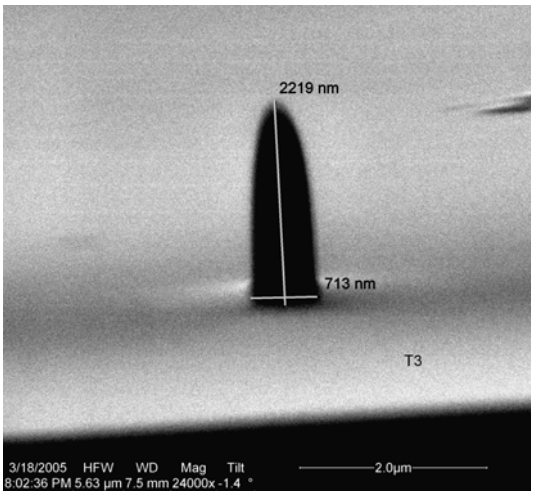

TFAR3 Measurements (HV=29 kV, BC=5400 pA, T=15.1 min)

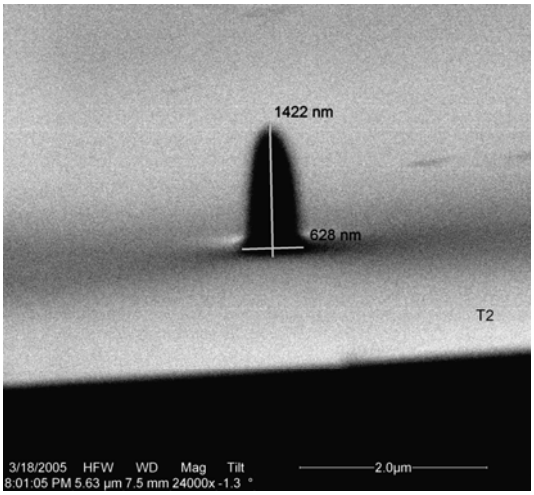

TFAR2 Measurements (HV=29 kV, BC=1378 pA, T=15.1 min)

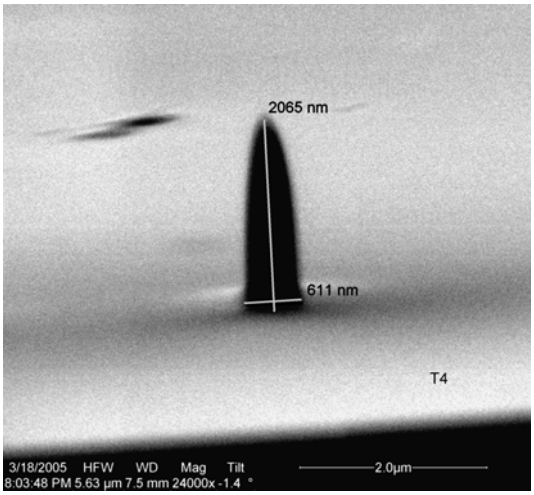

TFAR4 Measurements (HV=29 kV, BC=5400 pA, T=15.1 min)

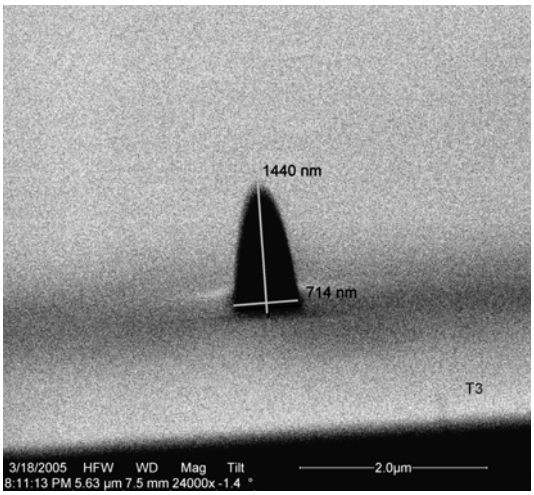

TFGR3 Measurements (HV=10 kV, BC=5,400 pA, T=5 min)

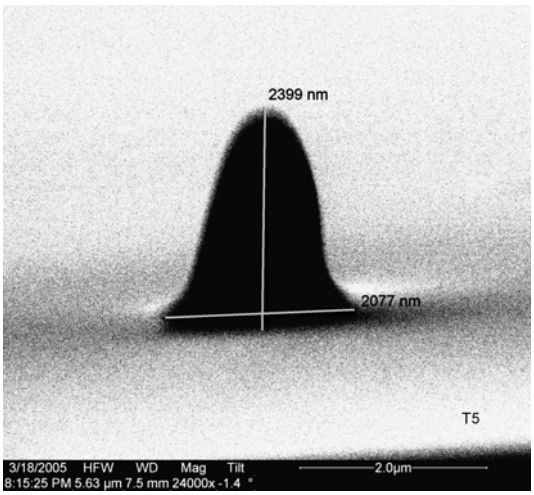

TFGR5 Measurements (HV=5 kV, BC=20,000 pA, T=5 min)

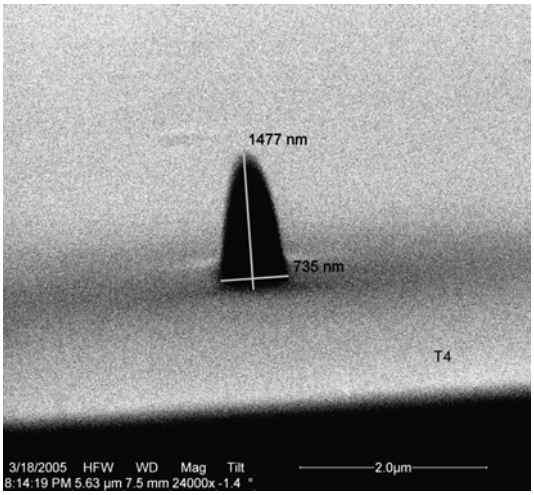

TFGR4 Measurements (HV=10 kV, BC=5,400 pA, T=5 min)

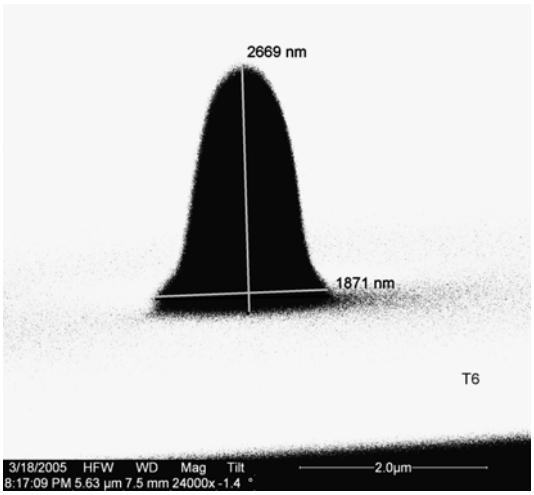

TFGR6 Measurements (HV=5 kV, BC=20,000 pA, T=5 min)

Appendix A.12: Carbon Fiber Growth Rate Study Measurements

Note: T = Deposition Time

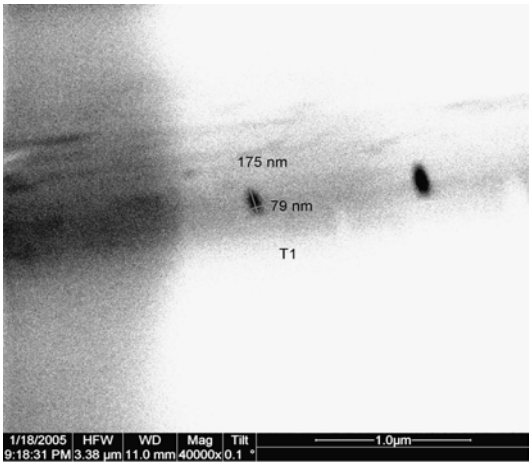

T1 Measurements (T=1 min)

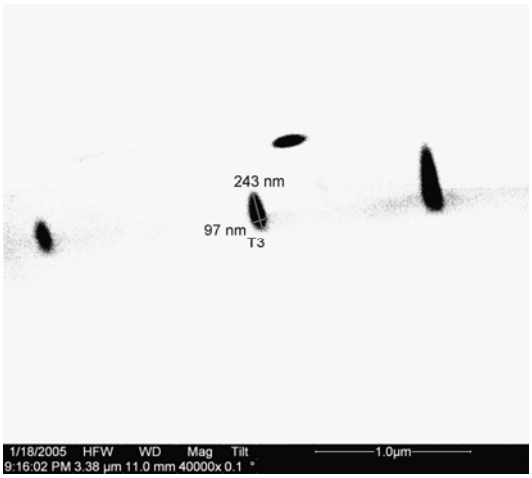

T3 Measurements (T=3 min)

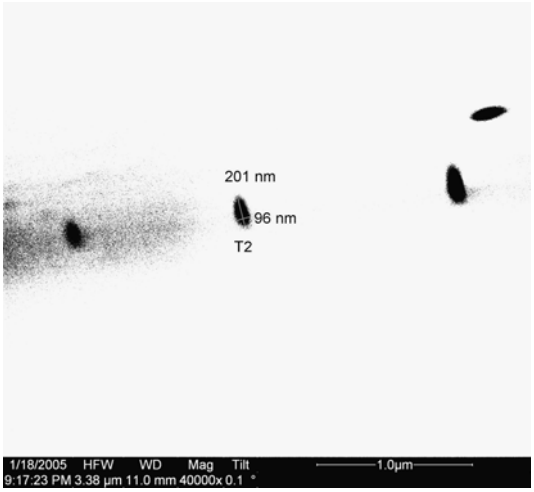

T2 Measurements (T=2 min)

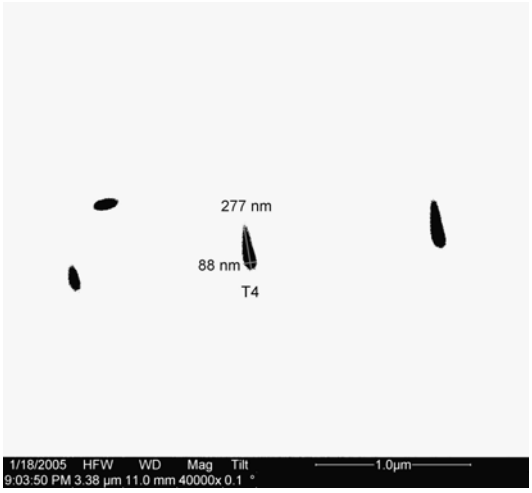

T4 Measurements (T=4 min)

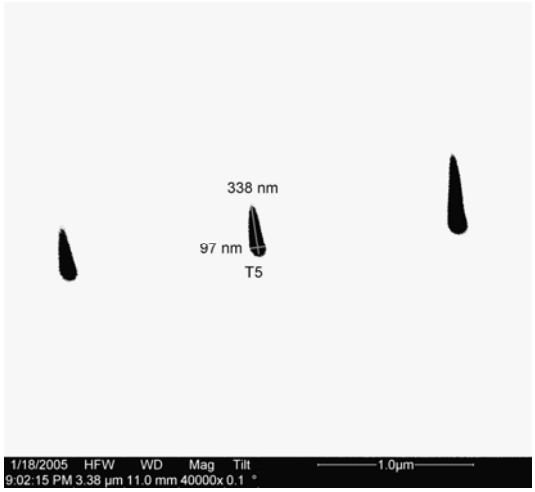

T5 Measurements (T=5 min)

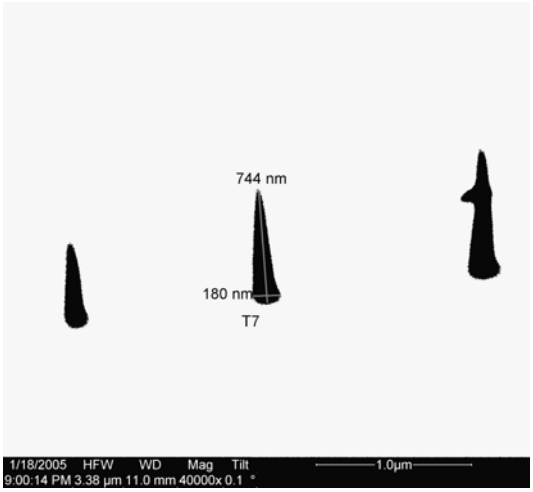

T7 Measurements (T=10 min)

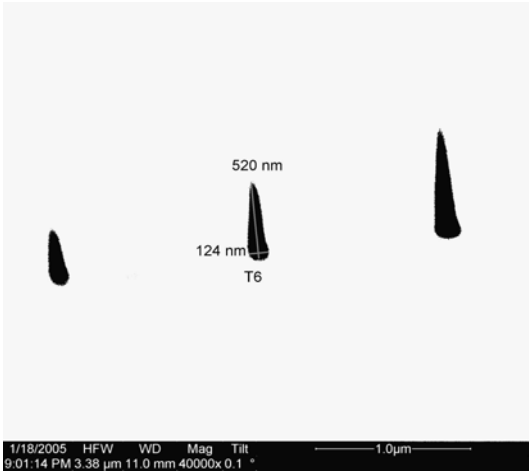

T6 Measurements (T=7 min)

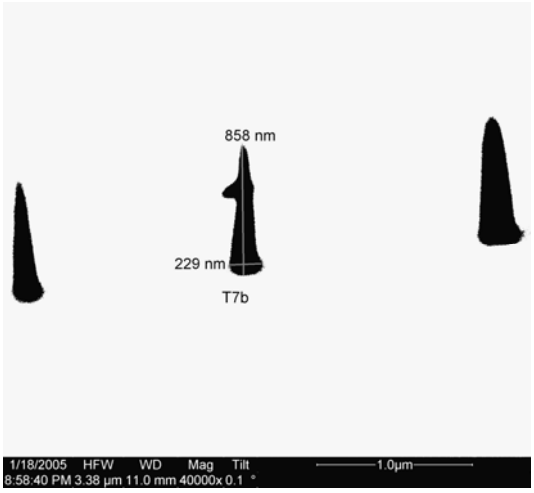

T7b Measurements (T=12 min)

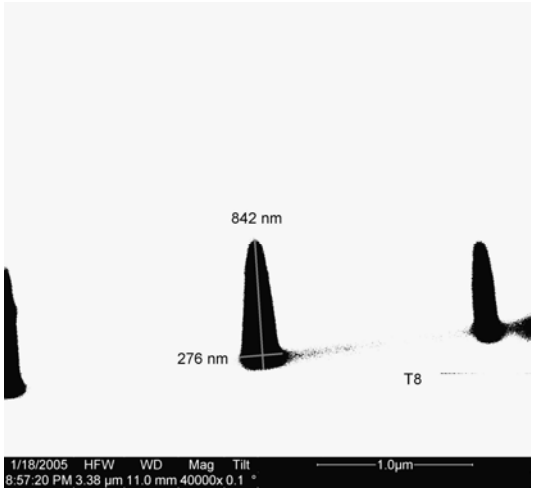

T8 Measurements (T=15 min)

Appendix A.13: Carbon Fiber Exploratory Experiment Measurements

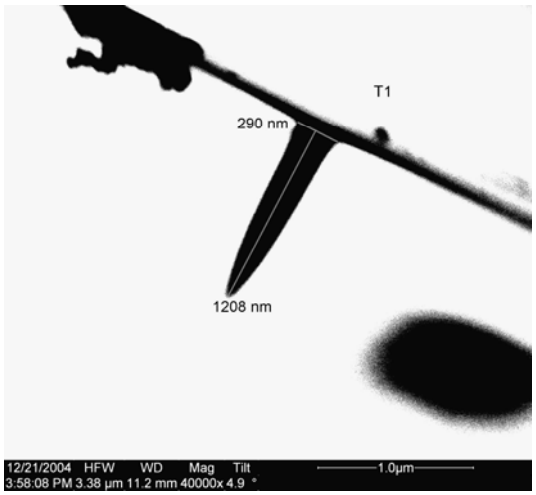

T1 Measurements

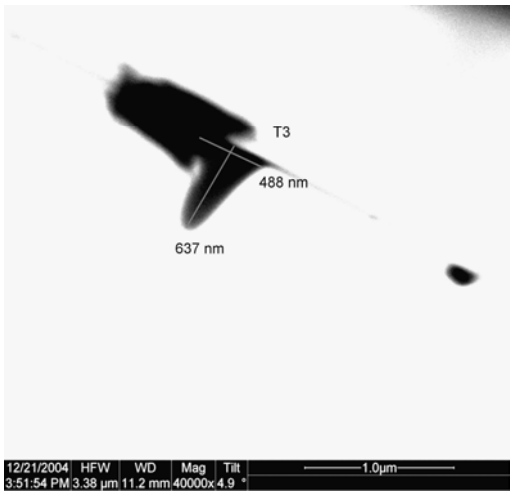

T3 Measurements

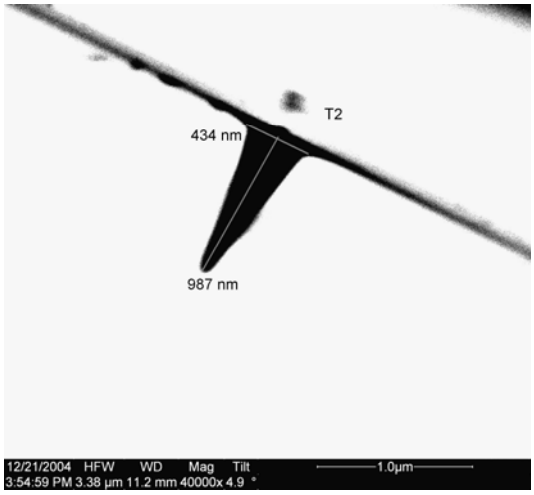

T2 Measurements

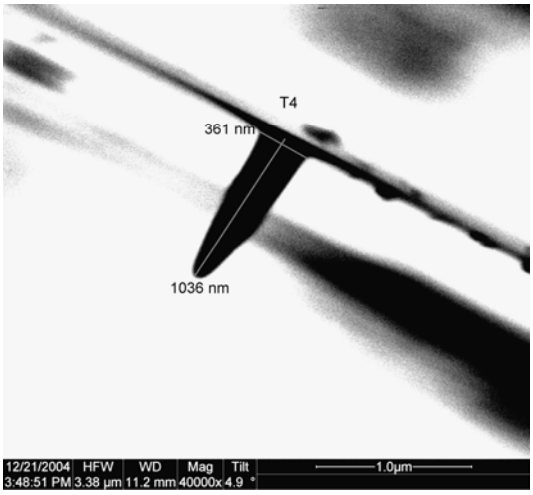

T4 Measurements

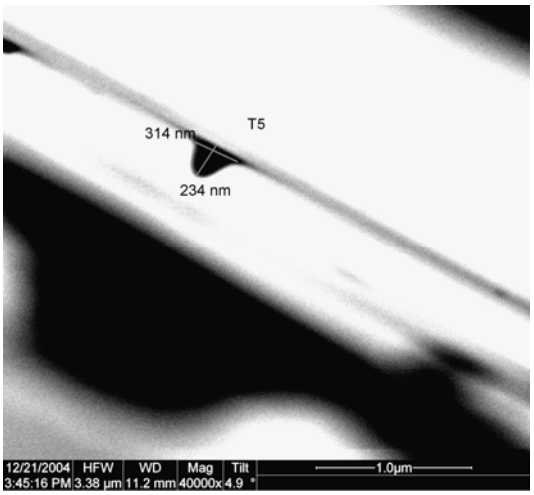

T5 Measurements

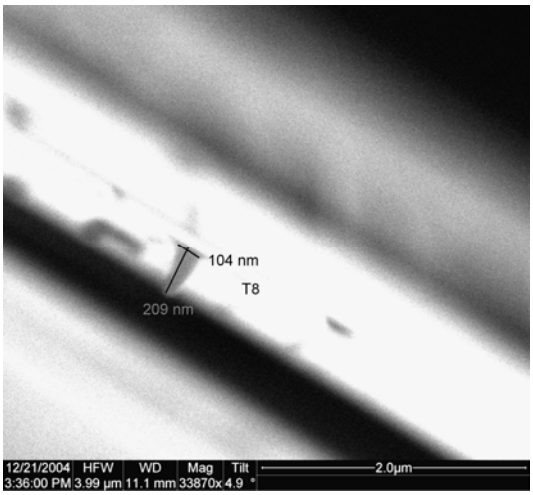

T8 Measurements

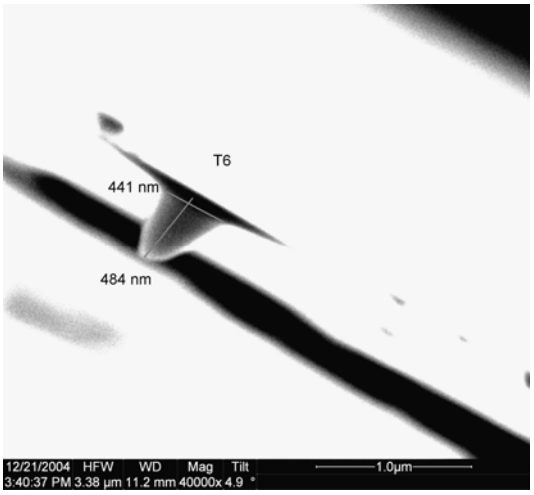

T6 Measurements

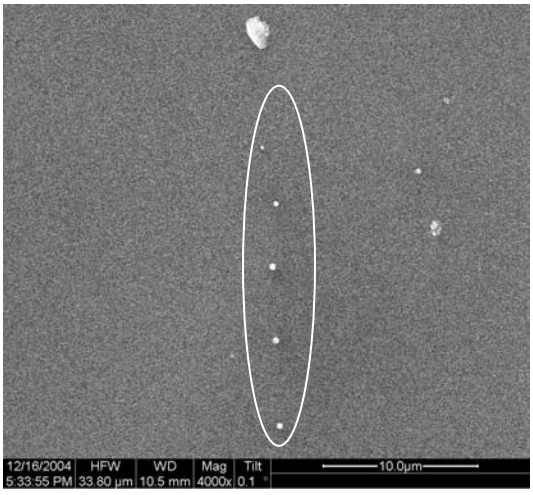

Overhead View of Fibers

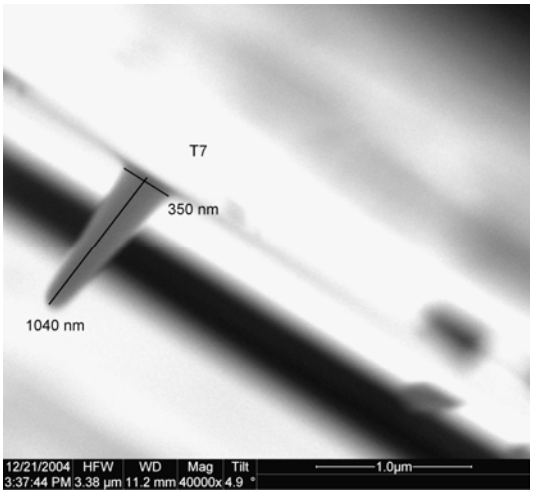

T7 Measurements

Appendix A.14: Carbon 2^3 Factorial Line Study Measurements

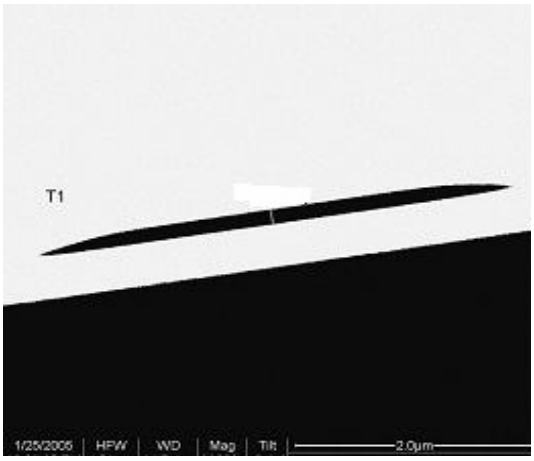

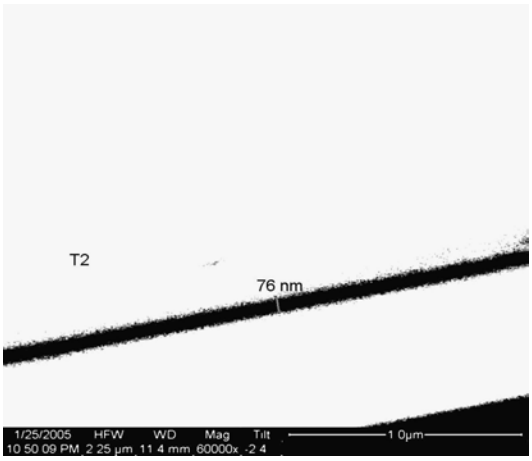

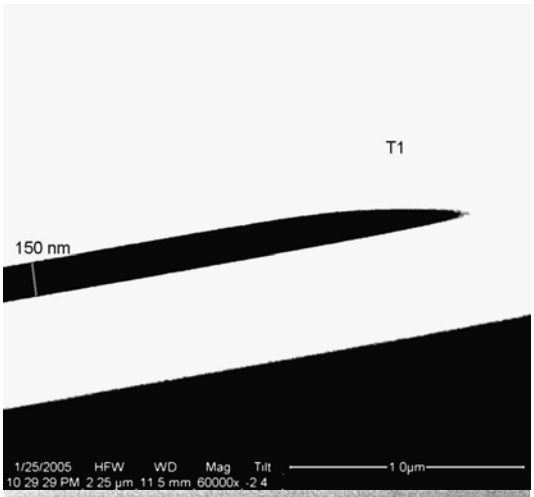

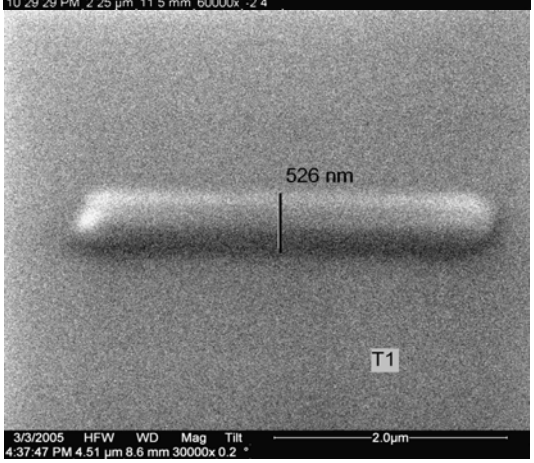

T1 Measurements (Settings: HV=10 kV, BC=5400 pA, DT=1000 µs, LT=1060 ms)

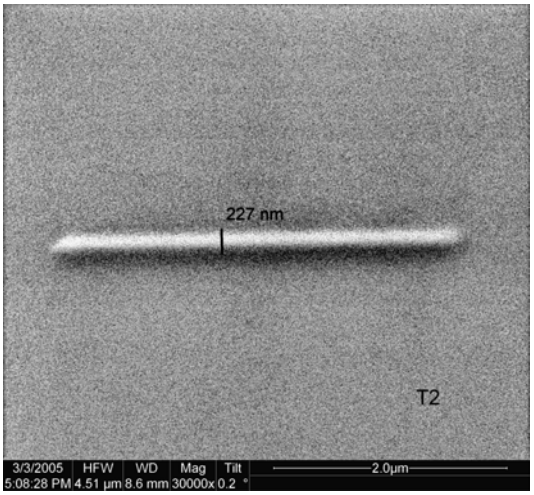

T2 Measurements (Settings: HV=10 kV, BC=50 pA, DT= 10 µs, LT=10.60 ms)

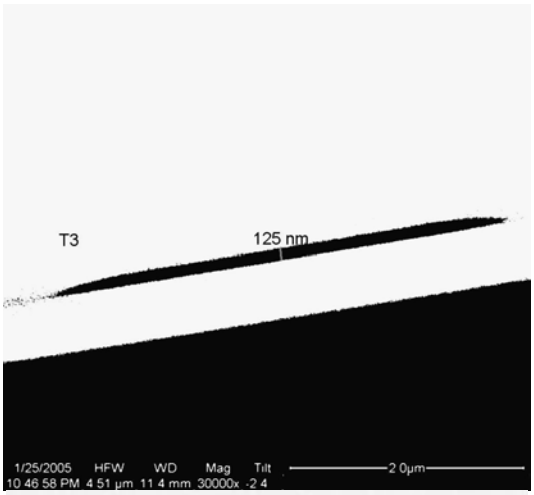

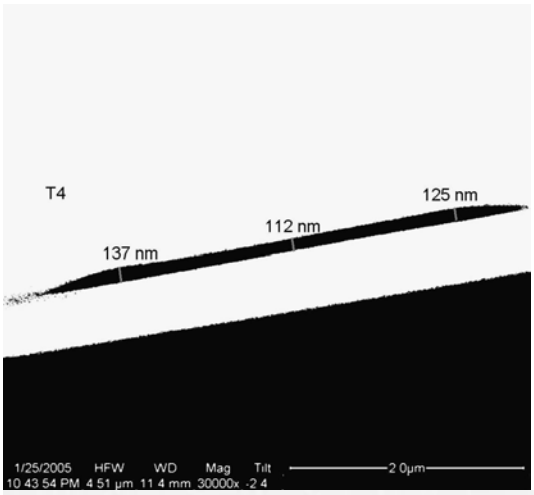

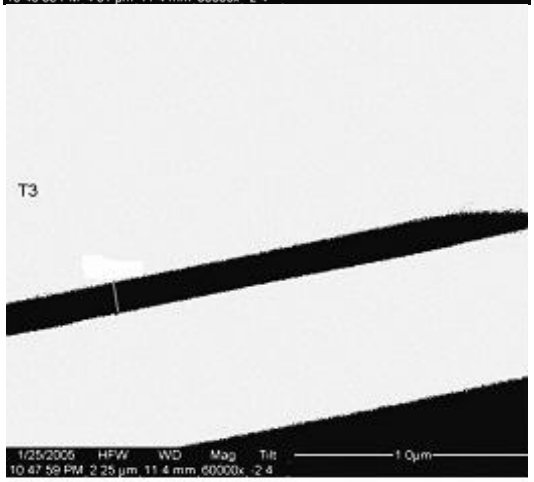

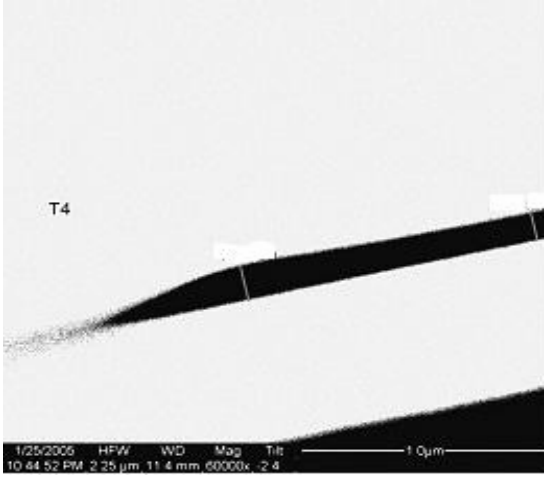

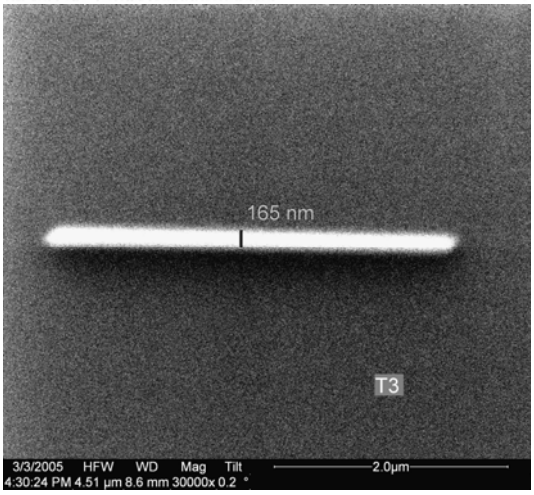

T3 Measurements (Settings: HV=30 kV, BC=50 pA, DT=10 µs, LT=10.60 ms)

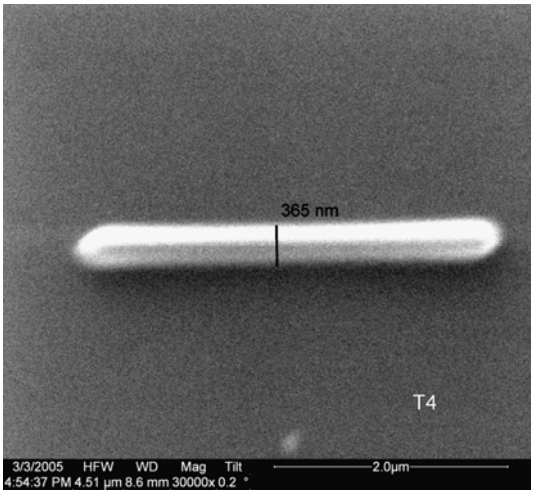

T4 Measurements (Settings: HV=30 kV, BC=5400 pA, DT=1000 µs, LT=1060 ms)

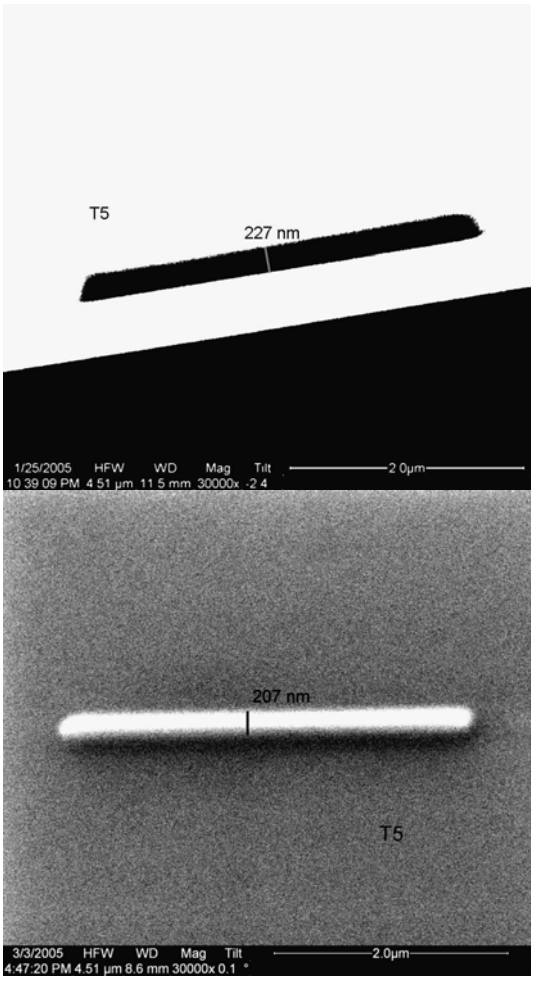

T5 Measurements (Settings: HV=30 kV, BC=50 pA, DT=1000 µs, LT=1060 ms)

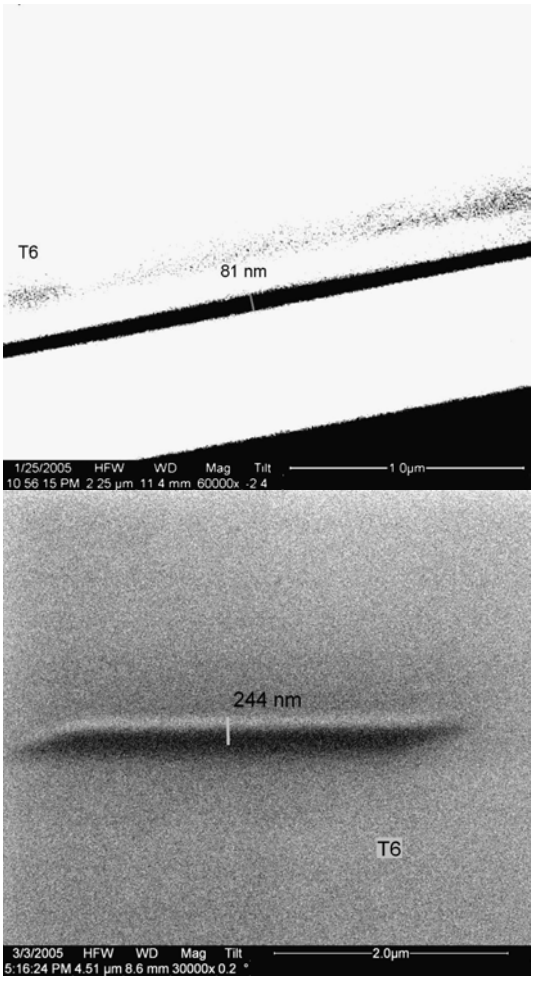

T6 Measurements (Settings: HV=10 kV, BC=50 pA, DT=1000 µs, LT=1060 ms)

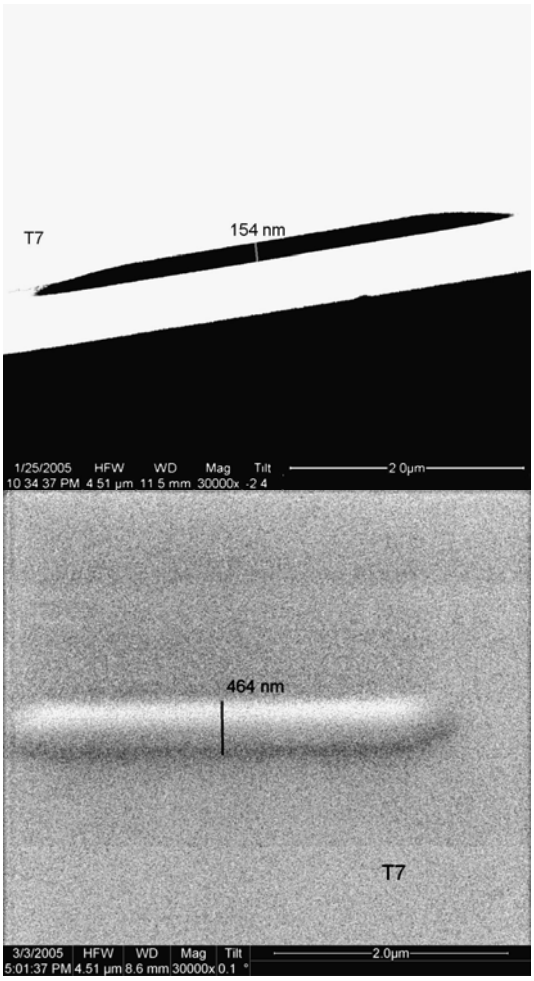

T7 Measurements (Settings: HV=10 kV, BC=5400 pA, DT=10 µs, LT=10.60 ms)

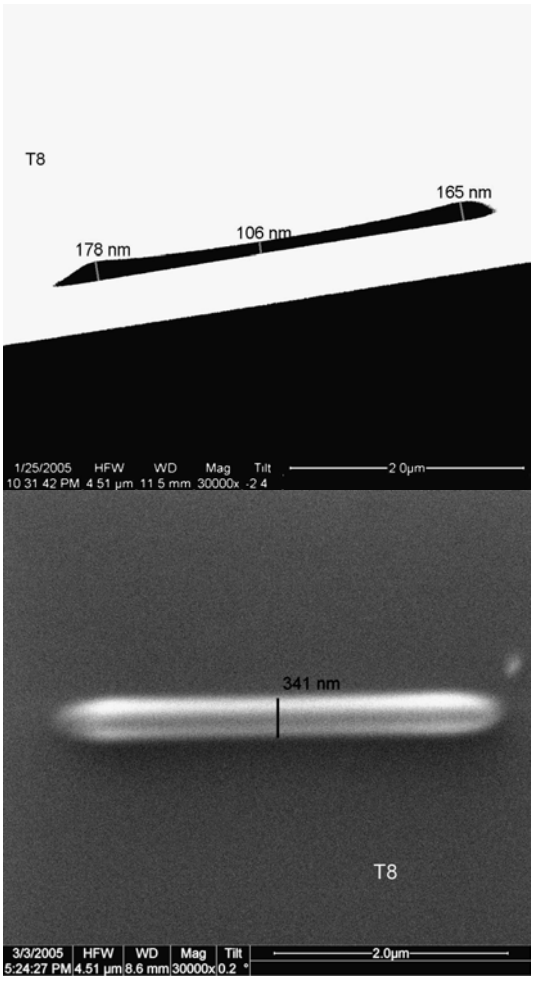

T8 Measurements (Settings: HV=30 kV, BC=5400 pA, DT=10 µs, LT=10.60 ms)

Appendix A.15. Carbon Line 2^3 Factorial Line Time Study Measurements

Note: HV = High Voltage, BC = Beam Current, LT = Line Time

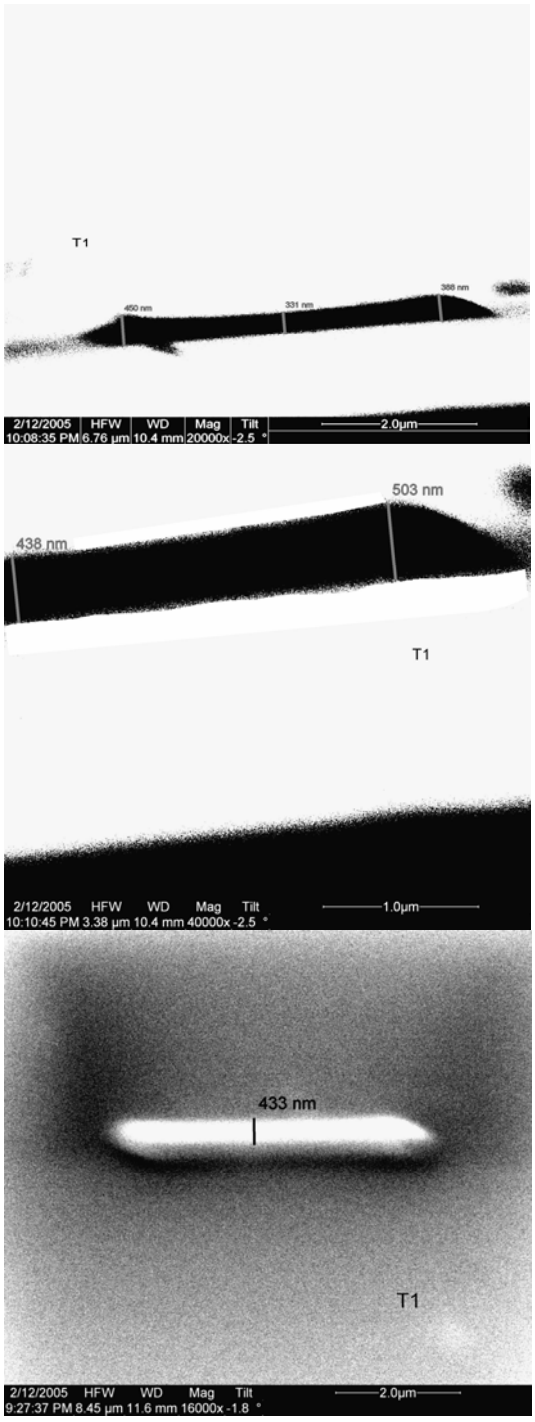

T1 Measurements (Settings: HV=30 kV, BC=5400 pA, LT=1.06 ms)

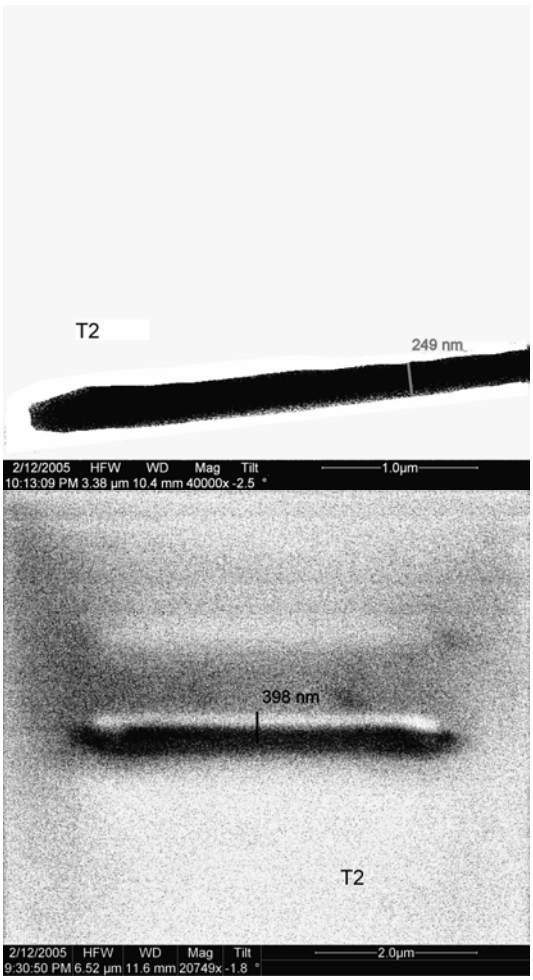

T2 Measurements (Settings: HV=10 kV, BC=100 pA, LT=2.12 ms)

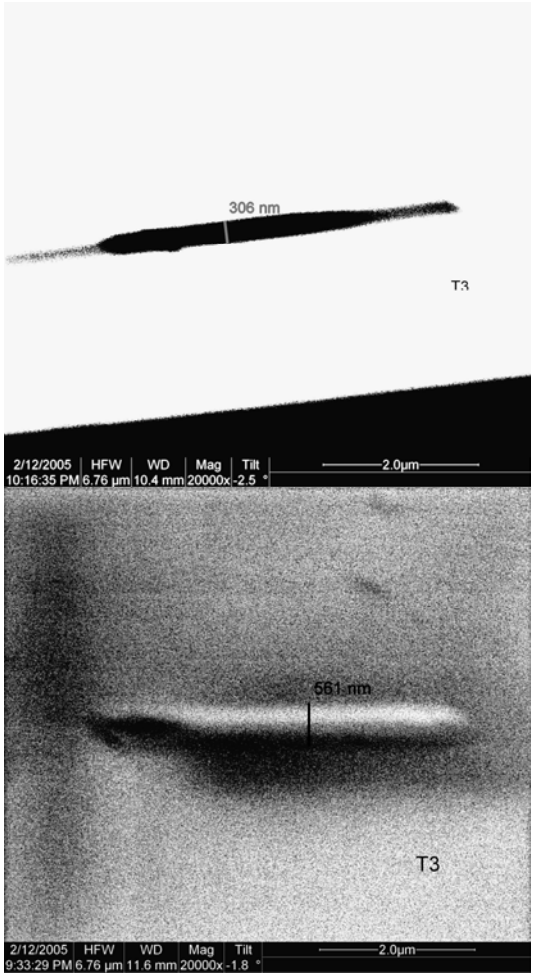

T3 Measurements (Settings: HV=30 kV, BC=100 pA, LT=2.12 ms)

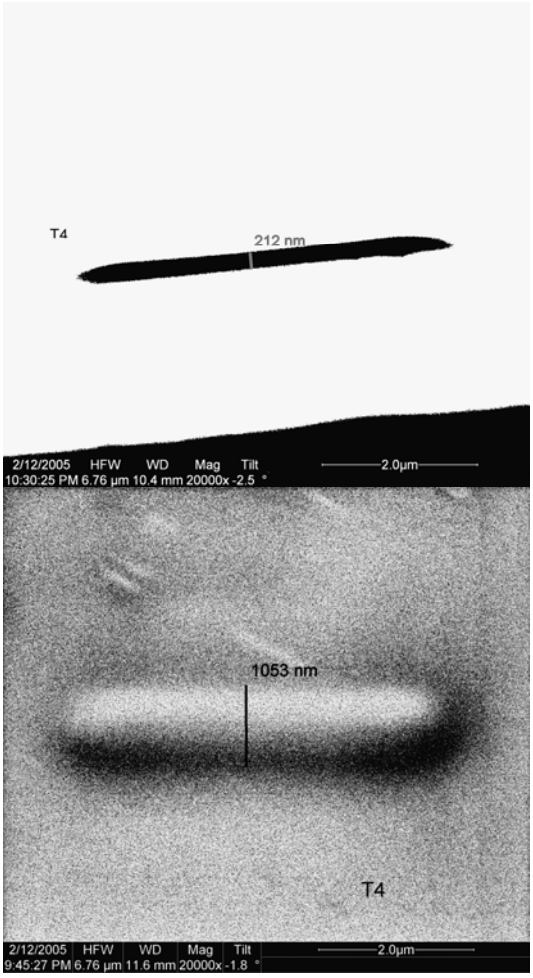

T4 Measurements (Settings: HV=10 kV, BC=5400 pA, LT=2.12 ms)

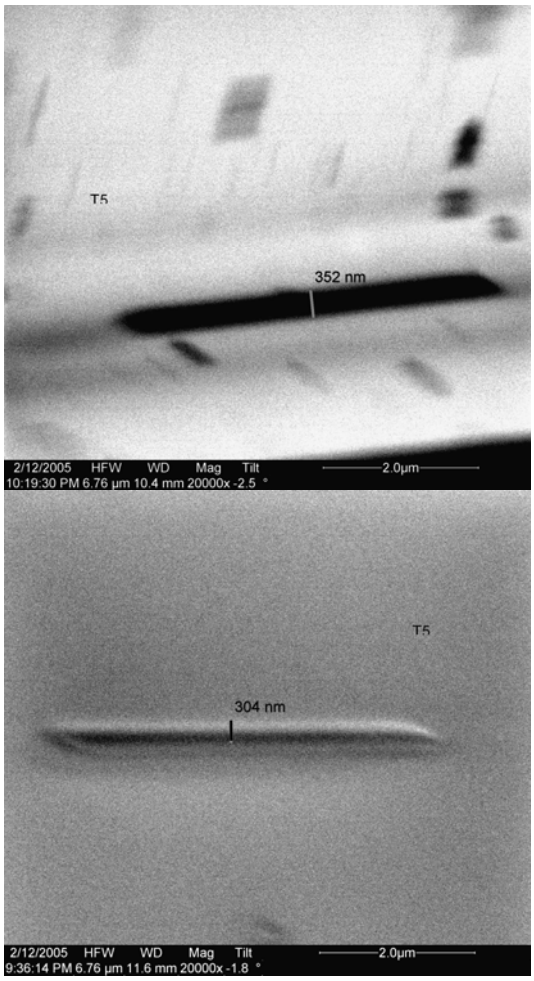

T5 Measurements (Settings: HV=30 kV, BC=100 pA, LT=1.06 ms)

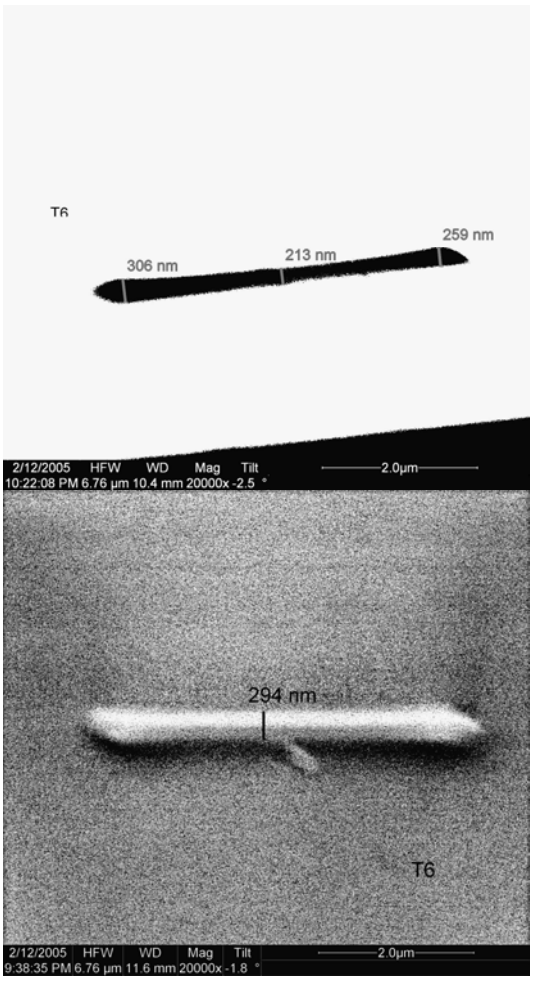

T6 Measurements (Settings: HV=30 kV, BC=5400 pA, LT=2.12 ms)

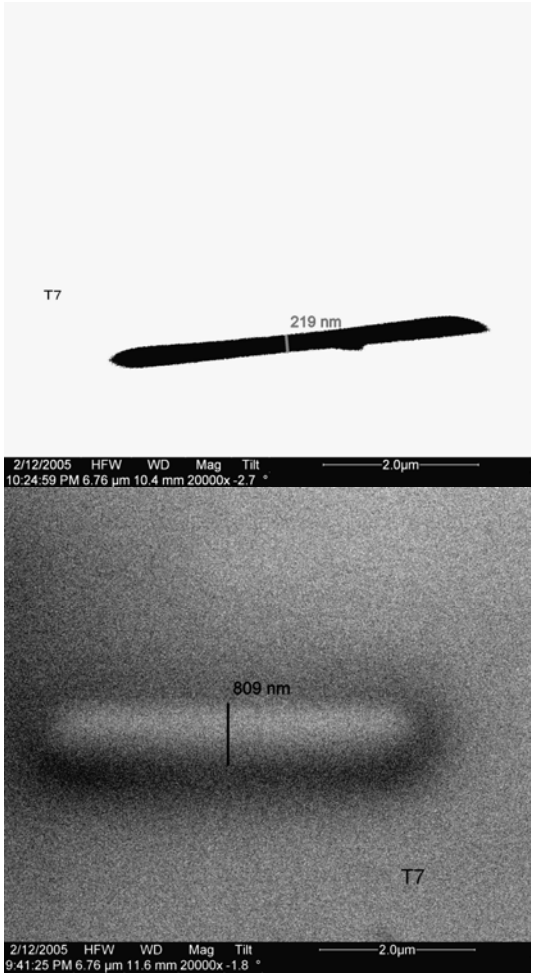

T7 Measurements (Settings: HV=10 kV, BC=5400 pA, LT=1.06 ms)

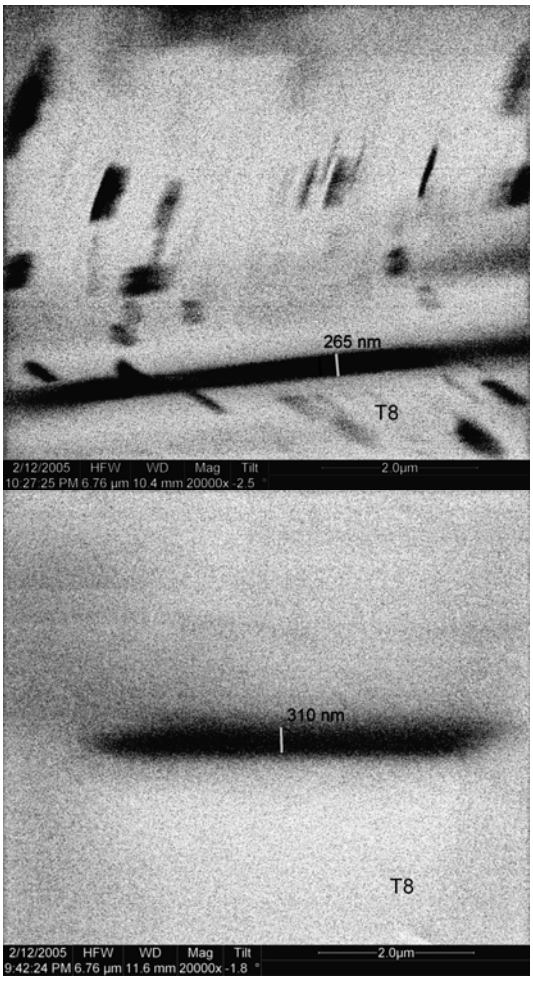

T8 Measurements (Settings: HV=10 kV, BC=100 pA, LT=1.06 ms)

APPENDIX B: ANOVA RESULTS

Analysis of Variance for Vertical Growth Rate

Source	Sum of Squares	Df	Mean Square	F-Ratio	P-Value
A:Voltage	0.0173228	1	0.0173228	9.03	0.0575
B:Beam Current	0.126169	1	0.126169	65.75	0.0039
C:Deposition Time	0.039256	1	0.039256	20.46	0.0202
BC	0.0267884	1	0.0267884	13.96	0.0334
Total error	0.0057568	3	0.00191893		
Total (corr.)	0.215293	7			

R-squared = 97.3261 percent
R-squared (adjusted for d.f.) = 93.7608 percent
Standard Error of Est. = 0.0438056
Mean absolute error = 0.0210333
Durbin-Watson statistic = 3.01996 (P=0.0754)
Lag 1 residual autocorrelation = -0.60068

ANOVA Data for Fiber Vertical Growth Rate for Platinum Fiber Factorial Study

Analysis of Variance for Base Dia Growth Rate

Source	Sum of Squares	Df	Mean Square	F-Ratio	P-Value
A:Voltage	0.00170139	1	0.00170139	1.93	0.2373
B:Beam Current	0.00280251	1	0.00280251	3.18	0.1493
C:Deposition Time	0.0243616	1	0.0243616	27.61	0.0063
Total error	0.00352988	4	0.000882469		
Total (corr.)	0.0323954	7			

R-squared = 89.1038 percent
R-squared (adjusted for d.f.) = 80.9316 percent
Standard Error of Est. = 0.0297064
Mean absolute error = 0.0178833
Durbin-Watson statistic = 3.18306 (P=0.0484)
Lag 1 residual autocorrelation = -0.615271

ANOVA Data for Fiber Base Diameter Growth Rate for Platinum Fiber Factorial Study

Analysis of Variance for Vertical Growth Rate

Source	Sum of Squares	Df	Mean Square	F-Ratio	P-Value
A:Voltage	0.0274404	1	0.0274404	14.95	0.0180
B:Beam Current	0.0768843	1	0.0768843	41.89	0.0029
C:Deposition Time	0.0195888	1	0.0195888	10.67	0.0309
Total error	0.00734067	4	0.00183517		
Total (corr.)	0.131254	7			

R-squared = 94.4073 percent
R-squared (adjusted for d.f.) = 90.2128 percent
Standard Error of Est. = 0.0428389
Mean absolute error = 0.0282667
Durbin-Watson statistic = 1.67449 (P=0.2663)
Lag 1 residual autocorrelation = -0.0234553

ANOVA Data for Fiber Vertical Growth Rate for 2nd Platinum Fiber Factorial Study

Analysis of Variance for Base Dia Growth Rate

Source	Sum of Squares	Df	Mean Square	F-Ratio	P-Value
A:Voltage	0.0595821	1	0.0595821	10.65	0.0470
B:Beam Current	0.0121728	1	0.0121728	2.18	0.2366
C:Deposition Time	0.177202	1	0.177202	31.68	0.0111
AC	0.05212	1	0.05212	9.32	0.0553
Total error	0.0167788	3	0.00559293		
Total (corr.)	0.317856	7			

R-squared = 94.7213 percent
R-squared (adjusted for d.f.) = 87.6829 percent
Standard Error of Est. = 0.0747859
Mean absolute error = 0.03796
Durbin-Watson statistic = 2.09545 (P=0.4372)
Lag 1 residual autocorrelation = -0.186358

ANOVA Data for Fiber Base Diameter Growth Rate for 2nd Platinum Fiber Factorial Study

Analysis of Variance for Vertical Growth Rate

Source	Sum of Squares	Df	Mean Square	F-Ratio	P-Value
A:Voltage	0.00785453	1	0.00785453	4.79	0.0512
B:Beam Current	0.0608492	1	0.0608492	37.08	0.0001
C:Deposition Time	0.0443158	1	0.0443158	27.00	0.0003
AA	0.00912541	1	0.00912541	5.56	0.0379
Total error	0.0180535	11	0.00164123		
Total (corr.)	0.140199	15			

R-squared = 87.1229 percent
R-squared (adjusted for d.f.) = 82.4403 percent
Standard Error of Est. = 0.0405121
Mean absolute error = 0.0257201
Durbin-Watson statistic = 2.36006 (P=0.1963)
Lag 1 residual autocorrelation = -0.209892

ANOVA Data for Fiber Vertical Growth Rate for Platinum Fiber Central Composite Study

Analysis of Variance for Dia Growth Rate

Source	Sum of Squares	Df	Mean Square	F-Ratio	P-Value
A:Voltage	0.000896703	1	0.000896703	0.08	0.7800
B:Beam Current	0.000690774	1	0.000690774	0.06	0.8062
C:Deposition Time	0.157595	1	0.157595	14.41	0.0030
CC	0.129895	1	0.129895	11.87	0.0055
Total error	0.120338	11	0.0109398		
Total (corr.)	0.409414	15			

R-squared = 70.6073 percent
R-squared (adjusted for d.f.) = 59.9191 percent
Standard Error of Est. = 0.104593
Mean absolute error = 0.0672015
Durbin-Watson statistic = 1.83268 (P=0.4278)
Lag 1 residual autocorrelation = 0.07882

ANOVA Data for Fiber Base Diameter Growth Rate for Platinum Fiber Central Composite Study

Analysis of Variance for Height per scan

Source	Sum of Squares	Df	Mean Square	F-Ratio	P-Value
A:Voltage	770.245	1	770.245	0.88	0.4186
B:Beam Current	62727.0	1	62727.0	71.27	0.0035
C:Dwell Time	224815.0	1	224815.0	255.42	0.0005
BC	59652.4	1	59652.4	67.77	0.0038
Total error	2640.53	3	880.177		
Total (corr.)	350605.0	7			

R-squared = 99.2469 percent
R-squared (adjusted for d.f.) = 98.2427 percent
Standard Error of Est. = 29.6678
Mean absolute error = 15.705
Durbin-Watson statistic = 3.0475 (P=0.0000)
Lag 1 residual autocorrelation = -0.57117

ANOVA Data for Height/scan (h) for Platinum Line Factorial Study

Analysis of Variance for Line Width

Source	Sum of Squares	Df	Mean Square	F-Ratio	P-Value
A:Voltage	0.117855	1	0.117855	9.84	0.0349
B:Beam Current	0.38325	1	0.38325	32.00	0.0048
C:Dwell Time	0.00567112	1	0.00567112	0.47	0.5292
Total error	0.0478995	4	0.0119749		
Total (corr.)	0.554676	7			

R-squared = 91.3644 percent
R-squared (adjusted for d.f.) = 84.8877 percent
Standard Error of Est. = 0.10943
Mean absolute error = 0.06125
Durbin-Watson statistic = 2.16999 (P=0.1324)
Lag 1 residual autocorrelation = -0.397727

ANOVA Data for Line Width for Platinum Line Factorial Study

Analysis of Variance for h

Source	Sum of Squares	Df	Mean Square	F-Ratio	P-Value
A:Voltage	1012.84	1	1012.84	5.16	0.0464
B:Beam Current	2355.24	1	2355.24	12.01	0.0061
C:Dwell Time	5585.5	1	5585.5	28.48	0.0003
AA	852.2	1	852.2	4.35	0.0637
BC	997.928	1	997.928	5.09	0.0477
Total error	1961.28	10	196.128		
Total (corr.)	12765.0	15			

R-squared = 84.6355 percent
R-squared (adjusted for d.f.) = 76.9532 percent
Standard Error of Est. = 14.0046
Mean absolute error = 9.38894
Durbin-Watson statistic = 0.780551 (P=0.0011)
Lag 1 residual autocorrelation = 0.539103

ANOVA Data for Height/scan (h) for Platinum Line Central Composite Study

Analysis of Variance for Line Width

Source	Sum of Squares	Df	Mean Square	F-Ratio	P-Value
A:Voltage	0.0124454	1	0.0124454	2.76	0.1311
B:Beam Current	0.000338097	1	0.000338097	0.07	0.7905
C:Dwell Time	0.0342123	1	0.0342123	7.58	0.0223
AA	0.0192825	1	0.0192825	4.27	0.0687
BC	0.0238711	1	0.0238711	5.29	0.0470
CC	0.0388066	1	0.0388066	8.60	0.0167
Total error	0.0406119	9	0.00451243		
Total (corr.)	0.157389	15			

R-squared = 74.1965 percent
R-squared (adjusted for d.f.) = 56.9942 percent
Standard Error of Est. = 0.0671746
Mean absolute error = 0.043073
Durbin-Watson statistic = 1.61808 (P=0.1688)
Lag 1 residual autocorrelation = 0.128672

ANOVA Data for Line Width for Platinum Line Central Composite Study

Analysis of Variance for Height per scan

Source	Sum of Squares	Df	Mean Square	F-Ratio	P-Value
A:Voltage	0.0844666	1	0.0844666	1.73	0.2593
B:Beam Current	0.30453	1	0.30453	6.22	0.0672
C:Line Time	0.626573	1	0.626573	12.80	0.0232
Total error	0.19584	4	0.04896		
Total (corr.)	1.21141	7			

R-squared = 83.8337 percent
R-squared (adjusted for d.f.) = 71.709 percent
Standard Error of Est. = 0.221269
Mean absolute error = 0.128606
Durbin-Watson statistic = 2.41506 (P=0.1748)
Lag 1 residual autocorrelation = -0.453227

ANOVA Data for Height/scan (h) for Platinum Line Factorial Line Time Study

Analysis of Variance for Line Width

Source	Sum of Squares	Df	Mean Square	F-Ratio	P-Value
A:Voltage	0.013778	1	0.013778	4.89	0.1139
B:Beam Current	0.052488	1	0.052488	18.64	0.0229
C:Line Time	0.0049005	1	0.0049005	1.74	0.2787
AB	0.06125	1	0.06125	21.76	0.0186
Total error	0.0084455	3	0.00281517		
Total (corr.)	0.140862	7			

R-squared = 94.0044 percent
R-squared (adjusted for d.f.) = 86.0103 percent
Standard Error of Est. = 0.0530581
Mean absolute error = 0.02775
Durbin-Watson statistic = 2.64016 (P=0.0400)
Lag 1 residual autocorrelation = -0.390866

ANOVA Data for Line Width for Platinum Line Factorial Line Time Study

Analysis of Variance for Line Height

Source	Sum of Squares	Df	Mean Square	F-Ratio	P-Value
A:Voltage	0.000561125	1	0.000561125	0.71	0.4620
B:Beam Current	0.0368561	1	0.0368561	46.49	0.0065
C:Dwell Time	0.000435125	1	0.000435125	0.55	0.5125
BC	0.00750313	1	0.00750313	9.46	0.0543
Total error	0.00237837	3	0.000792792		
Total (corr.)	0.0477339	7			

R-squared = 95.0174 percent
R-squared (adjusted for d.f.) = 88.374 percent
Standard Error of Est. = 0.0281566
Mean absolute error = 0.016125
Durbin-Watson statistic = 1.4317 (P=0.3493)
Lag 1 residual autocorrelation = 0.170383

ANOVA Data for Line Height for Platinum Factorial Dwell Time Study

Analysis of Variance for Line Width

Source	Sum of Squares	Df	Mean Square	F-Ratio	P-Value
A:Voltage	0.00195313	1	0.00195313	1.15	0.3620
B:Beam Current	0.0488281	1	0.0488281	28.77	0.0127
C:Dwell Time	0.00103512	1	0.00103512	0.61	0.4918
AC	0.00904513	1	0.00904513	5.33	0.1042
Total error	0.00509237	3	0.00169746		
Total (corr.)	0.0659539	7			

R-squared = 92.2789 percent
R-squared (adjusted for d.f.) = 81.9841 percent
Standard Error of Est. = 0.0412002
Mean absolute error = 0.020375
Durbin-Watson statistic = 0.697783 (P=0.0097)
Lag 1 residual autocorrelation = 0.523917

ANVOVA Data for Line Width for Platinum Dwell Time Factorial Study

Analysis of Variance for h

Source	Sum of Squares	Df	Mean Square	F-Ratio	P-Value
A:Voltage	224.762	1	224.762	0.57	0.4915
B:Beam Current	39.729	1	39.729	0.10	0.7664
C:Dwell Time	6158.81	1	6158.81	15.68	0.0167
Total error	1571.08	4	392.77		
Total (corr.)	7994.39	7			

R-squared = 80.3477 percent
R-squared (adjusted for d.f.) = 65.6085 percent
Standard Error of Est. = 19.8184
Mean absolute error = 11.6794
Durbin-Watson statistic = 2.3616 (P=0.3581)
Lag 1 residual autocorrelation = -0.324828

ANOVA Data for Height/scan (h) for Carbon Line Factorial Study

Analysis of Variance for Line Width

Source	Sum of Squares	Df	Mean Square	F-Ratio	P-Value
A:Voltage	0.022898	1	0.022898	9.55	0.0366
B:Beam Current	0.102152	1	0.102152	42.59	0.0028
C:Dwell Time	0.005	1	0.005	2.08	0.2223
Total error	0.0095935	4	0.00239838		
Total (corr.)	0.139644	7			

R-squared = 93.13 percent
R-squared (adjusted for d.f.) = 87.9775 percent
Standard Error of Est. = 0.0489732
Mean absolute error = 0.0296875
Durbin-Watson statistic = 1.27013 (P=0.1639)
Lag 1 residual autocorrelation = 0.247375

ANOVA Data for Line Width for Carbon Line Factorial Study

Analysis of Variance for Height per scan

Source	Sum of Squares	Df	Mean Square	F-Ratio	P-Value
A:Voltage	0.00186344	1	0.00186344	5.63	0.0766
B:Beam Current	0.00211082	1	0.00211082	6.38	0.0650
C:Line Time	0.0119936	1	0.0119936	36.23	0.0038
Total error	0.0013242	4	0.00033105		
Total (corr.)	0.017292	7			

R-squared = 92.3421 percent
R-squared (adjusted for d.f.) = 86.5987 percent
Standard Error of Est. = 0.0181948
Mean absolute error = 0.0106736
Durbin-Watson statistic = 1.40392 (P=0.1395)
Lag 1 residual autocorrelation = 0.198939

ANOVA Data for Height/scan for Carbon Line Factorial Line Time Study

Analysis of Variance for Line Width

Source	Sum of Squares	Df	Mean Square	F-Ratio	P-Value
A:Voltage	0.11956	1	0.11956	7.03	0.0769
B:Beam Current	0.129032	1	0.129032	7.59	0.0705
C:Line Time	0.0253125	1	0.0253125	1.49	0.3096
AB	0.208658	1	0.208658	12.27	0.0394
Total error	0.0510125	3	0.0170042		
Total (corr.)	0.533575	7			

R-squared = 90.4395 percent
R-squared (adjusted for d.f.) = 77.6922 percent
Standard Error of Est. = 0.1304
Mean absolute error = 0.069
Durbin-Watson statistic = 1.70313 (P=0.2604)
Lag 1 residual autocorrelation = -0.048928

ANOVA Data for Line Width for Carbon Line Factorial Line Time Study

REFRENCES

1. C. Duty, D. Jean, W.J. Lackey, "Laser Chemical Vapor Deposition: Materials, Modeling, and Process Control," *International Materials Reviews* **46(6)**, p.271-287 (2001)

2. S. Matsui, Y. Ochiai, "Focused Ion Beam Applications to Solid State Devices," *Nanotechnology* **7**, p.247-258 (1996)

3. S. Reyntjens, R. Puers, "A Review of Focused Ion Beam Applications in Microsystem Technology," *J. Micromech. Microeng.* **11**, p.287-300 (2001)

4. International Business Machines Corporation, "Nanometer Scale Probe for an Atomic Force Microscope, and Method for Making the Same." United States Patent Office, Patent Number 5,171,992. New York, NY:1991

5. R.L. Stewart, "Insulating Films Formed under Electron and Ion Bombardment" *Phys. Rev.*, **45**, p.488-490 (1934)

6. A.E. Ennos, "The Sources of Electron-Induced Contamination in Kinetic Vacuum Systems," *Brit. J. Appl. Phys*., **5**, p.27-31 (1954)
7. A.N. Broers, W.W. Molzen, J.J. Cuomo, N.D. Wittels, "Electron-Beam Fabrication of 80-Å Metal Structures," *Applied Physics Letters* **29**, p.596-598 (1976)

8. V. Scheuer, H. Koops, T. Tschudi, "Electron Beam Decomposition of Carbonyls on Silicon," *Microelectronic Engineering*, **5**, p.423-430 (1986)

9. H.W.P. Koops, R. Weiel, D.P. Kern, "High-Resolution Electron-Beam Induced Decomposition," *J. Vac. Sci. Technol. B.* **6(2)**, p.477-481 (1988)

10. S. Matsui, K. Mori, "New Selective Deposition Technology by Electron Beam Induced Surface Reaction," *Japanese Journal of Applied Physics* **23**, p.706-708 (1984)

11. A. Ishibashi, K. Funato, Y. Mori, "Electron-Beam-Induced Resist and Aluminum Formation," *J. Vac. Sci. Technol. B*. **9(1)**, p.169-172 (1991)
12. J. Drucker, R. Sharma, K. Weiss, B.L. Ramakrishna, J. Kouvetakis, "In Situ Real Time Observation of Chemical Vapor Deposition using an Environmental Transmission Electron Microscope," *Mat. Res. Symp. Proc*. **Vol. 404**, p.75-84 (1996)

13. J. Kouvetakis, R. Sharma, B.L. Ramakrishna, J. Drucker, P. Seidler, "Electron Beam Assisted Chemical Vapor Deposition of Gold in an Environmental TEM," *Mat. Res. Symp. Proc*. **Vol. 388**, p.323-328 (1995)

14. K. Molhave, D.N. Madsen, A.M. Rasmussen, A. Carlsson, C. Appel, M. Brorson, C. Jacobsen, P. Bøggild, "Solid Gold Nanostructures Fabricated by Electron Beam Deposition," *Nano Letters* **3**, p.1499-1503 (2003)

15. P. Hoffmann, I. Utke, F. Cicoira, B. Dwir, K. Leifer, E. Kapon, P. Doppelt, "Focused Electron Beam Induced Deposition of Gold and Rhodium," *Mat. Res. Soc. Symp. Proc., San Francisco* **624**, p.171-177 (2000)

16. H.W. Koops, C. Schössler, A. Kaya, M. Weber, "Conductive Dots, Wires, and Supertips for Field Electron Emitters Produced by Electron-Beam Induced Deposition on Samples having Increased Temperature," *J. Vac. Sci. Technol. B* **14(6)**, p.4105-4109 (1996)

17. N. Miura, H. Ishii, J. Shirakashi, A. Yamada, M. Konagai, "Electron-Beam-Induced Deposition of Carbonaceous Microstructures using Scanning Electron Microscopy," *Applied Surface Science* **113/114**, p.269-273 (1997)

18. I. Utke, T. Bret, D. Laub, P. Buffat, L. Scandella, P. Hoffmann, "Thermal Effects During Focused Electron Beam Deposition of Nanocomposite Magnetic-Cobalt-Containing Tips," *Microelectronic Engineering* **73-74**, p.553-558 (2004)

19. R.R. Kunz, T.E. Allen, T.M. Mayer, "Selective Area Decomposition of Metals using Low-energy Electron Beams," *J. Vac. Sci. Technol. B.* **5(5)**, p.1427-1430 (1987)

20. T. Bret, I. Utke, A. Bachmann, P. Hoffmann, "In situ Control of the Focused-Electron-Beam-Induced Deposition Process," *Applied Physics Letters* **83**, p.4005-4007 (2003)

21. S. Kiyohara, H. Takamatsu, K. Mori, "Microfabrication of Diamond Films by Localized Electron Beam Chemical Vapor Deposition," *Semicond. Sci. Technol*. **17**, p.1096-1100 (2002)

22. M. Shimojo, M. Takeguchi, M. Tanaka, K. Mitsuishi, K. Furuya, "Electron Beam-Induced Deposition using Iron Carbonyl and the Effects of Heat Treatment on Nanostructure," *Applied Physics A* **79**, p.1869-1872 (2004)

23. T. Takahashi, Y. Arakawa, M. Nishioka, T. Ikoma, "Selective Growth of GaAs Wire Structures by Electron Beam Induced Metalorganic Chemical Vapor Deposition," *Appl. Phys. Lett*., **60(1)**, p.68-70 (1992)

24. M. Weber, H.W.P. Koops, M. Rudolph, J. Kretz, G. Schmidt, "New Compound Quantum Dot Materials Produced by Electron-Beam Induced Deposition," *J. Vac. Sci. Technol. B*. **13(3)**, p.1364-1368 (1995)

25. F. Floreani, H.W. Koops, W. Elsäßer, "Operation of High Power Field Emitters Fabricated with Electron Beam Deposition and Concept of a Miniaturized Free Electron Laser," *Microelectronic Engineering* **57-58**, p.1009-1016 (2001)

26. L. Rotkina, J.F. Lin, J.P. Bird, "Nonlinear Current-Voltage Characteristics of Pt Nanowires and Nanowire Transistors Fabricated by Electron-Beam Deposition," *Applied Physics Letters* **83**, p.4426-4428 (2003)

27. H.W. Koops, A. Kaya, M. Weber, "Fabrication and Characterization of Platinum Nanocrystalline Material Grown by Electron-Beam Induced Deposition," *J. Vac. Sci. Technol. B* **13(6)**, p.2400-2403 (1995)

28. M. Takai, T. Kishimoto, H. Morimoto, Y.K. Park, S. Lipp, C. Lehrer, L. Frey, H. Ryssel, A. Hosono, S. Kawabuchi, "Fabrication of Field Emitter Array using Focued Ion and Electron Beam Induced Reaction," *Microelectronic Engineering* **41/42**, p.453-456 (1998)

29. K. Heinemann, T. Osaka, "Electron-Beam Enhanced Growth of CVD-Deposited Silicon on Alumina," *Journal of Crystal Growth* **59**, p.485-498 (1982)

30. A. Perentes, A. Bachmann, M. Leutenegger, I. Utke, C. Sandu, P. Hoffmann, "Focused Electron Beam Induced Deposition of a Periodic Transparent Nano-optic Pattern," *Microelectronic Engineering* **73-74**, p.412-416 (2004)

31. L.R. Thompson, J.J. Rocca, K.Emery, P.K. Boyer, G.J. Collins, "Electron Beam Assisted Chemical Vapor Deposition of SiO_2," *Applied Physics Letters* **43(8)**, p.777-779 (1983)

32. B.H. Chin, G. Ehrlich, "Formation of Silicon Nitride Structures by Direct Electron Beam Writing," *Applied Physics Letters* **38(4)**, p.253-255 (1981)

33. T. Ichihashi, S. Matsui, "In-situ Observation on Electron Beam Induced Chemical Vapor Deposition by Transmission Electron Microscope," *Extended Abstracts of the 19th Conference on Solid State Devices and Materials, Tokyo*, p.505-506 (1987)

34. S. Bauerdick, C. Burkhardt, R. Rudorf, W. Barth, V. Bucher, W. Nisch, "In-situ Monitoring of Electron Beam Induced Deposition by Atomic Force Microscopy in a Scanning Electron Microscope," *Microelectronic Engineering* **67-68**, p.963-969 (2003)

35. A. Folch, J. Tejada, C.H. Peters, M.S. Wrighton, "Electron Beam Deposition of Gold Nanostructures in a Reactive Environment," *Appl. Phys. Lett*. **66**(16), p. 2080-2082 (1995)

36. A. Folch, J. Servat, J. Esteve, J. Tejada, M. Seco, "High-Vacuum Versus "Environmental" Electron Beam Deposition," *J. Vac. Sci. Technol. B* **14**(4), p. 2609-2614 (1996)

37. R.R. Kunz, T.M. Mayer, "Electron Beam Induced Surface Nucleation and Low-Temperature Decomposition of Metal Carbonyls," *J. Vac. Sci. Technol. B*. **6(5)**, p.1557-1564 (1988)

38. Y. Akama, E. Nishimura, A. Sakai, H. Murakami, "New Scanning Tunneling Microscopy Tip for Measuring Surface Topography," *J. Vac. Sci. Technol. A*. **8(1)**, p.429-433 (1990)

39. K.I. Schiffmann, "Investigation of Fabrication Parameters for the Electron-Beam-Induced Deposition of Contamination Tips used in Atomic Force Microscopy," *Nanotechnology* **4**, p.163-169 (1993)

40. M. Komuro, H. Hiroshima, "Fabrication and Properties of Dot Array using Electron-Beam-Induced-Deposition," *Microelectronic Engineering* **35**, p.273-276 (1997)

41. I.W. Rangelow, T. Gotszalk, N. Abedinov, P. Grabiec, K. Edinger, "Thermal Nano-Probe," *Microelectronic Engineering* **57-58**, p.737-748 (2001)

42. P. Bøggild, T.M. Hansen, O. Kuhn, F. Grey, T. Junno, L. Montelius, "Scanning Nanoscale Multiprobes for Conductivity Measurements," *Rev. Sci. Instrum*. **71**, p.2781 (2000)

43. P. Hoffmann, I. Utke, F. Cicoira, "Limits of 3-D Nanostructures Fabricated by Focused Electron Beam (FEB) Induced Deposition," *10th Int. Symposium "Nanostructures: Physics and Technology", St. Petersburg, Russia, June 17-21, (2002)*

44. N. Silvis-Cividjian, C.W. Hagen, L.H.A. Leunissen, P. Kruit, "The Role of Secondary Electrons in Electron-Beam-Induced-Decomposition Spatial Resolution," *Microelectronic Engineering* **61-62**, p.693-699 (2002)

45. L. Reimer, *Scanning Electron Microscopy, 2nd ed*.; Springer:Berlin, **Vol. 45**, (1998)

46. M. Wendel, H. Lorenz, J.P. Kotthaus, "Sharpened Electron Beam Deposited Tips for High Resolution Atomic Force Microscope Lithography and Imaging," *Applied Physics Letters*, **67 (25)**, p.3732-3734 (1995)

47. K.T. Kohlmann-von Platen, L.M. Buchmann, H.C. Petzoid, W.H. Brunger, "Electron-Beam Induced Tungsten Deposition: Growth Rate Enhancement and Applications in Microelectronics," *J. Vac. Sci. Technol. B*. **10(6)**, p.2690-2694 (1992)

48. Z.Q. Liu, K. Mitsuishi, K. Furuya, "Effects of Focus Change of the Fabrication of Tungsten Nanowire by Electron-Beam-Induced Deposition," *Nanotechnology* **15**, p.S414-S419 (2004)

49. U. Hübner, R. Plontke, M. Blume, A. Reinhardt, H.W.P. Koops, "On-line Nanolithography Using Electron Beam-Induced Deposition Technique," *Microelectronic Engineering* **57-58**, p. 953-958 (2001)

50. P. Bøggild, T.M. Hansen, C. Tanasa, F. Grey, "Fabrication and Actuation of Customized Nanotweezers with a 25 nm Gap," *Nanotechnology* **12**, p.331-335 (2001)

51. T. Ooi, K. Matsumoto, M. Nakao, M. Otsubo, S. Shirakata, S. Tankaa, Y. Hatamura, "3D Nano Wire-Frame for Handling and Observing a Single DNA Fiber," *IEEE MEMS2000 Proceedings*, p.580-583, (2000)